

Aus dem Pathologisches Institut
Institut der Ludwig-Maximilians-Universität München



Dissertation

zum Erwerb des Doctor of Philosophy (Ph.D.)

an der Medizinischen Fakultät der
Ludwig-Maximilians-Universität München

Characterization of miR-34 effectors in colorectal cancer

vorgelegt von:

Zekai Huang

aus:

Chaozhou

Jahr:

2024

Mit Genehmigung der Medizinischen Fakultät der
Ludwig-Maximilians-Universität München

Erstes Gutachten von: Prof. Dr. Heiko Hermeking

Zweites Gutachten von: Prof. Dr. Roland Kappler

Drittes Gutachten von: Priv. Doz. Dr. Tobias Schwerd

Viertes Gutachten von: Prof. Dr. Frank Kolligs

Dekan: Prof. Dr. med. Thomas Gudermann

Datum der Verteidigung:

11.03.2024

Table of content

Table of content.....	3
Zusammenfassung (Deutsch):.....	5
Abstract (English):	7
List of abbreviations	10
1. Introduction	11
1.1 Colorectal cancer	11
1.1.1 CRC development pathways	12
1.1.2 Metastatic CRC therapy.....	14
1.1.3 Consensus Molecular Subtypes (CMS) of CRC.....	19
1.2 P53 and miR-34 family.....	20
1.2.1 Tumor suppressor p53.....	20
1.2.2 MicroRNAs and miR-34	21
1.2.3 P53/miR-34 axis in CRC.....	27
1.3 EMT in cancer metastasis.....	29
1.4 Autophagy in CRC	33
1.4.1 Autophagy.....	33
1.4.2 Autophagy inhibits apoptosis	36
1.4.3 Autophagy and therapy resistance in cancer.....	41
1.4.4 Autophagy and p53.....	43
1.4.5 Autophagy and miR-34	45
1.5 FOXM1.....	48
2. Aims of the study.....	52
3. Material.....	53
3.1 Chemicals and reagents	53
3.2 Buffers and solutions	55
3.3 Kits	56
3.4 siRNAs	57
3.5 Enzymes	57
3.6 Oligonucleotides	58
3.6.1 Sequence information for guide RNAs used for <i>miR-34a/b/c</i> deletion	58
3.6.2 Sequence information for genotyping primers used for selecting <i>miR-34a/b/c</i> homozygous deletion	58
3.6.3 Oligonucleotides used for qPCR.....	59
3.6.4 Oligonucleotides used for qChIP	59
3.7 Oligonucleotides used for reporter plasmids	60
3.8 List of antibodies	61
4. Methods	62
4.1 Cell culture and treatments.....	62
4.2 CRISPR/Cas9-mediated deletion of <i>miR-34</i>	62

4.3	RNA isolation and real-time polymerase chain reaction (qPCR) analysis.....	63
4.4	Chromatin immunoprecipitation	63
4.5	Modified Boyden-chamber assay	64
4.6	Wound healing assay.....	64
4.7	3'-UTR dual reporter assay.....	65
4.8	Western blot analysis.....	66
4.9	Apoptosis detection with FITC Annexin V staining	66
4.10	Apoptosis evaluation with cell cycle analysis by Propidium Iodide staining	67
4.11	Cell viability assay.....	67
4.12	Assessment of cell proliferation by real-time impedance measurement.....	68
4.13	Autophagic flux assay with GFP-LC3-RFP probe	68
4.14	RNA-Seq analysis.....	69
4.15	Analysis of gene expression and clinical data from public databases.....	70
4.16	Drug combination synergy scores analysis	72
4.17	Statistical analysis.....	72
5.	Results	74
5.1	Generation and characterization of <i>miR-34a/b/c</i> -deficient HCT116 cell lines	74
5.2	<i>miR-34a/b/c</i> inhibits cellular proliferation in HCT116 cells	77
5.3	Loss of <i>miR-34a/b/c</i> promotes EMT, migration and invasion in HCT116 cells	78
5.4	Loss of <i>miR-34a/b/c</i> mediates resistance to chemotherapeutic agents by enhancing autophagic flux.....	81
5.5	Loss of <i>miR-34a/b/c</i> consistently elevates autophagic flux after stress	89
5.6	Analysis of mediators of miR-34 function by expression profiling	93
5.7	<i>MiR-34a/b/c</i> inhibit multiple key autophagy-related genes	102
5.8	FOXM1 induces autophagy and transactivates <i>p62</i> and <i>ATG9A</i>	103
5.9	Silencing of <i>ATG9A</i> in <i>miR-34a/b/c</i> -KO cells inhibits autophagic flux and re-sensitizes to 5-FU	109
5.10	Synergistic effects of 5-FU and chloroquine in <i>miR-34a/b/c</i> -KO cells	112
5.11	Clinical relevance of <i>miR-34a/b/c</i> -KO-derived gene signatures	113
6.	Discussion.....	117
7.	References.....	133
8.	Appendix.....	144
	Table S1. List of mRNAs to generate the K-means clustering heatmap.	144
	Acknowledgements.....	174
	Affidavit.....	175
	Confirmation of congruency	176
	Curriculum vitae.....	177
	List of publications	178

Zusammenfassung (Deutsch):

Die Gene, die für microRNA-34a (miR-34a) und microRNA-34b/c (miR-34b/c) kodieren, wurden als direkte Ziele des p53-Transkriptionsfaktors charakterisiert und vermitteln vermutlich einen Teil der tumorsuppressiven Wirkung von p53. In dieser Studie wurden die funktionellen Rollen von miR-34a und miR-34b/c durch die Deletion von *miR-34a* und *miR-34b/c* entweder einzeln oder in Kombination unter Verwendung eines Clustered Regular Interspaced Palindromic Repeats (CRISPR)/Cas9-Ansatzes in der Darmkrebs (CRC) Zelllinie HCT116 untersucht. Die kombinierte Inaktivierung von *miR-34a/b/c* schwächte die p53-vermittelte Unterdrückung der Proliferation deutlich ab. Darüber hinaus verstärkte die gleichzeitige Deletion von *miR-34a/b/c* die Zell-Migration und -Invasion deutlich, vermutlich aufgrund der Aktivierung des epithelial-mesenchymalen Übergangs (EMT). Der Verlust von *miR-34a/b/c* führte auch zu einer verminderten chemotherapeutischen Empfindlichkeit und einer verringerten Apoptose, was vermutlich auf den erhöhten Stress-induzierten, autophagischen Fluss zurückzuführen ist. Die Inaktivierung von *miR-34a* oder *miR-34b/c* allein hatte jedoch kaum Auswirkungen auf die oben genannten Prozesse. Die Analyse der RNA-Sequenzierungs-Ergebnisse ergab, dass die kombinierte Deletion von *miR-34a/b/c* zu einer beeinträchtigten Genrepression durch die p53-DREAM-Achse (Dimerisierungspartner, RB-like, E2F und multi-vulvaler Klasse-B-Komplex), Aktivierung des EMT-Signalwegs und verminderten mitochondrialen und apoptotischen Signaturaktivitäten und Hochregulierung der Autophagie nach der Behandlung mit 5-Fluorouracil (5-FU) führte. Darüber hinaus zeigte eine Gensignatur, die deutlich hoch-regulierte Messenger-RNAs (mRNAs) umfasste und durch die kombinierte Inaktivierung von *miR-34a/b/c* verursacht wurde, eine signifikante Korrelation mit dem invasiven Dickdarmkrebs-Subtyp Consensus Molecular Subtype 4 (CMS4)

und einem ungünstigen Gesamtüberleben in zwei CRC Patientenkohorten und mit 5-FU-Resistenz in CRC-Zelllinien. In *miR-34a/b/c*-defizienten Zellen verstärkte die erhöhte Expression des miR-34-Ziels FOXM1 die Autophagie und reduzierte folglich die Apoptose durch direkte Induktion von *ATG9A* und *SQSTM1*, was die *miR-34a/b/c*-defizienten Zellen resistenter gegenüber einer 5-FU-Behandlung machte. Diese Resistenz wurde durch die Hemmung der Autophagie, die entweder durch die Stummschaltung von *ATG9A* oder die Verabreichung von Chloroquin erreicht wurde, deutlich abgeschwächt. Zusammengekommen unterstreichen diese Ergebnisse eine komplementäre Rolle von *miR-34a* und *miR-34b/c* bei der Modulation von EMT und Autophagie, die für zukünftige therapeutische Interventionen beim CRC relevant sein könnte.

Abstract (English):

The genes encoding *microRNA-34a* (*miR-34a*) and *microRNA-34b/c* (*miR-34b/c*) have been characterized as direct targets of the p53 transcription factor, and presumably mediate a portion of the tumor suppressive effects of p53. In this study, the functional roles of miR-34a and miR-34b/c were interrogated by the deletion of *miR-34a* and *miR-34b/c* either individually or in combination utilizing a Clustered Regularly Interspaced Palindromic Repeats (CRISPR)/Cas9 approach in the colorectal cancer (CRC) cell line HCT116. The combined inactivation of *miR-34a/b/c* significantly attenuated the p53-mediated repression of proliferation. Additionally, the concomitant deletion of *miR-34a/b/c* significantly enhanced cellular migration and invasion, presumably due to the activation of epithelial-mesenchymal transition (EMT). The concomitant loss of *miR-34a/b/c* also resulted in diminished chemotherapeutic sensitivity and decreased apoptosis, presumably resulting from the increased stress-induced autophagic flux. However, the inactivation of either *miR-34a* or *miR-34b/c* alone had little effect on the aforementioned processes. RNA sequencing analysis revealed that the combined deletion of *miR-34a/b/c* led to impaired gene repression by the p53-DREAM (dimerization partner, RB-like, E2F and multi-vulval class B complex) axis, activation of EMT pathway, decreased mitochondrial and apoptotic signature activities, and upregulation of the autophagy after 5-Fluorouracil (5-FU) treatment. Furthermore, a gene signature comprising of significantly up-regulated messenger RNAs (mRNAs) caused by the combined inactivation of *miR-34a/b/c* exhibited a significant correlation with the invasive colon cancer subtype Consensus Molecular Subtype 4 (CMS4) and adverse overall survival in two CRC patient cohorts, and with 5-FU resistance in CRC cell lines. In *miR-34a/b/c*-deficient cells, the

elevated miR-34 target FOXM1 augmented autophagy and consequently reduced apoptosis by directly inducing *ATG9A* and *SQSTM1*, which rendered the *miR-34a/b/c*-deficient cells more resistant to 5-FU treatment. This resistance was significantly attenuated by the inhibition of autophagy, achieved via either *ATG9A* silencing or chloroquine administration. Collectively, these findings underscore a complementary role of *miR-34a* and *miR-34b/c* in modulating EMT and autophagy, which may be relevant for future therapeutic interventions in CRC.

Part of the results in the dissertation have been published in a peer-reviewed journal [published open access under a CC BY license (Creative Commons Attribution 4.0 International license), authors retain copyright of their articles]:

Huang, Z., Kaller, M. & Hermeking, H. CRISPR/Cas9-mediated inactivation of *miR-34a* and *miR-34b/c* in HCT116 colorectal cancer cells: comprehensive characterization after exposure to 5-FU reveals EMT and autophagy as key processes regulated by miR-34. *Cell Death Differ* 30, 2017–2034 (2023). <https://doi.org/10.1038/s41418-023-01193-2>

In addition, I made contributions to the following articles, which are not further described here:

1. Rokavec, M., Huang, Z, Hermeking, H. Meta-analysis of miR-34 target mRNAs using an integrative online application. *Comput Struct Biotechnol J*, 2023. 21: p. 267-274. <https://doi.org/10.1016/j.csbj.2022.12.003>

2. Liu, C., Rokavec, M., Huang, Z. & Hermeking, H. Curcumin activates a ROS/KEAP1/NRF2/*miR-34a/b/c* cascade to suppress colorectal cancer metastasis. *Cell Death Differ* 30, 1771–1785 (2023). <https://doi.org/10.1038/s41418-023-01178-1>

List of abbreviations

5-FU	fluorouracil
ATG9A	autophagy related 9A
CCLE	Cancer Cell Line Encyclopedia
cDNA	complementary DNA
CQ	chloroquine
CMS	colorectal cancer molecular subtype
CRC	colorectal cancer
DNA	deoxyribonucleic acid
DREAM complex	DP, RB-like, E2F4, and multi-vulval class B (MuvB) complex
DOX	doxycycline
EMT	epithelial-mesenchymal transition
FOXM1	forkhead box protein M1
FDR	false discovery rate
GDSC	Genomics of Drug Sensitivity in Cancer database
GSVA	gene set variation analysis
miRNAs	microRNAs
<i>MIR34AHG</i>	MIR34A host gene
<i>MIR34BHG</i>	MIR34B and MIR34C host gene
MuvB complex	multi-vulval class B complex
SQSTM1	sequestosome 1
SMS	seed-matching sequence
siRNA	small interfering RNA
TCGA	the Cancer Genome Atlas

1. Introduction

1.1 Colorectal cancer

Colorectal cancer (CRC) represents the third most diagnosed cancer type and the second leading cause of cancer-associated mortality globally. In addition, CRC ranks as the second most common cancer diagnosed in women and the third in men. The gender disparity in incidence and mortality rates, with women having approximately 25% lower rates than men, adds another layer of complexity to the disease's epidemiology. The year 2020 alone saw an estimated 1.9 million new CRC cases and around 940,000 deaths, representing almost 10% of all cancer diagnoses and cancer-related deaths worldwide [1]. While the mortality rate of CRC has been decreasing for several decades and is down by more than 50% from its peak level, a concerning increase has been observed in the number of patients under 50 years old presenting with CRC, particularly rectal cancer and left-sided colon cancer [2].

The management of CRC presents significant challenges, particularly in advanced stages of the disease. While surgery remains the primary curative option for early-stage CRC, the picture is far more complex for advanced cases. An estimated 50% to 60% of CRC patients will develop metastases [3, 4], and a staggering 80% to 90% of these metastatic cases involve unresectable liver disease [5]. Compounding the issue is the fact that CRC often remains asymptomatic until it reaches an advanced stage. Approximately 21% of CRC cases are already at an advanced stage upon initial diagnosis. Despite advancements in our understanding of the disease's pathophysiology and improvements in therapeutic options, the prognosis for advanced CRC remains grim. The 5-year survival rate for

these cases is dishearteningly low, hovering around just 14% in the United States [6].

1.1.1 CRC development pathways

The majority of CRCs arise from a polyp, which is a neoplastic lesion derived from an aberrant crypt. It takes about 10 to 15-year period for a polyp to progress to CRC [2]. In addition, current understanding suggests that most CRCs originate from stem cells or stem-cell-like cells. These cells originate from the progressive accumulation of epigenetic and genetic changes that activate oncogenes, which are genes that have the potential to cause cancer, and deactivate tumor-suppressor genes, which are genes that protect a cell from one step on the path to cancer. Cancer stem cells presumably originate at the base of colonic crypts and are crucial in initiating and maintaining CRC [7].

There are three major development pathways for CRC: the traditional adenoma-carcinoma pathway, the serrated neoplasia pathway and the microsatellite instability pathway (**Figure 1.1**). The traditional adenoma-carcinoma pathway, aka the chromosomal instability sequence, accounts for 70-90% of all CRC cases. It is characterized by the accumulation of genetic mutations and chromosomal instability in colonic epithelial cells, leading to the formation of adenomatous polyps. This process typically begins with an initiating mutation in the *adenomatous polyposis coli* (*APC*) gene, which is a hallmark of familial adenomatous polyposis and a tumor suppressor gene that normally regulates division and cell growth. The mutation of *APC* gene results in uncontrolled cell growth and the formation of an adenoma. Additional mutations can occur in other genes such as *KRAS*, *BRAF*, *SMAD4* and *TP53*, which leads to further uncontrolled growth and the development of dysplasia and eventually progress to invasive cancer. In sum,

the traditional adenoma-carcinoma pathway is a stepwise process that involves multiple genetic changes over time [8].

The serrated neoplasia pathway is the other major pathways that result in the development of CRC, accounting for 10-20% of all CRC cases. It is characterized by the formation of serrated polyps, which are a type of precancerous lesion that can eventually progress to become malignant tumors. Serrated polyps can be divided into three main subtypes: sessile serrated lesions, traditional serrated adenomas, and hyperplastic polyps. The serrated neoplasia pathway is often initiated by genetic mutations in the *KRAS* or *BRAF* genes, and then progresses via the methylation of tumor-suppressor genes, leading to CpG island methylator phenotype (CIMP). CIMP can result in both microsatellite unstable and stable tumors, depending on which genes are epigenetically silenced as the lesions progress [9].

Microsatellite instability pathway accounts for 2 to 7% of CRC cases, which results from defective DNA repair due to the inactivation of DNA mismatch repair (MMR) genes, including *PMS2*, *MLH1*, *MSH2* and *MSH6*. Microsatellite instability pathway can occur through germline mutations in these genes, which is also seen in Lynch syndrome, a hereditary condition that results from germline mutations in MMR genes. Lynch syndrome accounts for 2 to 4% of all CRC cases and is the most common type of genetically determined CRC predisposition. Cells with deficiency of DNA mismatch repair (dMMR) tend to accumulate errors in DNA microsatellites, which are short, repetitive DNA sequences that make up about 3% of the human genome. These errors, known as microsatellite instability (MSI), occur when the MMR system fails to fix DNA replication errors and maintain genomic stability, resulting in high levels of microsatellite instability (MSI-H) and an

increased risk of developing CRC, and other types of cancer [10]. In sporadic CRC without MMR genes mutations, there are usually 3 to 6 driver mutations and multiple passenger mutations. However, CRC with MMR deficiency has 10 times more mutations, leading to a hypermutated phenotype [11].

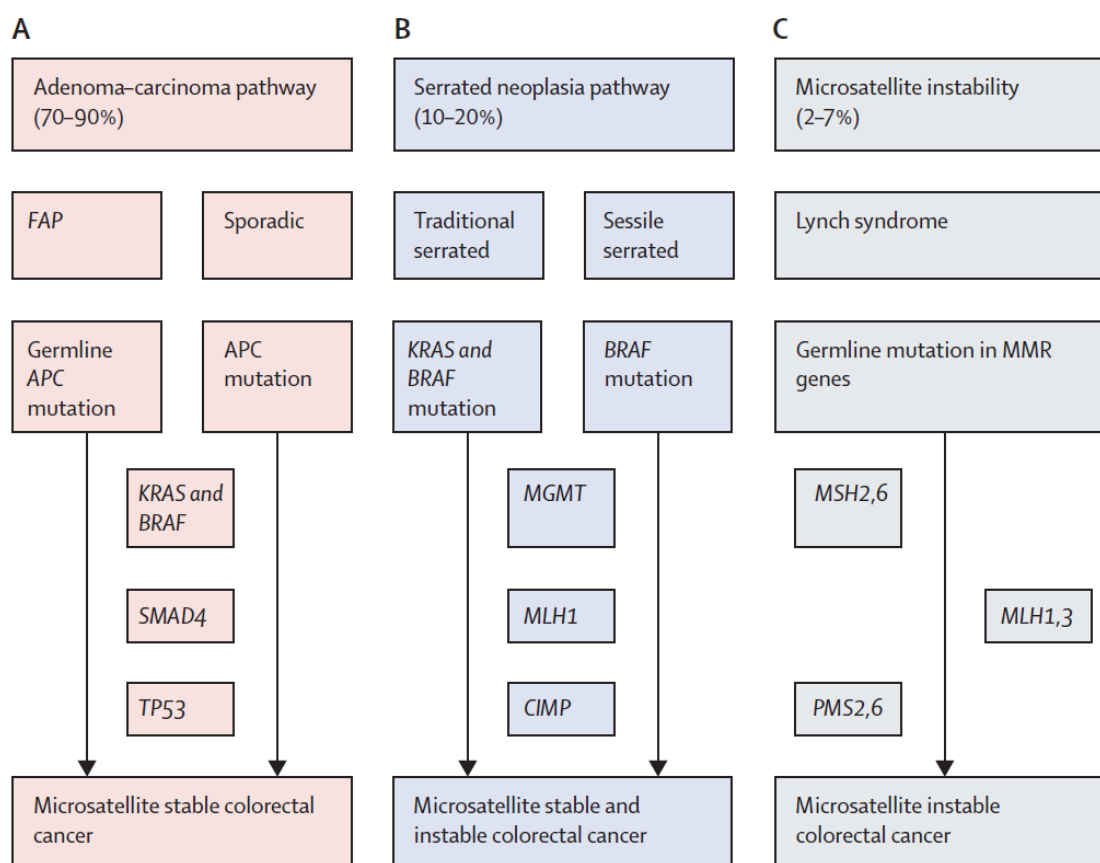


Figure 1.1. Colorectal cancer (CRC) development pathways. (Figure and legend are from Dekker et al.[2])

1.1.2 Metastatic CRC therapy

Surgical resection remains the primary curative intervention for early-stage CRC patients. However, the clinical management of CRC is complicated by the high propensity for metastatic spread, with an estimated 50% to 60% of individu-

als diagnosed with CRC ultimately manifesting colorectal metastases [3, 4]. Furthermore, a significant proportion of these patients, ranging from 80% to 90%, present with metastatic liver disease that is deemed unresectable [5, 12].

In such cases, systemic therapy becomes the primary treatment modality for metastatic CRC (mCRC). Standard systemic therapy for mCRC generally involves a chemotherapy backbone, which typically includes fluoropyrimidines, oxaliplatin, and irinotecan. This is often paired with a biologic agent, either an anti-VEGF (Vascular Endothelial Growth Factor) or anti-EGFR (Epidermal Growth Factor Receptor) antibody, the choice of which is guided by patient-specific and tumor-specific factors [2]. For patients with BRAF-V600E mutant CRCs, which are known to be particularly aggressive and less responsive to standard systemic therapies, combinatorial strategies have been developed. These often involve the use of anti-EGFR antibodies paired with BRAF inhibitors, MEK inhibitors, or additional chemotherapy agents. Such combinatorial approaches have demonstrated improved outcomes in several randomized clinical trials and are now recommended as part of the treatment regimen for these patients [13, 14]. In addition, newer therapeutic agents such as Regorafenib and TAS-102 have been approved for use in mCRC patients who are refractory to frontline systemic therapies. These drugs offer an alternative treatment option for patients who have exhausted other available therapies, thereby extending the therapeutic landscape for mCRC [15-17] (**Figure 1.2**).

Chemotherapies	Biologics	Novel or salvage therapy drugs	Targeted therapies or immunotherapy
Fluorouracil (capecitabine)	Anti-VEGF agents	Regorafenib	Immunotherapy
Oxaliplatin	Anti-EGFR drugs	TAS-102 (trifluridine plus tipiracil)	BRAF or BRAF plus MEK inhibitors
Irinotecan			

Figure 1.2 Different classes of drugs available for metastatic CRC patients. (Figure and legend are from Dekker et al., 2019 [2])

Fluorouracil (5-FU) remains a cornerstone in the standard of care for patients with mCRC [18]. As an antimetabolite agent, 5-FU is widely employed in the treatment of various malignancies, but it holds particular significance in the therapeutic regimen for CRC. Once administered, 5-FU undergoes intracellular conversion into several active metabolites, which includes fluorouridine triphosphate (FUTP), fluorodeoxyuridine monophosphate (FdUMP), and fluorodeoxyuridine triphosphate (FdUTP). The cytotoxic effects of 5-FU are primarily mediated through two mechanisms. First, FdUMP acts as an inhibitor to the enzyme thymidylate synthase (TS), which is essential for the synthesis of thymidine monophosphate (dTMP), a precursor of DNA. This inhibition disrupts DNA synthesis and results in cell cycle arrest and apoptosis. Second, FdUTP and FUTP are incorporated into DNA and RNA, respectively, thereby disrupting the normal function and synthesis of these nucleic acids. The dual action of 5-FU, both the inhibition of TS and the misincorporation of its active metabolites into DNA and RNA, results in significant DNA and RNA damage [19] (**Figure 1.3**).

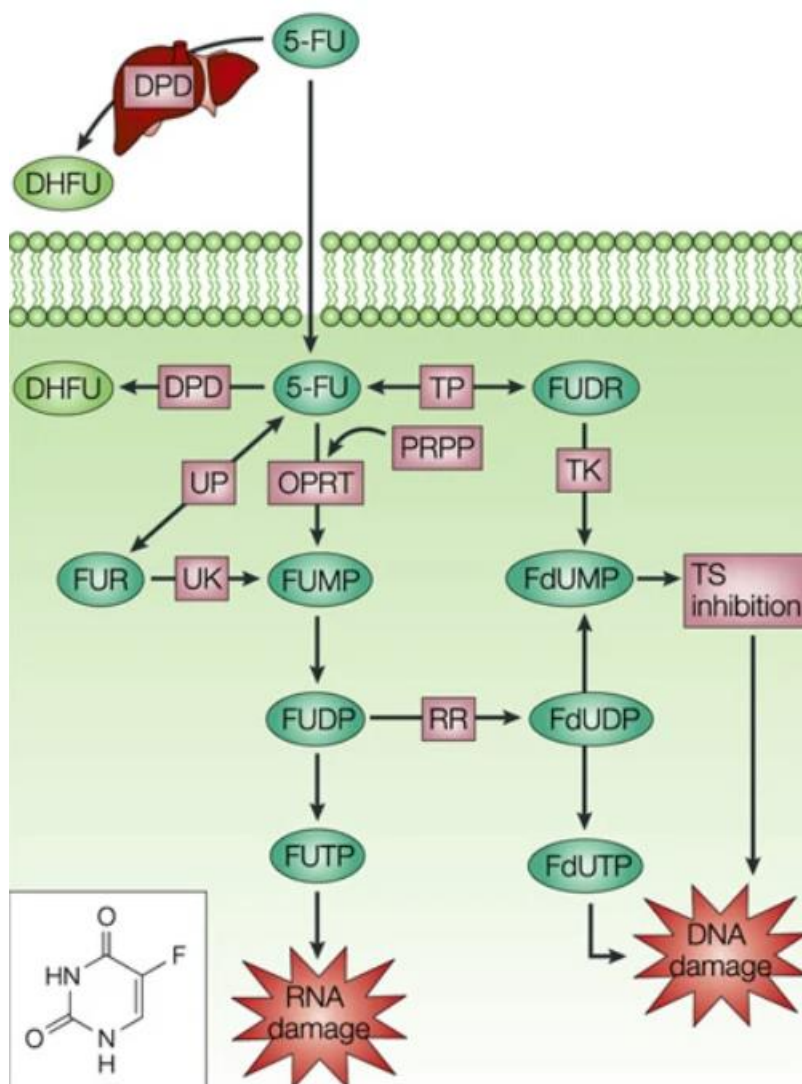


Figure 1.3 5-FU metabolism and mechanism of action. (Figure and legend are from Longley et al., 2003 [19])

The tumor suppressor protein p53 plays a critical role in safeguarding genomic integrity by orchestrating a range of cellular responses to DNA damage. Depending on the cellular context and the specific nature of the DNA damage incurred, p53 can induce cellular senescence, cell-cycle arrest, or apoptosis. Each of these outcomes serves to mitigate the risk of malignant transformation by either repairing the damaged DNA or eliminating the affected cell [20]. In the context of 5-FU-based chemotherapy, both the misincorporation of 5-FU metabolites into RNA and DNA, as well as the inhibition of thymidylate synthase (TS),

can lead to DNA damage that triggers the stabilization and activation of p53. The activated p53, in turn, initiates one of its downstream pathways to maintain genomic stability. For instance, p53 can halt the cell cycle to allow time for DNA repair mechanisms to correct the damage. Alternatively, if the damage is too extensive to be repaired, p53 can induce apoptosis to remove the damaged cell from the population [19] (**Figure 1.4**).

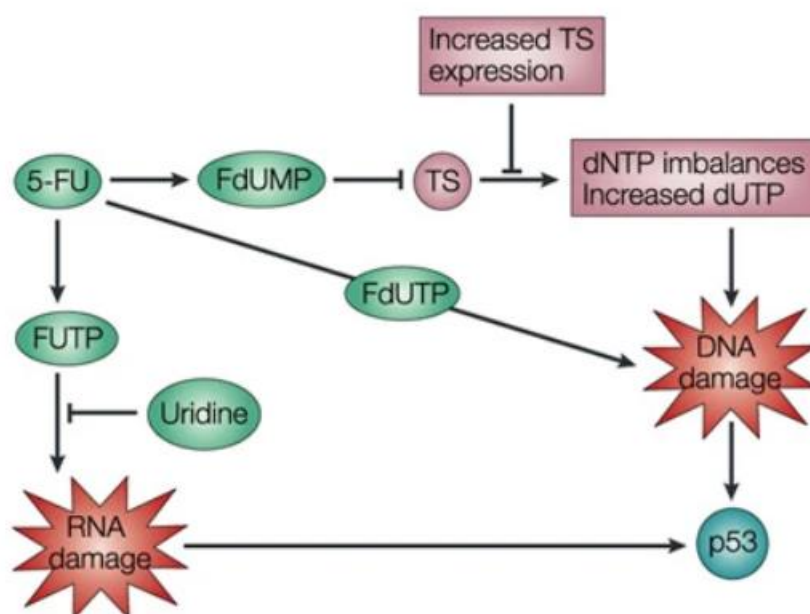


Figure 1.4 Activation of p53 by 5-FU. (Figure and legend are from Longley et al., 2003 [19])

While 5-FU continues to be a cornerstone in the standard treatment regimen for mCRC, its efficacy is not universal. The collective response rate to 5-FU-based chemotherapy in mCRC patients is estimated to be approximately 50% [21] and the emergence of drug resistance is an eventual likelihood [22]. Despite promising, targeted therapy and immunotherapy only benefit a subset of CRC patients [23, 24]. Given these limitations, there is an urgent imperative to deepen

our understanding of the gene regulatory networks and molecular mechanisms that govern the response of CRC cells to therapeutic interventions. Such insights could pave the way for the development of more effective, personalized treatment strategies.

1.1.3 Consensus Molecular Subtypes (CMS) of CRC

CRC is a notably complex and heterogeneous disease, characterized by significant variations in both prognosis and therapeutic response across different biological subtypes [25].

Recognizing the need for a unified classification system to better understand this heterogeneity, an international consortium integrated six independent classification systems into a consensus molecular subtypes (CMS) framework in 2014. This system delineates CRC into four distinct subtypes based on gene expression profiles, each with unique biological and clinical characteristics: CMS1 (microsatellite instability, immune), microsatellite unstable, hypermutated and strong immune activation; CMS2 (canonical), epithelial, marked MYC and WNT signaling activation; CMS3 (metabolic), evident metabolic dysregulation and epithelial; CMS4 (mesenchymal), stromal invasion, prominent transforming growth factor- β activation and angiogenesis. Importantly, CMS4 tumors display the poorest relapse-free and overall survival rate [25]. The CMS classification is currently assessed in clinical trials for its utility as a predictive or prognostic marker. The aim is to tailor therapeutic strategies more effectively based on the molecular subtype, thereby improving patient outcomes [26, 27].

In summary, the CMS classification represents a significant step toward a more nuanced understanding of CRC, offering the potential for more personalized and effective treatment strategies. However, further research is needed to

validate the clinical utility of this classification system in guiding therapeutic decision-making and improving patient outcomes.

1.2 P53 and miR-34 family

1.2.1 Tumor suppressor p53

The p53 tumor suppressive protein is encoded by the *TP53* gene and commonly referred to as “the guardian of the genome” for its prominent biological function in protecting the integrity of cellular DNA. The *TP53* gene is the most frequently mutated gene in a wide variety of cancer types and the wild-type p53 protein functions are commonly compromised in many types of cancers [28]. P53 has been shown to regulate various biological processes, including cell cycle arrest [29], senescence [30], DNA repair [31], apoptosis [32], epithelial-mesenchymal transition [33] as well as autophagy [34].

P53 is a transcription factor which is activated by several cellular stresses including DNA damage, oncogene activation, hypoxia, metabolic stress and oxidative stress [35]. In response to these cellular stresses, p53 undergoes post-translational modifications and initiates cellular responses through transcriptional activation or repression of genes implicated in specific cellular responses according to the type of stress and thereby controlling the fate of the cell [36].

P53 has been reported to mediate its tumor suppressive functions not only through protein-coding genes but also through non-coding RNAs, among which are microRNAs (miRNAs) [37]. P53 directly induces the expression of tumor-suppressive miRNAs, such as those belonging to the *miR-34*, *miR-15/16*, *miR-200*

and *miR-192/194/215* families, as well as the *miR-145*. For example, p53 represses the proto-oncogene *c-Myc* through direct induction of miR-145 via a p53 response element in the promoter of the *miR-145* gene [38]. In addition, p53 suppresses EMT and metastasis through the induction of the *miR-200* family members [33, 39]. Besides the transcriptional regulation of the miRNAs expression, p53 also affects the expression of miRNAs in a transcription-independent manner by modulating the miRNA biogenesis process. P53 has been demonstrated to interact with the Drosha processing complex and promotes the processing of specific primary miRNAs to precursor miRNAs to increase the mature miRNAs level, such as miR-143, miR-16-1 and miR-145 [40].

1.2.2 MicroRNAs and miR-34

MicroRNAs (miRNAs) are small, approximately 22-nucleotide long, regulatory RNA molecules that play a crucial role in the post-transcriptional regulation of messenger RNA (mRNA) targets. They are instrumental in modulating the expression of a majority of mRNAs in humans and other mammals. The biogenesis of canonical miRNAs in humans involves a multi-step process that is highly regulated. Initially, canonical miRNAs are transcribed by RNA Polymerase II to form primary miRNAs (pri-miRNAs). These pri-miRNAs are subsequently processed in the nucleus by Drosha, a specialized RNase III enzyme, to yield precursor miRNAs (pre-miRNAs) that are ~60 nucleotides in length and have a stem-loop structure. Following their nuclear processing, pre-miRNAs are exported to the cytoplasm, where they undergo further cleavage by Dicer, an endonuclease containing two RNase III domains. This cleavage results in a miRNA duplex that is approximately 20 nucleotides in length with a 2-nucleotide 3' overhang on each end and a 5' phosphate group. Subsequently, one strand of the miRNA duplex is

incorporated into an Argonaute protein to form an RNA-induced silencing complex (RISC), whereas the other strand is typically degraded. Once part of the RISC, the miRNA guides the complex to specific sites on the 3' untranslated region (3' UTR) of target mRNAs, resulting in their post-transcriptional repression through mRNA degradation or translational inhibition [41] (**Figure 1.5**).

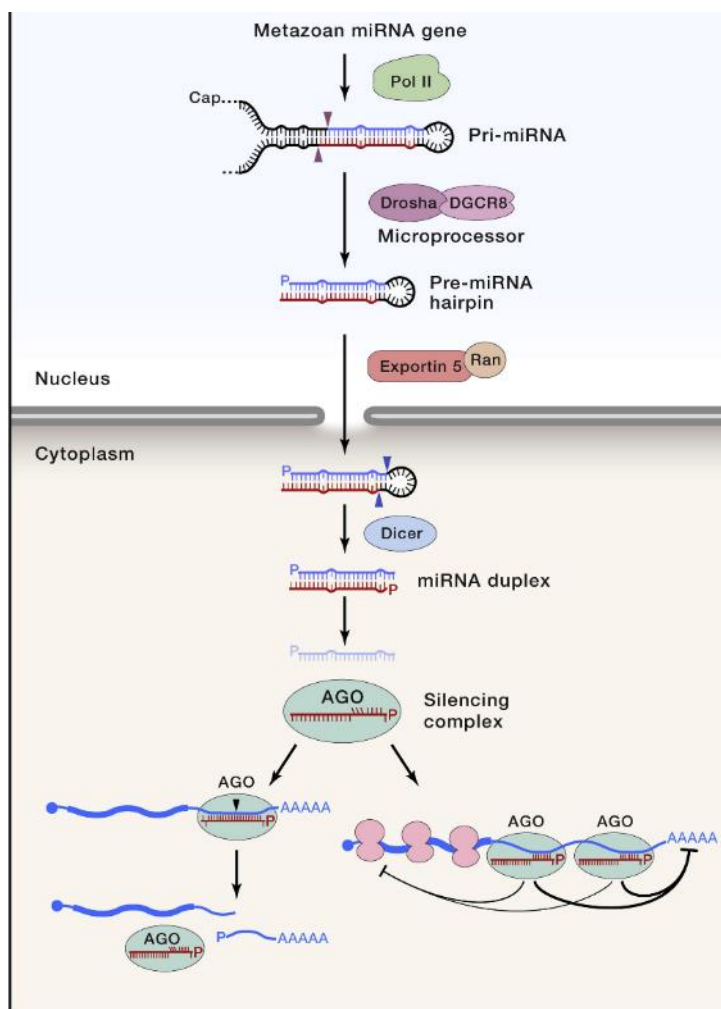


Figure 1.5 The biogenesis and function of a canonical miRNA. (Figure and legend are from Bartel et al., 2018 [41].)

The discovery of the first miRNA, *lin-4*, in *Caenorhabditis elegans* (*C. elegans*) in 1993 marked a seminal moment in the field of molecular biology [42]. Subsequent research revealed that miRNAs are abundant in both vertebrate and inver-

tebrate species, with some miRNAs displaying high levels of evolutionary conservation [43, 44]. The first evidence implicating miRNAs in human cancer came with the observation of frequent downregulation and inactivation of *miR-15* and *miR-16-1* in chronic lymphocytic leukemia (CLL) [45]. These miRNAs were later identified as tumor suppressors, as they were shown to induce apoptosis [46], and their deletion in mouse models recapitulated CLL-associated phenotypes observed in humans [47]. In the ensuing years, an expanding corpus of evidence has demonstrated that miRNA expression is frequently dysregulated in various human cancers. This dysregulation can occur through multiple mechanisms, including aberrant transcriptional control of miRNA genes, genomic deletions or amplifications affecting miRNA coding regions, defects in the miRNA biogenesis machinery, and dysregulated epigenetic changes [48]. Importantly, such dysregulation has been shown to contribute to the hallmarks of cancer, which include evading growth suppressors, sustaining proliferative signaling, activating invasion and metastasis, resisting cell death, and inducing angiogenesis [48].

In 2007, several research groups independently reported that the tumor suppressor protein p53 directly modulates the expression of the miR-34 family of microRNAs, specifically miR-34a, miR-34b, and miR-34c [49-54]. The three miR-34 family members are encoded by two different genes. MiR-34a is encoded by the *MIR34AHG* gene, situated on chromosome 1p36, a region frequently deleted in neuroblastomas. In contrast, miR-34b and miR-34c are co-transcribed from a common primary transcript encoded by the *MIR34BHG* gene located on chromosome 11q23 [55]. The primary transcript for *miR-34a* is generated through the splicing of two exons from the *MIR34AHG* gene, which are separated by approximately 30 kilobases. Conversely, *miR-34b* and *miR-34c* are processed from a single primary transcript, which harbors their coding regions in close proximity

[50]. Both *MIR34AHG* and *MIR34BHG* genes contain multiple p53-responsive elements within their promoter regions. p53 can directly interact with these elements, thereby activating the transcription of both *miR-34* genes [55-57] (**Figure 1.6A**). Intriguingly, homologs of the p53, namely p63 and p73, have also been demonstrated to induce the expression of miR-34a. They achieve this by directly binding to the p53-responsive elements present within the *miR-34a* gene promoter [58, 59].

In addition to being regulated by p53, miR-34a has been shown to participate in positive feedback loops that enhance p53 activity. For instance, Yamakuchi et al. reported that miR-34a increases the level of acetylated p53 and subsequently increases the expression of p53 transcriptional targets, e.g., PUMA and p21, by inhibiting the expression of *SIRT1*, which is an NAD-dependent deacetylase, through a miR-34a-binding site within the 3' UTR of *SIRT1* [60]. Additionally, miR-34a has been demonstrated to activate p53 by targeting *MDM4*, a potent negative regulator of p53. By repressing *MDM4*, miR-34a effectively removes an inhibitory influence on p53, thereby contributing to its activation [61, 62].

These findings illustrate the complexity of the regulatory network involving miR-34a and p53. Not only does p53 regulate miR-34a expression, but miR-34a also feeds back to enhance p53 activity. This intricate interplay forms a robust regulatory loop that amplifies p53-mediated cellular responses, thereby reinforcing its role in tumor suppression.

While p53 is a well-known regulator of *miR-34* genes, there is also evidence of p53-independent mechanisms regulating *miR-34* genes (**Figure 1.6A, B**). For example, *ELK1*, which is a member of the E26 transformation-specific (ETS) family of transcription factors, was shown to directly induce *miR-34a* independently

of p53 during oncogene-induced senescence [63]. Additionally, C/EBP α directly induces miR-34a, which in turn targets E2F3 to inhibit myeloid cell proliferation during the process of granulopoiesis [64]. Remarkably, miR-34a expression is also subject to negative regulation by EMT-transcription factors (EMT-TFs). For example, EMT-TFs, such as ZEB1 and SNAIL, have been shown to bind directly to E-boxes in the promoter regions of *miR-34a* and *miR-34b/c* genes, thereby repressing their expression [65]. Also, STAT3, which is an oncogenic transcription factor, has been reported to directly repress miR-34a expression via a STAT3-binding site located within the first intron of the *miR-34a* gene. This repression occurs during IL-6–induced EMT and invasion in colorectal cancer (CRC) cells harboring p53 mutations. [66]. Interestingly, the expression of *miR-34b/c* is reported to be directly regulated by FOXO3, which is a member of the forkhead family of transcription factors [67, 68]. This highlights the complexity of the regulatory networks governing *miR-34* gene expression, which involve not only p53 but also a variety of other transcription factors that can induce miR-34 expression in a context-dependent manner.

The loss of *miR-34a/b/c* is a recurrent event in a variety of cancer types. For instance, frequent deletion of *miR-34a* gene, which resides on chromosome 1p36, was observed in neuroblastoma as well as in other tumor types [69]. Moreover, epi-genetic silencing of *miR-34a* and *miR-34b/c* by DNA methylation was identified in a variety of primary tumor samples and cancer cell lines from various tissue origins, including colon, bladder, breast, lung, kidney, pancreas cancer and melanoma [70, 71].

Intriguingly, miR-34a and miR-34c possess identical seed-matching sequences, suggesting that they likely target similar mRNA transcripts for post-transcriptional regulation. On the other hand, the seed sequence of miR-34b is similar but not identical to those of miR-34a and miR-34c. This implies that while miR-34b may share some mRNA targets with miR-34a and miR-34c, it could also have unique targets, thereby potentially exerting distinct regulatory effects [72] (**Figure 1.6C**)

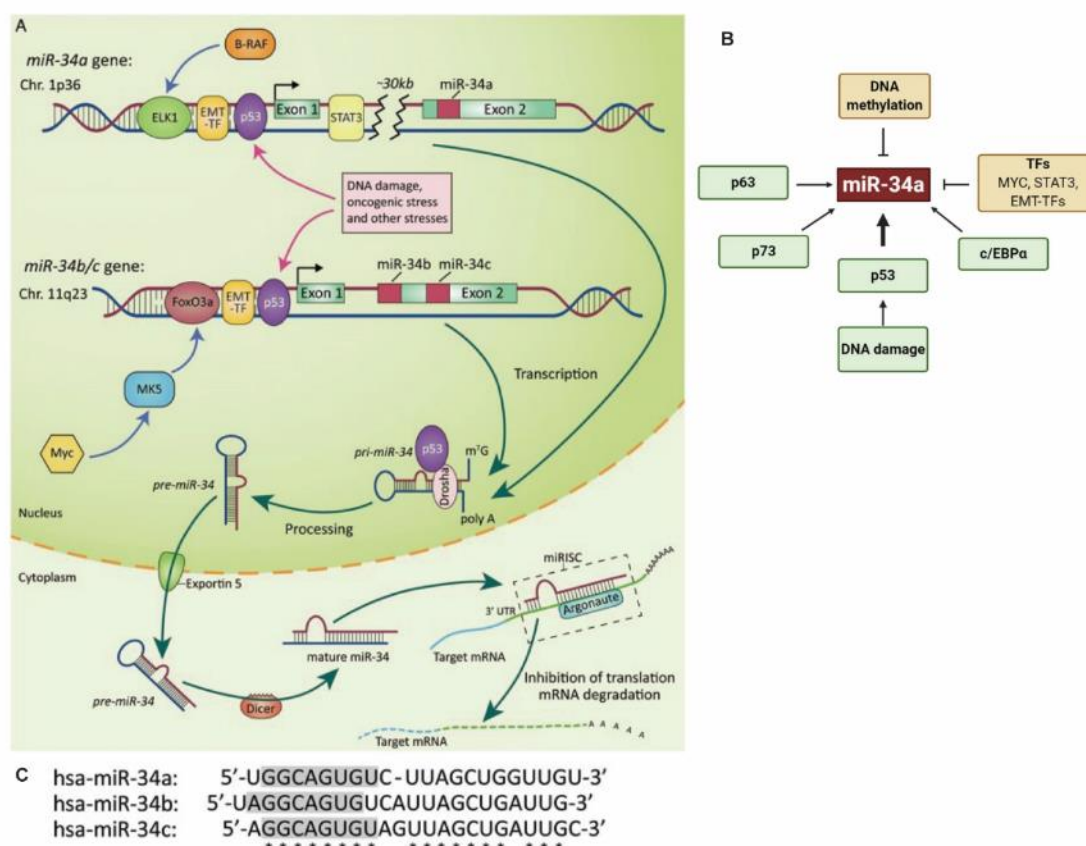


Figure 1.6 (A) Genomic structure of the human *miR-34a* and *miR-34b/c* encoding genes. (B) Factors that regulate *miR-34a* expression. (C) Mature miR-34a, miR-34b, and miR-34c molecule sequences and seed sequences. (Figure and legend are from Rokavec et al., 2014 [57] and Li et al. 2021 [73])

1.2.3 P53/miR-34 axis in CRC

Among the miRNAs that are transcriptionally induced by p53, the miR-34 family (comprising miR-34a, miR-34b, and miR-34c) exhibits the most pronounced induction [55]. These miR-34 genes are direct transcriptional targets of p53 [74], and p53 presumably exerts some of its tumor-suppressive functions through the miR-34 family by downregulating specific target mRNAs [55]. Research has indicated that miR-34a plays a multifaceted role in inhibiting tumor growth and cancer progression. It acts on various processes that are pivotal to cancer development, including EMT, metastasis, cell cycle regulation, stemness, and tumor immunity. Concurrently, miR-34a promotes processes that inhibit carcinogenesis, such as cellular senescence and apoptosis (**Figure 1.7**). The regulatory effects of miR-34 on these processes are mediated through the post-transcriptional repression of their mRNA targets. For example, ectopic expression of *miR-34a/b/c* has been demonstrated to induce cell cycle arrest in diverse cancer cell lines through targeting and repressing key cell cycle regulators like Cyclin E1 (CCNE1), Cyclin D1 (CCND1), cyclin-dependent kinase 4 (CDK4), and cyclin-dependent kinase 6 (CDK6), all of which are critical for the G₁- to S-phase transition of the cell cycle [50, 75, 76]. In addition, a study by Bommer et al. showed that p53-mediated activation of *miR-34* directly represses the expression of B-cell leukemia/lymphoma 2 (*BCL2*), a prominent regulator of apoptosis, thereby leading to induction of apoptosis [53].

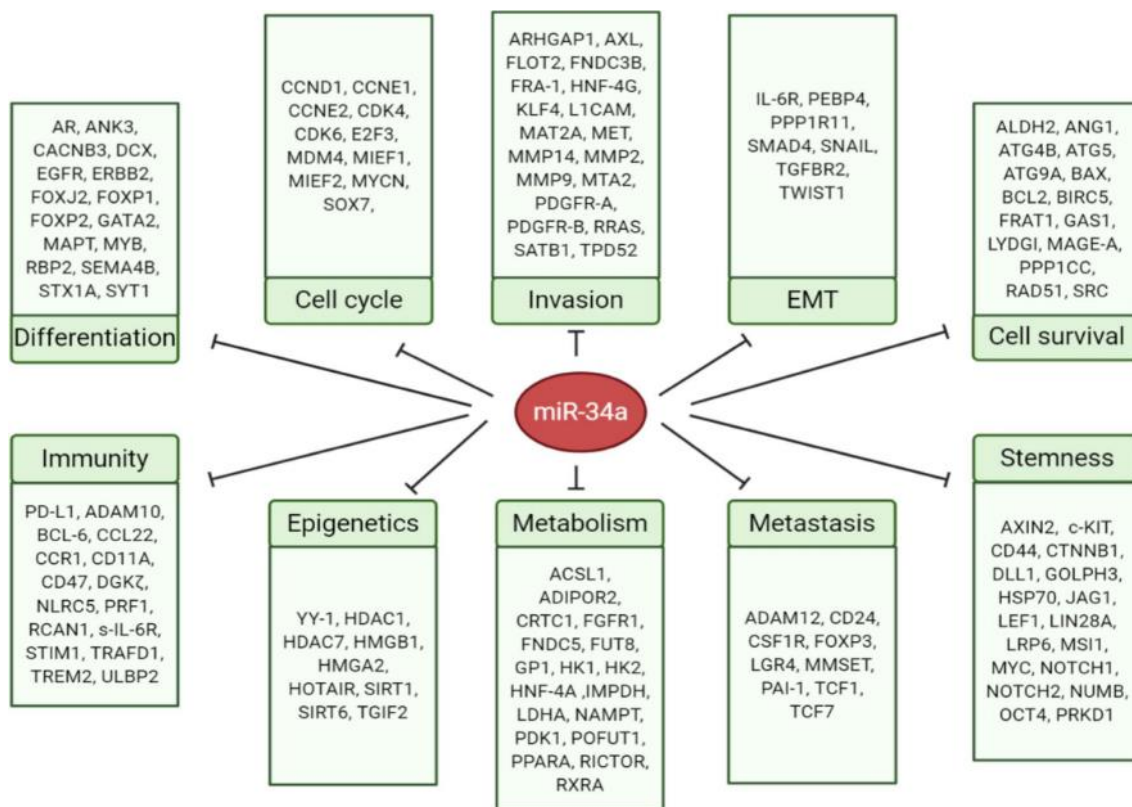


Figure 1.7 MiR-34 regulates a variety of cancer-relevant cellular pathways and processes by repressing key factors. (Figure and legend are modified from Li et al, 2021 [73])

The genes encoding *miR-34a* and *miR-34b/c* are frequently subject to epigenetic silencing through DNA methylation in CRC, underscoring their significance in this malignancy [70, 71]. In addition, concomitant deletion of both *Mir34a* and *Mir34b/c* has been shown to accelerate intestinal tumorigenesis and reduce the survival rates of *Apc*^{Min/+} mice, which carry a mutant *Apc* (adenomatous polyposis coli) allele [77]. Furthermore, the concurrent silencing of *p53* and *Mir34a* has been demonstrated to expedite the development and progression of CRC in azoxymethane (AOM)-treated mice, a model that mimics sporadic CRC [78]. Moreover, miR-34a inhibits EMT-mediated invasion and metastasis of CRC by disrupting an *IL6R/STAT3/miR-34a* feedback loop [66]. Besides, DNA-methylation-mediated inactivation of *miR-34a* is significantly correlated with increased

incidences of lymph node and liver metastasis in CRC patients [79]. Collectively, these findings strongly suggest that miR-34a, miR-34b, and miR-34c serve as tumor suppressors in CRC. Their frequent inactivation, whether through genetic deletion or epigenetic silencing, appears to contribute to the pathogenesis and progression of CRC.

1.3 EMT in cancer metastasis

Despite considerable progress in cancer diagnosis and treatment modalities, metastasis remains the predominant cause of cancer-related mortality, accounting for over 90% of such deaths. Metastasis is a complex, multi-step process in which cancer cells initially migrate from the primary tumor, intravasate into the circulatory system, and eventually colonize distant anatomical sites [80].

Epithelial-mesenchymal transition (EMT) is an evolutionarily conserved biological process initially identified in embryogenesis, and has been implicated in the acquisition of metastatic traits in cancer cells, including enhanced stemness, motility, invasiveness, and resistance to apoptosis [81]. EMT involves a cellular reprogramming event where epithelial cells transition into a mesenchymal phenotype. Given the striking similarities between cellular plasticity in embryogenesis and carcinogenesis, EMT has been posited as a critical mechanism underlying the malignancy of epithelial-derived tumors [82]. Activation of EMT induces a cascade of morphological alterations in cancer cells, which encompass the dissolution of tight junctions, disruption of apical-basal polarity, and reorganization of the cytoskeletal architecture. These changes facilitate the detachment of cancer cells

from the primary tumor, invasion into adjacent tissues, survival during hematogenous or lymphatic dissemination, and ultimately, the establishment of secondary tumors at distant sites [83]. Notably, EMT is predominantly observed at the invasive front of tumors, characterized by reduced cell-cell adhesion, a hallmark of the mesenchymal phenotype, while the central mass of the tumor generally retains its epithelial characteristics [84] (**Figure 1.8**).

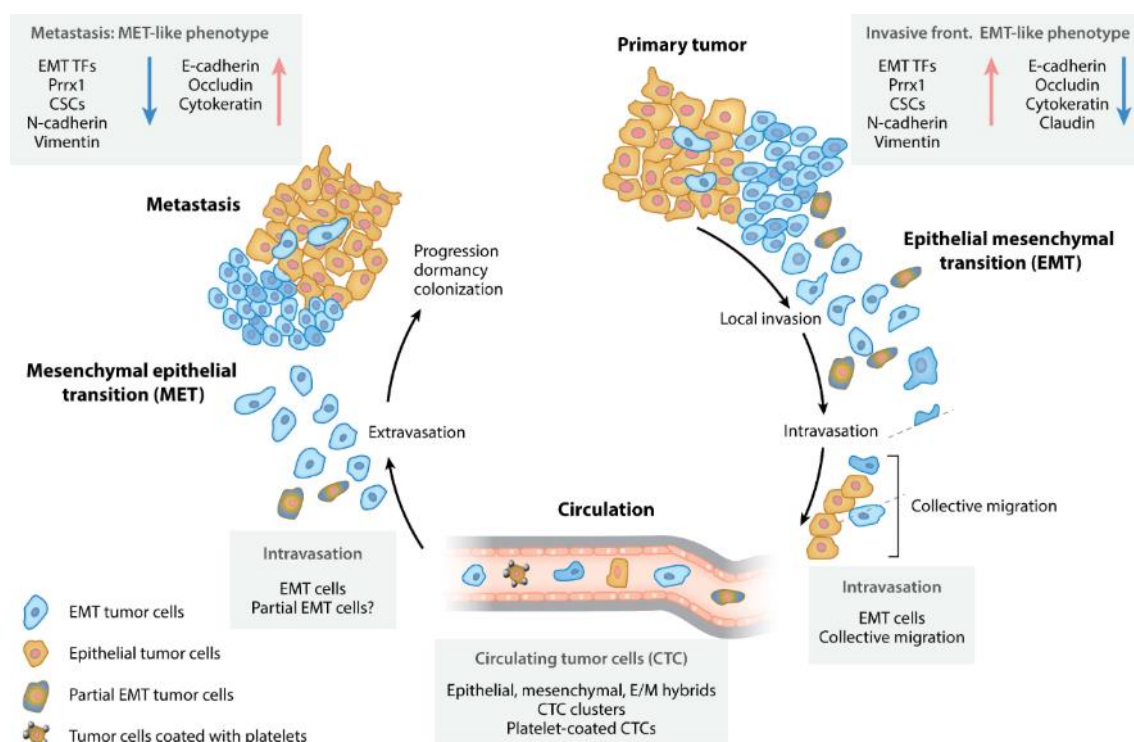


Figure 1.8 Cancer cells within primary tumors that undergo EMT exhibit a reduction in cell-cell adhesion, facilitating local migration and invasion, intravasation, extravasation, and the colonization of metastatic sites. (Figure and legend are from Mittal et al., 2018 [81])

The orchestration of EMT is a complex interplay involving multiple signaling cascades, notably the Wnt/ β -catenin, transforming growth factor (TGF), NF- κ B, hypoxia, and Notch pathways. These signaling networks act in concert to upregulate key EMT-inducing transcription factors (EMT-TFs), including members of the ZEB, Snail, and TWIST families [81, 85]. The Snail family comprises SNAIL

(SNAI1), SLUG (SNAI2) and SMUC (SNAI3). EMT instigated by SNAIL is characterized by the down-regulation of epithelial markers such as E-cadherin (CDH1) and claudins, and the up-regulation of mesenchymal markers like vimentin (VIM) and fibronectin. The attenuation of E-cadherin levels is a hallmark of EMT, contributing to the destabilization of adherens junctions. Concurrently, the suppression of genes encoding claudins leads to the disassembly of apical tight junctions [85]. Importantly, increased expression of SNAIL is correlated with poor clinical outcomes in metastatic cancer. Concurrently, tumors with elevated SNAIL expression are refractory to current therapeutic treatments [86]. TWIST, another EMT-TF, promotes EMT through a distinct mechanism, repressing E-cadherin while upregulating N-cadherin, independently of SNAIL [87]. Similarly, ZEB proteins induce EMT and repress E-cadherin expression through the recruitment of the SWI/SNF chromatin-remodeling complex component BRG1 [88]. In summary, EMT-TFs such as those from the Snail and ZEB families, as well as TWIST, are instrumental in the down-regulation of epithelial gene expression and the concomitant activation of mesenchymal genes. These transcriptional regulators thus play a critical role in the molecular reprogramming that underlies EMT, contributing to the complexity and heterogeneity observed in metastatic cancers [89] (**Figure 1.9**).

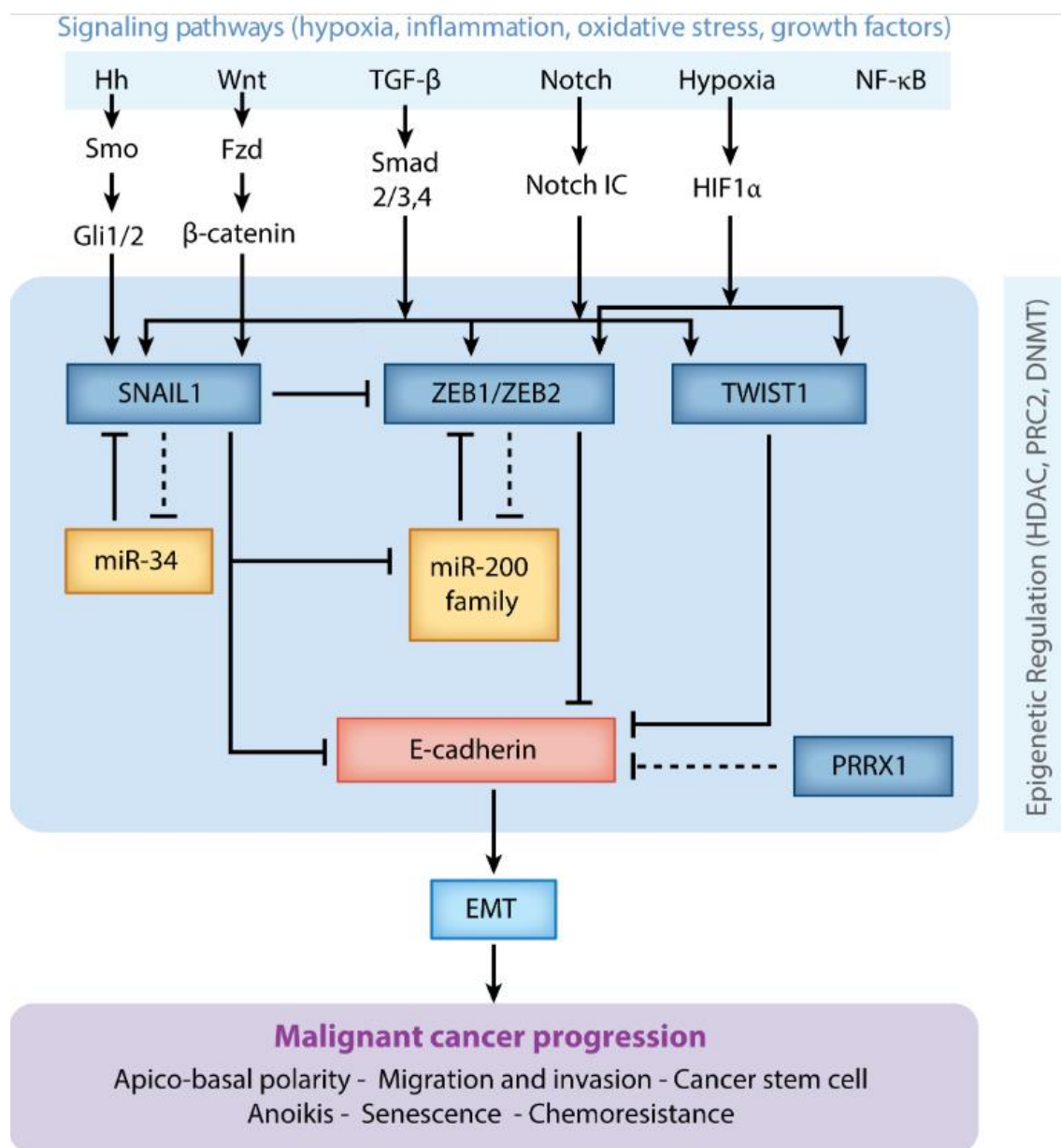


Figure 1.9 EMT is driven by SNAIL, ZEB and TWIST transcription factors which function to suppress the expression of genes associated with the epithelial phenotype and induce the expression of mesenchymal marker genes. (Figure is from Mittal et al, 2018 [81])

The role of p53 in negatively regulating EMT through miRNA-dependent mechanisms adds another layer of complexity to the intricate network of signaling pathways and transcription factors that govern this process. The p53 tumor suppressor has been shown to directly induce miRNAs like miR-200c and miR-34a/b/c, which in turn target EMT-inducing transcription factors (EMT-TFs) such

as ZEB1/2, SNAIL, SLUG, and TWIST [90]. For instance, p53-induced miR-200c specifically targets and inhibits ZEB1, a key EMT-TF. Interestingly, this regulation is reciprocal, as ZEB1 also directly represses the transcription of the gene encoding *miR-200c*. This sets up a double-negative feedback loop that tightly regulates the EMT process [33]. Similarly, p53 activation leads to the induction of *miR-34a/b/c* genes, which target and downregulate the EMT-TF SNAIL. SNAIL, in turn, represses the expression of miR-34a/b/c by binding to E-boxes located within the promoter regions of these miRNA genes. This also establishes a double-negative feedback loop, providing a tightly controlled mechanism for regulating EMT [65]. Feedback loops, such as the miR-34-SNAIL and miR-200-ZEB1 axes, serve as regulatory circuits that maintain a dynamic equilibrium between epithelial and mesenchymal states. They allow for fine-tuned control over EMT, which is crucial for processes like wound healing and tissue regeneration, and their deregulation [33, 65].

1.4 Autophagy in CRC

1.4.1 Autophagy

Autophagy (“self-eating”) encompasses a suite of processes by which cellular constituents, including proteins and organelles, are targeted to lysosomes for degradation. Three distinct forms of autophagy have been delineated, each characterized by a unique mode of cargo delivery to the lysosome: macroautophagy, microautophagy, and chaperone-mediated autophagy [91] (**Figure 1.10**).

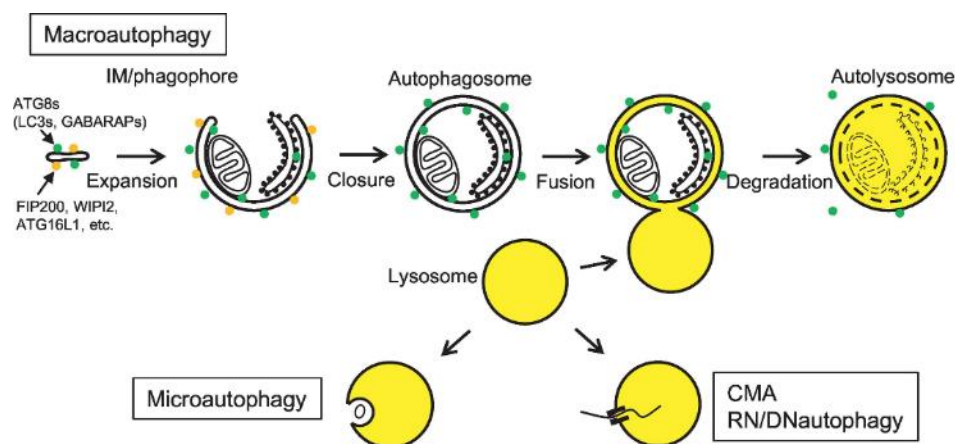


Figure 1.10 Three distinct forms of autophagy are characterized by a unique mode of cargo delivery to the lysosome. (Figure and legend are from Mizushima et al, 2020 [92])

Macroautophagy (herein referred to as autophagy) is the major form of autophagy and a key homeostatic pathway that facilitates the degradation and recycling of cellular materials. In autophagy, a thin membrane structure, referred to as the phagophore or isolation membrane, emerges in proximity to the endoplasmic reticulum (ER), undergoes elongation and bending, and ultimately undergoes membrane fission to form a double-membraned vesicle known as the autophagosome, which sequesters a portion of the cytoplasm. The autophagosome subsequently fuses with a lysosome, and upon fusion of the outer autophagosomal and lysosomal membranes, lysosomal enzymes degrade the inner autophagosomal membrane and its contents [93] (**Figure 1.10**).

Autophagy is a process orchestrated by the coordinated action of multiple protein complexes encoded by evolutionarily conserved autophagy-related genes (ATG), originally identified in yeast [91]. Initiation is induced by the activation of the ULK1 complex, which in turn activates a class III PI3K complex (comprising Beclin 1, ATG14, VPS15, and VPS34). This complex generates phospho-

tidylinositol 3-phosphate (PI3P) on autophagosomal precursor membranes. Subsequently, the ATG5-ATG12 complex conjugates with ATG16 to expand the autophagosome membrane. Subsequently, the members of the GABARAP and LC3 protein families are conjugated to the lipid phosphatidylethanolamine (PE), followed by recruitment to the membrane. In conjunction with ATG7, ATG4B conjugates LC3-I and PE to form LC3-II, a lipid-conjugated form of LC3 that acts as a distinctive marker for autophagosomes. As the fusion between autophagosomes and lysosomes occurs, the contents within the autophagosome undergo degradation. The resultant macromolecular precursors are then either repurposed or utilized in metabolic pathways. Notably, the adaptor protein SQSTM1/p62, which guides specific substrates to autophagosomes, and LC3-II, alongside other cargo proteins, undergo degradation, which serves as an indicative measure of autophagic flux [94] (**Figure 1.11**).

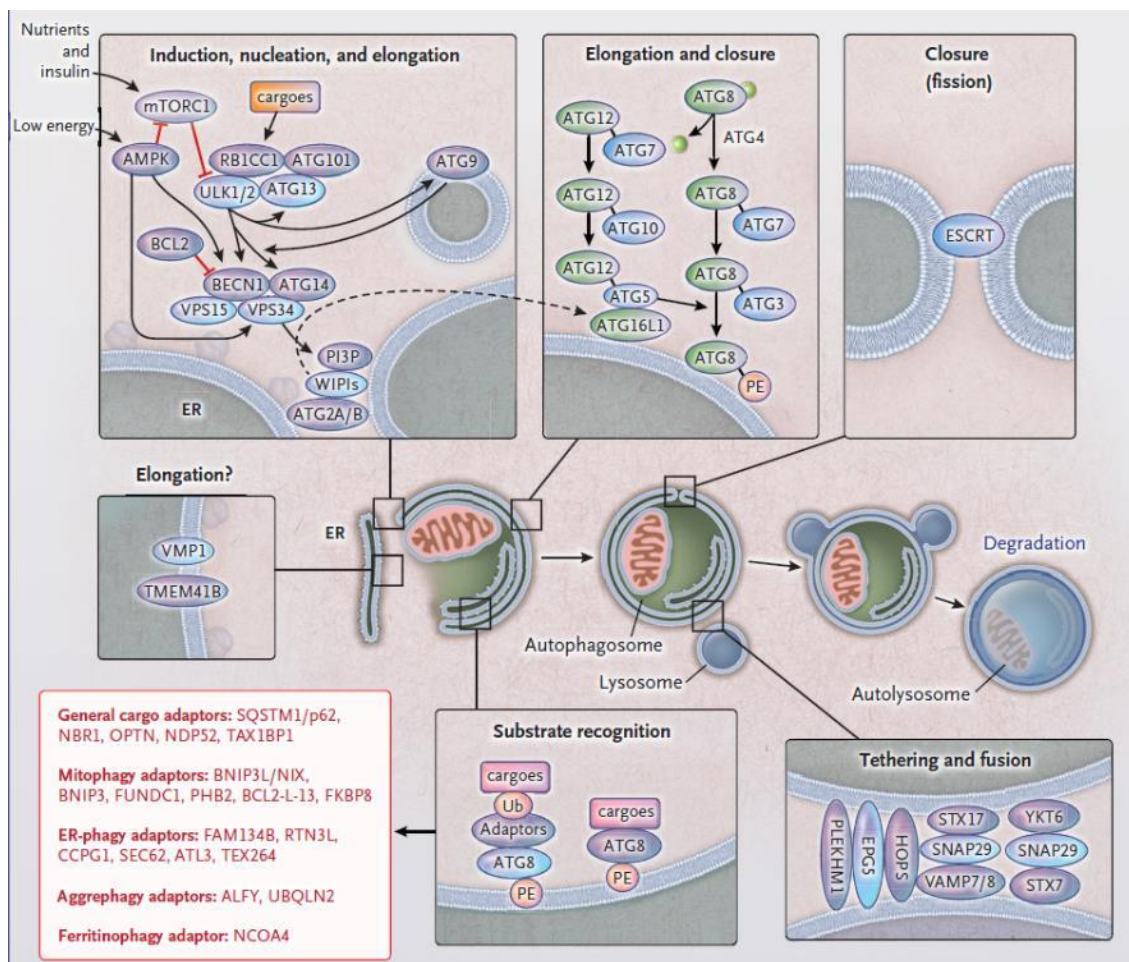


Figure 1.11 In macroautophagy/autophagy, autophagosome formation and degradation are central processes. Autophagy is mediated by the autophagosome, which is formed when a portion of the cytoplasm is sequestered by the isolation membrane. Upon fusion with lysosomes, the material enclosed within the autophagosome is degraded by lysosomal enzymes within autolysosomes. (Figure and legend are from Mizushima et al., 2020 [91])

1.4.2 Autophagy inhibits apoptosis

Apoptosis, often referred to as programmed cell death, plays a critical role in numerous physiological processes, encompassing normal cell turnover, chemical-induced cell death, embryonic development, proper development and functioning of the immune system, and hormone-dependent atrophy [95].

Apoptosis is characterized by an array of morphological and biochemical hallmarks that delineate it as a distinct form of programmed cellular demise. Morphologically, the process manifests through nuclear condensation and fragmentation, coupled with plasma membrane blebbing, culminating in the formation of discrete vesicular structures known as apoptotic bodies. Biochemically, apoptosis is accompanied by a well-defined sequence of molecular events, including the permeabilization of the mitochondrial outer membrane (MOMP), the subsequent activation of effector caspases such as caspase-3, -6, and -7, as well as the initiation of catabolic hydrolases that facilitate the comprehensive degradation of cellular macromolecules. The regulation and execution of this complex cellular disassembly process are mediated by the caspase family of cysteine proteases, which selectively target a multitude of cellular proteins for restricted proteolytic cleavage. This targeted proteolysis serves not merely to dismantle cellular structures, but also to modulate various biochemical pathways, thereby ensuring a highly controlled and regulated process of cell death. Furthermore, apoptosis possesses functional implications beyond the mere elimination of cells; it also prepares the dying cells for efficient phagocytic clearance, thereby minimizing the risk of eliciting an adverse immunological response. This dual role underscores the multifaceted significance of apoptosis in maintaining cellular and tissue homeostasis, as well as in the regulation of immune responses [96].

Autophagy and apoptosis represent two discrete yet interconnected catabolic pathways that govern cellular homeostasis through the regulated degradation of intracellular components and the orchestrated demise of cells, respectively. Termed from the Greek words for 'self-eating', autophagy is primarily responsible for the turnover of cytoplasmic organelles and other cellular constituents. It func-

tions as a homeostatic mechanism to maintain cellular integrity by recycling cellular components under conditions of nutrient deprivation or stress. Conversely, apoptosis, derived from the Greek term meaning 'falling off,' as leaves from a tree, is a form of programmed cell death that serves to eliminate damaged or superfluous cells. This process contributes to tissue development, immune regulation, and the prevention of pathological conditions [97].

A primary mechanism by which autophagy modulates the propensity for cells to undergo apoptosis is through a specialized form of autophagy known as mitophagy, which is dedicated to the selective degradation of mitochondria [98]. Mitochondria serve as a critical 'battleground' where both pro-survival and pro-death signals coalesce to influence the activation of the intrinsic apoptotic pathway, a process notably characterized by mitochondrial outer membrane permeabilization (MOMP). Upon the initiation of cell death, MOMP facilitates the cytoplasmic release of pro-apoptotic proteins, including endonuclease G (EndoG), apoptosis-inducing factor (AIF), and cytochrome c, as well as second mitochondria-derived activator of caspase (SMAC). This precipitates the dissipation of the inner mitochondrial transmembrane potential, leading to a bioenergetic catastrophe that marks a cellular 'point-of-no-return' during intrinsic apoptosis. Mitophagy serves to delay this irreversible commitment to apoptosis by selectively targeting damaged mitochondria for autophagic degradation, thereby attenuating the release of pro-apoptotic factors. Given that compromised mitochondria are particularly susceptible to initiating the apoptotic cascade, their removal via mitophagy effectively elevates the threshold required for the induction of apoptosis. This, in turn, fosters cellular adaptability and enhances the prospects for survival, thereby illustrating the intricate and nuanced interplay between autophagy and apoptosis in the regulation of cellular fate [97] (**Figure 1.12A**).

The initiation of the extrinsic pathway of apoptosis occurs through the binding of trimeric ligands to specific death receptors, notably including the Tumor Necrosis Factor Receptor 1 (TNFR1) and the TNF-Related Apoptosis-Inducing Ligand (TRAIL) receptors. A pivotal event in this signaling cascade is the enzymatic activation of caspase-8 [99]. Recent evidence suggests that the selective autophagic clearance of active caspase-8 within the cytosolic compartment may serve to postpone the initiation of extrinsic apoptosis subsequent to death receptor engagement [100]. Additionally, the execution of caspase-8-mediated apoptosis frequently necessitates the proteolytic cleavage and activation of the BH3-only protein BID. BID acts as a potent inducer of MOMP, which is a critical event in both intrinsic and extrinsic apoptotic pathways. Given mitophagy's role in the selective degradation of compromised mitochondria, and consequently the attenuation of MOMP, it is conceivable that mitophagy may serve to inhibit lethal signaling pathways activated via death receptors [97] (**Figure 1.12B**).

Anoikis, a term derived from the Greek word for 'homelessness,' represents a specialized form of apoptosis that is induced when cells lose their attachment to the appropriate extracellular matrix (ECM), thereby disrupting integrin-mediated signaling pathways. This mechanism serves a critical homeostatic function by efficiently eliminating cells that have become detached from their native ECM substrate. By doing so, anoikis prevents these displaced cells from aberrantly reattaching to new matrices, thereby inhibiting their potential for dysplastic growth [101]. Autophagy has been shown to modulate the activity of the SRC kinase, which becomes hyperactivated in response to the disruption of focal adhesion kinase (FAK) signaling pathways. Specifically, autophagic targeting of SRC serves as a regulatory mechanism that enables cancer cells to evade anoikis (**Figure 1.12C**). This suggests that autophagy can play a role in modulating cell-

matrix interactions, particularly in pathological contexts such as cancer, where the evasion of anoikis can contribute to malignant progression. This adds another dimension to the complex interplay between autophagy and apoptosis, further emphasizing the need for comprehensive investigations to elucidate the multifaceted roles these processes play in cellular homeostasis and disease pathogenesis.

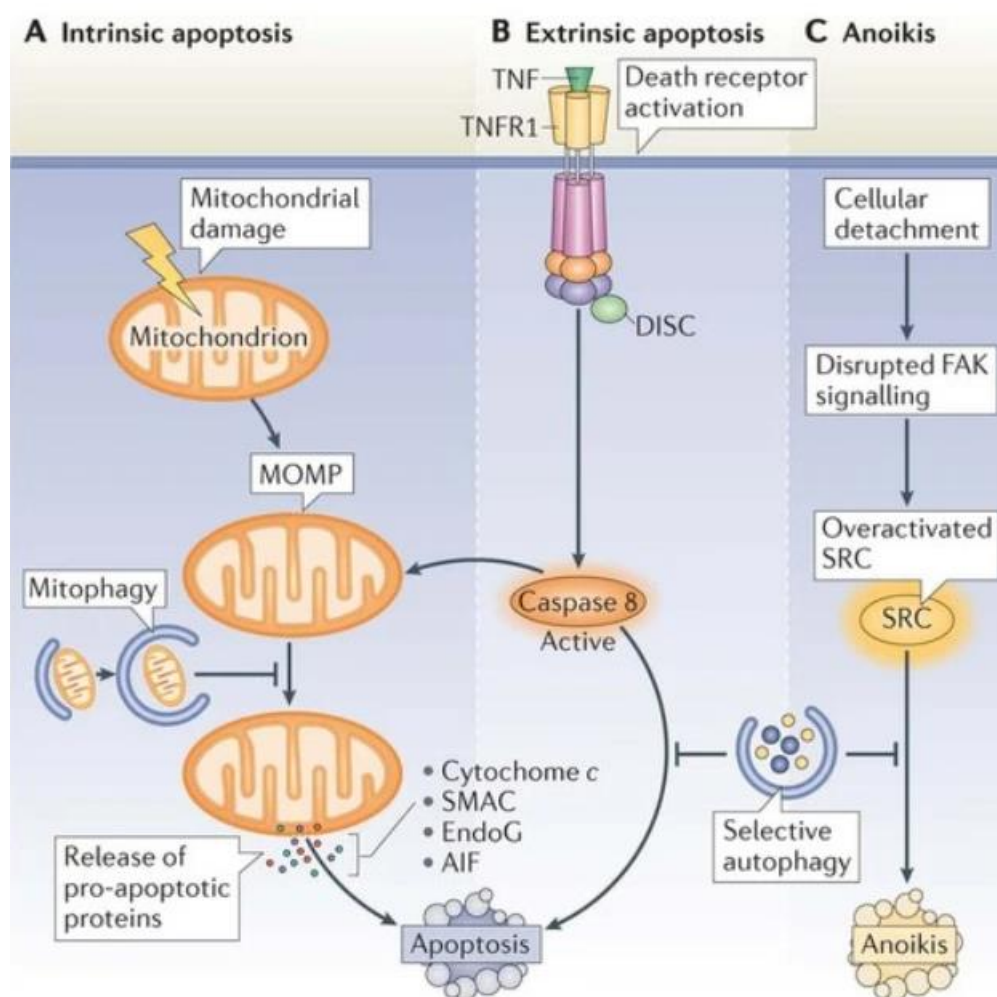


Figure 1.12 (A) Autophagy inhibits intrinsic apoptosis (B) Autophagy inhibits extrinsic apoptosis. (C) Autophagy inhibits anoikis, a specialized form of apoptosis that is triggered when cells lose their anchorage to the extracellular matrix (ECM). (Figure and legend are from Mariño et al., 2012 [97])

1.4.3 Autophagy and therapy resistance in cancer

The primary tenets of cancer therapy revolve around the induction of cell death and the inhibition of cell survival mechanisms, aimed at eradicating malignant cells while sparing normal tissue. However, a significant impediment to the efficacy of cancer treatment is the development of resistance to anticancer drugs.

Autophagy is increasingly recognized as a pivotal regulator in cellular responses to both metabolic and therapeutic stresses. Functioning as a catabolic process, autophagy aims to maintain or restore metabolic homeostasis by facilitating the lysosomal degradation of superfluous or damaged proteins, as well as injured or senescent organelles. This capacity for intracellular recycling and waste management enables cells to adapt to adverse conditions, thereby contributing to cellular survival mechanisms. Importantly, the induction of autophagy has been identified as a significant factor in the development of resistance to therapeutic interventions, particularly in the context of cancer treatment. By mitigating the cytotoxic effects of anti-cancer agents, autophagy allows cancer cells to evade programmed cell death, thereby undermining the efficacy of anticancer therapies [102]. For instance, patients with melanoma tumors have been observed to develop resistance to the BRAF inhibitor Vemurafenib through a mechanism involving endoplasmic reticulum (ER) stress-induced cytoprotective autophagy. This autophagic response serves to mitigate the cytotoxic effects of Vemurafenib, thereby enabling the tumor cells to evade drug-induced apoptosis and continue proliferating. Intriguingly, pharmacological inhibition of autophagy has been shown to reverse this acquired resistance to Vemurafenib, thereby potentiating the drug's cytotoxic effects and inducing greater levels of cell death. Furthermore, combinatorial approaches that simultaneously target both BRAF

and autophagic pathways have demonstrated efficacy in promoting tumor regression in xenograft models that had developed resistance to Vemurafenib [103]. Similarly, high rates of induced autophagy were observed in BRAF mutant central nervous system (CNS) tumor cells. Pharmacologic and genetic inhibition of autophagy re-sensitized BRAF inhibitor-resistant cancer cells and *ex vivo* primary culture to BRAF inhibitor [104]. Thus, in this type of patients, the tumors could be re-sensitized by the treatment with an autophagy inhibitor. Emerging preclinical evidence further substantiates the role of autophagy as a mediator of resistance to targeted therapies, extending beyond melanoma to include various other cancer types. For example, studies have demonstrated that the inhibition of autophagy can effectively overcome resistance to tyrosine kinase inhibitors in a range of malignancies, such as bladder cancer [105], thyroid cancer [106], non-small cell lung cancer (NSCLC) [107] and ALK-positive lung cancer [108]. These findings suggest that autophagy serves as a common adaptive response mechanism that cancer cells exploit to evade the cytotoxic effects of targeted therapies.

Autophagy has also been increasingly implicated as a key factor in mediating resistance to a variety of standard chemotherapeutic agents, further emphasizing its role in the complex landscape of cancer therapy. Specifically, autophagy is often activated as a cytoprotective mechanism that enables cancer cells to acquire a resistant phenotype during the course of chemotherapy. For instance, studies have demonstrated that the induction of autophagy is associated with resistance to the chemotherapeutic agent paclitaxel in ovarian cancer [109]. The role of autophagy in mediating resistance to chemotherapy extends to various types of cancer and therapeutic agents. For example, resistance to the chemotherapeutic drug cisplatin has been attributed to the induction of autophagy in both ovarian [110] and esophageal cancer [111]. In addition, ER stress-induced

autophagy has been implicated in the development of resistance to cyclin-dependent kinase (CDK) inhibitors in chronic lymphocytic leukemia cells [112], as well as resistance to histone deacetylase (HDAC) inhibitors in glioblastoma cell lines [113]. These findings collectively strengthen the emerging paradigm that positions autophagy as a central player in the development of resistance to a diverse array of therapeutic interventions. As the mechanistic link between autophagy and therapy resistance becomes increasingly substantiated, the targeting of autophagy is poised to evolve as a promising avenue in the advancement of cancer therapy [102].

1.4.4 Autophagy and p53

Autophagy, an evolutionarily conserved cellular mechanism, is instrumental in maintaining cellular homeostasis through the degradation and recycling of malfunctioning cytoplasmic organelles and accumulated misfolded proteins. The tumor suppressor, p53, is integral in modulating this process, yet its interaction with autophagy is complex and remains an area of active investigation [114].

Emerging researches have delineated that p53 can function both as an inhibitor and an activator of autophagy, depending on its subcellular localization and mode of action [34]. This duality in p53's function has profound ramifications in oncogenesis and therapeutic interventions. Specifically, when resident in the nucleus, p53 augments autophagy. Under conditions of DNA damage or cellular stresses, nuclear p53 orchestrates the transcriptional upregulation of genes vital for autophagy initiation and maturation. Notably, p53 has been shown to increase the expression of damage-regulated autophagy modulator (DRAM) [115], and AMP-activated protein kinase (AMPK) β 1 and β 2 subunits [116], as well as tuber-

ous sclerosis protein 2 (TSC2) [117]. In contrast, upon its cytoplasmic localization, p53 exhibits an inhibitory effect on autophagy. Specifically, p53 mediates this suppression by attenuating the activity of AMPK and concurrently promoting mTOR activation. This modulation culminates in the hyper-phosphorylation of key molecules such as AMPK, TSC2, and acetyl CoA carboxylase (ACC). Conversely, there is a marked hypo-phosphorylation of the mTOR substrate, p70S6K, further emphasizing the intricate regulatory role of p53 in the autophagic process [34].

Furthermore, autophagy reciprocally modulates p53 concentrations and functionality. Studies have elucidated that impaired autophagy, resultant from the allelic loss of beclin1, a pivotal autophagy regulator, predisposes mammary epithelial cells to metabolic challenges and expedites lumen formation in mammary acini. Such autophagic anomalies also instigate the DNA damage response both *in vitro* and in mammary carcinomas *in vivo*, fostering gene amplification and, in conjunction with compromised apoptosis, propelling mammary tumorigenesis [118]. This underscores autophagy's protective role against DNA damage. Remarkably, diminished autophagy, coupled with an inability to uphold metabolic homeostasis, correlates with escalated DNA damage, gene amplification, and chromosomal aberrations, positing that autophagy curtails tumor progression by curtailing chromosomal instability [119].

In sum, the relationship between autophagy and p53 is complex. While autophagy can attenuate p53, pivotal for tumorigenesis and potentially averting tissue degeneration, p53's modulation of autophagy is context dependent. Deciphering the mechanisms underpinning this interrelation holds significant promise for disease understanding and therapeutic innovations.

1.4.5 Autophagy and miR-34

Emerging evidence has substantiated the role of miR-34 as a negative regulator of autophagy across a range of biological contexts. A study conducted by Yang et al. in 2013 utilized the *Caenorhabditis elegans* model to demonstrate that loss-of-function mutations in mir-34 substantially mitigate age-related physiological decline, extend overall lifespan, and enhance resistance to both thermal and oxidative stress. Notably, deletion of ATG9A reversed the life-extending effects of mir-34 loss, indicating that ATG9A up-regulation is a mediator of these effects of mir-34 inactivation. Therefore, this study established a mechanistic link between repression of ATG9A by miR-34 and the positive effects of enhanced autophagy, marking it as the first publication to identify miR-34 as an autophagy inhibitor [120].

Subsequent to the initial identification of miR-34 as an autophagy repressor, a number of literatures has corroborated this role across diverse biological models by elucidating the mechanism of action of miR-34. Specifically, miR-34 has been shown to inhibit autophagy through targeting multiple autophagy-related genes. For example, Rothe *et al.* revealed that miR-34a inhibits autophagy by targeting *ATG4B* in the context of chronic myeloid leukemia (CML) [121]. Similarly, a study conducted by Wu *et al.* revealed that miR-34c inhibits pirarubicin-induced cytoprotective autophagy, thereby amplifying the susceptibility of cervical cancer cells to pirarubicin treatment. This inhibitory effect was found to be mediated through the downregulation of *ATG4B*, a key autophagy-related gene [122]. Additional studies have shown that miR-34a represses autophagy and potentiates chemotherapy-induced apoptosis by targeting High Mobility Group Box 1 (HMGB1), which is a multifaceted protein with a key role in autophagy, in retinoblastoma cells [123]. Intriguingly, another dimension to the role of miR-34a as

an autophagy repressor has been revealed in the context of acute lung injury. Specifically, miR-34a has been reported to inhibit autophagy in murine alveolar type II epithelial cells by downregulating the expression of the transcription factor FoxO3 [124].

Further complexity in the role of miR-34 in autophagy regulation has been revealed in cardiovascular pathology. Specifically, miR-34a modulates autophagy in human coronary artery endothelial cells under conditions of chronic intermittent hypoxia, an effect mediated through the Bcl-2/Beclin 1 signaling pathway, another pivotal pathway for autophagy [125]. This finding adds another layer of complexity to our understanding of the role of miR-34 in autophagy regulation. It suggests that miR-34a can influence autophagic activity through multiple signaling pathways, depending on the cellular context and specific stressors involved. In this case, the involvement of the Bcl-2/Beclin 1 pathway indicates a potentially critical role for miR-34a in cardiovascular pathologies related to hypoxic conditions. In addition, miR-34c has also been implicated in regulating autophagy in cardiovascular pathology. A study investigated the role of miR-34c in cardiac hypertrophy, a significant precursor to heart failure. Elevated levels of miR-34c were found in heart tissues from mice treated with isoprenaline (ISO), as well as in primary cultures of neonatal rat cardiomyocytes (NRCMs). The study showed that increasing miR-34c levels led to cellular hypertrophy and elevated expression of fetal-type genes in NRCMs. Conversely, inhibiting miR-34c mitigated ISO-induced hypertrophic responses. In mouse models, enforced expression of miR-34c resulted in cardiac dysfunction and hypertrophy, while its inhibition protected against these effects. Mechanistically, miR-34c was found to suppress autophagy

by targeting the ATG4B, contributing to hypertrophy. Inhibition of miR-34c reversed these detrimental effects by restoring ATG4B levels and increasing autophagy [126].

Further expanding the multifaceted role of miR-34a in autophagy regulation, a study by Kim *et al.* showed that the upregulation of miR-34a, induced by the Liver X Receptor alpha (LXR α), which is a nuclear receptor pivotal in lipid metabolism, serves to inhibit autophagy in hepatocytes. This repressive effect is executed through the targeting of key autophagy-related proteins, specifically ATG4B [127].

Further investigation has elucidated that miR-34a acts as a negative modulator of the mitophagy pathway, a specialized form of autophagy focused on the degradation of damaged mitochondria, primarily through the downregulation of PTEN-induced kinase 1 (PINK1) expression levels. In particular, miR-34a impedes the accumulation of phosphorylated Ser65-ubiquitin (pS65-Ub), a critical step for initiating mitophagy. MiR-34a also hampers the recruitment of the E3 ubiquitin ligase Parkin to damaged mitochondria, an essential event for the ubiquitination and subsequent degradation of these organelles. As a result, miR-34a attenuates the ubiquitination process and thereby delays the efficient clearance of damaged mitochondria from the cell [128].

Additionally, the hosting lab of Prof. Hermeking has identified IRE1A and XBP-1 as potential targets of miR-34a, both of which are integral components of the unfolded protein response activated under stress conditions like ER stress and hypoxia. Following exposure to hypoxic conditions and DNA damage, the tumor suppressor p53 suppressed the expression levels of IRE1A and XBP-1 through miR-34a mediation. Conversely, in the absence of p53, an upregulation of IRE1A

and the spliced, active form of XBP-1 (XBP-1(S)) was observed. In p53-deficient colorectal cancer cells, the activation of IRE1A/XBP-1(S) was found to be essential for hypoxia-induced EMT, migration, and chemotherapy resistance. Intriguingly, this chemo-resistance in hypoxic conditions was driven by enhanced autophagy. Ectopic expression of miR-34a inhibited autophagy, thereby sensitizing cells to chemotherapy in hypoxic conditions. Thus, the inactivation of p53 and miR-34a in tumors could lead to IRE1A/XBP-1(S)-mediated autophagy and EMT, thereby promoting chemoresistance and metastasis [129].

1.5 FOXM1

The transcription factor Forkhead Box M1 (FOXM1) belongs to the larger Forkhead Box (FOX) family of transcription factors, distinguished by their characteristic forkhead DNA-binding domains. FOXM1 plays a pivotal role in regulating a broad spectrum of biological processes, thereby serving as a key modulator of cellular physiology [130].

FOXM1 serves a crucial function in embryonic development, and its aberrant expression has been implicated in the initiation and progression of a multitude of cancer types [131]. In a comprehensive pan-cancer analysis encompassing approximately 18,000 cancer cases, FOXM1 expression and its co-expressed gene network were identified as a major predictor of adverse outcomes of cancer patients [132]. This underscores the potential utility of FOXM1 as a prognostic biomarker and possibly as a therapeutic target. Moreover, FOXM1 has been specifically highlighted as a prognostic marker in CRC [133].

FOXM1 represents a key activator for cell cycle progression and cellular proliferation. It is known to upregulate the expression of a multitude of genes that are

integral to DNA replication and the transitions from G₁ to S phase and from G₂ to M phase of the cell cycle [134]. Interestingly, FOXM1 presumably indirectly induces cell cycle-related genes through its interaction with the DP, RB-like, E2F4, and multi-vulval class B (MuvB) core complex [134]. The MuvB core complex interacts with the RB-related proteins p107 or p130, and E2F5 or E2F4 as well as DP to form the Dimerization Partner, RB-like, E2F and Multi-vulval class B (DREAM) complex, which is a transcriptional repressor that represses the expression of a broad array of cell cycle-related genes, thereby leading to cell cycle arrest [135]. FOXM1 can disrupt this repressive action by competing with the DREAM complex for binding to the MuvB core complex. This competition effectively switches the functional orientation of the MuvB-containing complexes from a repressive DREAM configuration to an activating B-MYB-MuvB-FOXM1 configuration. This switch has the effect of promoting the expression of cell cycle-related genes, thereby facilitating cell cycle progression rather than arrest [134] (Figure 1.13).

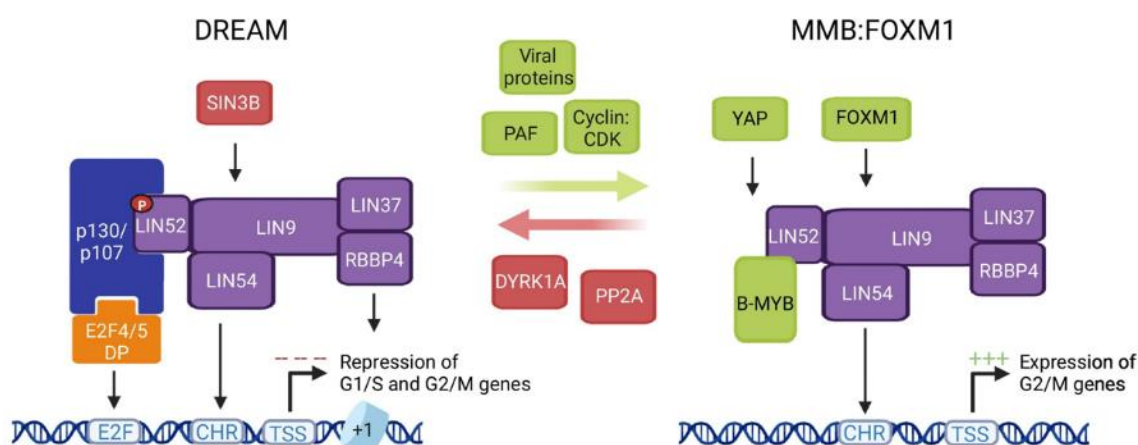


Figure 1.13 The MuvB core complex, which is indicated in purple, serves as a foundational component in the assembly of the DREAM complex. In this configuration, the MuvB core complex associates with p107/p130, E2F4/5, as well as DP to form the DREAM complex, which acts as a transcriptional repressor. The DREAM complex exerts its repressive function in a phase-specific manner: it binds to G₁/S gene promoters through the interaction with E2F promoter sites, and is recruited to G₂/M gene promoters via LIN54 interacting with Cell Cycle

Homology Region (CHR) elements. The repressive activity of the DREAM complex can be disrupted by the competitive binding of B-MYB and FOXM1 to the MuvB core complex. This competition effectively shifts the functional orientation of the MuvB-based complex from a repressive DREAM configuration to an activating B-MYB-MuvB-FOXM1 configuration. In this activated state, the complex promotes the expression of cell cycle-related genes. (Figure and legend are from Fischer et al., 2022 [134])

In addition to its well-established role in cell cycle regulation and cellular proliferation, FOXM1 has also been identified as a key inducer of autophagy, further expanding its functional repertoire. For example, FOXM1 has been shown to induce autophagy by transcriptionally upregulating key autophagy-related genes, such as *LC3* and *Beclin-1*, in triple-negative breast cancer cells [136]. Also, FOXM1 has been implicated in the activation of AMP-activated protein kinase (AMPK)/mammalian target of rapamycin (mTOR)-mediated autophagy, a pathway that is particularly relevant in the context of drug resistance. Specifically, the activation of this autophagic pathway by FOXM1 has been demonstrated to contribute to resistance against docetaxel in castration-resistant prostate cancer [137].

These findings highlight the multifaceted role of FOXM1 in both cell cycle regulation and autophagy, two critical cellular processes with significant implications for cancer biology. The ability of FOXM1 to induce autophagy suggests a complex interplay between cell cycle progression, autophagy, and therapy resistance. This complexity underscores the potential of FOXM1 as a therapeutic target, particularly in types of cancers in which autophagy serves as a mechanism of drug resistance.

Interestingly, FOXM1 exhibits a remarkable functional versatility, regulating a diverse array of biological processes via distinct mechanisms. For instance, in

the context of cell cycle regulation, FOXM1 indirectly modulates the expression of genes such as Cyclin B1 (*CCNB1*) by interacting with the MuvB complex, which in turn binds to the CHR elements (TTTGAA) in the promoters of these genes [138]. Conversely, when regulating genes implicated in other biological processes (e.g., *MAT1A* [139] and *NURR1* [140]), FOXM1 directly binds to the consensus Forkhead (FKH) motif (RYAAAYA) located within their promoter regions. This dual mode of action underscores the multifaceted role of FOXM1 in cellular physiology, allowing it to serve as a key regulatory node in various cellular pathways. The ability of FOXM1 to modulate gene expression both directly and indirectly adds an additional layer of complexity to its regulatory functions, making it a particularly intriguing target for further research.

In addition, *FOXM1* has been characterized as a target of miR-34a, adding another layer of regulatory complexity to its diverse functions. For example, miR-34a has been shown to induce cellular senescence in hepatocellular carcinoma by modulating telomerase activity through the targeting of the FOXM1/c-Myc signaling pathway [141]. Additionally, miR-34a has been involved in the regulation of triple-negative breast cancer growth and invasion by repressing the FOXM1/eukaryotic elongation factor 2 kinase (eEF2-kinase) axis [142]. The ability of miR-34a to modulate multiple pathways involving FOXM1 underscores the intricate regulatory networks that govern cellular processes like cell cycle progression, autophagy, senescence, and cancer invasion. Understanding these complex interactions could provide valuable insights for the development of targeted therapeutic strategies aimed at modulating FOXM1 activity and its downstream effects.

2. Aims of the study

The present study had the following aims:

(1) Characterization of the effects of the inactivation of *miR-34a* and *miR-34b/c* alone or in combination in the CRC cell line HCT116.

(2) Identification of mediators of *miR-34a/b/c* function relevant for the regulation of chemo-resistance and autophagy induction.

3. Material

3.1 Chemicals and reagents

Application	Chemical compound	Supplier
Cell culture	Fetal bovine serum	Life Technologies
	Penicillin-Streptomycin (10,000 U/mL)	Life Technologies
	McCoy's 5A (Modified) Medium	Life Technologies
	HBSS, no calcium, no magnesium, no phenol red	Life Technologies
	Earle's Balanced Salt Solution (EBSS)	Life Technologies
	5-Fluorouracil (5-FU)	Sigma-Aldrich
	SN-38	Sigma-Aldrich
	Dimethyl sulphoxide (DMSO)	Carl Roth
	Chloroquine	Sigma-Aldrich
	puromycin dihydrochloride	Sigma-Aldrich
	Fast SYBR Green Master Mix	Applied Biosystems
WB	APS	Carl Roth
	TEMED	Carl Roth
	β -mercaptoethanol	Sigma-Aldrich
	complete mini protease inhibitor cocktail	Roche
	PageRuler™ Plus Prestained Protein Ladder, 10 to 250 kDa	Thermo Fisher Scientific
	Immobilon-P PVDF Membrane (0.45 μ m)	Merck Millipore
	skim milk powder	Sigma-Aldrich
	Methanol	Carl Roth

	ECL/HRP substrate	Merck Millipore
	Rotiphorese gel 30 (37,5:1)	Carl Roth
Luciferase reporter assays	ampicillin	Sigma-Aldrich
	LB-Agar (Lennox)	Carl Roth
	LB-Medium (Luria/Miller)	Carl Roth
	Hi-Di™ Formamide	Applied Biosystems
	HiPerFect Transfection Reagent	Qiagen
	Opti-MEM® Reduced Serum Medium	Life Technologies
	ethidium bromide	Carl Roth
	Ruler 1kb DNA ladder	Life Technologies
Wound healing	Mitomycin C	Sigma-Aldrich
Modified Boyden-chamber assay	Crystal violet	Carl Roth
	Matrigel matrix	Corning
ChIP	37% formaldehyde	Merck Millipore
	Phosphate buffered saline (PBS)	Carl Roth
Generation of CRISPR plasmids	ampicillin	Sigma-Aldrich
	LB-Agar	Carl Roth
	LB-Medium	Carl Roth

Hi-Di™ Formamide	Applied Biosystems
ethidium bromide	Carl Roth
Lipofectamine® LTX Reagent	Invitrogen
Opti-MEM® Reduced Serum Medium	Life Technologies

3.2 Buffers and solutions

1. 2x Laemmli Buffer:
 - Tris-HCl: 125 mM, pH 6.8
 - 4% Sodium Dodecyl Sulfate (SDS)
 - 20% Glycerol
 - 0.05% Bromophenol Blue (dissolved in H₂O)
 - 10% β-Mercaptoethanol (added immediately prior to utilization)
2. Vogelstein PCR Buffer (10x):
 - Ammonium Sulfate (NH₄SO₄): 166 mM
 - Tris: 670 mM, pH 8.8
 - Magnesium Chloride (MgCl₂): 67 mM
 - β-Mercaptoethanol: 100 mM
3. RIPA Buffer:
 - 1% Nonidet P-40 (NP40)
 - 0.5% Sodium Deoxycholate
 - 0.1% SDS
 - Sodium Chloride (NaCl): 250 mM
 - Tris-HCl: 50 mM, pH 8.0
4. Towbin Buffer:
 - Glycine: 200 mM
 - Methanol: 20%
 - Tris Base: 25 mM, pH 8.6
5. 10x TBS-T (5 Liters):
 - Tris: 500 mL of 1M, pH 8.0
 - Sodium Chloride (NaCl): 438.3 g
 - Tween 20: 50 mL
 - Diluted to 5L with deionized water (ddH₂O)
6. 10x PBS (1L):
 - NaCl: 80 g
 - Potassium Chloride (KCl): 1 g
 - Disodium Hydrogen Phosphate Dihydrate (Na₂HPO₄•2H₂O): 14.42 g
 - Potassium Dihydrogen Phosphate (KH₂PO₄): 2 g
 - Diluted to 1L with deionized water (ddH₂O)

7. SDS Buffer:

- Tris: 50 mM, pH 8.1
- NaCl: 100 mM
- SDS: 0.5%
- Ethylenediaminetetraacetic Acid (EDTA): 5 mM

3.3 Kits

Application	Kit	Supplier
qPCR	High Pure RNA Isolation Kit	Roche
	Verso cDNA Kit	Thermo Fisher Scientific
	Pierce™ BCA Protein Assay Kit	Thermo Fisher Scientific
	miRNeasy Mini Kit	QIAGEN
	miRURY LNA Universal RT kit	QIAGEN
	miRURY LNA Universal RT mi-croRNA PCR kit	QIAGEN
Generation of vectors	Monarch® DNA Gel Extraction Kit	New England Biolabs
	Monarch® PCR & DNA Cleanup Kit	New England Biolabs
	DyeEx® 2.0 Spin Kit	QIAGEN
	QIAprep Spin Miniprep Kit	QIAGEN
	BigDye® Terminator v1.1 Cycle Sequencing Kit	Life Technologies
	QuikChange II XL Site-Directed Mutagenesis Kit	Agilent Technologies
Luciferase reporter assays	Dual-Luciferase® Reporter Assay System	Promega
WB	BCA Protein Assay Kit	Thermo Fisher Scientific
qChIP	iDeal ChIP-qPCR kit	Diagenode

Cell viability	Cell Counting Kit-8 (CCK-8)	Dojindo EU GmbH
Apoptosis detection	FITC Annexin V Apoptosis Detection Kit I	BD Pharmingen™

3.4 siRNAs

FlexiTube GeneSolution (GS2305), a pool of four distinct siRNAs designed to target FOXM1, along with their corresponding control siRNAs were obtained from Qiagen (Hilden, Germany). For ATG9A knockdown, two specific siRNAs (#s35506 and #s35505) and their negative controls were acquired from ThermoFisher Scientific (Waltham, MA, USA).

3.5 Enzymes

Application	Enzyme	Supplier
cell culture	Trypsin-EDTA	Invitrogen
qPCR	DNase I	Sigma-Aldrich
vectors generation	T4 DNA ligase	Thermo Fisher Scientific
vectors generation	Platinum® Taq DNA polymerase	Invitrogen
vectors generation	restriction endonucleases	New England Biolabs

3.6 Oligonucleotides

3.6.1 Sequence information for guide RNAs used for *miR-34a/b/c* deletion

	Sequence information (5'-3')
miR-34a guide RNA 1 forward	CACCGGCCGGTCCACGGCATCCGGA
miR-34a guide RNA 1 reverse	AAACTCCGGATGCCGTGGACCGGCC
miR-34a guide RNA 2 forward	CACCGCTAGAAGTGCTGCACGTTGT
miR-34a guide RNA 2 reverse	AAACACAACGTGCAGCACTTCTAGC
miR-34b/c guide RNA 1 forward	CACCGCCTCGGACCCCATTTACCG
miR-34b/c guide RNA 1 reverse	AAACCGGTGAAATGGGGTCCGAGGC
miR-34b/c guide RNA 2 forward	CACCGGTGCATCATCAATGTGCGTG
miR-34b/c guide RNA 2 reverse	AAACCACGCACATTGATGATGCACC

3.6.2 Sequence information for genotyping primers used for selecting *miR-34a/b/c* homozygous deletion

	Sequence information (5'-3')
<i>miR-34a</i> genotyping primer forward	GTTTTGAACTTCTCGCCTCA
<i>miR-34a</i> genotyping primer reverse 1	CACAACAACCAGCTAAGACACT
<i>miR-34a</i> genotyping primer reverse 2	TACTATTCTCCCTACGTGCAA
<i>miR-34b/c</i> genotyping primer forward	GAACTGAAGCCTGGCGTGAAG
<i>miR-34b/c</i> genotyping primer reverse 1	TTTTGCTTTCCTGGCATGAGAC
<i>miR-34b/c</i> genotyping primer reverse 2	ATGGCAGGAACAACCTTAACCAC

3.6.3 Oligonucleotides used for qPCR

mRNA	Forward (5'-3')	Reverse (5'-3')
<i>CCNB1</i>	GACCTGTGTCAGGCTTTCTCTG	GGTATTTTGGTCTGACTGCTTGC
<i>FOXM1</i>	TCTGCCAATGGCAAGGTCTCCT	CTGGATTCGGTCGTTTCTGCTG
<i>ATG5</i>	GCAGATGGACAGTTGCACACAC	GAGGTGTTTCCAACATTGGCTCA
<i>ULK2</i>	TCCACGGAGTTCTGACTGGTTC	GACGAGTAACCAAGGCTAACAGG
<i>pri-miR-34a</i>	CGTCACCTCTTAGGCTTGA	CATTGGTGTCGTTGTGCTCT
<i>pri-miR-34b/c</i>	GAGCTGCCTGTGCATCATC	GGATGAAATCAGCATTTTCCA
<i>SQSTM1/p62</i>	CCCTACAGATGCCAGAATCCG	GCCTTCATCAGAGAAGCCCAT
<i>ATG13</i>	AGATGACATTCTTCCGATGGAC	TCCACAAAGGCATCAAACCTCG
<i>E-cadherin</i>	CCCGGGACAACGTTTATTAC	GCTGGCTCAAGTCAAAGTCC
<i>VIM</i>	TACAGGAAGCTGCTGGAAGG	ACCAGAGGGAGTGAATCCAG
<i>SNAIL</i>	GCACATCCGAAGCCACAC	GGAGAAGGTCCGAGCACAC
<i>XBP1</i>	GCTGAGTCCGCAGCAGGTG	GCTGGCAGGCTCTGGGGAAG
<i>IRE1A</i>	CGGGAGAACATCACTGTCCC	CCCGGTAGTGGTGCTTCTTA
<i>ATG4B</i>	ATGACTTCAATGATTGGTGCC	AGAAGAATCTGGACTTGGCAG
<i>ATG9A</i>	TCCTCTTTGTGGTTGCCTTC	AGTGACCTTGACGGGTTTCAG
<i>ULK1</i>	TCATCTTCAGCCACGCTGT	CACGGTGCTGGAACATCTC

3.6.4 Oligonucleotides used for qChIP

Gene	Forward (5'-3')	Reverse (5'-3')
<i>CCNB1</i>	CGCGATCGCCCTGGAAACGCA	CCCAGCAGAAACCAACAGCCGT
<i>ATG9A</i>	GTAACGGAGGAAGGGGCG	GCAGCTCCCAACAGCGGACAACC

<i>16q22</i>	CTACTCAC- TTATCCATCCAGGCTAC	ATTTCACACACTCAGACATCACAG
<i>SQSTM1/p62</i>	CTCAGGGGACTCACGGTGA	GTGAGTCAGCGTCCCATGAC

3.7 Oligonucleotides used for reporter plasmids

Oligo	Forward (5'-3')	Reverse (5'-3')
<i>FOXM1</i> 3'-UTR	AAAGAATTCAGCCCTGCCCTT- GCCCCTGTGC	AAAAC TAGTGCATGTCCAC- CTTCGCTTTTATTGAG
miR-34a/b/c-5p	CTTAGATCATTATCCAGAG-	CATCCTACCCACCTTCCTCTG-
Δ SMS	GAAGGTGGGTAGGATG	GATAATGATCTAAG

3.8 List of antibodies

epitope	Species	Catalog No.	Company	Use	Dilution	Source
Primary						
antibodies						
β -actin	Human	# A2066	Sigma-Aldrich	WB	1:1000	rabbit
FOXM1	Human	# 20459	Cell Signaling	WB	1:1000	rabbit
ATG9A	Human	# 13509	Cell Signaling	WB	1:1000	rabbit
PARP	Human	# 9542	Cell Signaling	WB	1:1000	rabbit
LC3B	Human	# 2775	Cell Signaling	WB	1:1000	rabbit
SQSTM1/p62	Human	# 88588	Cell Signaling	WB	1:1000	mouse
SNAIL	Human	# 3879	Cell Signaling	WB	1:1000	rabbit
E-cadherin	Human	# 33-4000	Invitrogen	WB	1:1000	mouse
P53	Human	# sc-126	Santa Cruz	WB	1:1000	mouse
Secondary						
antibodies						
Anti-mouse HRP	N.A.	# W4021	Promega	WB	1:10,000	goat
Anti-rabbit HRP	N.A.	# A0545	Sigma-Aldrich	WB	1:10,000	goat

4. Methods

4.1 Cell culture and treatments

CRC cell lines HCT116, HCT15, and SW480 were cultured under standardized conditions in McCoy's 5A medium, supplemented with 1% penicillin/streptomycin and 10% fetal bovine serum (FBS). The cells were incubated at 37°C with 5% CO₂. MiR-34a/b/c-5p mimics and their corresponding negative controls were sourced from Qiagen. For ectopic expression of FLAG-tagged human FOXM1c, we utilized the pCW57.1-FOXM1c plasmid (a gift from Adam Karpf; #68810, obtained from Addgene), which is inducible by doxycycline [143]. Conditional expression of *pri-miR-34a* from pRTR vectors was achieved using doxycycline at a final concentration of 100 ng/ml. Cells harboring pRTR vectors were maintained in a medium containing 4 µg/ml puromycin.

4.2 CRISPR/Cas9-mediated deletion of *miR-34*

Two single-guide RNAs (sgRNAs) were designed to target the flanking regions of the pre-miRNA encoding locus (**Section 3.6.1**), utilizing the Clustered Regularly Interspaced Palindromic Repeats (CRISPR) design tool available at benchling.com. These sgRNAs were cloned into the *BbsI* sites of pSpCas9(BB)-2A-GFP [144] via two complementary DNA oligonucleotides to generate sgRNA expression plasmids, following established protocols [145]. HCT116 cells were transfected with 2.5 µg of each constructed sgRNA-pSpCas9(BB)-2A-GFP plasmid. As a control, cells were also transfected with an "empty" pSpCas9(BB)-2A-GFP vector that did not contain any sgRNA. After transfection for 48 hours, GFP-positive cells were isolated utilizing a FACSARIA cell sorter (BD Biosystems) and

seeded into 96-well plates to expand as single-cell clones over a two-week period. Control cells transfected with the "empty" pSpCas9(BB)-2A-GFP vector were similarly processed to generate wild-type single-cell clones. Genomic DNA from these clones was then subjected to genotyping PCR to screen for successful deletions in the pre-miRNA encoding regions, employing two pairs of genotyping screening primers as detailed in **Section 3.6.2**. Clones confirmed to have deletions in both alleles of the pre-miRNA encoding regions were further validated by qPCR to ascertain the absence of mature miRNA expression.

4.3 RNA isolation and real-time polymerase chain reaction (qPCR) analysis

Total RNA was isolated from cultured cells utilizing the High Pure RNA Isolation Kit from Roche, following the manufacturer's guidelines. Subsequently, cDNA was synthesized from 1 µg of the isolated total RNA using the Verso cDNA Synthesis Kit from Thermo Scientific. For the quantification of mRNA levels, qPCR was conducted employing the Fast SYBR Green Master Mix from Applied Biosystems and analyzed on a LightCycler 480 instrument from Roche. For the specific isolation of mature miRNAs, the miRNeasy Mini Kit from QIAGEN was employed. The sequence information for the primers used in these qPCR analyses is detailed in **Section 3.6.3** of the Materials.

4.4 Chromatin immunoprecipitation

Chromatin Immunoprecipitation (ChIP) assays were conducted in HCT116 cells, adhering to the protocol outlined in the iDeal ChIP-qPCR kit supplied by Diagenode, Belgium. The primers utilized for the quantitative ChIP (qChIP) assays are detailed in **Section 3.6.4** of the Materials. As a negative control for the

qChIP experiments, we selected the 16q22 genomic region, which lack enriched FOXM1 signal (**Figure 5.31D**), as evidenced by publicly available FOXM1 ChIP-seq data sourced from the Cistrome Data Browser [146].

4.5 Modified Boyden-chamber assay

We employed modified Boyden-chamber assays to assess cellular migration and invasion, as previously described [66]. Briefly, 1×10^5 cells suspended in serum-free medium were seeded in the upper chamber (characterized by 8.0 μM pore size membrane; Corning). The lower chamber was filled with medium containing 10% FBS to serve as a chemoattractant. For the migration assay, cells were incubated for 24 hours. For the invasion assay, the chamber membrane was pre-coated with 100 μl of Matrigel matrix (Corning) at a concentration of 300 $\mu\text{g/ml}$ in serum-free medium. Following seeding, cells were cultured for an additional 48 hours. After incubation, non-motile cells on the upper side of the membrane were carefully removed. The cells in the bottom chamber were fixed using ice-cold methanol for 20 minutes at room temperature and subsequently stained with a 0.5% crystal violet solution for 30 minutes. The fold change of migrated cells was quantified by normalizing the results to corresponding control groups.

4.6 Wound healing assay

A wound-healing assay was conducted to evaluate cell migration using Culture-inserts (IBIDI, 80241, Martinsried, Germany). Cells were seeded into these inserts and cultured until a confluent monolayer was established. Prior to the removal of the Culture-inserts, which creates a cell-free gap mimicking a wound, cells were treated with 10 $\mu\text{g/mL}$ of mitomycin C (M4287; Sigma-Aldrich, Germany) for 2 hours to inhibit cell proliferation. Following the removal of the Culture-

inserts, cells were washed twice with Hank's Balanced Salt Solution (HBSS) to remove residual mitomycin C and any detached cells. The medium was then re-filled. The cell-free gap was immediately imaged using a phase-contrast microscope, and additional images were captured after a 36-hour period.

4.7 3'-UTR dual reporter assay

The full length 3'-UTR of the human *FOXM1* gene was PCR-amplified from cDNA derived from HCT116 cells and subsequently cloned into the pGL3-control-MCS vector [69]. To investigate the interaction between miR-34a/b/c and *FOXM1*, the seed-matching sequence (SMS) for miR-34a/b/c in the *FOXM1* 3'-UTR was deleted using the QuikChange II XL Site-Directed Mutagenesis Kit (Stratagene, San Diego, CA, USA). All constructs were validated through Sanger sequencing. The oligonucleotides used for cloning and mutagenesis were listed in **Section 3.7**. For luciferase reporter assays, HCT116 *miR-34a/b/c-KO* cells were seeded in 12-well plates at a density of 3×10^4 cells per well and cultured for 24 hours prior to transfection. These cells were then transfected with 100 ng of the indicated reporter vectors, 10 nM of indicated miRNA mimics, as well as 20 ng of a Renilla luciferase plasmid for normalization. Transfections were performed using HiPerFect Transfection Reagent (Qiagen). After 48 hours of incubation with the indicated treatments, luciferase activity was quantified using a Dual Luciferase Reporter Assay Kit (Promega) in accordance with the manufacturer's guidelines. Measurements were taken using an Orion II Microplate Lumiometer (Berthold, Germany) equipped with integrated Simplicity software.

4.8 Western blot analysis

Cell lysates were prepared using RIPA lysis buffer, supplemented with PhosSTOP Phosphatase Inhibitor Cocktail Tablets and complete mini protease inhibitors (Roche, Basel, Switzerland). The lysates were sonicated and subsequently centrifuged at 13,000 rpm for 20 minutes at 4°C to remove cellular debris. Protein concentrations in the lysates were determined using a BCA Protein Assay Kit (Thermo Fisher Scientific) as per the manufacturer's guidelines. For Western blot analysis, 30 µg of protein per lane was separated by 12% SDS-PAGE gels and transferred to the PVDF membranes (Millipore). Protein detection was carried out using the ECL system (Millipore) and visualized with a LI-COR Odyssey FC imaging system (Bad Homburg, Germany). Quantification of Western blot signals was performed using Image Studio software (LI-COR). The specific antibodies employed for Western blotting are detailed in **Section 3.8** of the study.

4.9 Apoptosis detection with FITC Annexin V staining

Apoptosis was assessed using flow cytometry with the FITC Annexin V Apoptosis Detection Kit I (Catalog No. 556547, BD Pharmingen™), following the manufacturer's guidelines. Briefly, the supernatant containing apoptotic cells was collected prior to trypsinization and cell harvesting. These cells were washed twice and subsequently resuspended in 1X Binding Buffer to achieve a concentration of 1×10^6 cells/ml. A 100 µl aliquot of this cell suspension, containing 1×10^5 cells, was incubated with 5 µl of Propidium Iodide (PI) and 5 µl of FITC Annexin V. The incubation was carried out at room temperature, shielded from light, for a duration of 15 minutes. Following incubation, 400 µl of 1X Binding Buffer was added to each sample. Flow cytometric analysis was conducted within one hour

of sample preparation, utilizing an Accuri C6 flow cytometry instrument (BD Biosciences).

4.10 Apoptosis evaluation with cell cycle analysis by Propidium Iodide staining

Cells were plated at a density of 2×10^5 cells per well in 6-well plates and allowed to adhere for 24 hours. Subsequently, the cells were subjected to designated treatments for 48 hours. Both adherent and floating cells from the supernatant were collected and pooled together. The cells were then washed twice with HBSS and fixed using ice-cold 70% ethanol, added dropwise, and stored overnight at -20°C . Following fixation, the cells were washed once with HBSS and then resuspended in a Propidium Iodide (PI) staining solution. The DNA content of the cells was assessed using flow cytometry on an Accuri C6 instrument (BD Biosciences). Data analysis was performed using CFlow software, with the sub- G_1 cell population serving as an indicator of apoptotic cells.

4.11 Cell viability assay

Cell viability was assessed using the Cell Counting Kit-8 (CCK-8) from Dojindo EU GmbH, following the instructions of the manufacturer. In brief, cells were plated in 96-well plates at a density of 3,000 cells per well and subjected to various treatments with indicated cytostatic agents for designated time periods. At the end point of the treatment, each well received a 10% CCK-8 solution and was incubated for 2 hours. The absorbance was then measured at a wavelength of 450 nm using a Berthold Orio II Microplate Luminometer (Berthold, Germany). Dose-response curves were generated using GraphPad Prism software (v9.31; GraphPad Software, USA), which were subsequently utilized to calculate the half-

maximal inhibitory concentration (IC₅₀) values for the respective cytostatic agents.

4.12 Assessment of cell proliferation by real - time impedance measurement

Cell proliferation was assessed by real-time cellular impedance measurement using the xCELLigence Real Time Cell Analyzer (RTCA) (Roche Diagnostics GmbH, Germany), as previously described [147]. Cells were seeded into E-plates at a density of 3,000 cells per well and subjected to specified treatments after a 24-hour incubation period. Impedance was monitored every hour for a duration of 96 hours and is reported as a dimensionless unit termed the Cell Index by the RTCA software. The Cell Index is not only dependent on cell number, but also influenced by various factors including cell size, cell morphology, and the degree of cell adherence to the substrate coating the plate [148]. To validate the impedance measurements, end-point cell number counting was performed. This is crucial as the Cell Index is not solely dependent on cell number. For this validation, cells were simultaneously seeded into 96-well plates and treated in an identical manner. At the end point, cell numbers were quantified using a Neubauer chamber.

4.13 Autophagic flux assay with GFP-LC3-RFP probe

Cells with stable expression of GFP-LC3-RFP were established by transfecting them with a GFP-LC3-RFP plasmid, which was sourced from Addgene and originally provided by Noboru Mizushima (Plasmid #84573). The transfection was carried out using Lipofectamine LTX (Invitrogen), and cells were subsequently selected using puromycin for a two-week period. To evaluate the intensities of

GFP and RFP fluorescence, cells were exposed to specified stress conditions and then analyzed via flow cytometry, utilizing an Accuri C6 instrument (BD Biosciences).

4.14 RNA-Seq analysis

Total RNAs from HCT116 cells were extracted using a High Pure RNA Isolation Kit (Roche), following the manufacturer's guidelines, which included an on-column DNase digestion. Random primed cDNA libraries were constructed and sequenced on the NovaSeq 6000 platform (Illumina, San Diego, CA, USA) by GATC (Konstanz, Germany). The sequencing yielded a minimum of 30 million paired-end read pairs, each with a length of 150 bp for every sample. The RNA sequencing (RNA-Seq) FASTQ files underwent processing utilizing the RNA-Seq module within CLC Genomics Workbench v20.0.2 (Qiagen Bioinformatics, Germany) and were aligned to the GRCh38/hg38 human reference genome using specified settings, including insertion cost = 2, mismatch cost = 2, length fraction = 0.8, deletion cost = 3, and similarity fraction = 0.8. Post-alignment, the RNA-Seq data underwent filtering to eliminate transcripts with low expression levels (< 20 reads mapped to exons in all samples) and upper quartile normalization by the RUVSeq package (Version 1.18.0) R/Bioconductor package [149]. DESeq2 (Version 1.24.0) was used to perform differential gene expression analysis [150] after normalization by the RUVg approach from the RUVSeq package to remove technical variations between RNA samples that was resulted from the differences in library preparation processes. The implementation of Principal Component Analysis (PCA) was carried out utilizing the PCA functionality embedded within the EDASeq package. For miR-34 target identification, the top 1000 ranked targets of miR-34a, as delineated in a recently published list of miR-34 targets, were

utilized. These targets were generated by the METAmiR34TARGET website [151]. The over-representation analysis (ORA) of pathways was performed by the “enricher” function, which utilizes a hypergeometric testing method as implemented in the clusterProfiler 4.0 R package [152]. The AUTOPHAGY_CORE signature was retrieved from a publication by Bordi et al. [153]. The other gene sets used in this study were retrieved from the Molecular Signatures database (MSigDB) [154]. Sample-wise pathway activity variations were estimated non-parametrically in a unsupervised manner using the GSEA R package [155]. The interaction effects between genotype and treatment condition were tested using EdgeR, which helped identify mRNAs showing genotype-dependent differences in regulation after 5-FU treatment [156].

4.15 Analysis of gene expression and clinical data from public databases

For the examination of human CRC samples, gene expression profiles and associated clinical metadata of the TCGA-CRC samples and a large integrated CRC samples were retrieved from the Genomic Data Commons (GDC) portal [157] and the Gene Expression Omnibus (GEO) repository [158], respectively. For the TCGA-CRC dataset, the TCGAbiolinks R package [159] was employed to extract both the read counts of the TCGA-CRC samples and their corresponding clinical and phenotypic information from the GDC portal. Following data retrieval, a filtration process was executed to exclude genes with low expression levels using the “filterByExpr” function from the edgeR package [160]. The remaining read counts were then normalized utilizing the TMM method [161], as implemented in the edgeR package [160]. For the GEO-CRC data, integrated clinical and phenotypic data for 1,273 CRC samples were acquired from the study conducted by Martinez R. et al. [158]. The raw CEL expression files pertinent to

these samples were downloaded directly from the GEO repository. These raw CEL expression files were subsequently imported and subjected to normalization using the Robust Multi-array Average (RMA) method, as implemented by the oligo R package [162]. Following the normalization process, the ComBat algorithm [163], as implemented in the sva package, was employed to mitigate batch effects. To assess the efficacy of this batch effect removal, Principal Component Analysis (PCA) was conducted both pre- and post-application of the ComBat algorithm. This dual-phase PCA served as a quality control measure to validate the successful elimination of batch effects, thereby ensuring the integrity and comparability of the analyzed datasets.

The CMScaller package (version 2.0.1) [164] was employed to classify CRC samples into consensus molecular subtypes (CMS) [25], a system that has been shown to have prognostic and therapeutic implications. In accordance with the package guidelines, CMS subtype predictions were executed using the pre-defined template incorporated within the CMScaller package using the nearest template prediction algorithm [165]. Sample categorization was performed based on the minimal Euclidean distance to the respective subtype templates. To ascertain the robustness of these classifications, a permutation analysis was conducted with 1,000 iterations. A classification was deemed statistically significant if it yielded a FDR-adjusted P-value less than 0.05.

Additionally, we utilized data from the Cancer Cell Line Encyclopedia (CCLE) [166], and the Genomics of Drug Sensitivity in Cancer (GDSC) database [167] to correlate 5-FU sensitivity with gene expression profiles in CRC cell lines. We applied the Cox proportional-hazards model to assess the association between

overall patient survival time and *miR-34-a/b/c-KO*-derived signatures scores in the specified CRC patient cohorts by determining the respective hazard ratio.

4.16 Drug combination synergy scores analysis

To rigorously evaluate the synergistic effects of combining Chloroquine (CQ) and 5-Fluorouracil (5-FU), synergy scores were computed using SynergyFinder 2.0 [168], a specialized software tool designed for this purpose. The analysis employed the Loewe model [169], a widely accepted mathematical framework for assessing drug interactions. The dose-response matrix, which was obtained from cell viability assays, served as the empirical basis for this computational analysis. By utilizing this methodological approach, we aimed to provide a quantitative measure of the extent to which the drug combination enhances therapeutic efficacy beyond what would be expected from the sum of their individual effects.

4.17 Statistical analysis

Statistical analyses were conducted using GraphPad Prism (v9.31; GraphPad Software, USA) and R (version 4.2.2). Each experimental condition was replicated a minimum of three times. To assess the statistical significance of differences between two groups of samples, an unpaired two-tailed Student's t-test was employed. A p-value threshold of less than 0.05 was set for statistical significance, with varying levels of significance denoted as follows: * for $p < 0.05$, ** for $p < 0.01$, *** for $p < 0.001$, and **** for $p < 0.0001$; n.s. indicates no statistical significance. To correct for multiple testing errors, the Benjamini-Hochberg method was utilized to calculate the false discovery rate (FDR), which is crucial for controlling the rate of Type I errors.

The results that follow are in part derived from the manuscript: Huang et al., CRISPR/Cas9-mediated inactivation of *miR-34a* and *miR-34b/c* in HCT116 colorectal cancer cells: comprehensive characterization after exposure to 5-FU reveals EMT and autophagy as key processes regulated by miR-34. *Cell Death Differ* 30, 2017–2034 (2023). This manuscript has been published in a peer-reviewed journal and is available open access under a CC BY license (Creative Commons Attribution 4.0 International License). The publisher has stated that this material can be used in the author's doctoral thesis without obtaining permission from the publisher.

5. Results

5.1 Generation and characterization of *miR-34a/b/c*-deficient HCT116 cell lines

To characterize the functions of the three *p53*-inducible *miR-34* family members, the genomic regions encoding mature *miR-34a* and *miR-34b/c* within their respective host genes were deleted alone or concomitantly in the HCT116 CRC cell line utilizing a Clustered Regularly Interspaced Palindromic Repeats (CRISPR)/Cas9 approach. The single-guide RNAs (sgRNAs) targeting the sequence flanking the genomic regions of precursor *miR-34a* or *miR-34b/c* are illustrated in **Figure 5.1A, C** and **Section 3.6.1**. Three independent single-cell-derived clones for each genotype (i.e., *miR-34a-KO*, *miR-34b/c-KO* and *miR-34a/b/c-KO*) were obtained. Serving as controls, three independent single-cell-derived clones for wild-type cells (*WT*) were also generated by transfection of HCT116 cells with pSpCas9 plasmids not harboring sgRNAs. The deletion of the *miR-34a* and/or *miR-34b/c* genomic loci was validated by PCR (**Figure 5.1B, D** and **Section 3.6.2**).

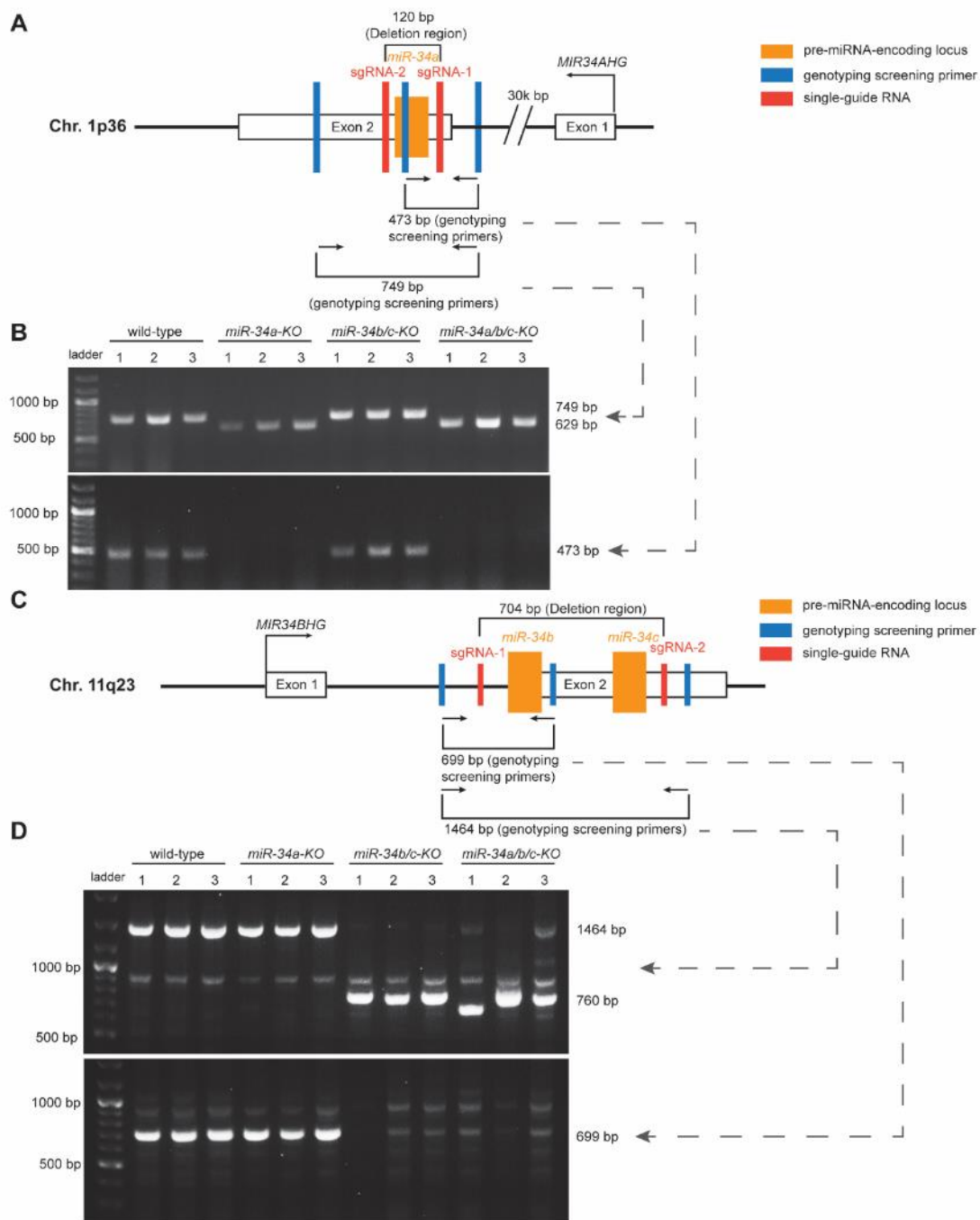


Figure 5.1 Schematic representations of deleting *miR-34* using a CRISPR/Cas9 approach and genotyping screening results. **(A)** A graphical representation of *miR-34a* genomic location and deletion of the precursor *miR-34a* encoding region utilizing a CRISPR/Cas9 approach. *miR-34a* coding locus is indicated by an orange column and two sgRNAs targeted regions are shown by red columns. Three genotyping screening primers indicated in blue were designed to determine cells with homozygous *miR-34a* deletion. **(B)** Genotyping results of deletion of the *miR-34a* locus. Intact *miR-34a* locus displayed 749 bp bands, while deletion of it resulted in 629 bp bands (upper panel). The absence of *miR-34a* locus was validated by the failure to detect the 473 bp products (lower panel). **(C)** A schematic

of *miR-34b* and *miR-34c* loci and deletion of the precursor miRNAs encoding regions utilizing a CRISPR/Cas9 approach. *miR-34b* and *miR-34c* coding genomic loci are indicated by orange columns and two sgRNAs targeted regions are shown by red columns. Three genotyping screening primers indicated in blue were designed to determine cells with homozygous *miR-34b/c* deletion. **(D)** Genotyping results of the deletion of *miR-34b/c* loci. Intact *miR-34b/c* loci displayed 1464 bp bands, while deletion of them resulted in 760 bp bands (upper panel). The absence of *miR-34b/c* loci was validated by the failure to detect the 699 bp products (lower panel).

Additionally, the absence of *miR-34a* and/or *miR-34b/c* expression was confirmed by qPCR analysis subsequent to p53 activation by the addition of Nutlin-3a, which is a highly selective inhibitor of MDM2 [170] **(Figure 5.2)**.

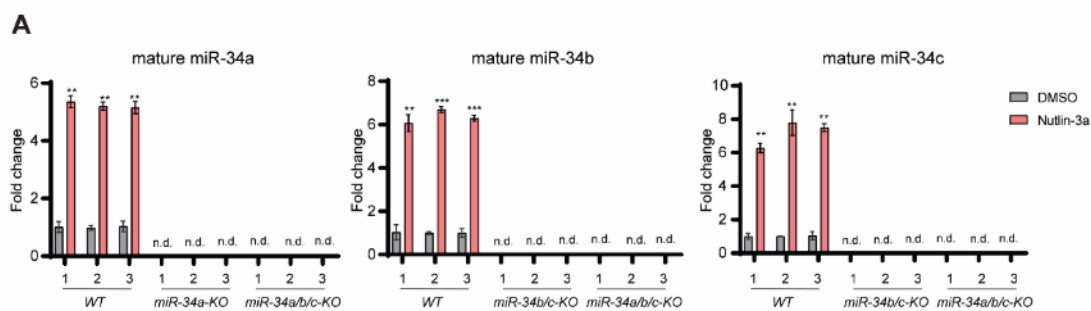


Figure 5.2 qPCR analysis of mature miR-34 expression following treatment of either DMSO or 10 μ M of Nutlin-3a for 48 h. Results are presented as the mean \pm SD (n = 3) with **: $p < 0.01$, ***: $p < 0.001$. n.d. indicates not detectable.

Intriguingly, mature miR-34b and miR-34c exhibited a significantly increased expression following the inactivation of *miR-34a* in HCT116 cells **(Figure 5.3)**, indicating that the loss of miR-34a functions may be partially compensated by the increased expression *miR-34b/c*. The inactivation of *miR-34b/c* in HCT116 cells led to a slight increase of the expression of mature miR-34a **(Figure 5.3)**, presumably due to the basal expression levels of miR-34b and miR-34c being relatively low in HCT116 cells in comparison to miR-34a [171].

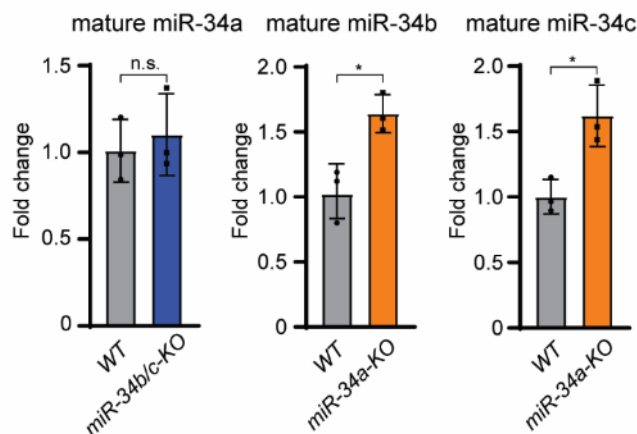


Figure 5.3 qPCR assessments of mature miR-34 expression in HCT116 *miR-34a-KO* and *miR-34b/c-KO* cells. Results are presented as the mean \pm SD ($n = 3$) with *: $p < 0.05$, **: $p < 0.01$, n.s.: no significance.

5.2 *miR-34a/b/c* inhibits cellular proliferation in HCT116 cells

Subsequently, we investigated the impact of the absence of miR-34a/b/c on cellular proliferation via real-time impedance measurements. The loss of *miR-34a/b/c* in HCT116 cells led to minor effects on proliferation relative to wild-type cells, which however were not consistently statistically significant (**Figure 5.4**). However, upon the activation of p53 via the addition of Nutlin-3a, the *miR-34*-deficient cells were partially refractory to Nutlin-3a in comparison to *WT* cells, with *miR-34a/b/c-KO* cells showing the highest rate of proliferation in the presence of Nutlin-3a (**Figure 5.4**). These findings suggest that a significant fraction of p53-mediated suppression of proliferation is orchestrated by the collective action of *miR-34a/b/c*. Additionally, these data imply that inactivation of one isoform of *miR-34* is not sufficient to alleviate the p53-induced proliferation inhibition.

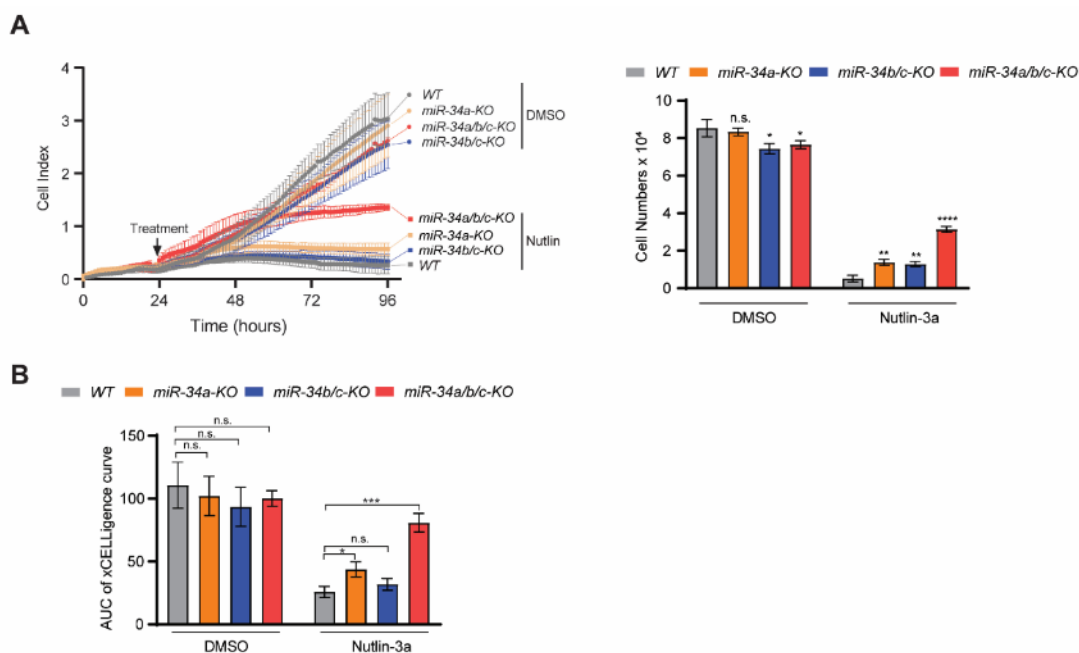


Figure 5.4 (A) The proliferation of HCT116 *miR-34*-deficient cells was measured by a real-time cellular impedance assay by the xCELLigence system. Cell numbers were counted at the end point of the experiment. **(B)** A bar graph delineating the Area Under the Curve (AUC) of the xCELLigence growth curves presented in **A**. Results are presented as the mean \pm SD ($n = 3$) with *: $p < 0.05$, **: $p < 0.01$, ***: $p < 0.001$, ****: $p < 0.0001$, n.s.: no significance.

5.3 Loss of *miR-34a/b/c* promotes EMT, migration and invasion in HCT116 cells

Subsequently, we explored whether the deficiency of *miR-34* affects the migratory and invasive capabilities of HCT116 cells. Indeed, *miR-34a/b/c-KO* cells displayed significantly enhanced migration and invasion relative to wild-type cells by Boyden-chamber assays (**Figure 5.5**).

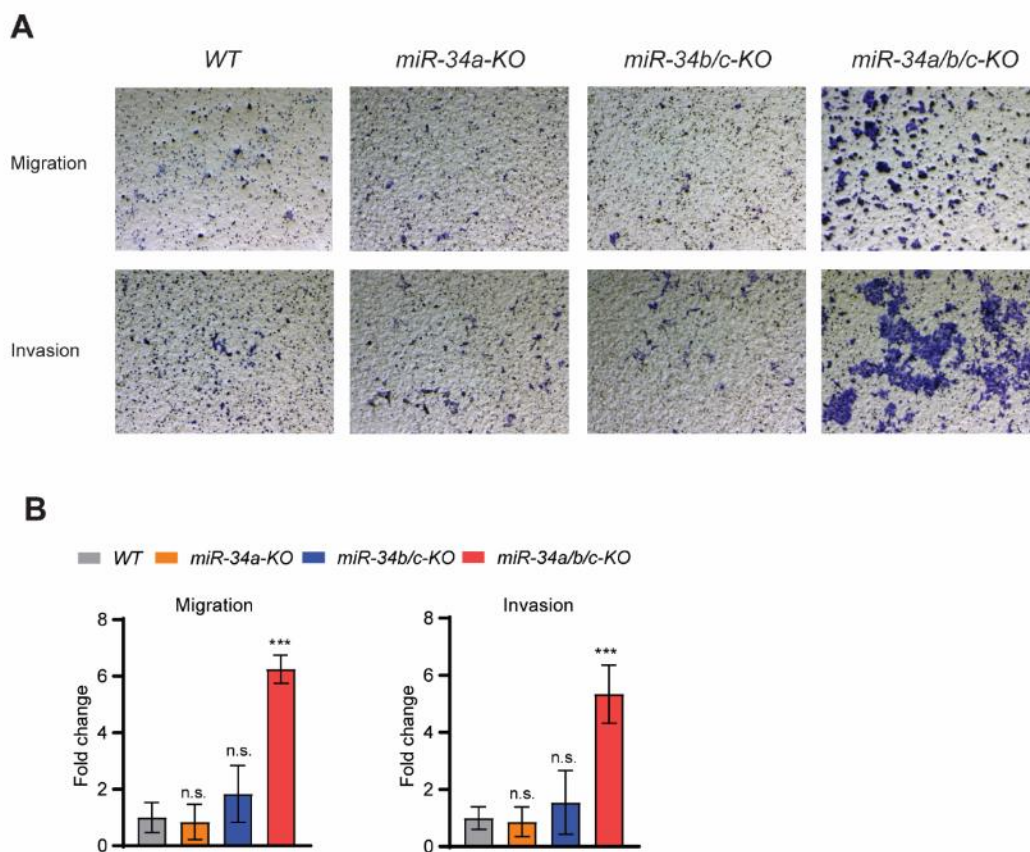


Figure 5.5 (A) Representative images showcasing the determination of cellular migratory and invasive capacities via Boyden-chamber assays. **(B)** Quantification of cellular migration or invasion as determined by the Boyden-chamber assays in **A**. Results are presented as the mean \pm SD ($n = 3$) for **B** with ***: $p < 0.001$, ****: $p < 0.0001$, n.s.: no significance.

Enhanced migration of *miR-34a/b/c*-deficient cells was further substantiated by a wound healing assay conducted both in the presence and absence of Nutlin-3a treatment (**Figure 5.6**).

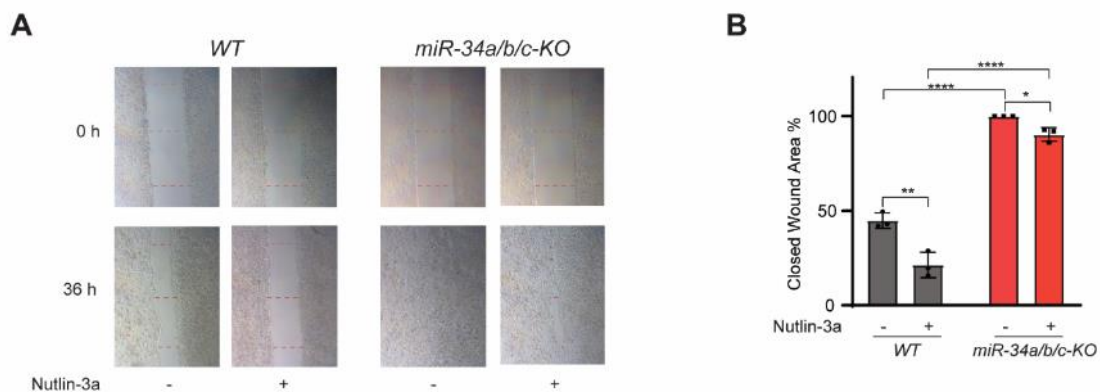


Figure 5.6 (A) Representative images showcasing the determination of cellular migration for indicated cells, treated with either DMSO or Nutlin-3a, utilizing a wound healing assay. **(B)** Quantification of results of wound healing assays in **A**. Results are presented as the mean \pm SD ($n = 3$) for **B** with *: $p < 0.05$, **: $p < 0.01$, ***: $p < 0.001$, ****: $p < 0.0001$.

Given that epithelial-mesenchymal transition (EMT) serves as a pivotal mechanism underpinning cellular migration and invasion, we tested EMT markers to determine whether the loss of *miR-34* affects EMT. Protein levels of E-cadherin, a hallmark epithelial marker, were decreased in *miR-34*-deficient cells in comparison to wild-type cells, while the expression of SNAIL, a mesenchymal marker, was increased across all *miR-34*-deficient cells (**Figure 5.7A**). qPCR analysis revealed a significant elevation in the expression of *VIM* and *SNAIL* in *miR-34a/b/c*-deficient cells relative to wild-type cells, but for *SNAIL* not in either *miR-34a*-deficient or *miR-34b/c*-deficient cells (**Figure 5.7B**). Additionally, the mRNA expression of *E-cadherin* was reduced in all *miR-34*-deficient cells, although this reduction was not statistically significant (**Figure 5.7B**). Thus, the alterations in the expression of EMT-related genes may at least in part explain the increased migration and invasion observed in *miR-34a/b/c*-deficient cells.

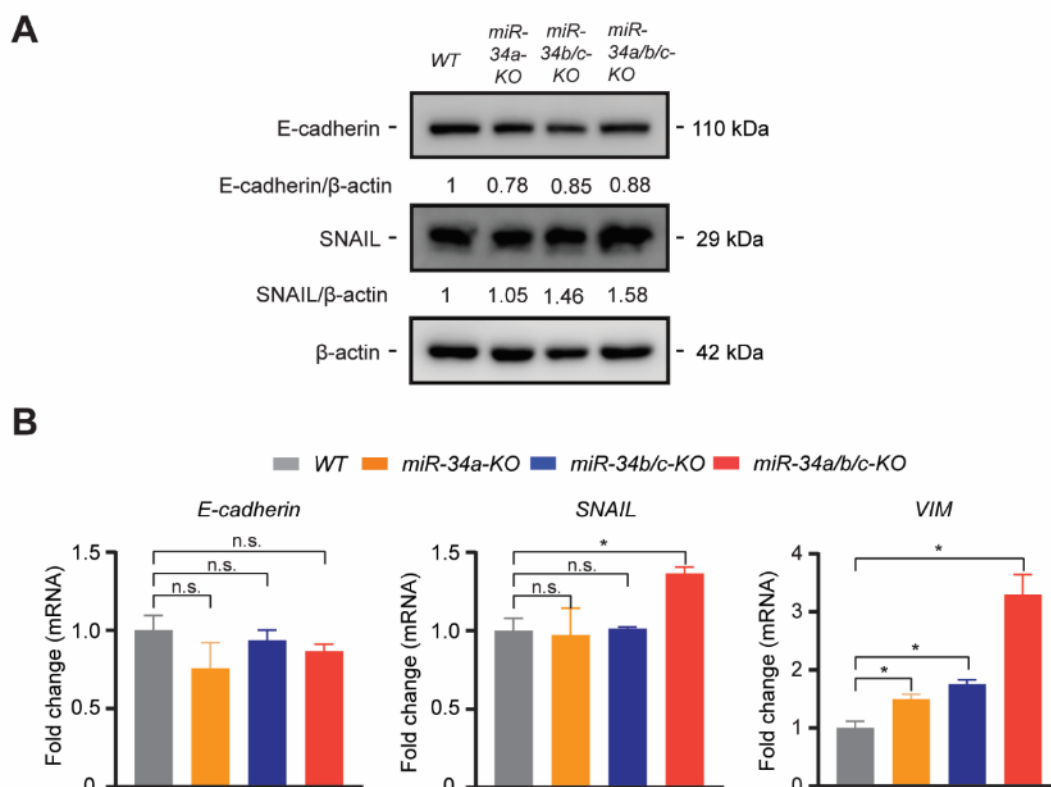


Figure 5.7 (A) Western blot analysis and (B) qPCR analysis of EMT markers. Results are presented as the mean \pm SD ($n = 3$) for B with *: $p < 0.05$, n.s.: no significance.

5.4 Loss of *miR-34a/b/c* mediates resistance to chemotherapeutic agents by enhancing autophagic flux

In addition, we asked whether miR-34 deficiency affects the cellular response to chemotherapeutic agents. 5-Fluorouracil (5-FU) and SN-38 (the active metabolite of Irinotecan) are frequently used chemotherapeutic agents in the treatment of CRC. HCT116 WT and *miR-34*-deficient cells were exposed to a wide range of concentrations of 5-FU or SN-38, and then subjected to an assessment of cell viability and determination of IC₅₀ values. Notably, only *miR-34a/b/c*-KO cells exhibited a significant, ca. two-fold elevation in IC₅₀ values for both 5-FU and SN-38. In contrast, singular deletion of *miR-34a* or *miR-34b/c* led to a marginal

increase in IC50 values (**Figure 5.8**). *P53-KO* cells exhibited a ca. two-fold increase in IC50 values for both 5-FU and SN-38 relative to *p53-WT* cells (**Figure 5.8**), indicating that only the combined inactivation of *miR-34a* and *miR-34b/c* has a similar effect as *p53*-deficiency on the response to chemotherapeutic agents.

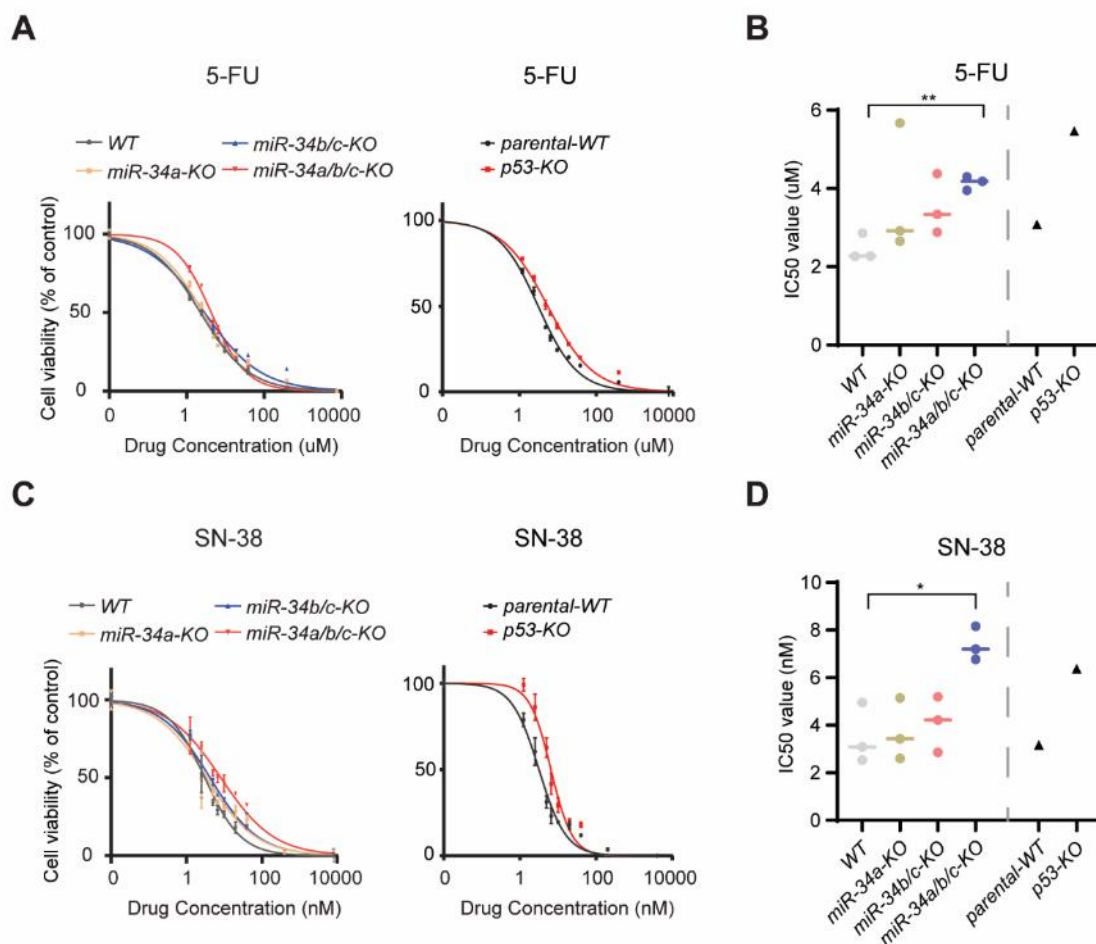


Figure 5.8 (A, C) Representative dose-response curves for HCT116 cells of varying *miR-34* or *p53* genotypes when exposed to 5-FU or SN-38. Cells were exposed to a wide range of concentration of specified therapeutic agents for 72 h and then subjected to assessment of cell viability by the CCK-8 assays. **(B, D)** Determination of IC50 values for HCT116 cells of varying *miR-34* or *p53* genotypes when exposed to 5-FU or SN-38. The corresponding dose-response curves, from which the IC50 values were derived, are shown in **A** and **C**. Results are presented as the mean \pm SD ($n = 3$) for **B** and **D** with *: $p < 0.05$, **: $p < 0.01$, ***: $p < 0.001$.

As an alternative method to assess sensitivity towards chemotherapeutic agents, we evaluated apoptosis through identifying Annexin V positive cells by flow cytometry. Only *miR-34a/b/c*-deficient cells exhibited a significant decrease in apoptosis after treatment of 5-FU in comparison to *WT* cells (**Figure 5.9**), suggesting that concomitant loss of both *miR-34a* and *miR-34b/c* is required for increased chemo-resistance.

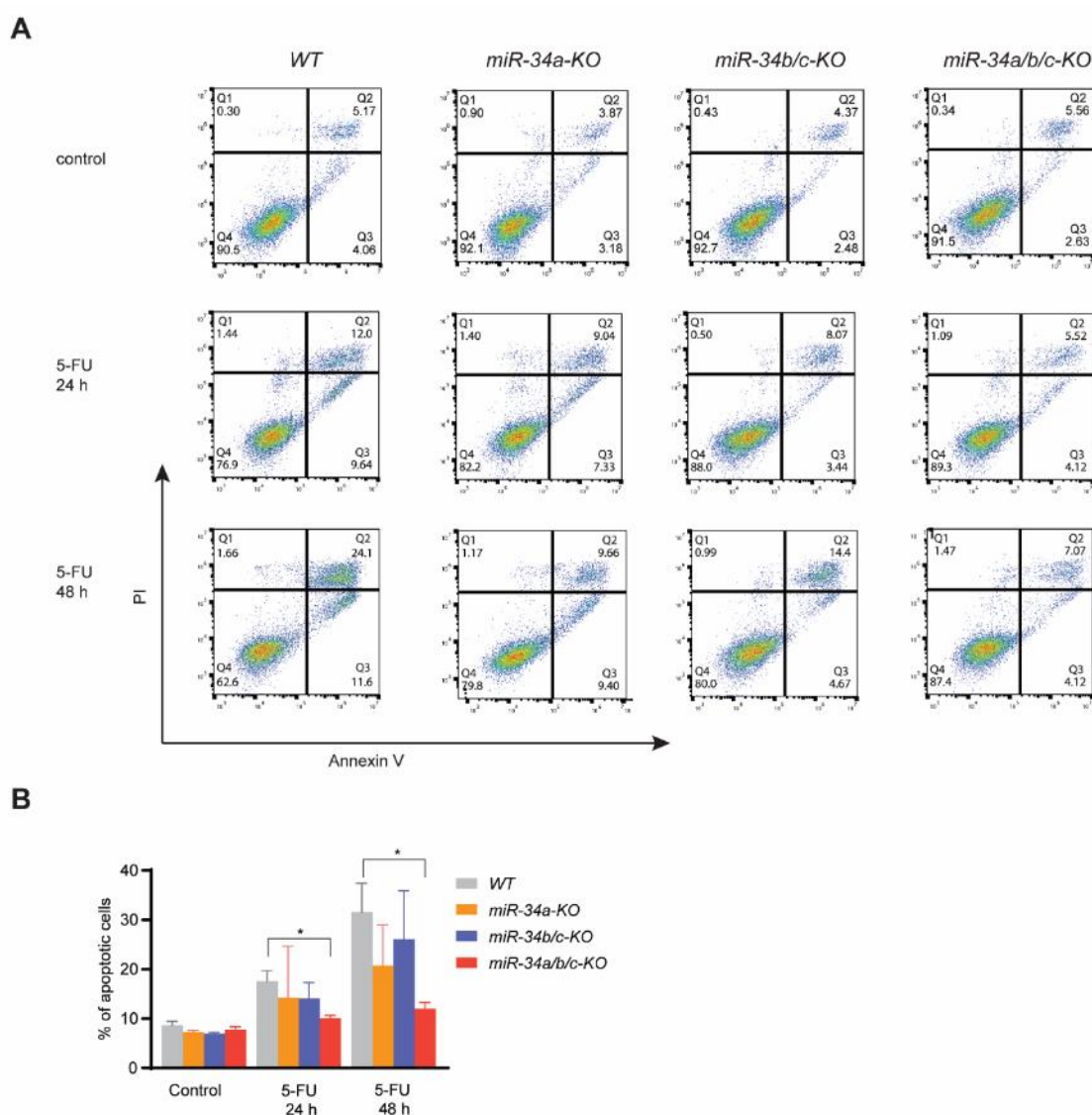


Figure 5.9 (A) Representative flow cytometry results. The indicated cells were exposed to 5-FU for 24 or 48 hours and subjected to FITC Annexin V staining and flow cytometric analysis to detect apoptotic cells. (B) Quantification of apoptotic cells in A. Results are presented as the mean \pm SD ($n = 3$) for B with *: $p < 0.05$.

The reduced sensitivity of *miR-34a/b/c*-deficient cells to 5-FU was further substantiated through DNA content analysis via flow cytometry, which revealed a reduction of cells in the sub-G₁ phase in *miR-34a/b/c*-deficient cells following treatment with 5-FU for 48 hours in comparison to wild-type cells (**Figure 5.10**).

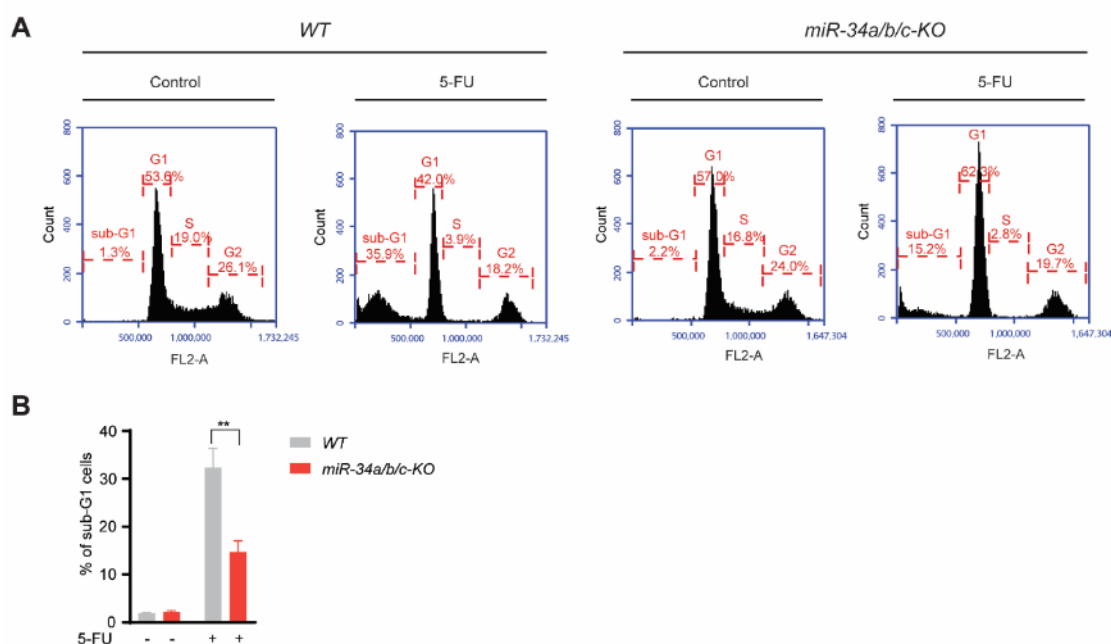


Figure 5.10 (A) Representative results of DNA content analysis conducted using flow cytometry. The indicated cells were treated with DMSO or 5-FU for 48 h and then subjected to PI staining and flow cytometric analysis to determine the sub-G₁ population. **(B)** Quantification of sub-G₁ cell population in **A**. Results are presented as the mean \pm SD ($n = 3$) for **B** with **: $p < 0.01$.

Furthermore, *miR-34a/b/c*-deficient cells exhibited a significantly reduction in the cleavage of PARP, a hallmark of apoptosis, after exposure to 5-FU relative to wild-type cells as determined by Western blot analysis (**Figure 5.11**). Collectively, these findings suggest that the absence of *miR-34a/b/c* rendered HCT116 cells chemo-resistant by attenuating apoptosis.

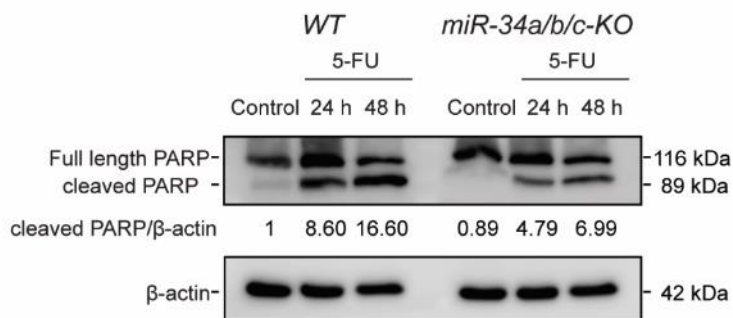


Figure 5.11 Immunoblotting analysis of cleaved-PARP when exposed to either DMSO or 5-FU for the indicated durations.

Macroautophagy/autophagy, a cellular process in which specialized organelles called autophagosomes deliver intracellular constituents to the lysosome for degradation, has been involved in the inhibition of apoptosis, thereby leading to resistance against therapeutic interventions [172]. By facilitating the degradation and reduction of damaged mitochondria and pro-apoptotic proteins (such as active caspase 8), autophagy mitigates apoptosis and promote cellular adaptation and survival [97]. Given this background, we asked whether enhanced autophagy contributes to the observed chemo-resistance in *miR-34a/b/c*-deficient cells. To assess autophagic flux, an indicator of autophagic degradation activity, we generated cells stably expressing GFP-LC3-RFP, which is an established fluorescent marker for autophagic flux [173]. Utilizing this probe, autophagy activity was estimated by calculating the GFP-LC3/RFP signal ratio. This probe undergoes cleavage by the ATG4 protease, yielding equimolar quantities of GFP-LC3 and RFP. Following this, GFP-LC3 is integrated into autophagosomes and undergoes degradation, while RFP remains undegraded by autophagy and persists

in the cytosol, thereby acting as an internal control. As a result, a lower GFP-LC3/RFP signal ratio is indicative of an elevated autophagic flux (**Figure 5.12**).

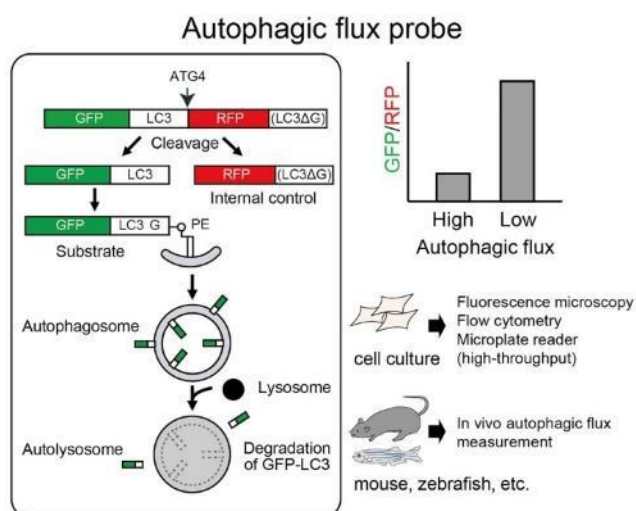


Figure 5.12 A schematic illustration of the GFP-LC3-RFP probe is from Kaizuka et al., 2016 [173].

An example is demonstrated in **Figure 5.13**, where GFP-LC3 signal intensity was reduced after exposed to 5-FU while RFP signal intensity remained unchanged.

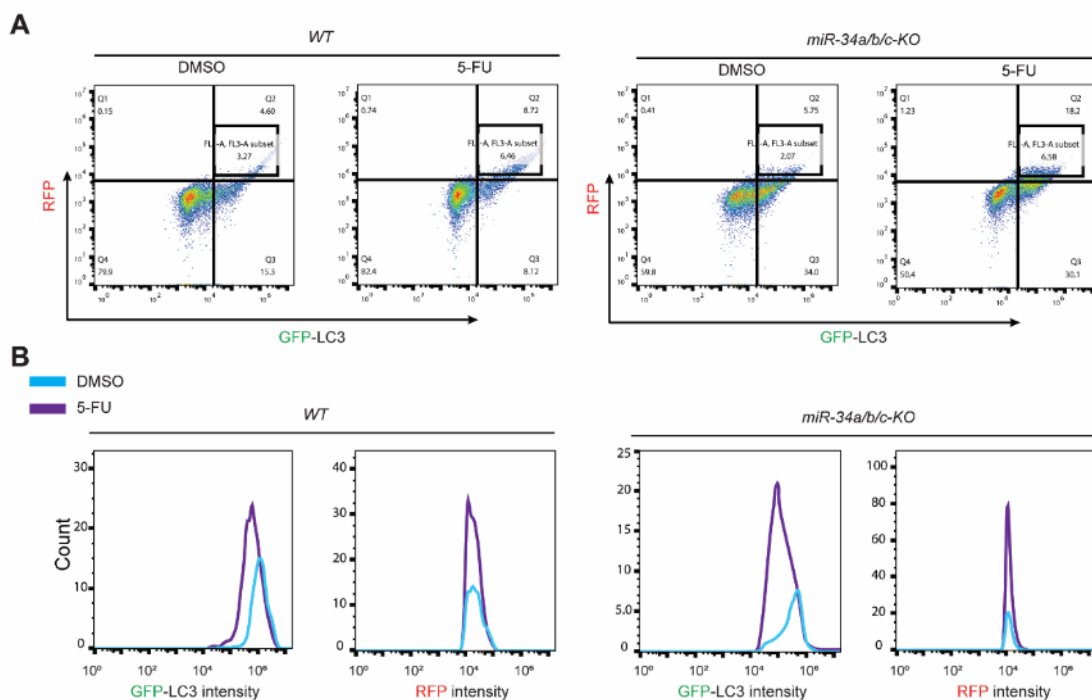


Figure 5.13 (A) An example of gating displaying cells stably expressing GFP-LC3-RFP after treatment with DMSO or 5-FU. (B) An example of flow cytometry histograms displaying cell counts versus fluorescence intensity in cells stably expressing GFP-LC3-RFP after treatment with DMSO or 5-FU.

When *miR-34a/b/c*-deficient and *WT* cells stably expressing a GFP-LC3-RFP were exposed to 5-FU for 24 or 48 hours, it resulted in a significant elevation of autophagic flux in *miR-34a/b/c*-deficient cells, as evidenced by a significantly larger reduction in GFP-LC3/RFP ratio in *miR-34a/b/c*-deficient cells in comparison to *WT* cells (**Figure 5.14A**). As an alternative method to evaluate autophagic flux, a Western blot analysis was employed to measure the lysosomal turnover of SQSTM1/p62, an autophagy receptor protein, and LC3-II, a widely recognized autophagosome marker, in the presence and absence of chloroquine (CQ), an inhibitor of lysosome [174]. Consistent with the findings from the GFP-LC3-RFP probe, after exposure to 5-FU for 24 or 48 hours, *miR-34a/b/c*-deficient cells exhibited a significantly enhanced turnover of endogenous p62 and LC3-II in comparison to wild-type cells (**Figure 5.14B**), indicating that *miR-34a/b/c*-deficient cells exhibit an elevated level of autophagic flux following 5-FU treatment.

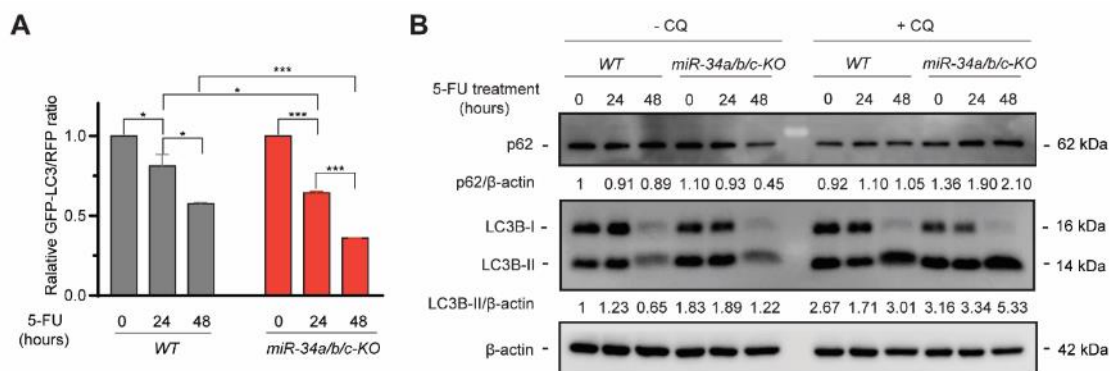


Figure 5.14 (A) Quantification of the GFP-LC3/RFP ratio via FACS analysis of cells stably expressing GFP-LC3-RFP probe after exposed to DMSO or 5-FU. Lower GFP-LC3/RFP signal ratio, resulting from enhanced GFP-LC3 degradation, is indicative of higher autophagic flux. **(B)** *miR-34a/b/c-KO* and *WT* cells were exposed to DMSO or 5-FU for the specified durations and subjected to immunoblotting analysis. Chloroquine (CQ) at a concentration of 20 μM was introduced 4 hours prior to cell harvesting. Results are presented as the mean \pm SD ($n = 3$) for **A** with *: $p < 0.05$, **: $p < 0.01$, ***: $p < 0.001$, ****: $p < 0.0001$, n.s.: no significance.

Additionally, the *miR-34a/b/c*-deficient cells consistently exhibited an increased autophagic flux in response to 5-FU in a dose-dependent manner. In contrast, the *WT* cells demonstrated a more subdued autophagic response (**Figure 5.15**). Notably, even at elevated concentrations of 5-FU, the *WT* cells did not consistently display increased autophagic flux. Taken together, these findings demonstrate that autophagy is significantly induced in *miR-34a/b/c*-deficient cells after exposure to 5-FU in comparison to wild-type cells. This suggests that autophagy presumably plays a critical role in the observed chemo-resistance of *miR-34a/b/c*-deficient cells in response to 5-FU.

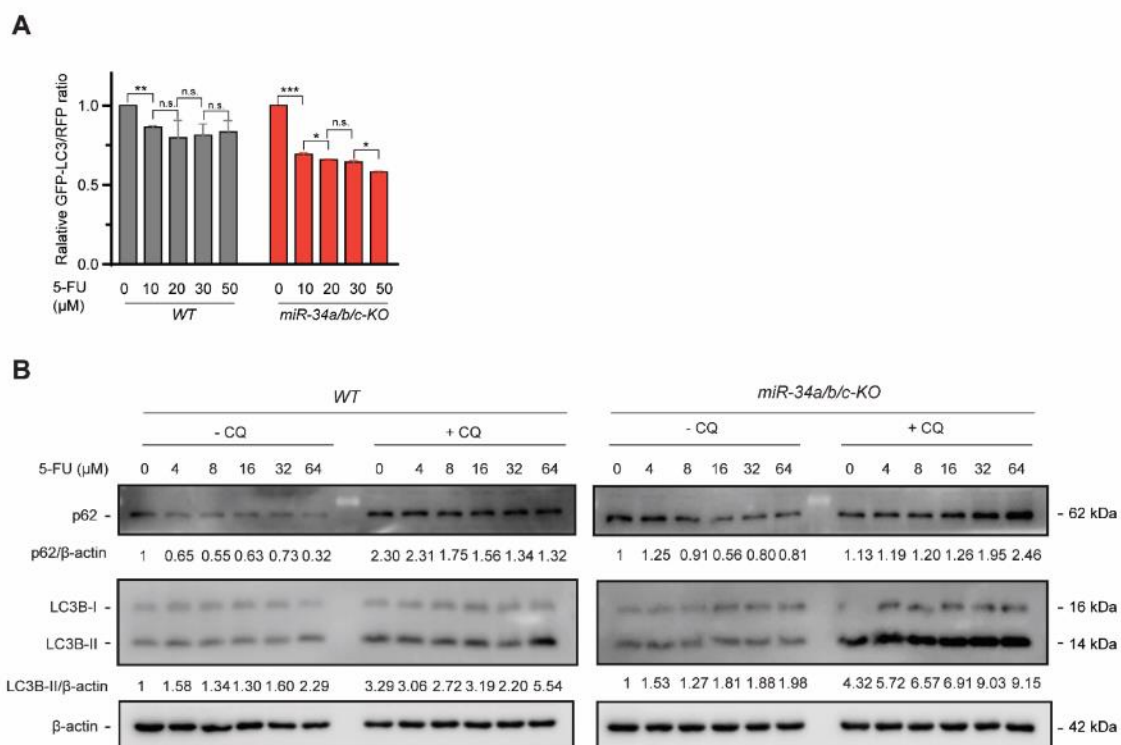


Figure 5.15 (A) Quantification of GFP-LC3/RFP ratio via FACS analysis of cells stably expressing GFP-LC3-RFP after exposure to DMSO or varying concentrations of 5-FU. **(B)** Cells were exposed to DMSO or 5-FU at the specified concentrations. 20 μM of CQ was introduced 4 hours prior to cell harvesting. Results are presented as the mean \pm SD ($n = 3$) for **A** with *: $p < 0.05$, **: $p < 0.01$, ***: $p < 0.001$, n.s.: no significance.

5.5 Loss of *miR-34a/b/c* consistently elevates autophagic flux after stress

To test if *miR-34a/b/c*-deficient cells also exhibit an elevated autophagic flux when autophagy is triggered by other mechanisms, cells were exposed to amino acid and serum deprivation by being cultured in Earle's Balanced Salt Solution (EBSS). Additionally, cells were treated with Tunicamycin, known to induce ER-stress. Under EBSS conditions, *miR-34a/b/c*-deficient cells exhibited significantly

elevated autophagic flux relative to *WT* cells, as indicated by the increased turnover of LC3-II and p62 (**Figure 5.16A**), was further corroborated by the increased degradation of GFP-LC3 as determined through FACS analysis (**Figure 5.16B**).

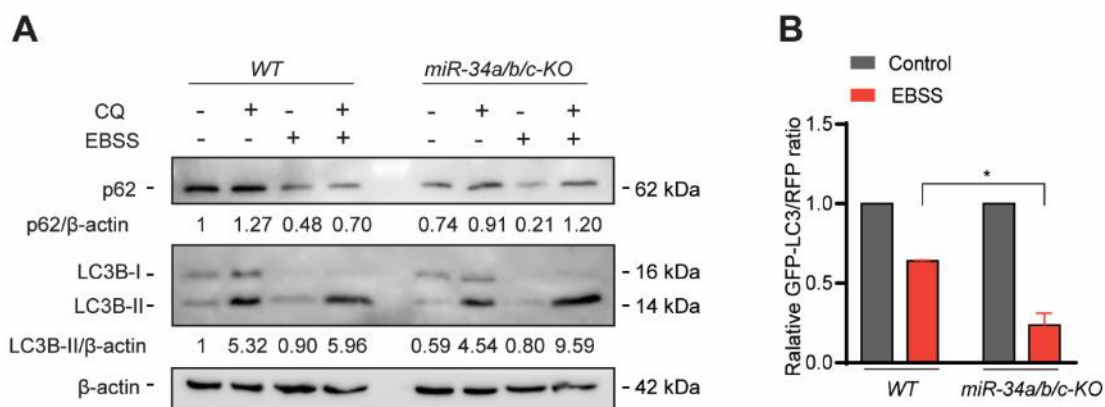


Figure 5.16 (A) Cells were cultured either in complete medium or in EBSS for 24 hours. 20 μ M CQ was introduced 4 hours prior to cell harvesting. (B) Cells stably expressing GFP-LC3-RFP probe were cultured either in complete medium or in EBSS for 24 hours, followed by FACS analysis. Results are presented as the mean \pm SD ($n = 3$) for B with *: $p < 0.05$.

Similarly, treatment with Tunicamycin resulted in significantly elevated autophagic flux in *miR-34a/b/c*-deficient cells (**Figure 5.17A, B**). However, an unexpected accumulation of p62 protein was observed (**Figure 5.17A**). A possible rationale for this phenomenon could be the transcriptional activation of p62, as evidenced in our findings (**Figure 5.17C**). This transcriptional activation might be orchestrated by the NRF2 transcription factor, which is known to be activated by Tunicamycin and has been previously identified as a regulator of p62 [175, 176].

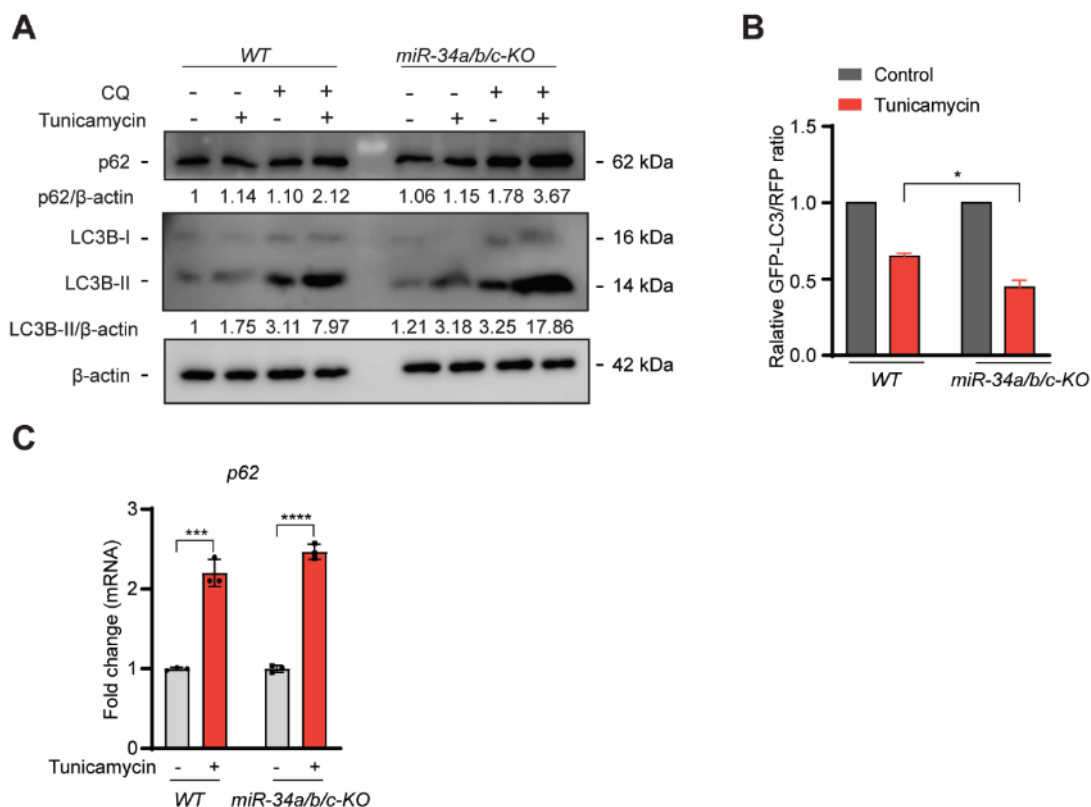


Figure 5.17 (A) Cells were exposed to DMSO or Tunicamycin for 24 h. 20 μ M CQ was introduced 4 hours prior to cell harvesting. (B) FACS analysis was conducted on cells stably expressing the GFP-LC3-RFP after exposure to DMSO or Tunicamycin for 24 hours. (C) qPCR analysis was performed to assess *p62* levels after treating HCT116 cells with Tunicamycin at a concentration of 1 μ g/ml for 24 hours. Results are presented as the mean \pm SD ($n = 3$) for B and C with *: $p < 0.05$, **: $p < 0.01$, ***: $p < 0.001$, n.s.: no significance.

Additionally, ectopic expression of *pri-miR-34a* from an episomal pRTR vector led to the suppression of basal autophagy in SW480 (Figure 5.18A) and HCT15 cells (Figure 5.18B).

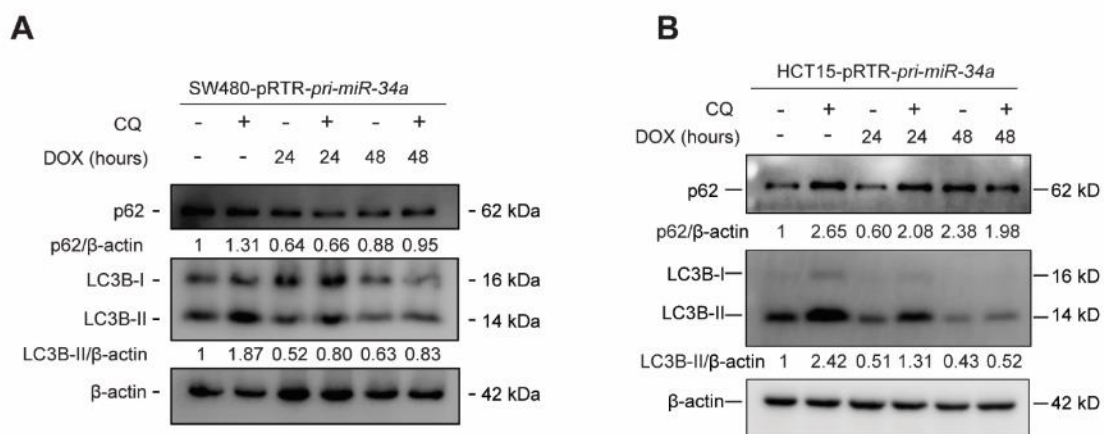


Figure 5.18 Doxycycline was administered as indicated to induce the ectopic expression of *pri-miR-34a* in SW480 cells (**A**) and HCT15 cells (**B**). 20 μ M CQ was introduced 4 hours prior to cell harvesting.

Because 5-FU also led to a significantly increased autophagic flux in HCT116 *p53*-deficient cells in comparison to *WT* cells (**Figure 5.19**), the loss of *miR-34a/b/c* at least partially recapitulated the effects of *p53* deficiency on autophagy. Collectively, these findings corroborate that *miR-34a* and *miR-34b/c* function as negative regulators of autophagy in HCT116 cells.

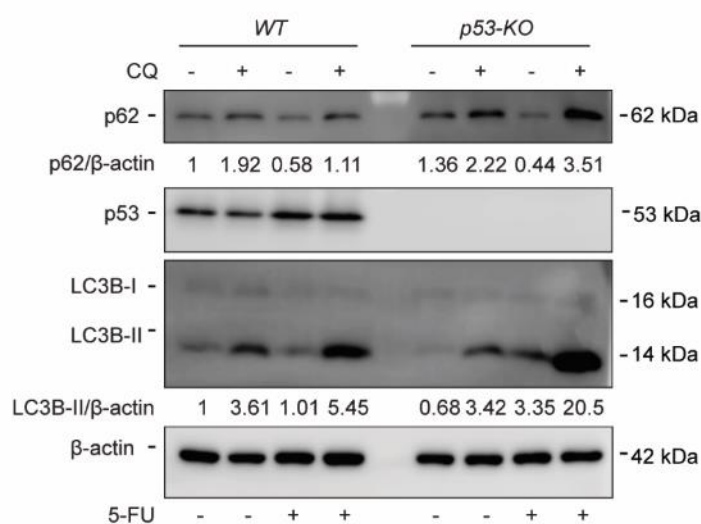


Figure 5.19 *p53-KO* and *WT* cells were exposed to DMSO or 5-FU for the specified durations, followed by Western blot analysis. 20 μ M CQ was introduced 4 hours prior to cell harvesting.

5.6 Analysis of mediators of miR-34 function by expression profiling

To comprehensively characterize the mediators through which *miR-34a* and *miR-34b/c* exert their functions and regulate the processes mentioned above and others, we explored the mRNA expression profiles of HCT116 *miR-34a/b/c-KO* cells and corresponding *WT* cells after treated with 5-FU (4 μ M) for 48 hours using RNA sequencing (RNA-Seq) analysis. Libraries were constructed from RNAs isolated from three biological replicates across four conditions: *miR-34a/b/c-KO* and *WT* HCT116 cells exposed to 5-FU or, as a control, exposed to DMSO. The RNA-Seq analysis was conducted with more than 30 million paired-end reads for each library. The Principal Component Analysis (PCA) highlighted that the predominant variations were driven by 5-FU treatment, as captured by principal component (PC) 1. The loss of *miR-34a/b/c*, on the other hand, led to significantly altered expression profiles, which were predominantly captured by PC2 (**Figure 5.20A**). The differential RNA expression analysis was conducted using DESeq2, and differentially expressed mRNAs (with an FDR < 0.05 and an absolute fold-change > 1.5) in both unstressed or 5-FU-treated cells are demonstrated in the volcano plots (**Figure 5.20B**). The deletion of *miR-34a/b/c* in untreated HCT116 cells led to a significant up-regulation of 966 mRNAs and down-regulation of 562 mRNAs in comparison to *WT* cells (left panel, **Figure 5.20B**). Moreover, 5-FU treatment led to a significantly up-regulation of 1971 mRNAs and down-regulation of 1296 mRNAs in *WT* cells in comparison to DMSO control (middle panel, **Figure 5.20B**). Similarly, 5-FU treatment resulted in a significantly up-regulation of 1675 mRNAs and down-regulation of 1243 mRNAs in *miR-34a/b/c*-deficient cells in comparison to DMSO control (right panel, **Figure 5.20B**). Intriguingly, the overlap between mRNAs either down- or up-regulated (> 1.5-fold change) in *WT* or *miR-34a/b/c-KO* cells when exposed to 5-FU was not

complete (**Figure 5.20C**). This indicated that while the response to 5-FU treatment shared considerable similarities (as previously hinted by the PCA), there were distinct differences dependent on *miR-34a/b/c*. Additionally, a limited overlap was observed between mRNAs that exhibited strong opposing regulation (> 1.5 -fold change in either down- or up-regulation) (**Figure 5.20C**). Notably, among the 8 mRNAs that were down-regulated in *WT* cells and up-regulated in *miR-34a/b/c*-deficient cells, 5 (*CCNE2*, *SKA1*, *RAD51AP1*, *EXO1*, *ESCO2*) were associated with cell proliferation-related pathways such as cell cycle regulation (*CCNE2*), mitosis (*SKA1*, *ESCO2*), as well as DNA replication and repair (*RAD51AP1*, *EXO1*), indicating that loss of *miR-34a/b/c* may affect cell cycle progression after exposed to 5-FU.

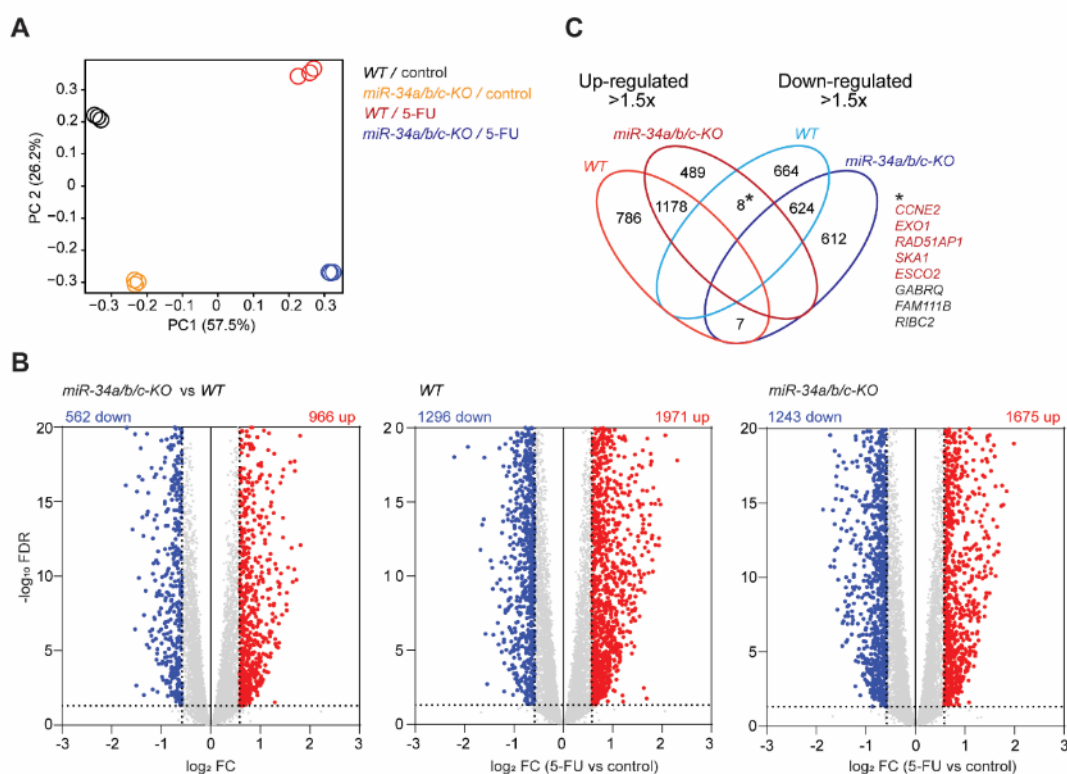


Figure 5.20 (A) PCA analysis of mRNAs expression in HCT116 *miR-34a/b/c*-KO and *WT* cells exposed to DMSO or 5-FU for 48 hours. **(B)** Volcano plots demonstrating differential mRNA expression with FDR on a $-\log_{10}$ scale and fold change on a \log_2 scale. Significantly down- and up-regulated mRNAs are highlighted in blue and red, respectively. Non-significantly regulated mRNAs are depicted in

grey. **(C)** A Venn diagram illustrating the number of differentially expressed mRNAs shared between *miR-34a/b/c-KO* and *WT* cells (5-FU vs control). Dr. Markus Kaller performed the analysis and generated the figures.

To identify the molecular and cellular pathways that might be differentially affected by the loss of *miR-34a/b/c*, we conducted an over-representation analysis (ORA) of pathways utilizing gene sets from the MSigDB database [177] (**Figure 5.21**). The pathways that were enriched among the mRNAs that saw an up-regulation in *miR-34a/b/c*-deficient cells were characterized by gene sets encompassing genes implicated in endoplasmic reticulum (ER) stress, ER and Golgi apparatus, EMT, the positive regulation of autophagy, as well as extracellular matrix, and p53 pathway activation. Conversely, the gene sets that were over-represented among the mRNAs that were down-regulated encompassed those representing the organization of epithelial cells (CELL_CELL_JUNCTION, TIGHT_JUNCTION), and relating to cell proliferation, such as DREAM_TARGETS, E2F_TARGETS, and CELL CYCLE. These findings from the ORA analysis largely validated our initial observations that *miR-34a/b/c*-deficient cells display a more mesenchymal phenotype, as well as enhanced autophagy.

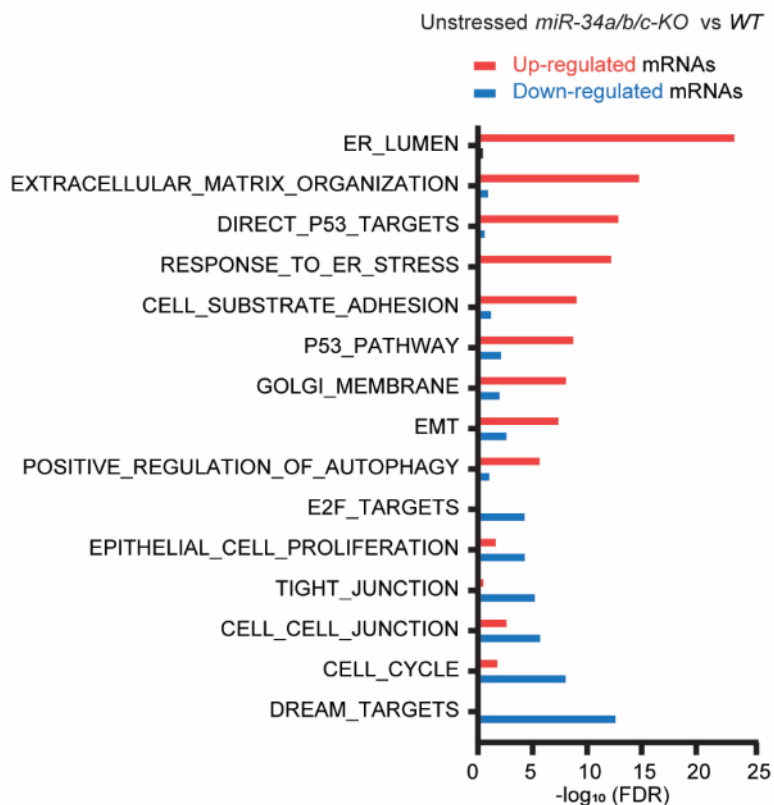


Figure 5.21 ORA analysis of mRNAs significantly regulated in unstressed *miR-34a/b/c-KO* vs. *WT* cells. Dr. Markus Kaller performed the analysis and generated the figure.

The ORA method was further utilized to analyze the molecular and cellular pathways that were significantly altered after 5-FU treatment of *miR-34a/b/c-KO* and *WT* cells (**Figure 5.22**). Pathways over-represented among the up-regulated mRNAs were similar between *miR-34a/b/c-KO* and *WT* cells, which encompassed p53 activation, EMT, apoptosis, and pathways related to cell migration. The activation of p53 and the induction of apoptosis are expected responses to 5-FU treatment, as 5-FU is a chemotherapeutic agent that induces DNA damage, leading to p53-mediated cell cycle arrest and apoptosis. Intriguingly, profound differences in pathways over-represented among the down-regulated mRNAs between *miR-34a/b/c-KO* and *WT* cells after treatment with 5-FU were observed. Specifically, the down-regulation of cell proliferation associated pathways, though

still significant, was markedly diminished in *miR-34a/b/c-KO* cells. This observation aligns with the earlier findings (**Figure 5.20C**), and strongly indicated that loss of *miR-34a/b/c* may abrogate the cell cycle arrest observed in *WT* cells after 5-FU treatment.

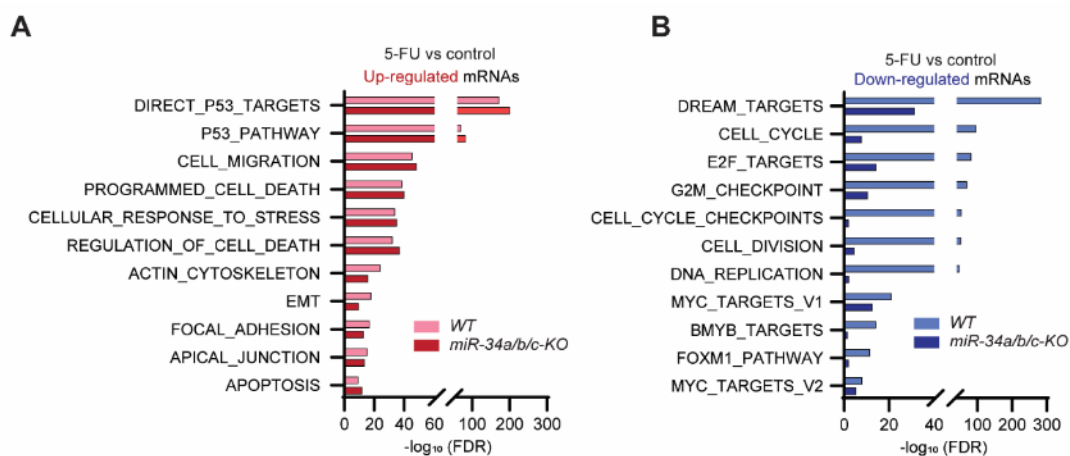


Figure 5.22 (A, B) ORA analysis of mRNAs significantly regulated in 5-FU-treated *miR-34a/b/c-KO* and *WT* cells. Dr. Markus Kaller performed the analysis and generated the figures.

In addition, we explored how the differential gene expression resulted from the deletion of *miR-34a/b/c* may cause the aforementioned alterations observed for specific cellular processes. First, we delineated the set of mRNAs displaying genotype-dependent variations (> 1.5-fold) in regulation following 5-FU treatment. We conducted K-means clustering with the resulting set of 1691 mRNAs displaying differential regulation (**Figure 5.23A** and **Table S1**) and identified both predicted and published miR-34 targets within each cluster (**Table S1**). Individual published or predicted miR-34a targets did not adhere to a particular pattern of differential regulation between *miR-34a/b/c*-deficient and wild-type cells and were present in all of the clusters. Nonetheless, miR-34 targets were markedly over-represented in cluster 6 (and to a lesser degree in cluster 2), which was predominantly characterized by genes engaged in cell-cycle regulation (**Figure 5.23B**).

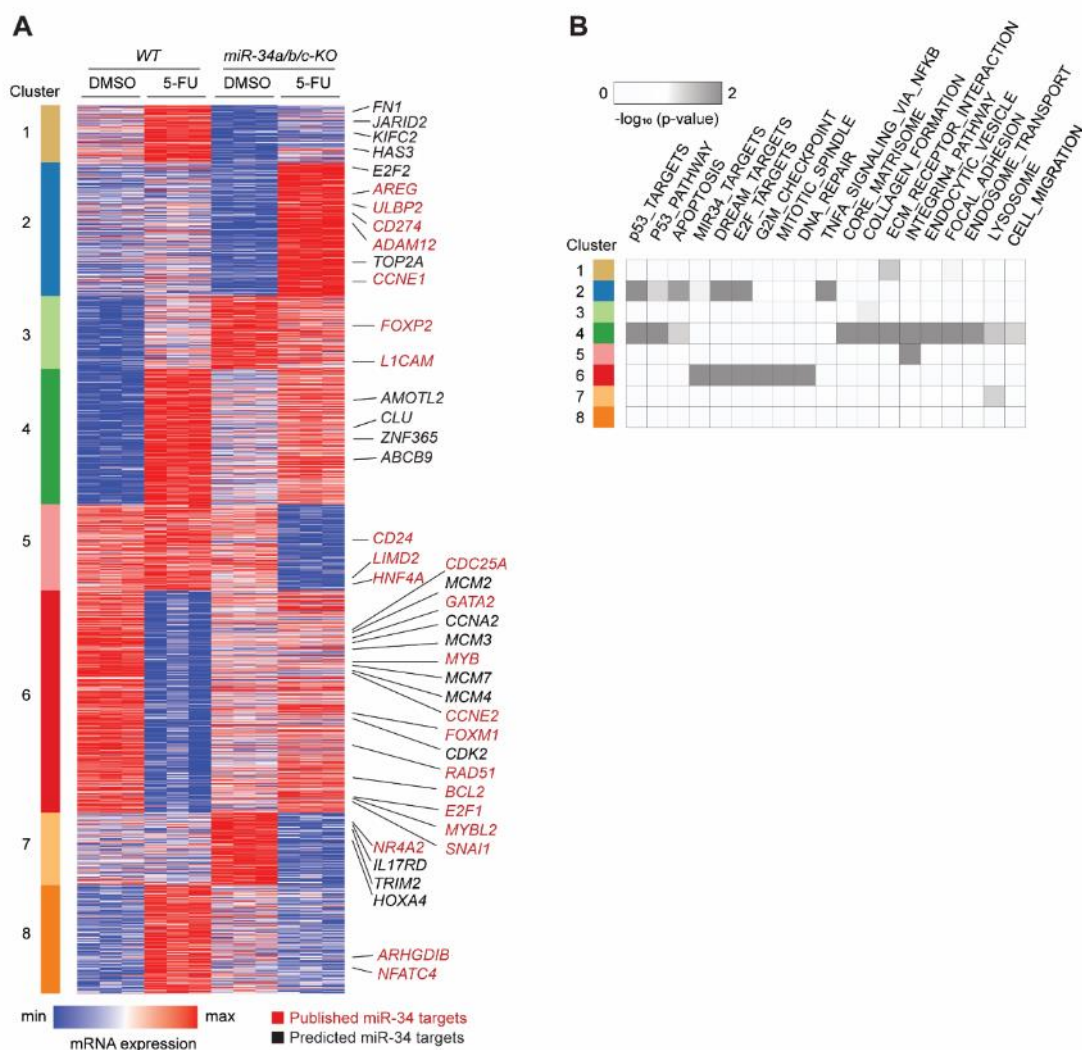


Figure 5.23 (A) A heatmap representation of expression of mRNAs that exhibited significantly genotype-dependent differences (> 1.5 -fold) in regulation following 5-FU treatment, organized into distinct transcriptional clusters. Selected miR-34a targets are demarcated by color, with published targets in red and predicted ones in black **(B)** A heatmap that displays the enrichment of specific pathways and functional categories within the expression clusters as shown in **(A)**. The statistical significance of these enrichments was calculated by Fisher's exact test. Dr. Markus Kaller performed the analysis and generated the figures.

These mRNAs were characterized by significantly elevated up-regulation in *miR-34a/b/c*-deficient cells or strongly diminished down-regulation in *miR-34a/b/c*-deficient cells (**Figure 5.24A**). While miR-34 targets did not manifest a uniform pattern of expression alteration in wild-type cells following 5-FU exposure, collectively, they showed either activation or de-repression in *miR-34a/b/c*-deficient cells. Notably, of the 266 DREAM targets identified within clusters 2 and

6, 42 (15.8 %) were either predicted or previously documented as *miR-34a/b/c* targets (**Figure 5.24B** and **Table S1**), hinting that the DREAM complex and miR-34a/b/c share a substantial overlap of targets and presumably cooperatively suppress these genes following p53 activation. Given the considerable overlap between the E2F and DREAM target gene signatures, which is due to the binding of both E2F and DREAM complexes to E2F sites, shared targets between miR-34 and E2F were also identified, such as Cyclin E1/CCNE1, which exhibited up-regulation in *miR-34a/b/c*-deficient cells (**Figure 5.24B** and **Table S1**). Taken together, these findings indicate that miR-34 may contribute to the repression of mRNAs, which are also subjected to down-regulation through the mediation of the DREAM complex [135].

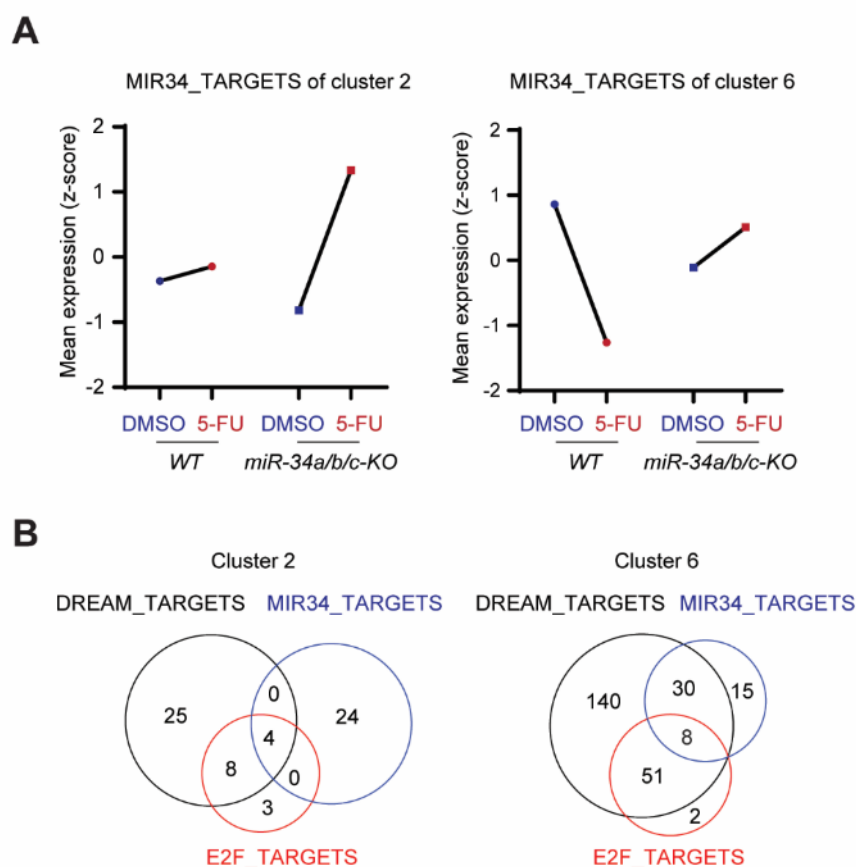


Figure 5.24 (A) Line plots showed the mean z-scores of normalized RNA expression of all miR-34 targets that demonstrated statistically significant genotype-de-

pendent variations following 5-FU treatment, organized into the specified transcriptional clusters (B) Venn diagrams highlighting the overlap between DREAM targets, miR-34 targets and E2F targets within the designated transcriptional clusters. Dr. Markus Kaller performed the analysis and generated the figures.

Subsequently, we utilized the Gene Set Variation Analysis (GSVA) [155], a method for the sample-wise pathway enrichment analysis, to explore the pathways that were significantly altered in *miR-34a/b/c-KO* vs. *WT* cells following 5-FU exposure, by estimating the pathway activities variations of various pathway in an unsupervised manner (Figure 5.25). Notably, the pathways related to p53 activation and the upregulation of direct p53 targets were not significantly altered between *miR-34a/b/c-KO* and *WT* cells following 5-FU treatment. A marked difference in the regulation of the miR-34 target set was observed between *miR-34a/b/c-KO* and *WT* cells, which was down-regulated in *WT*, but up-regulated in *miR-34a/b/c-KO* following 5-FU treatment (Figure 5.25). As already hinted by the ORA analysis, the differential regulation of mRNAs associated with cell proliferation (E2F_TARGETS, DREAM_TARGETS, etc.) was significantly changed in *miR-34a/b/c*-deficient cells, which demonstrated a severely diminished repression relative to *WT* cells (Figure 5.25). Additionally, pathways associated with mitochondria functions and apoptosis were differentially down-regulated in *miR-34a/b/c*-deficient cells following 5-FU treatment. We also observed a differential regulation of genes implicated in organization of the ER and Golgi apparatus, EMT, and gene sets representing diverse autophagy pathways, which either showed enhanced basal levels, and/or increased up-regulation in *miR-34a/b/c*-deficient cells.

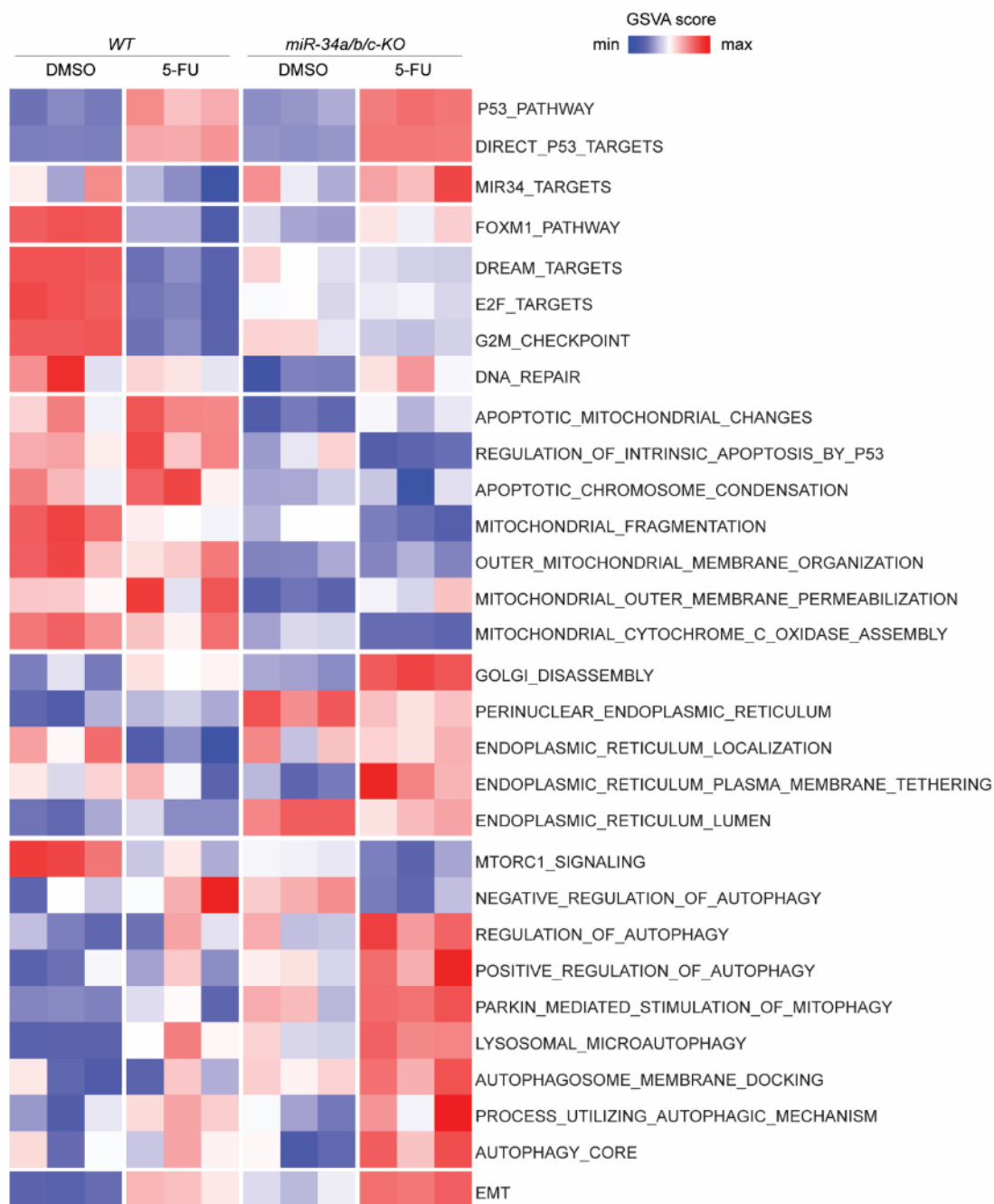


Figure 5.25 A heatmap representation of the GSVAscore analysis, highlighting the alterations in the activities of specified pathways due to the inactivation of *miR-34a/b/c* following 5-FU treatment. Dr. Markus Kaller performed the analysis and generated the figure.

5.7 *MiR-34a/b/c* inhibit multiple key autophagy-related genes

We further explored the role of *miR-34a* and *miR-34b/c* in the autophagic response to 5-FU treatment. As expected, the *pri-miR-34a* and *pri-miR-34b/c* transcripts were significantly induced in HCT116 *WT* cells after treated with 5-FU (**Figure 5.26A**). Concurrently, mature *miR-34a*, *miR-34b* and *miR-34c* were significantly up-regulated in HCT116 *WT* cells after exposed to 5-FU, but not detectable in HCT116 *miR-34a/b/c-KO* cells (**Figure 5.26B**).

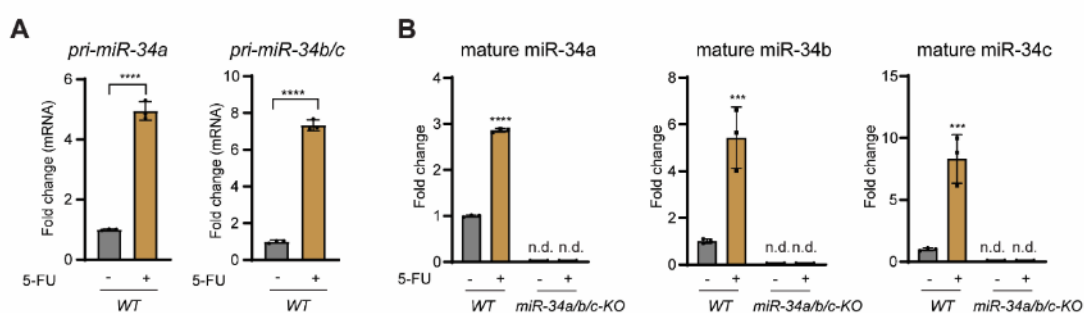


Figure 5.26 (A) qPCR analyses of *pri-miR-34a* and *pri-miR-34b/c* after exposure to DMSO or 5-FU for 48 h in HCT116 *WT* cells. **(B)** qPCR analyses of mature *miR-34* in HCT116 *miR-34a/b/c-KO* or *WT* cells after exposed to DMSO or 5-FU for 48 h. Results are presented as the mean \pm SD ($n = 3$) for **A**, **B** with *: $p < 0.05$, **: $p < 0.01$, ***: $p < 0.001$, ****: $p < 0.0001$, n.s.: no significance.

Consistent with the GSEA findings presented in **Figure 5.25**, qPCR analysis of key autophagy-related mRNAs, which are either predicted (*ULK2*, *ATG13*) or known (*ULK1* [178], *ATG4B* [122], *ATG9A* [179], *XBP1* [180], *ATG5* [181], *IRE1A* [182]) to be directly targeted by *miR-34*, revealed that these mRNAs were either significantly elevated in *miR-34a/b/c*-deficient cells or diminished in *WT* cells after exposed to 5-FU (**Figure 5.27A**). Moreover, the ectopic expression of *miR-34a* significantly repressed the expression of the aforementioned autophagy-related

genes in SW480 cells (**Figure 5.27B**). Consequently, *miR-34* presumably represses autophagy processes by targeting multiple key autophagy-related mRNAs in CRC HCT116 cells.

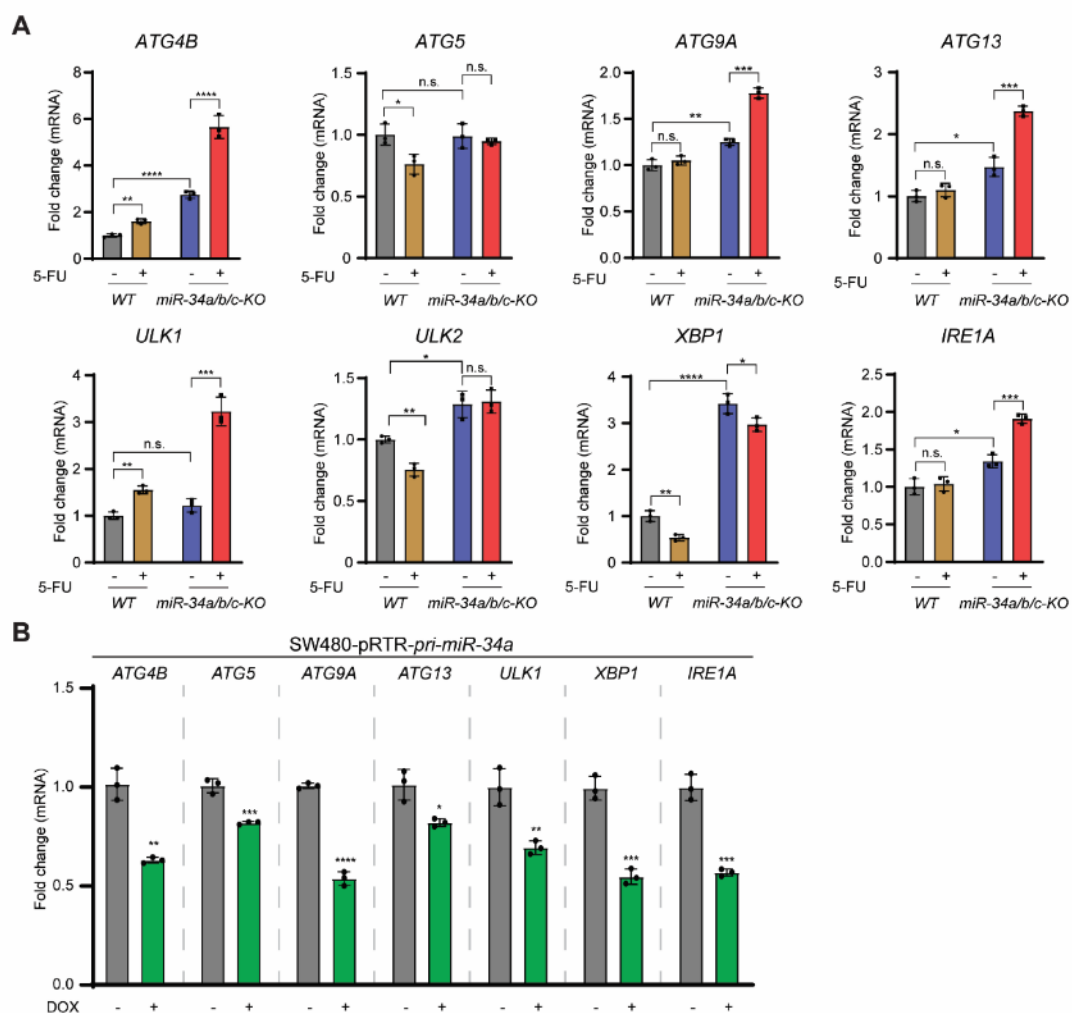


Figure 5.27 (A) qPCR analyses of selected autophagy-related mRNAs that are targets of *miR-34*. **(B)** qPCR analyses of selected autophagy-related *miR-34* target mRNAs following ectopic expression of *pri-miR-34a* from an episomal pRTR vector in SW480 cells by addition of doxycycline for 48 hours. n.d. indicates not detected. Results are presented as the mean \pm SD ($n = 3$) for **A**, **B** with *: $p < 0.05$, **: $p < 0.01$, ***: $p < 0.001$, ****: $p < 0.0001$, n.s.: no significance.

5.8 FOXM1 induces autophagy and transactivates *p62* and *ATG9A*

Among the recognized *miR-34* targets exhibiting differential up-regulation in *miR-34a/b/c*-deficient cells following 5-FU exposure (**Figure 5.23**), *FOXM1*

emerged as a potential autophagy mediator, given its prior association with autophagy regulation [136, 137]. Given that the up-regulation of *FOXM1* may be responsible for the enhanced expression of the autophagy gene sets observed in *miR-34a/b/c*-deficient cells after exposed to 5-FU (**Figure 5.25**), we analyzed whether *FOXM1* mediates the *miR-34* effects on autophagy. The up-regulation of *FOXM1* in *miR-34a/b/c*-deficient cells after exposed to 5-FU was first validated by qPCR (**Figure 5.28A**). Subsequently, a dual luciferase reporter assay was used to confirm that *FOXM1* mRNA is a target of *miR-34a/b/c* in HCT116 *miR-34a/b/c*-deficient cells (**Figure 5.28B**). Specifically, the luciferase activity of a human *FOXM1* 3'-UTR reporter was repressed after co-transfected with *miR-34a/b/c* mimics. In contrast, the luciferase activity of a reporter with a mutant *miR-34* seed-matching sequence (SMS) was refractory (**Figure 5.28B**). The repression of *FOXM1* mRNA by *miR-34a/b/c* was further substantiated by referencing the METAmiR34TARGET database [151], which indicated that *FOXM1* mRNA was repressed following the ectopic introduction of *miR-34a/b/c* across various cell lines (**Figure 5.28C**). Subsequently, the repression of *FOXM1* mRNA and protein by *miR-34* was validated through the ectopic introduction of *pri-miR-34a* in SW480 cells (**Figure 5.28D, E**).

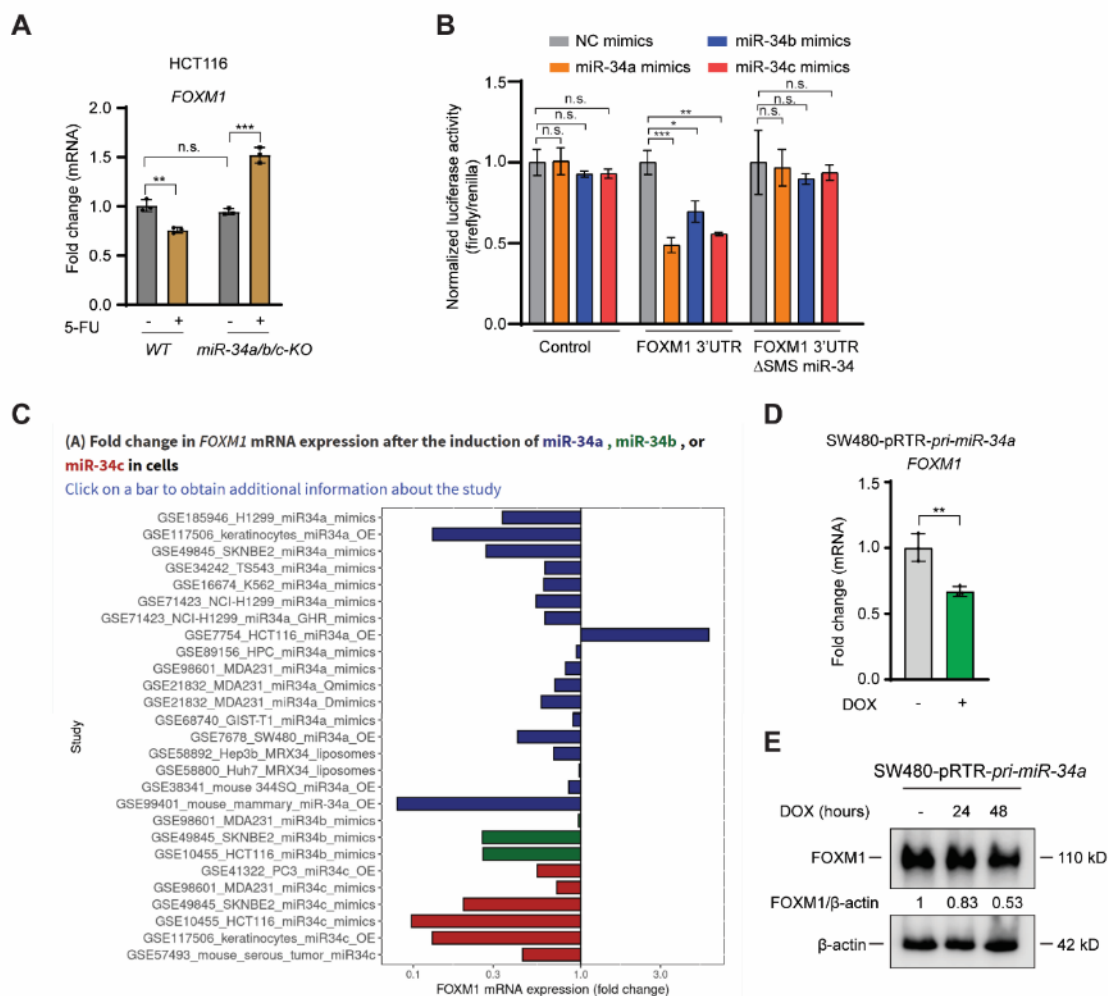


Figure 5.28 (A) qPCR analysis of *FOXM1* in HCT116 *miR-34a/b/c-KO* or *WT* cells after exposure to DMSO or 5-FU for 48 h. (B) A dual luciferase reporter assay conducted 48 hours after transfection of HCT116 *miR-34a/b/c*-deficient cells with the specified miRNA mimics and reporter vector. (C) Data from the METAmiR34TARGET platform, illustrating the fold change in *FOXM1* mRNAs following ectopic expression of miR-34a/b/c across various cell lines. (D) qPCR analysis of *FOXM1* mRNAs and (E) immunoblotting analysis of FOXM1 protein following the ectopic expression of *pri-miR-34a* from an episomal pRTR vector in SW480 cells. Results are presented as the mean \pm SD ($n = 3$) for A, B and D with *: $p < 0.05$, **: $p < 0.01$, ***: $p < 0.001$, ****: $p < 0.0001$, n.s.: no significance.

In addition, down-regulation of FOXM1 using a specific siRNA pool (Figure 5.29A) led to a significantly reduction in autophagic flux in both *miR-34a/b/c*-deficient and *WT* cells, which was demonstrated by the diminished turnover of endogenous LC3-II and p62 (Figure 5.29B), supporting the assumption that *miR*-

34a/b/c inhibits autophagic flux by repressing *FOXM1*. Unexpectedly, the *FOXM1* depletion also repressed p62 (**Figure 5.29B**). p62 is an autophagy cargo receptor. Therefore, its accumulation would typically be anticipated if autophagy is inhibited due to the reduced autophagy-mediated degradation of p62 [174, 183]. Consequently, the repression of p62 following the down-regulation of *FOXM1* cannot be ascribed to autophagy inhibition. Instead, it hinted that *FOXM1* may transactivate p62 and possibly other autophagy-related genes. Indeed, *FOXM1* depletion led to a repression of p62 mRNA and also a down-regulation of *ATG9A* at both the mRNA and protein levels (**Figure 5.29C, D**). *CCNB1* (*Cyclin B1*), a *bona fide* *FOXM1* target [184], also exhibited significantly repression following *FOXM1* depletion (**Figure 5.29C**).

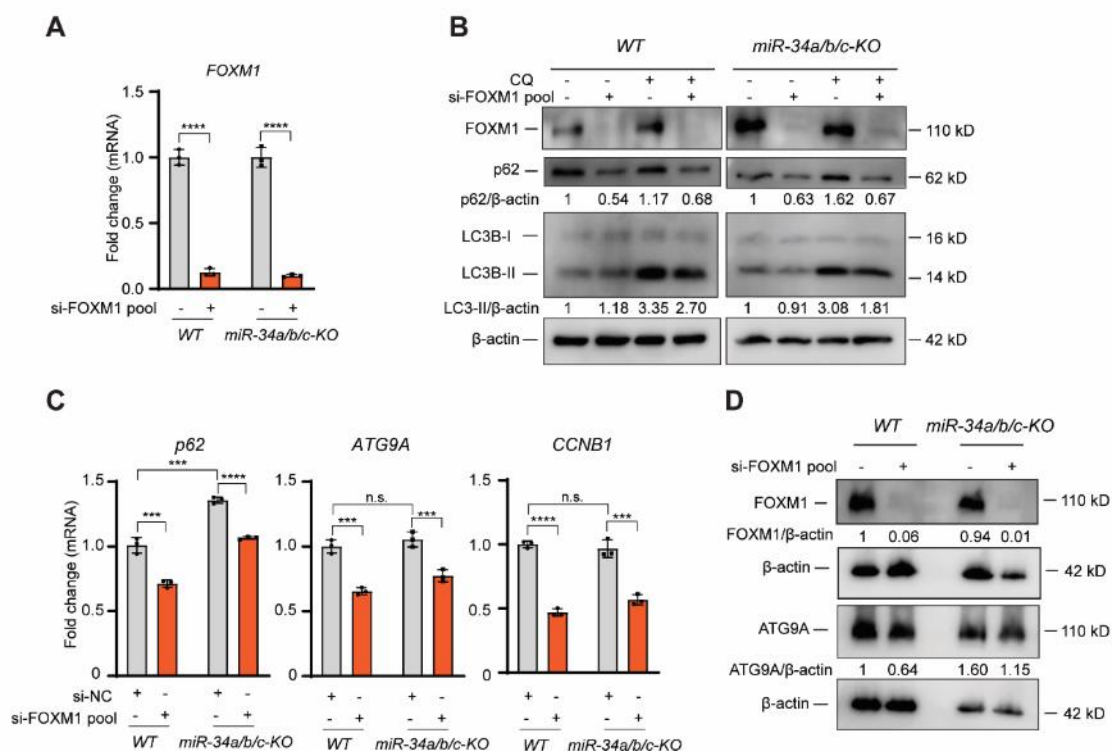


Figure 5.29 (A) qPCR analysis of *FOXM1* after transfection of cells with a 10 nM of si-*FOXM1* pools (specific siRNAs pools targeting *FOXM1*) for 48 h. (B) Western blot analysis of autophagic flux after transfection of cells with a 10 nM si-*FOXM1* pools for 48 h. 20 μ M CQ was introduced 4 hours prior to cell harvesting. (C) qPCR analyses of the specified mRNAs in HCT116 *miR-34a/b/c-KO* or WT cells transfected with si-*FOXM1* pools for 48 h. (D) Immunoblotting analysis of

indicated protein after transfection of cells with si-NC or si-FOXM1 pools for 48 h. Results are presented as the mean \pm SD ($n = 3$) for **A** and **C** with *: $p < 0.05$, **: $p < 0.01$, ***: $p < 0.001$, ****: $p < 0.0001$, n.s.: no significance.

Furthermore, the ectopic expression of FOXM1 in HCT116 wild-type cells significantly elevated the expression of ATG9A and p62 at both the mRNA and protein levels (**Figure 5.30**).

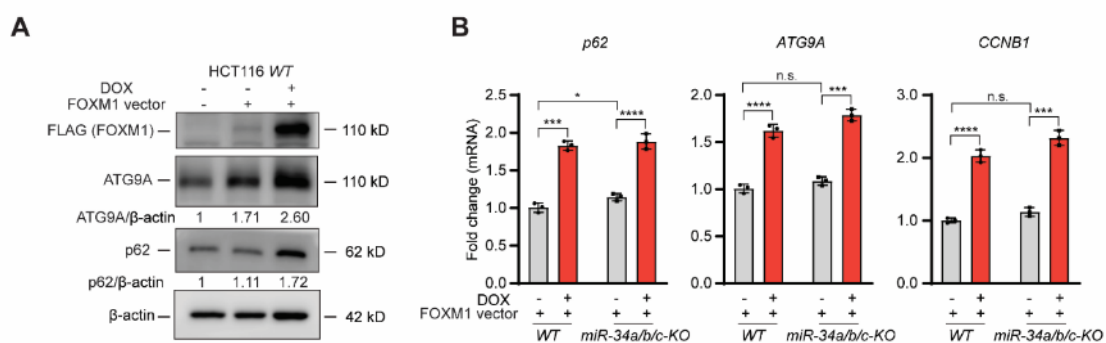


Figure 5.30 (A) Western blot analysis of the specified proteins and (B) qPCR analysis of the specified mRNAs in cells transfected with a FOXM1 expression plasmid and addition of DOX for 48 h. Results are presented as the mean \pm SD ($n = 3$) for **B** with *: $p < 0.05$, **: $p < 0.01$, ***: $p < 0.001$, ****: $p < 0.0001$, n.s.: no significance.

Additionally, the occupancy of FOXM1 at the promoter regions of *ATG9A* and *p62* was detected through querying publicly accessible FOXM1 ChIP-Seq datasets (**Figure 5.31A**) from the Cistrome Data Browser [146]. Given that a FOXM1 binding motif (**Figure 5.31B**) was also identified within the corresponding FOXM1 ChIP-Seq peaks (**Figure 5.31A**), FOXM1 presumably directly interacts with the promoter regions of the *ATG9A* and *p62* genes and modulates their expression. The occupancy of FOXM1 at the promoters of *ATG9A* and *p62* was further corroborated through qChIP experiments (**Figure 5.31C**).

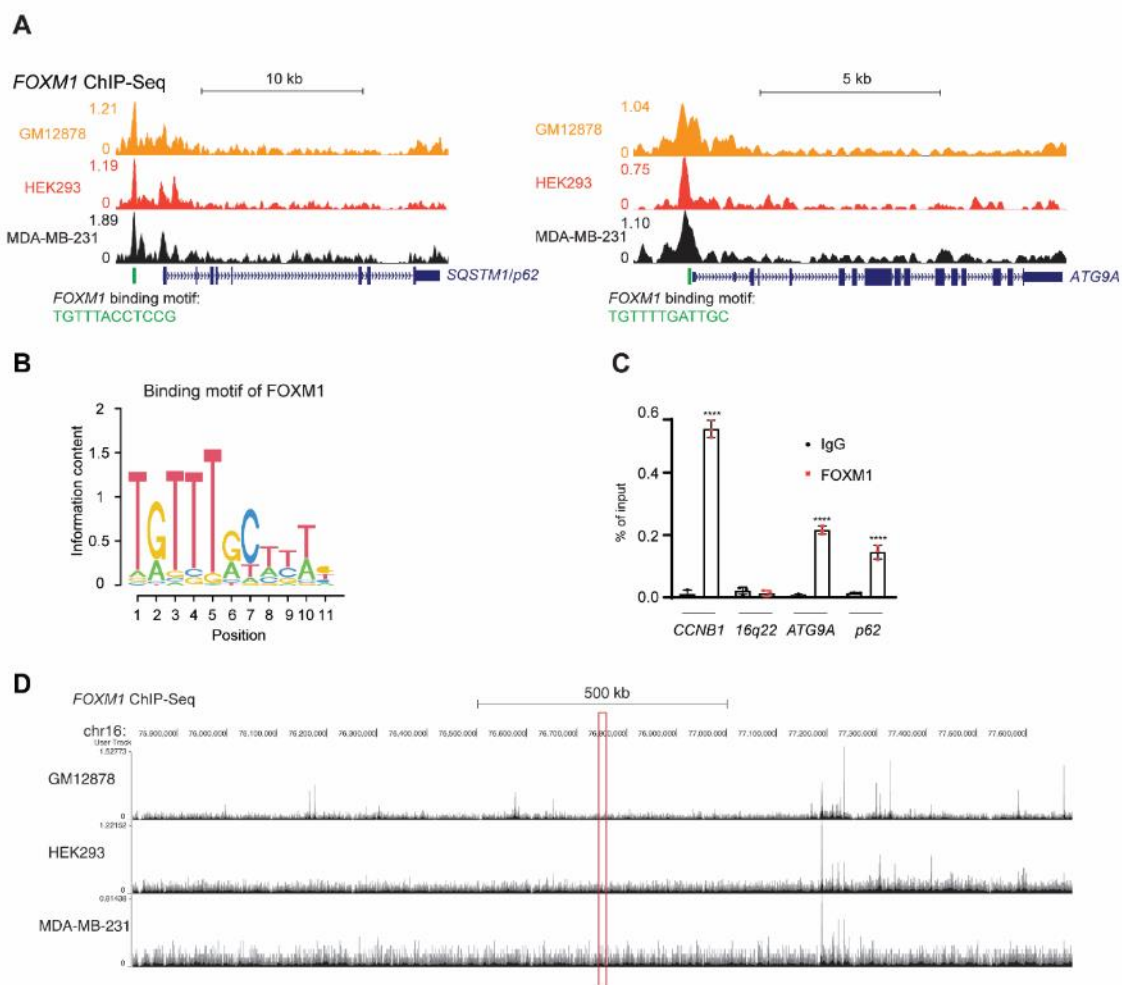


Figure 5.31 (A) A graphical representation from the Cistrome Data Browser showcasing *FOXM1* ChIP-Seq profiles at the genomic loci of *ATG9A* and *p62*. (B) A sequence logo showing the *FOXM1* binding motif from the HOCOMOCO v11 database. (C) qChIP analysis demonstrating the occupancy of *FOXM1* at the promoters of *ATG9A* and *p62*. Chromatin was enriched by anti-rabbit-IgG or anti-*FOXM1* antibodies. *16q22* and *CCNB1* served as negative and positive control, respectively. (D) A depiction from the Cistrome Data Browser showcasing *FOXM1* ChIP-Seq profiles at the genomic locus of *16q22*. The region amplified by the qChIP primers used here (see **Section 3.6.4**) is indicated by a red rectangle. Results are presented as the mean \pm SD ($n = 3$) for **C** with **: $p < 0.01$ and for **D** with ****: $p < 0.0001$.

Notably, the ectopic *FOXM1* expression significantly induced autophagic flux in *miR-34a/b/c*-deficient cells, and effectively counteracted the suppressive effects of *miR-34a* mimics on autophagic flux (**Figure 5.32A**), supporting that *miR-34* inhibits autophagy by repressing *FOXM1*. Given that *miR-34a/b/c* represent

direct targets of p53, we propose a regulatory framework wherein the p53-miR-34 axis negatively modulates autophagy by repressing the expression of multiple autophagy-related genes through a coherent feed-forward regulation. Specifically, miR-34 inhibits autophagy by directly targeting *ATG9A* and *FOXM1* mRNAs, as well as by indirectly repressing the transcription of *ATG9A* and *p62* through targeting *FOXM1* (**Figure 5.32B**).

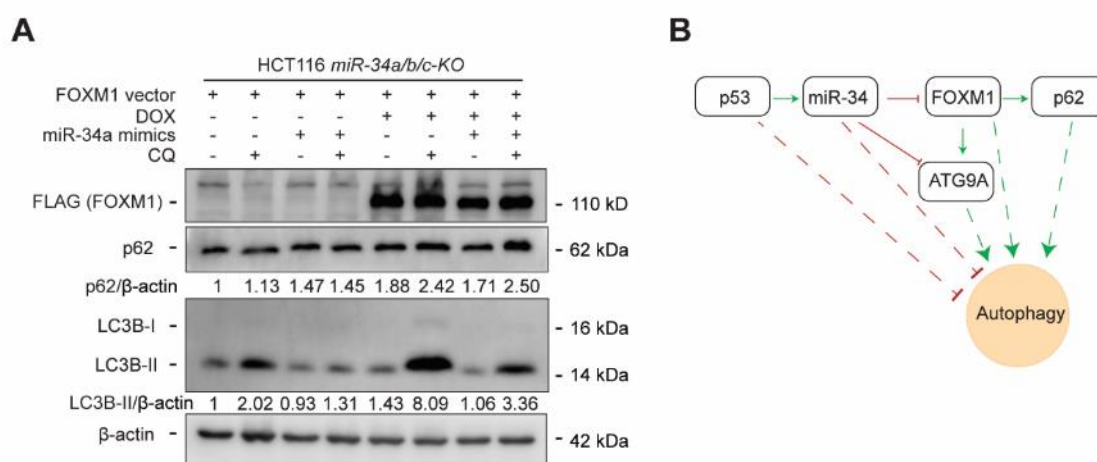


Figure 5.32 (A) Western blot analysis of autophagic flux of *miR-34a/b/c-KO* cells co-transfected with FOXM1 expression plasmid and the indicated miRNAs mimics. 20 μ M CQ was introduced 4 hours prior to cell harvesting. **(B)** A schematic representation elucidating the regulatory interplay between the p53, miR-34, ATG9A FOXM1, and p62.

5.9 Silencing of *ATG9A* in *miR-34a/b/c-KO* cells inhibits autophagic flux and re-sensitizes to 5-FU

We hypothesized that if enhanced autophagy is responsible for the reduced sensitivity of *miR-34a/b/c*-deficient cells to 5-FU, then repression of autophagy should counteract this effect. To evaluate this hypothesis, *ATG9A*, a key mediator of autophagy, was depleted using siRNA pools specifically targeting *ATG9A* mRNA. *ATG9A* was inhibited by ca. 85% at the mRNA level and also effectively at the protein level (**Figure 5.33A, B**). Intriguingly, *ATG9A* protein levels were

elevated in *miR-34a/b/c*-deficient cells but diminished in wild-type cells following treatment with 5-FU, indicating autophagy induction following 5-FU exposure may indeed be mitigated by the repressive effects of *miR-34* on autophagy-related genes (**Figure 5.33B**).

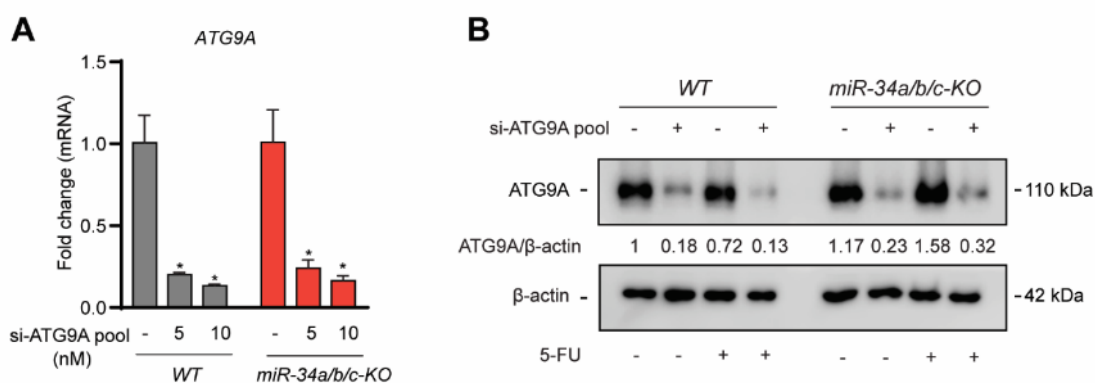


Figure 5.33 (A) qPCR analysis of *ATG9A* after cells transfected with indicated concentration of si-*ATG9A* pools for 48 h. (B) Western blot analysis of *ATG9A* protein after transfection of cells with a 10 nM si-*ATG9A* pools and treated with DMSO or 5-FU for 48 h. Results are presented as the mean \pm SD ($n = 3$) for A with *: $p < 0.05$.

Surprisingly, *ATG9A* silencing elicited only a modest inhibition of 5-FU-induced autophagic flux in wild-type cells, but significantly repressed 5-FU-induced autophagic flux in *miR-34a/b/c*-deficient cells (**Figure 5.34**), indicating *ATG9A* might play a pivotal role in mediating autophagy in *miR-34a/b/c*-deficient cells but not in wild-type cells.

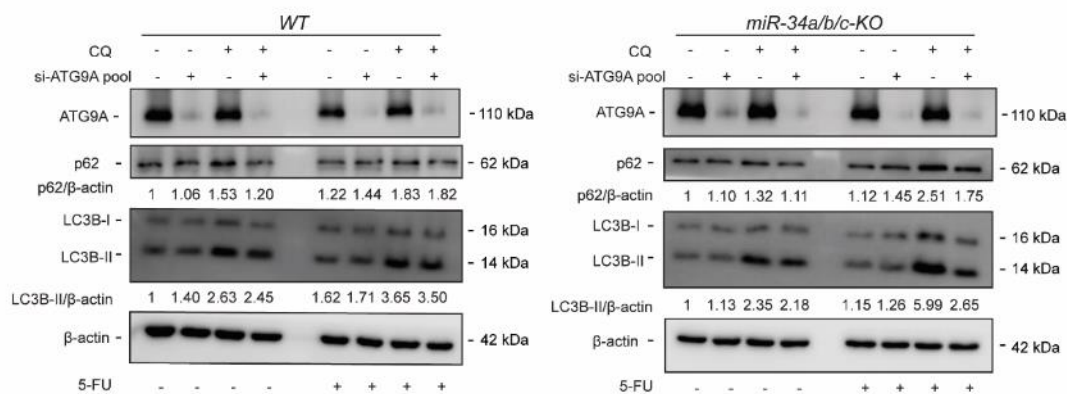


Figure 5.34 Western blot analysis after transfection of cells with a 10 nM si-NC or si-ATG9A pools for 24 h, followed by exposure to DMSO or 5-FU for 48 h. 20 μ M CQ was introduced 4 hours prior to cell harvesting.

Furthermore, cell viability assays revealed that depletion of *ATG9A* significantly re-sensitized *miR-34a/b/c*-deficient cells to 5-FU, but had little impact in wild-type cells (**Figure 5.35A**). In addition, *ATG9A* silencing elevated the protein levels of cleaved-PARP, a hallmark of apoptosis, in *miR-34a/b/c*-deficient cells to a significantly greater degree relative to wild-type cells following 5-FU exposure (**Figure 5.35B**). Collectively, these findings indicate that *ATG9A* plays a critical role in conferring resistance to 5-FU in *miR-34a/b/c*-deficient cells, presumably by increasing autophagy and mitigating apoptosis.

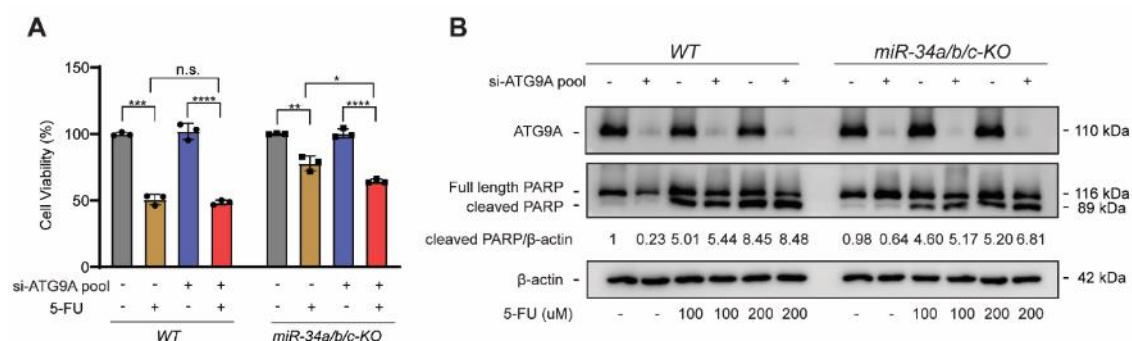


Figure 5.35 (A) After transfection with a 10 nM si-NC or si-ATG9A pools for 48 h, cells were re-seeded into 96-well plates and allowed to incubate for an additional 24 h. Following this, cells were exposed to DMSO or 5-FU for 72 h before

assessing cell viability. **(B)** Immunoblotting analysis of cleaved-PARP after transfection of cells with si-ATG9A pools for 48 h and then exposed to DMSO or 5-FU for 24 h. Results are presented as the mean \pm SD ($n = 3$) for **A** with *: $p < 0.05$, **: $p < 0.01$, ***: $p < 0.001$, ****: $p < 0.0001$, n.s.: no significance.

5.10 Synergistic effects of 5-FU and chloroquine in *miR-34a/b/c-KO* cells

Next, we utilized chloroquine (CQ) as an alternative autophagy inhibitor to explore whether it may also re-sensitize *miR-34a/b/c-KO* cells to 5-FU as observed upon ATG9A silencing. Indeed, the concomitant administration of CQ and 5-FU resulted in a synergistic cytotoxicity in *miR-34a/b/c*-deficient cells, whereas wild-type cells displayed an additive effect (**Figure 5.36A**), as determined by the SynergyFinder 2.0 [168] algorithm. To corroborate the findings from the synergy map, cells were exposed to a dual-drug regimen at concentrations corresponding to the region of highest synergistic score (highlighted by a yellow square in **Figure 5.36A**). Indeed, the combined administration of 2.5 μ M of CQ and 6.25 μ M of 5-FU resulted in a significantly enhanced reduction in cell viability for *miR-34a/b/c*-deficient cells compared to wild-type cells (**Figure 5.36B**). These findings suggest that the 5-FU-resistance of CRC cells with defects in the p53/*miR-34a/b/c* pathway may be attenuated by a combined therapeutic approach involving 5-FU and CQ.

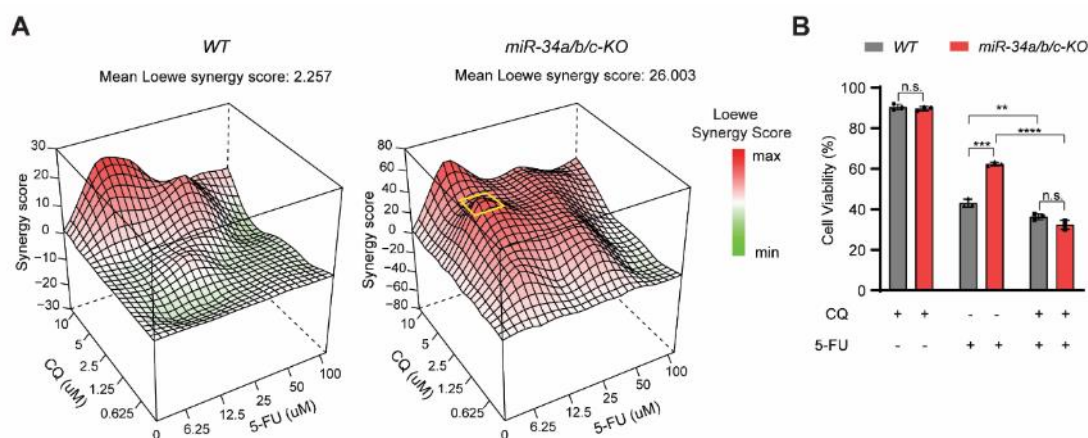


Figure 5.36 (A) Synergistic effects analysis of cells treated with 5-FU and CQ in combination. Following exposure to the specified concentration of 5-FU and/or CQ for 48 h, cells were subjected to cell viability analysis and estimation of Loewe synergy score. The concentration pair exhibiting the highest synergy is demarcated by a yellow square. **(B)** Cell viability assays elucidating the cytotoxic effects of 6.25 μM 5-FU, 2.5 μM CQ, or their combined application. Results are presented as the mean \pm SD ($n = 3$) for **B** with *: $p < 0.05$, **: $p < 0.01$, ***: $p < 0.001$, ****: $p < 0.0001$, n.s.: no significance.

5.11 Clinical relevance of *miR-34a/b/c-KO*-derived gene signatures

Subsequently, we determined the association between *miR-34a/b/c-KO*-derived signatures and the chemotherapeutic response of CRC cells, utilizing the Genomics of Drug Sensitivity in Cancer (GDSC) datasets [167]. We first defined two *miR-34a/b/c-KO*-derived gene signatures ($\Delta miR-34_Up$ and $\Delta miR-34_Down$), which encompass genes that were significantly up- and down-regulated in *miR-34a/b/c*-deficient cells in comparison to wild-type cells. Utilizing the GSVA algorithm, we computed single-sample *miR-34a/b/c-KO*-derived signature scores for CRC cell lines in an unsupervised manner. Intriguingly, the $\Delta miR-34_Up$ signature score exhibited a significant, positive correlation with the IC50 values of 5-FU in CRC cell lines, whereas the $\Delta miR-34_Down$ signature score exhibited no significant correlation (**Figure 5.37**). This suggests that the resistance to 5-FU observed in HCT116 *miR-34a/b/c-KO* cells may also be found in other CRC cell lines that display analogous gene expression profiles.

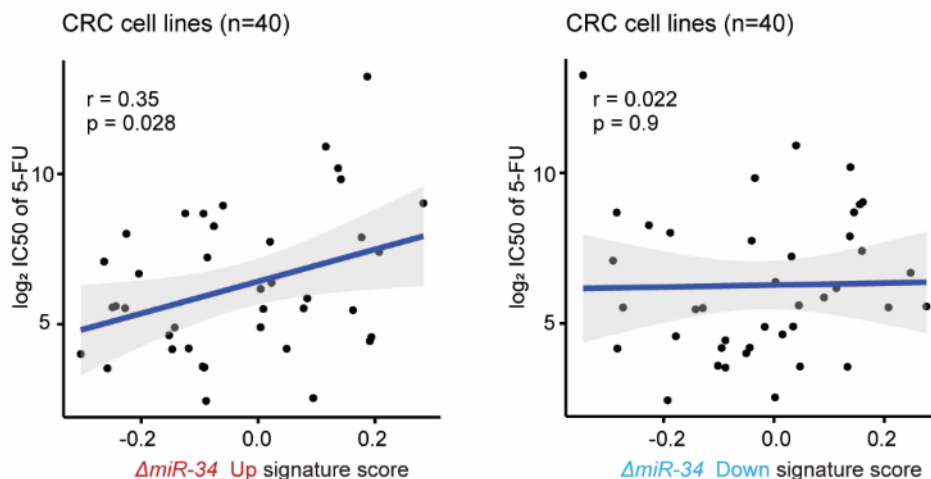


Figure 5.37 Scatter plots elucidating the association between the specified *miR-34a/b/c-KO*-derived signature scores and the IC50 values of 5-FU in CRC cell lines. Two-sided Pearson correlation coefficient r and p values were indicated.

We next explored whether the identified regulatory interaction among *miR-34*, *FOXM1*, *ATG9A* and *p62* is conserved in primary CRCs. To this end, we examined RNA expression datasets available in the TCGA database (TCGA-CRC) ($n=642$) [185]. Notably, the expression of mature *miR-34a* exhibited a significantly negative correlation with both *ATG9A* and *FOXM1*, whereas *FOXM1* manifested a significantly positive correlation with *ATG9A* and *p62* as well as *CCNB1* (**Figure 5.38**), a *bona fide* *FOXM1* target. This suggests that the *FOXM1*-mediated regulation of *ATG9* and *p62* is presumably conserved in primary CRCs. Collectively, these findings indicate that the modulation of autophagy by *miR-34a* through the repression of *FOXM1* may be relevant in primary CRCs.

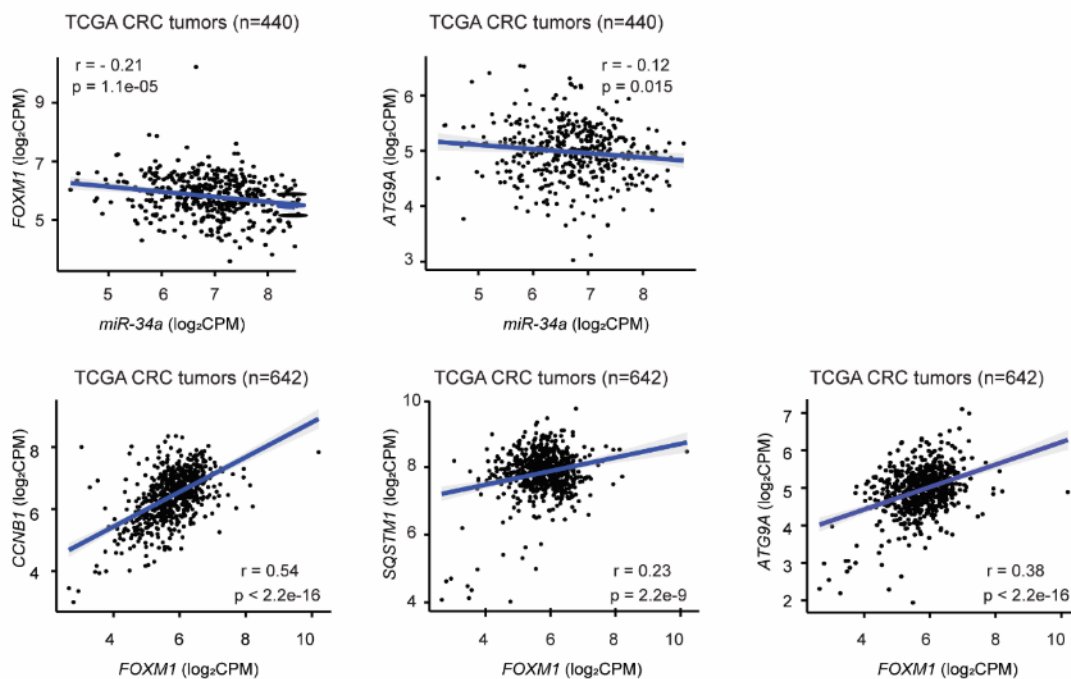


Figure 5.38 Scatter plots delineating the associations between the expressions of the selected genes within the TCGA-CRC patient cohort. Pearson correlation coefficient r and p values were indicated.

Finally, we aimed to explore the associations between the *miR-34a/b/c-KO*-derived gene signatures and the clinical parameters in primary CRC patient cohorts. For this, samples from both the TCGA-CRC and a large, integrated GEO-CRC ($n=1273$) patient cohort [158] were included in this analysis. The GSVA algorithm was once again employed to compute the *miR-34a/b/c-KO*-derived signature scores for CRC patient samples. Consistent with prior findings showing the repression of EMT by miR-34 [65], $\Delta miR-34_Up$ signature scores were highest in CMS4 (**Figure 5.39A**), the consensus molecular subtype (CMS) characteristic for mesenchymal-like CRCs, which are associated with poorest overall patient survival rates [25]. Reinforcing this observation, an analysis using a Cox proportional-hazards model revealed that $\Delta miR-34_Up$ signature scores were significantly correlated with poor overall patient survival in both CRC cohorts,

while $\Delta miR-34_Down$ signature scores exhibited no significant correlation (**Figure 5.39B**), underscoring a tumor suppressive role of miR-34a/b/c. Moreover, $\Delta miR-34_Up$ signature scores were also significantly correlated with poor overall patient survival rates in 17 out of the 33 TCGA cancer types (**Figure 5.39C**), suggesting that these observations may extend beyond CRC, given that inactivation of *p53* and *miR-34a/b/c* is common in many tumor types.

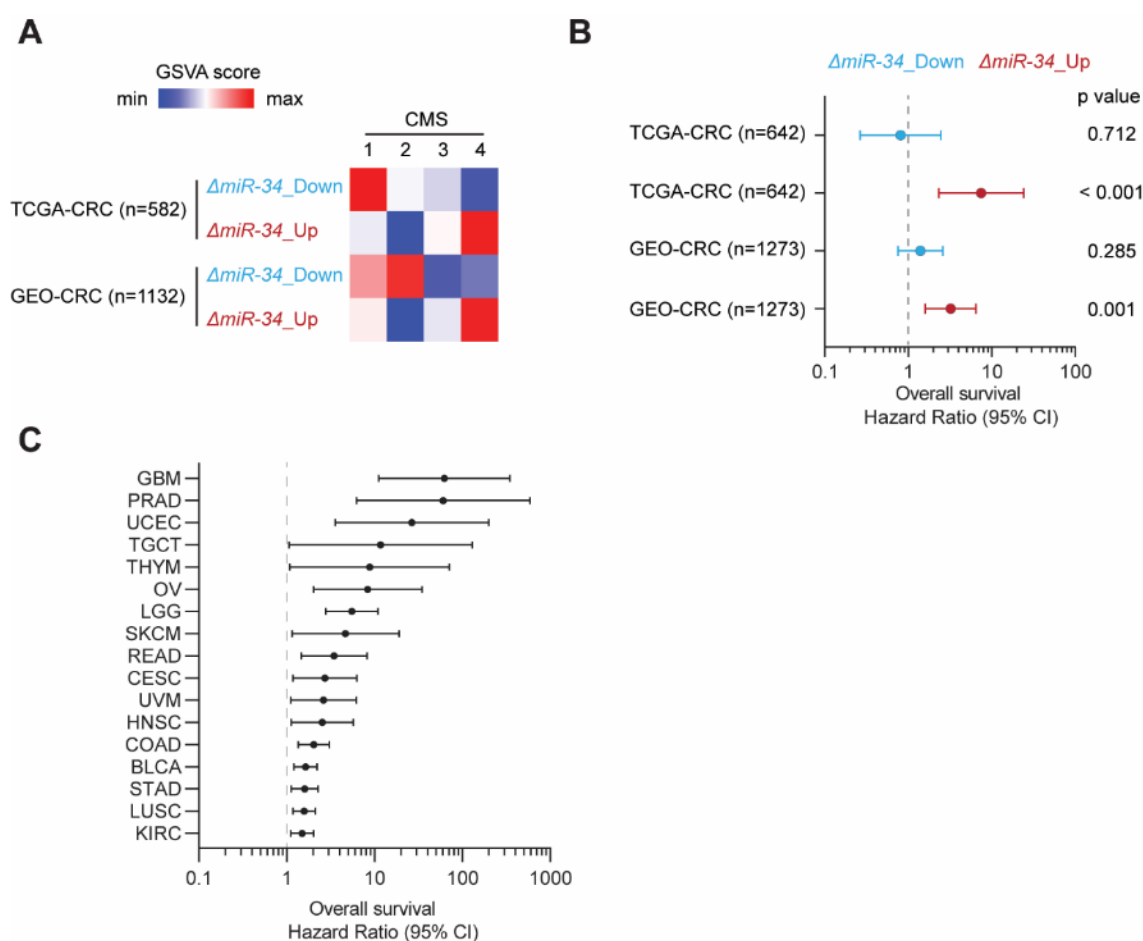


Figure 5.39 (A) The relationship between *miR-34a/b/c*-KO-derived signature scores and the CMS subtypes within the specified CRC patient cohorts (B) The results from the Cox regression model, illustrating the associations of *miR-34a/b/c*-KO-derived signature scores with overall survival in the designated CRC patient groups. (C) The results from the Cox regression model, illustrating the associations of $\Delta miR-34_Up$ signature score with overall patient survival across various TCGA pan-cancer cohorts.

6. Discussion

In this study, we delineate a complementary functional role of *miR-34a* and *miR-34b/c* in modulating various cellular processes that are integral to oncogenesis. Our results show that the concomitant genetic ablation of both *miR-34a* and *miR-34b/c* isoforms led to a significant attenuation in the anti-proliferative effects subsequent to p53 activation. Concurrently, this combined deletion enhances cellular migration and invasion, and induces epithelial-mesenchymal transition (EMT), while concomitantly attenuating cellular responsiveness to chemotherapeutic treatments. Notably, the observed reduction in chemotherapeutic sensitivity was attributable to an augmented stress-induced autophagic flux, concomitant with the transcriptional up-regulation of autophagy-related genes following 5-FU exposure. This induced autophagic activity led to a reduced rate of apoptosis. Importantly, pharmacological and genetic inhibition of autophagy effectively re-sensitized the *miR-34a/b/c*-deficient cells to 5-FU, thereby reinstating their chemotherapeutic vulnerability. Utilizing genome-wide transcriptomic analysis in the HCT116 *miR-34a/b/c*-deficient CRC cell lines, we observed that the absence of *miR-34a/b/c* compromises the gene-repressive functionalities mediated by the p53-DREAM axis, while concomitantly potentiating autophagic responses subsequent to 5-FU exposure. This potentiation of autophagy appears to be orchestrated by the transcription factor FOXM1, a known downstream target of miR-34a/b/c, which is indispensable for the observed autophagy induction, presumably via the transactivation of *SQSTM1/p62* and *ATG9A*. We hereby propose a feed-forward regulatory circuit wherein miR-34 serves as a negative regulator of autophagy, exerting its effects both directly by targeting *FOXM1* and *ATG9A* mRNA, and indirectly by repressing the transcription of *p62* and *ATG9A* via

FOXM1 (Figure 6.1). Intriguingly, a gene signature comprising genes significantly up-regulated consequent to the concomitant deletion of *miR-34a* and *miR-34b/c* exhibited a robust correlation with adverse clinical outcomes and 5-FU resistance. Furthermore, synergistic cytotoxic effects were observed upon the co-administration of autophagy inhibitors and chemotherapeutic agents in a *miR-34*-deficient context. Collectively, these findings not only contribute to the elucidation of the intricate regulatory networks involving p53, miR-34 and FOXM1, but also underscore their prospective clinical implications, particularly with respect to chemoresistance mechanisms.

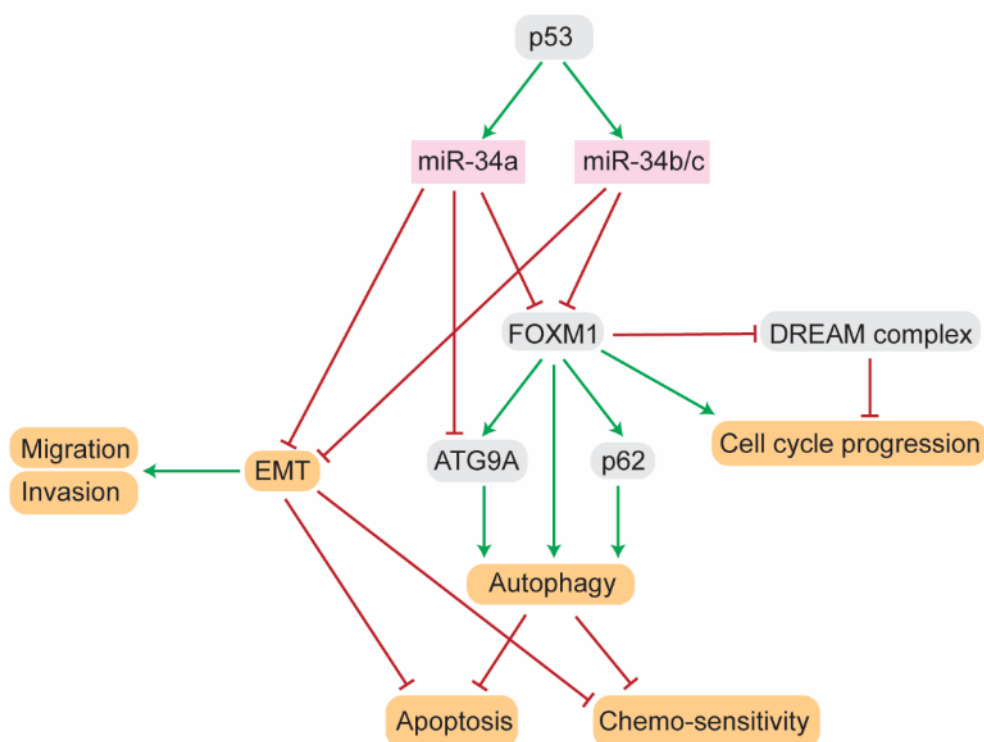


Figure 6.1 A summarizing model of the p53/miR-34/FOXM1/ATG9A/p62 regulatory connections that explains the key processes regulated by miR-34. Green arrow indicates activation. Red line indicates inhibition.

We observed that the combined inactivation of *miR-34a* and *miR-34b/c* in HCT116 CRC cells under non-stress conditions led to a marked increase in cellular migration and invasion capabilities, accompanied by an upregulation of EMT

markers. The induction of SNAIL in *miR-34a/b/c*-deficient cells is presumably due to the loss of its inhibition by miR-34a/b/c, as the *SNAIL* represents a *bona fide* target of miR-34a/b/c [65]. The repression of E-cadherin protein is presumably a consequence of the induction of SNAIL, which directly represses E-cadherin by interacting with the E-boxes present in the *E-cadherin* promoter regions [186, 187]. Further validation of the elevated EMT phenotype was obtained through RNA-Seq analysis, which revealed a significant enrichment of EMT-associated pathways in *miR-34a/b/c*-deficient cells. Moreover, a strong correlation was identified between the $\Delta miR-34_Up$ signature score and reduced survival rates in CRC patients, which is also indicative of induced EMT, given that EMT induction significantly correlates with poor patient survival [188]. Interestingly, the individual deletion of either *miR-34a* or *miR-34b/c* did not yield significant alterations in cellular migration, invasion, or EMT, thereby underscoring the complementary roles of these microRNA isoforms in the regulation of these critical cellular processes. Taken together, these findings elucidate a complementary role of *miR-34a* and *miR-34b/c* in modulating EMT and related oncogenic behaviors, and they highlight the potential clinical implications of miR-34 family inactivation in the prognosis and treatment of CRC.

MiR-34a/b/c have been implied as autophagy repressors by targeting key autophagy mediators, such as *ATG4B* [189], *ATG5* [181], and *ATG9A* [120, 179]. However, these observations were mainly based on overexpression of miRNAs at supraphysiological levels. In this study, we employed a CRISPR/Cas9-mediated genetic approach to ablate the endogenous expression of *miR-34a*, *miR-34b/c*, or both, thereby providing a more physiologically relevant context than previous studies that relied on miRNA overexpression at supraphysiological levels that may exaggerate physiological importance [190]. Our findings reveal that

the concurrent deletion of *miR-34a* and *miR-34b/c* exerts a pronounced impact on the promotion of stress-induced autophagic flux and attenuates the cellular sensitivity to chemotherapeutic agents. In contrast, the individual inactivation of either *miR-34a* or *miR-34b/c* did not confer chemoresistance, underscoring the complementary role of these miRNA isoforms in modulating cellular responses to stress and drug treatment. The diminished chemosensitivity observed in *miR-34a/b/c*-deficient cells is presumably a consequence of enhanced autophagic activity, which serves to elevate the cellular stress threshold necessary for the induction of apoptosis. This is achieved through the removal of damaged mitochondria and other potentially cytotoxic organelles [97]. Intriguingly, our data also suggest that the induction of EMT by the loss of *miR-34a/b/c* may further contribute to reduced chemosensitivity. EMT is a key regulator of the cancer stem cell (CSC) phenotype, which is characterized by heightened resistance to chemotherapeutic agents relative to differentiated cells. Mechanisms underlying CSC-mediated drug resistance include the upregulation of anti-apoptotic proteins, increased expression of ABC/ATP-binding cassette and transmembrane protein transporters that facilitate drug efflux, as well as a slower proliferation rate [191].

Importantly, prior investigations implicating *miR-34a/b/c* as inhibitors of autophagy have mainly relied on methodologies such as immunoblotting or fluorescence detection of LC3 in a steady-state condition. These approaches are limited in their interpretive value, as they neglect the fact that the lysosomal turnover of LC3, rather than the steady-state level of LC3, is a marker of autophagy [192]. The steady-state level of LC3 is not a reliable indicator of autophagic activity, as elevated LC3 levels could either signify the induction of autophagy at an early stage or a blockade of autophagy at a later stage [193]. Therefore, the quantification of autophagic flux, representing the rate of autophagic degradation, is a

more robust measure of autophagic activity [92]. For instance, thapsigargin, an endoplasmic reticulum (ER) stressor, was initially thought to induce autophagy due to its ability to accumulate LC3-positive autophagosomes. However, subsequent research demonstrated that thapsigargin actually inhibits autophagic degradation by preventing the fusion of autophagosomes with lysosomes [194]. In the present study, we utilized two methods to determine autophagic flux, which is a more robust measure of autophagy activity compared to the measurements of the steady level of LC3 [92, 192]. On one hand, we utilized immunoblotting assays to assess the turnover of p62 and LC3-II, thereby providing a quantitative assessment of autophagic activity. In addition, we generated cell lines stably expressing a GFP-LC3-RFP autophagy probe to quantitatively assess the cumulative degradation of GFP-LC3. Our findings reveal that cells deficient in *miR-34a/b/c* consistently exhibit elevated autophagic flux under conditions of chemotherapeutic exposure, starvation, or ER stress. This suggests that miR-34a/b/c plays a critical role in the suppression of stress-induced autophagy, thereby offering a more nuanced understanding of the regulatory mechanisms underlying autophagy and its implications for cancer therapy.

The selection of experimental approaches in gene expression studies can significantly influence the outcomes and insights derived from the research. The importance of this choice cannot be overstated as it lays the foundation for the validity and reliability of the findings obtained. In the realm of gene expression studies, various methodologies have been employed, each with its unique set of advantages and limitations.

Previous studies [52, 53, 195-205] have predominantly employed the overexpression of miR-34a/b/c, achieved through the transfection of cells with miRNA

mimics or expression vectors, and microarray analysis as their preferred experimental approaches for transcriptome profiling to elucidate the functions and mediators of miR-34. As mentioned earlier, one of the primary limitations associated with the overexpression of miRNAs is the potential exaggeration of the physiological importance of miR-34a/b/c. Overexpressing these molecules may not accurately mimic their natural levels and functions within cells, which could result in findings that may not accurately represent physiological conditions. This methodological reliance on over-expression raises concerns regarding the generalizability and applicability of the findings obtained from these studies [190].

In addition to the reliance on overexpression, it is noteworthy that these studies have predominantly employed microarray technology to profile mRNA expressions. Gene expression profiling by microarray enables genome-wide analysis of gene expression, providing a snapshot of the cellular processes occurring at a specific time point. This technique has played a pivotal role in elucidating the functionalities of miR-34 and characterizing its mediators in various contexts, thereby contributing valuable insights to the study of miR-34. However, it is important to acknowledge that while powerful and widely used, microarray technology does have its set of limitations. One of the primary constraints of microarrays is their reliance on a pre-determined set of probes. This reliance limits the range of transcripts that can be assayed, potentially leading to incomplete or biased profiles of gene expression. Furthermore, the values obtained through microarray technology are constrained to a narrower range due to the influence of background signals and the saturation of probe sets. This limitation can impact the sensitivity and accuracy of gene expression measurements, potentially hindering the detection of low-abundance transcripts and subtle changes in gene expression levels [206].

Considering the limitations of microarray technology, the present study has opted for a different experimental approach for gene expression analysis. Specifically, we have employed RNA-Seq technology, a powerful and versatile tool that has revolutionized the field of gene expression studies. RNA-Seq offers several advantages over microarray technology, rendering it the preferred choice for conducting comprehensive genome-wide gene expression analyses. One of the standout features of RNA-Seq is its ability to assay unknown transcripts. Unlike microarrays, RNA-Seq is not bound to a pre-determined set of probes. This characteristic allows for the detection and quantification of a broader spectrum of transcripts, including those that have not been previously identified or characterized. This capability proves to be especially valuable in exploratory studies, where the discovery of novel transcripts can yield fresh insights into cellular processes and functions, potentially uncovering previously uncharted aspects of biology. Furthermore, gene count values derived from RNA-Seq are known for their dynamism, surpassing the constraints often encountered with microarray data. RNA-Seq has the capacity to detect and quantify a wider range of expression levels, spanning from low-abundance transcripts to highly expressed genes. This expanded dynamic range in gene count values significantly enhances the sensitivity and resolution of gene expression analysis. Consequently, RNA-Seq empowers researchers to construct a more comprehensive and accurate profile of gene expression, capturing subtle nuances and variations that may have previously gone undetected [206].

The incorporation of the CRISPR/Cas9 gene editing system and RNA-Seq technology in the present study underscores a deliberate effort to surmount the limitations associated with the overexpression approach and microarray technology. By combining the precision of the CRISPR/Cas9 methodology with the depth

of RNA-Seq analysis, we aimed to provide a more reliable and representative examination of gene expression resulting from the deletion of miR-34a/b/c. This strategic choice contributes a wealth of valuable data and insights to the ongoing discourse surrounding the functionalities and mediators of miR-34. The findings derived from this study, underpinned by the robustness of the CRISPR/Cas9 system and the comprehensive capabilities of RNA-Seq technology, hold the promise of illuminating the intricate functionalities and mediators of miR-34. This enhanced understanding of these molecules and their roles in cellular processes could enrich our knowledge and potentially opens new avenues for therapeutic intervention. In summary, while previous studies have made significant contributions to the field, they have often relied on methodologies that carry the potential to exaggerate the physiological importance of miR-34a/b/c and provide a limited profile of gene expression. In contrast, the present study has effectively addressed these limitations through the adoption of the CRISPR/Cas9 system and RNA-Seq technology, offering a more physiologically relevant and comprehensive analysis of gene expression. This approach not only strengthens the foundation of our knowledge but also paves the way for more precise and nuanced investigations into the roles of miR-34 in various biological contexts.

In addition, utilization of the Gene Set Variation Analysis (GSVA) algorithm in RNA-Seq analysis substantiated the observed increase in autophagic flux in *miR-34a/b/c*-deficient cells following 5-FU exposure. Specifically, the GSVA analysis showed an upregulation of autophagy-associated pathways in these cells, thereby corroborating our empirical findings. Consistently, pathways involved in negative regulation of autophagy and MTORC1 signaling, which also negatively regulates autophagy by preventing ULK1 activation [207], were down-regulated in *miR-34a/b/c*-deficient cells following 5-FU treatment. Additionally, our analysis

indicated a differential upregulation of pathways related to organization of ER and Golgi apparatus in *miR-34a/b/c*-deficient cells following 5-FU exposure. This suggests an enhanced trafficking of proteins and lipids from the Golgi and ER to the isolation membrane, which is a critical step in autophagosome formation [208]. Moreover, pathways associated with mitochondrial function and apoptosis were differentially down-regulated in *miR-34a/b/c-KO* cells following 5-FU exposure. Expectedly, pathways involved in mitochondrial outer membrane permeabilization (MOMP), which is a hallmark of intrinsic apoptosis [209], as well as those related to the release of cytochrome c, which is a known caspase activator [210], were also found to be down-regulated in *miR-34a/b/c*-deficient cells following 5-FU exposure.

Intriguingly, our RNA-Seq data revealed a marked attenuation in the repression of genes associated with cell proliferation in *miR-34a/b/c*-deficient cells following 5-FU treatment. A substantial subset of these genes previously has been characterized as direct targets of the DREAM complex, thereby implicating compromised DREAM complex functionality in the *miR-34a/b/c*-deficient cellular context. Given that the DREAM complex is known to modulate both E2F and FOXM1 target genes through its binding affinity to E2F and CHR binding sites, respectively [134], we observed a concomitant abrogation of repression across both sets of FOXM1 and E2F targets in *miR-34a/b/c*-deficient cells. Furthermore, our analysis indicated that miR-34 modulates several upstream signaling elements that influence the activity of the DREAM complex. Notably, these components exhibited either diminished repression or up-regulation in *miR-34a/b/c*-deficient cells following 5-FU exposure. Among these are CCNE1 (Cyclin E1) [76] and CCNE2 (Cyclin E2) [50]. The upregulation of these cyclins in the absence of *miR-34a/b/c*

presumably enhances the phosphorylation of p130 via CDK2, thereby leading to the disassembly of the DREAM complex [134].

A significant overlap in target genes between DREAM complex and miR-34a/b/c was observed, suggesting a cooperative mechanism of DREAM complex and miR-34a/b/c for gene suppression following p53 activation. Among these shared targets are key transcription factors that modulate DREAM complex activity, including MYBL2 (B-MYB) [211], E2F1 [211], and FOXM1 [141]. These transcription factors were found to be upregulated in *miR-34a/b/c*-deficient cells subsequent to 5-FU treatment. The up-regulation of B-MYB in the context of *miR-34a/b/c* deficiency is posited to compete with the DREAM complex for binding to the MuvB core complex. This competition likely facilitates the assembly of the B-MYB-MuvB-FOXM1 complex, given that the interaction between B-MYB and MuvB is a prerequisite for the recruitment of FOXM1 [212]. Additionally, the observed upregulation of E2F1 in *miR-34a/b/c*-deficient cells appears to counteract the DREAM-mediated repression of E2F target genes. This suggests that the inactivation of *miR-34a/b/c* not only disrupts the repressive function of the DREAM complex but also potentially shifts the cellular equilibrium toward alternative regulatory complexes that promote gene activation.

FOXM1 serves as a pivotal regulator of cell cycle progression [134], and has been identified as a prognostic marker in CRC [213]. In the context of *miR-34a/b/c* deficiency following 5-FU exposure, we observed a significant upregulation of FOXM1. This upregulation is hypothesized to compete with the DREAM complex for binding to the MuvB core complex. As a result, the cellular machinery appears to transition from a DREAM-mediated repressive state to an activated state gov-

erned by the B-MYB-MuvB-FOX M1 complex, thereby exerting opposing regulatory functions [134, 135]. Collectively, these observations suggest that the concomitant loss of *miR-34a/b/c* has a multifaceted impact on biological processes regulation. Specifically, it appears to compromise the repressive capabilities of the DREAM complex while concurrently activating target genes of E2F and FOX M1, particularly in the context of p53 activation. Such a scenario suggests that *miR-34a/b/c* deficiency may lead to a cellular state where the balance of cell cycle regulation is disrupted, potentially promoting uncontrolled cell proliferation and survival. This intricate interplay between *miR-34a/b/c*, the DREAM complex, and FOX M1 provides a more profound understanding of the regulatory landscape following chemotherapeutic intervention and underscores the need for further investigation into these combinatorial effects for therapeutic optimization.

In addition, FOX M1 is not only a recognized autophagy inducer [136, 137], but also a known target of *miR-34a* [141], positioning it as a likely central effector of *miR-34* in this context. In this study, we extend this understanding by demonstrating that FOX M1 is also a direct target of *miR-34b* and *miR-34c*. This comprehensive targeting by the *miR-34* family underscores the significance of FOX M1 in *miR-34*-mediated regulatory networks. Importantly, the observed increase in autophagic flux following the deletion of *miR-34a/b/c* can be attributed, at least in part, to the upregulation of FOX M1. To further elucidate the role of FOX M1 in modulating autophagic activity, we conducted experiments involving the depletion and ectopic expression of FOX M1. Our data revealed a significant reduction in autophagic flux upon the depletion of FOX M1, whereas its ectopic expression resulted in a marked increase in autophagic flux. These findings provide compelling evidence for the pivotal role of FOX M1 in regulating autophagic activity, particularly in the context of *miR-34a/b/c* deficiency.

In this study, we elucidate that FOXM1 promotes autophagy, presumably by transactivating its target genes, *ATG9A* and *p62*. Notably, p62 serves as a critical autophagy receptor [214], and functions as an intersection between the ubiquitin-proteasome system and autophagy. It accomplishes this by linking these two principal cellular quality control mechanisms responsible for degradation of proteins and organelles in eukaryotic cells via its LC3-binding and ubiquitin-associated domains, which enable it to interact with LC3 and ubiquitinated cargo, respectively [215]. The up-regulation of *p62* caused by the dysregulation of *miR-34/FOXM1* axis presumably has dual implications: it not only augments autophagic activity but also potentially disrupts proteasomal function, thereby affecting cellular homeostasis.

Interestingly, the induction of p62 due to elevated FOXM1 expression could have further-reaching consequences in cellular stress responses. Specifically, it could activate the transcription factor NRF2, which is a master regulator of the cellular antioxidant response [216]. The activation of NRF2 occurs through p62's interaction with the NRF2-binding site on Keap1, which is a component of the Cullin-3-type ubiquitin ligase complex responsible for the degradation of NRF2 [217]. The stabilization of NRF2 via p62 interaction leads to enhanced expression of antioxidant proteins through NRF2's binding to antioxidant response elements (AREs) in the promoter regions of genes encoding cytoprotective proteins [218]. This NRF2 activation could confer a protective advantage to cancer cells against chemotherapeutic agents, thereby facilitating tumor progression [219]. This dual role of p62 in autophagy and the antioxidant response highlights its multifaceted role in cellular homeostasis and adaptation to stress.

ATG9A, an integral component of the autophagy machinery, has the unique distinction of being the sole transmembrane protein within the core autophagy machinery [220]. In the context of autophagy, ATG9A plays a pivotal role by being integrated into a specialized vesicle known as the ATG9A vesicle, which has a critical role in the early stages of autophagosome formation. Upon the induction of autophagy, the ATG9A vesicle is recruited to the pre-autophagosomal structure (PAS), functioning as the initial membrane source for the formation of the isolation membrane, also referred to as the phagophore [221, 222]. The phagophore is the precursor structure that eventually engulfs the cellular cargo targeted for degradation within the autophagosome. Concurrently, ATG9A relocates to the expanding periphery of the isolation membrane in coordination with the ATG2-ATG18 complex, another essential component of the autophagy machinery. This relocation establishes a contact site with the endoplasmic reticulum (ER) exit site [223, 224], where ATG2 is involved in phospholipid acquisition [225]. In essence, ATG9A vesicles act as nucleation points that facilitate the formation of autophagosomes by establishing critical contact sites and supplying the initial membrane components required for this *de novo* biogenesis process [226, 227].

Given this pivotal role of ATG9A in the *de novo* formation of autophagosomes, its down-regulation mediated by miR-34 could conceivably impair the formation and expansion of autophagosomes, thereby inhibiting autophagy. Notably, an inverse correlation was observed between the expression levels of mature miR-34a and the levels of both *ATG9A* and *FOXM1*. Conversely, *FOXM1* exhibited a significant positive correlation with the expression levels of *ATG9A* and *p62* in the TCGA-CRC patient cohort. The observed correlations between miR-34a, *FOXM1*, *p62*, and *ATG9A* suggest that such regulatory interactions may also ex-

ist in primary CRCs, underscoring the potential clinical relevance of these findings. It is plausible that miR-34a, by targeting both FOXM1 and ATG9A, exerts a regulatory influence on autophagy in CRC. The role of FOXM1 in regulating autophagy-related genes and its positive correlation with ATG9A, a core component of autophagy machinery, and p62, a key receptor of autophagy, hint at a potential regulatory loop that merits further investigation. Further investigations into these regulatory networks are essential for unraveling the intricate mechanisms of autophagy in CRC and for developing targeted therapies that leverage these insights for clinical benefit.

Chloroquine (CQ) and its derivative, hydroxychloroquine, are pharmacological agents traditionally employed in the treatment of malaria [228], amebiasis [229] and various rheumatoid conditions [230]. Critically, beyond their conventional applications, these drugs have attracted attention for their unique property of inhibiting autophagy. Specifically, CQ has been identified as a potent inhibitor of autophagy, acting at a late stage by obstructing the fusion between autophagosomes and lysosomes [231]. This property has led to its exploration in clinical trials as a potential anti-cancer therapeutic [232, 233]. One of the intriguing aspects of CQ's potential in cancer therapy is its ability to enhance the cytotoxic effects of chemotherapeutic agents, including 5-FU, in various cancer cell lines [234, 235]. 5-FU, a pyrimidine analog, is widely used in the treatment of CRC. It exerts its cytotoxic effects by disrupting DNA and RNA synthesis, ultimately leading to cell death [19]. Given the previous promising results of CQ in combination with 5-FU, our study aimed to elucidate the underlying mechanisms of this synergy and assess its relevance in the context of CRC. Our results unveiled a remarkable discrepancy in the cytotoxic response to the combination of CQ and 5-FU depending on the miR-34a/b/c expression status in CRC cells. Our findings

indicated that the co-administration of 5-FU and CQ resulted in a synergistic cytotoxic effect specifically in the context of *miR-34a/b/c* deficiency. In contrast, a merely additive effect was noted in CRC cells with proficient *miR-34a/b/c* expression. This intriguing observation suggests that the inactivation or silencing of *miR-34a/b/c* may render tumor cells more susceptible to autophagy inhibition.

The potential mechanisms underlying this observed synergy could be a higher dependence of autophagy for survival in cancer cells deficient in *miR-34a/b/c*. *MiR-34a/b/c* have been implicated in the negative regulation of autophagy [120, 123, 189, 236]. Their down-regulation in cancer cells leads to increased autophagic activity, making these cells more reliant on autophagy for survival. Consequently, the inhibition of autophagy by CQ could have a more pronounced cytotoxic effect in *miR-34a/b/c*-deficient cells.

Moreover, our study raises important questions about the broader implications of this synergistic cytotoxicity. Given the significance of autophagy in cancer biology and therapy, it is essential to explore whether similar combinations of autophagy inhibitors and 5-FU analogs exhibit analogous effects in tumor cells with defects in the p53/*miR-34a/b/c* signaling pathway. This avenue of research could unveil novel strategies for enhancing the efficacy of chemotherapy in various cancer types with compromised p53/*miR-34a/b/c* function.

Furthermore, the clinical translation of our findings warrants careful consideration. While our study provides valuable insights into the potential therapeutic synergy between CQ and 5-FU in specific CRC contexts, it is crucial to acknowledge the complexity of cancer biology. Clinical trials should be designed

to evaluate the safety and efficacy of such combination therapies in human patients, taking into account the heterogeneity of tumors and the potential for off-target effects.

7. References

1. Sung, H., et al., *Global Cancer Statistics 2020: GLOBOCAN Estimates of Incidence and Mortality Worldwide for 36 Cancers in 185 Countries*. CA Cancer J Clin, 2021. **71**(3): p. 209-249.
2. Dekker, E., et al., *Colorectal cancer*. Lancet, 2019. **394**(10207): p. 1467-1480.
3. Van Cutsem, E., et al., *Towards a pan-European consensus on the treatment of patients with colorectal liver metastases*. Eur J Cancer, 2006. **42**(14): p. 2212-21.
4. Yoo, P.S., et al., *Liver resection for metastatic colorectal cancer in the age of neoadjuvant chemotherapy and bevacizumab*. Clin Colorectal Cancer, 2006. **6**(3): p. 202-7.
5. Dawood, O., A. Mahadevan, and K.A. Goodman, *Stereotactic body radiation therapy for liver metastases*. Eur J Cancer, 2009. **45**(17): p. 2947-59.
6. Siegel, R.L., et al., *Cancer statistics, 2023*. CA Cancer J Clin, 2023. **73**(1): p. 17-48.
7. Nassar, D. and C. Blanpain, *Cancer Stem Cells: Basic Concepts and Therapeutic Implications*. Annu Rev Pathol, 2016. **11**: p. 47-76.
8. Raskov, H., et al., *Driver Gene Mutations and Epigenetics in Colorectal Cancer*. Ann Surg, 2020. **271**(1): p. 75-85.
9. East, J.E., et al., *British Society of Gastroenterology position statement on serrated polyps in the colon and rectum*. Gut, 2017. **66**(7): p. 1181-1196.
10. Hampel, H., et al., *Feasibility of screening for Lynch syndrome among patients with colorectal cancer*. J Clin Oncol, 2008. **26**(35): p. 5783-8.
11. Raskov, H., et al., *Colorectal carcinogenesis--update and perspectives*. World J Gastroenterol, 2014. **20**(48): p. 18151-64.
12. Alberts, S.R., et al., *Oxaliplatin, fluorouracil, and leucovorin for patients with unresectable liver-only metastases from colorectal cancer: a North Central Cancer Treatment Group phase II study*. J Clin Oncol, 2005. **23**(36): p. 9243-9.
13. Kopetz, S., et al., *Randomized Trial of Irinotecan and Cetuximab With or Without Vemurafenib in BRAF-Mutant Metastatic Colorectal Cancer (SWOG S1406)*. J Clin Oncol, 2021. **39**(4): p. 285-294.
14. Kopetz, S., et al., *Encorafenib, Binimetinib, and Cetuximab in BRAF V600E-Mutated Colorectal Cancer*. N Engl J Med, 2019. **381**(17): p. 1632-1643.
15. Grothey, A., et al., *Regorafenib monotherapy for previously treated metastatic colorectal cancer (CORRECT): an international, multicentre, randomised, placebo-controlled, phase 3 trial*. Lancet, 2013. **381**(9863): p. 303-12.
16. Mayer, R.J., et al., *Randomized trial of TAS-102 for refractory metastatic colorectal cancer*. N Engl J Med, 2015. **372**(20): p. 1909-19.
17. Kasi, P.M., et al., *Chemotherapy induced neutropenia at 1-month mark is a predictor of overall survival in patients receiving TAS-102 for refractory metastatic colorectal cancer: a cohort study*. BMC Cancer, 2016. **16**: p. 467.
18. Holch, J., S. Stintzing, and V. Heinemann, *Treatment of Metastatic Colorectal Cancer: Standard of Care and Future Perspectives*. Visc Med, 2016. **32**(3): p. 178-83.
19. Longley, D.B., D.P. Harkin, and P.G. Johnston, *5-fluorouracil: mechanisms of action and clinical strategies*. Nat Rev Cancer, 2003. **3**(5): p. 330-8.
20. Biegging, K.T., S.S. Mello, and L.D. Attardi, *Unravelling mechanisms of p53-mediated tumour suppression*. Nat Rev Cancer, 2014. **14**(5): p. 359-70.
21. Goldberg, R.M., et al., *A randomized controlled trial of fluorouracil plus leucovorin, irinotecan, and oxaliplatin combinations in patients with previously untreated metastatic colorectal cancer*. J Clin Oncol, 2004. **22**(1): p. 23-30.
22. Vodenkova, S., et al., *5-fluorouracil and other fluoropyrimidines in colorectal cancer: Past, present and future*. Pharmacol Ther, 2020. **206**: p. 107447.

23. Weng, J., et al., *Exploring immunotherapy in colorectal cancer*. J Hematol Oncol, 2022. **15**(1): p. 95.
24. Xie, Y.H., Y.X. Chen, and J.Y. Fang, *Comprehensive review of targeted therapy for colorectal cancer*. Signal Transduct Target Ther, 2020. **5**(1): p. 22.
25. Guinney, J., et al., *The consensus molecular subtypes of colorectal cancer*. Nat Med, 2015. **21**(11): p. 1350-6.
26. Stahler, A., et al., *Consensus Molecular Subtypes as Biomarkers of Fluorouracil and Folinic Acid Maintenance Therapy With or Without Panitumumab in RAS Wild-Type Metastatic Colorectal Cancer (PanaMa, AIO KRK 0212)*. J Clin Oncol, 2023. **41**(16): p. 2975-2987.
27. Ten Hoorn, S., et al., *Clinical Value of Consensus Molecular Subtypes in Colorectal Cancer: A Systematic Review and Meta-Analysis*. J Natl Cancer Inst, 2022. **114**(4): p. 503-516.
28. Hainaut, P. and G.P. Pfeifer, *Somatic TP53 Mutations in the Era of Genome Sequencing*. Cold Spring Harb Perspect Med, 2016. **6**(11).
29. Engeland, K., *Cell cycle regulation: p53-p21-RB signaling*. Cell Death Differ, 2022. **29**(5): p. 946-960.
30. Rufini, A., et al., *Senescence and aging: the critical roles of p53*. Oncogene, 2013. **32**(43): p. 5129-43.
31. Williams, A.B. and B. Schumacher, *p53 in the DNA-Damage-Repair Process*. Cold Spring Harb Perspect Med, 2016. **6**(5).
32. Aubrey, B.J., et al., *How does p53 induce apoptosis and how does this relate to p53-mediated tumour suppression?* Cell Death Differ, 2018. **25**(1): p. 104-113.
33. Chang, C.J., et al., *p53 regulates epithelial-mesenchymal transition and stem cell properties through modulating miRNAs*. Nat Cell Biol, 2011. **13**(3): p. 317-23.
34. Tasdemir, E., et al., *Regulation of autophagy by cytoplasmic p53*. Nat Cell Biol, 2008. **10**(6): p. 676-87.
35. Hernández Borrero, L.J. and W.S. El-Deiry, *Tumor suppressor p53: Biology, signaling pathways, and therapeutic targeting*. Biochim Biophys Acta Rev Cancer, 2021. **1876**(1): p. 188556.
36. Bode, A.M. and Z. Dong, *Post-translational modification of p53 in tumorigenesis*. Nat Rev Cancer, 2004. **4**(10): p. 793-805.
37. Hermeking, H., *MicroRNAs in the p53 network: micromanagement of tumour suppression*. Nat Rev Cancer, 2012. **12**(9): p. 613-26.
38. Sachdeva, M., et al., *p53 represses c-Myc through induction of the tumor suppressor miR-145*. Proc Natl Acad Sci U S A, 2009. **106**(9): p. 3207-12.
39. Kim, T., et al., *p53 regulates epithelial-mesenchymal transition through microRNAs targeting ZEB1 and ZEB2*. J Exp Med, 2011. **208**(5): p. 875-83.
40. Suzuki, H.I., et al., *Modulation of microRNA processing by p53*. Nature, 2009. **460**(7254): p. 529-33.
41. Bartel, D.P., *Metazoan MicroRNAs*. Cell, 2018. **173**(1): p. 20-51.
42. Lee, R.C., R.L. Feinbaum, and V. Ambros, *The C. elegans heterochronic gene lin-4 encodes small RNAs with antisense complementarity to lin-14*. Cell, 1993. **75**(5): p. 843-54.
43. Lee, R.C. and V. Ambros, *An extensive class of small RNAs in Caenorhabditis elegans*. Science, 2001. **294**(5543): p. 862-4.
44. Lau, N.C., et al., *An abundant class of tiny RNAs with probable regulatory roles in Caenorhabditis elegans*. Science, 2001. **294**(5543): p. 858-62.

45. Calin, G.A., et al., *Frequent deletions and down-regulation of micro- RNA genes miR15 and miR16 at 13q14 in chronic lymphocytic leukemia*. Proc Natl Acad Sci U S A, 2002. **99**(24): p. 15524-9.
46. Cimmino, A., et al., *miR-15 and miR-16 induce apoptosis by targeting BCL2*. Proc Natl Acad Sci U S A, 2005. **102**(39): p. 13944-9.
47. Calin, G.A., et al., *MiR-15a and miR-16-1 cluster functions in human leukemia*. Proc Natl Acad Sci U S A, 2008. **105**(13): p. 5166-71.
48. Peng, Y. and C.M. Croce, *The role of MicroRNAs in human cancer*. Signal Transduct Target Ther, 2016. **1**: p. 15004.
49. Tarasov, V., et al., *Differential regulation of microRNAs by p53 revealed by massively parallel sequencing: miR-34a is a p53 target that induces apoptosis and G1-arrest*. Cell Cycle, 2007. **6**(13): p. 1586-93.
50. He, L., et al., *A microRNA component of the p53 tumour suppressor network*. Nature, 2007. **447**(7148): p. 1130-4.
51. Raver-Shapira, N., et al., *Transcriptional activation of miR-34a contributes to p53-mediated apoptosis*. Molecular cell, 2007. **26**(5): p. 731-43.
52. Chang, T.-C., et al., *Transactivation of miR-34a by p53 broadly influences gene expression and promotes apoptosis*. Molecular cell, 2007. **26**(5): p. 745-52.
53. Bommer, G.T., et al., *p53-mediated activation of miRNA34 candidate tumor-suppressor genes*. Curr Biol, 2007. **17**(15): p. 1298-307.
54. Corney, D.C., et al., *MicroRNA-34b and MicroRNA-34c are targets of p53 and cooperate in control of cell proliferation and adhesion-independent growth*. Cancer Res, 2007. **67**(18): p. 8433-8.
55. Hermeking, H., *The miR-34 family in cancer and apoptosis*. Cell Death Differ, 2010. **17**(2): p. 193-9.
56. Wong, K.Y., L. Yu, and C.S. Chim, *DNA methylation of tumor suppressor miRNA genes: a lesson from the miR-34 family*. Epigenomics, 2011. **3**(1): p. 83-92.
57. Rokavec, M., et al., *The p53/miR-34 axis in development and disease*. J Mol Cell Biol, 2014. **6**(3): p. 214-30.
58. Su, X., et al., *TAp63 suppresses metastasis through coordinate regulation of Dicer and miRNAs*. Nature, 2010. **467**(7318): p. 986-90.
59. Agostini, M., et al., *Neuronal differentiation by TAp73 is mediated by microRNA-34a regulation of synaptic protein targets*. Proc Natl Acad Sci U S A, 2011. **108**(52): p. 21093-8.
60. Yamakuchi, M., M. Ferlito, and C.J. Lowenstein, *miR-34a repression of SIRT1 regulates apoptosis*. Proc Natl Acad Sci USA, 2008. **105**(36): p. 13421-6.
61. Navarro, F. and J. Lieberman, *miR-34 and p53: New Insights into a Complex Functional Relationship*. PLoS One, 2015. **10**(7): p. e0132767.
62. Okada, N., et al., *A positive feedback between p53 and miR-34 miRNAs mediates tumor suppression*. Genes Dev, 2014. **28**(5): p. 438-50.
63. Christoffersen, N.R., et al., *p53-independent upregulation of miR-34a during oncogene-induced senescence represses MYC*. Cell Death Differ, 2010. **17**(2): p. 236-45.
64. Pulikkan, J.A., et al., *C/EBP α regulated microRNA-34a targets E2F3 during granulopoiesis and is down-regulated in AML with CEBPA mutations*. Blood, 2010. **116**(25): p. 5638-49.
65. Siemens, H., et al., *miR-34 and SNAIL form a double-negative feedback loop to regulate epithelial-mesenchymal transitions*. Cell Cycle, 2011. **10**(24): p. 4256-71.
66. Rokavec, M., et al., *IL-6R/STAT3/miR-34a feedback loop promotes EMT-mediated colorectal cancer invasion and metastasis*. J Clin Invest, 2014. **124**(4): p. 1853-67.

67. Kress, T.R., et al., *The MK5/PRAK kinase and Myc form a negative feedback loop that is disrupted during colorectal tumorigenesis*. Mol Cell, 2011. **41**(4): p. 445-57.
68. Masui, K., et al., *mTOR complex 2 controls glycolytic metabolism in glioblastoma through FoxO acetylation and upregulation of c-Myc*. Cell Metab, 2013. **18**(5): p. 726-39.
69. Welch, C., Y. Chen, and R.L. Stallings, *MicroRNA-34a functions as a potential tumor suppressor by inducing apoptosis in neuroblastoma cells*. Oncogene, 2007. **26**(34): p. 5017-22.
70. Lodygin, D., et al., *Inactivation of miR-34a by aberrant CpG methylation in multiple types of cancer*. Cell Cycle, 2008. **7**(16): p. 2591-600.
71. Vogt, M., et al., *Frequent concomitant inactivation of miR-34a and miR-34b/c by CpG methylation in colorectal, pancreatic, mammary, ovarian, urothelial, and renal cell carcinomas and soft tissue sarcomas*. Virchows Arch, 2011. **458**(3): p. 313-22.
72. Hermeking, H., *The miR-34 family in cancer and apoptosis*. Cell death and differentiation, 2010. **17**(2): p. 193-9.
73. Li, W.J., et al., *MicroRNA-34a: Potent Tumor Suppressor, Cancer Stem Cell Inhibitor, and Potential Anticancer Therapeutic*. Front Cell Dev Biol, 2021. **9**: p. 640587.
74. Hermeking, H., *p53 enters the microRNA world*. Cancer Cell, 2007. **12**(5): p. 414-8.
75. Sun, F., et al., *Downregulation of CCND1 and CDK6 by miR-34a induces cell cycle arrest*. FEBS letters, 2008. **582**(10): p. 1564-8.
76. Han, Z., et al., *miR-497 and miR-34a retard lung cancer growth by co-inhibiting cyclin E1 (CCNE1)*. Oncotarget, 2015. **6**(15): p. 13149-63.
77. Jiang, L. and H. Hermeking, *miR-34a and miR-34b/c Suppress Intestinal Tumorigenesis*. Cancer Res, 2017. **77**(10): p. 2746-2758.
78. Öner, M.G., et al., *Combined Inactivation of TP53 and MIR34A Promotes Colorectal Cancer Development and Progression in Mice Via Increasing Levels of IL6R and PAI1*. Gastroenterology, 2018. **155**(6): p. 1868-1882.
79. Siemens, H., et al., *Detection of miR-34a promoter methylation in combination with elevated expression of c-Met and β -catenin predicts distant metastasis of colon cancer*. Clin Cancer Res, 2013. **19**(3): p. 710-20.
80. Mehlen, P. and A. Puisieux, *Metastasis: a question of life or death*. Nat Rev Cancer, 2006. **6**(6): p. 449-58.
81. Mittal, V., *Epithelial Mesenchymal Transition in Tumor Metastasis*. Annu Rev Pathol, 2018. **13**: p. 395-412.
82. Thiery, J.P., *Epithelial-mesenchymal transitions in tumour progression*. Nat Rev Cancer, 2002. **2**(6): p. 442-54.
83. Zhang, N., et al., *Novel therapeutic strategies: targeting epithelial-mesenchymal transition in colorectal cancer*. Lancet Oncol, 2021. **22**(8): p. e358-e368.
84. Nieto, M.A., et al., *EMT: 2016*. Cell, 2016. **166**(1): p. 21-45.
85. Lamouille, S., J. Xu, and R. Derynck, *Molecular mechanisms of epithelial-mesenchymal transition*. Nat Rev Mol Cell Biol, 2014. **15**(3): p. 178-96.
86. Kaufhold, S. and B. Bonavida, *Central role of Snail1 in the regulation of EMT and resistance in cancer: a target for therapeutic intervention*. J Exp Clin Cancer Res, 2014. **33**(1): p. 62.
87. Yang, J., et al., *Twist, a master regulator of morphogenesis, plays an essential role in tumor metastasis*. Cell, 2004. **117**(7): p. 927-39.
88. Sánchez-Tilló, E., et al., *ZEB1 represses E-cadherin and induces an EMT by recruiting the SWI/SNF chromatin-remodeling protein BRG1*. Oncogene, 2010. **29**(24): p. 3490-500.
89. Amack, J.D., *Cellular dynamics of EMT: lessons from live in vivo imaging of embryonic development*. Cell Commun Signal, 2021. **19**(1): p. 79.

90. Parfenyev, S., et al., *Interplay between p53 and non-coding RNAs in the regulation of EMT in breast cancer*. Cell Death Dis, 2021. **12**(1): p. 17.
91. Mizushima, N. and B. Levine, *Autophagy in Human Diseases*. N Engl J Med, 2020. **383**(16): p. 1564-1576.
92. Mizushima, N. and L.O. Murphy, *Autophagy Assays for Biological Discovery and Therapeutic Development*. Trends Biochem Sci, 2020. **45**(12): p. 1080-1093.
93. Klionsky, D.J., et al., *Autophagy in major human diseases*. Embo j, 2021. **40**(19): p. e108863.
94. Levy, J.M.M., C.G. Towers, and A. Thorburn, *Targeting autophagy in cancer*. Nat Rev Cancer, 2017. **17**(9): p. 528-542.
95. Elmore, S., *Apoptosis: a review of programmed cell death*. Toxicol Pathol, 2007. **35**(4): p. 495-516.
96. Taylor, R.C., S.P. Cullen, and S.J. Martin, *Apoptosis: controlled demolition at the cellular level*. Nat Rev Mol Cell Biol, 2008. **9**(3): p. 231-41.
97. Mariño, G., et al., *Self-consumption: the interplay of autophagy and apoptosis*. Nat Rev Mol Cell Biol, 2014. **15**(2): p. 81-94.
98. Youle, R.J. and D.P. Narendra, *Mechanisms of mitophagy*. Nat Rev Mol Cell Biol, 2011. **12**(1): p. 9-14.
99. Tummers, B. and D.R. Green, *Caspase-8: regulating life and death*. Immunol Rev, 2017. **277**(1): p. 76-89.
100. Hou, W., et al., *Autophagic degradation of active caspase-8: a crosstalk mechanism between autophagy and apoptosis*. Autophagy, 2010. **6**(7): p. 891-900.
101. Taddei, M.L., et al., *Anoikis: an emerging hallmark in health and diseases*. J Pathol, 2012. **226**(2): p. 380-93.
102. Sui, X., et al., *Autophagy and chemotherapy resistance: a promising therapeutic target for cancer treatment*. Cell Death Dis, 2013. **4**(10): p. e838.
103. Ma, X.H., et al., *Targeting ER stress-induced autophagy overcomes BRAF inhibitor resistance in melanoma*. J Clin Invest, 2014. **124**(3): p. 1406-17.
104. Levy, J.M., et al., *Autophagy inhibition improves chemosensitivity in BRAF(V600E) brain tumors*. Cancer Discov, 2014. **4**(7): p. 773-80.
105. Kang, M., et al., *Concurrent Autophagy Inhibition Overcomes the Resistance of Epidermal Growth Factor Receptor Tyrosine Kinase Inhibitors in Human Bladder Cancer Cells*. Int J Mol Sci, 2017. **18**(2).
106. Wang, W., et al., *Targeting Autophagy Sensitizes BRAF-Mutant Thyroid Cancer to Vemurafenib*. J Clin Endocrinol Metab, 2017. **102**(2): p. 634-643.
107. Zou, Y., et al., *The autophagy inhibitor chloroquine overcomes the innate resistance of wild-type EGFR non-small-cell lung cancer cells to erlotinib*. J Thorac Oncol, 2013. **8**(6): p. 693-702.
108. Ji, C., et al., *Induction of autophagy contributes to crizotinib resistance in ALK-positive lung cancer*. Cancer Biol Ther, 2014. **15**(5): p. 570-7.
109. Zhang, S.F., et al., *TXNDC17 promotes paclitaxel resistance via inducing autophagy in ovarian cancer*. Autophagy, 2015. **11**(2): p. 225-38.
110. Wang, J. and G.S. Wu, *Role of autophagy in cisplatin resistance in ovarian cancer cells*. J Biol Chem, 2014. **289**(24): p. 17163-73.
111. Yu, L., et al., *Induction of autophagy counteracts the anticancer effect of cisplatin in human esophageal cancer cells with acquired drug resistance*. Cancer Lett, 2014. **355**(1): p. 34-45.
112. Mahoney, E., et al., *ER stress and autophagy: new discoveries in the mechanism of action and drug resistance of the cyclin-dependent kinase inhibitor flavopiridol*. Blood, 2012. **120**(6): p. 1262-73.

113. Li, Z.Y., et al., *A novel HDAC6 inhibitor Tubastatin A: Controls HDAC6-p97/VCP-mediated ubiquitination-autophagy turnover and reverses Temozolomide-induced ER stress-tolerance in GBM cells*. *Cancer Lett*, 2017. **391**: p. 89-99.
114. Mrakovcic, M. and L.F. Fröhlich, *p53-Mediated Molecular Control of Autophagy in Tumor Cells*. *Biomolecules*, 2018. **8**(2).
115. Crighton, D., et al., *DRAM, a p53-induced modulator of autophagy, is critical for apoptosis*. *Cell*, 2006. **126**(1): p. 121-34.
116. Feng, Z., et al., *The regulation of AMPK beta1, TSC2, and PTEN expression by p53: stress, cell and tissue specificity, and the role of these gene products in modulating the IGF-1-AKT-mTOR pathways*. *Cancer Res*, 2007. **67**(7): p. 3043-53.
117. Budanov, A.V. and M. Karin, *p53 target genes sestrin1 and sestrin2 connect genotoxic stress and mTOR signaling*. *Cell*, 2008. **134**(3): p. 451-60.
118. Karantza-Wadsworth, V., et al., *Autophagy mitigates metabolic stress and genome damage in mammary tumorigenesis*. *Genes Dev*, 2007. **21**(13): p. 1621-35.
119. Mathew, R., et al., *Autophagy suppresses tumor progression by limiting chromosomal instability*. *Genes Dev*, 2007. **21**(11): p. 1367-81.
120. Yang, J., et al., *MiR-34 modulates Caenorhabditis elegans lifespan via repressing the autophagy gene atg9*. *Age*, 2013. **35**(1): p. 11-22.
121. Rothe, K., et al., *The core autophagy protein ATG4B is a potential biomarker and therapeutic target in CML stem/progenitor cells*. *Blood*, 2014. **123**(23): p. 3622-34.
122. Wu, Y., et al., *Targeting the MIR34C-5p-ATG4B-autophagy axis enhances the sensitivity of cervical cancer cells to pirarubicin*. *Autophagy*, 2016. **12**(7): p. 1105-17.
123. Liu, K., et al., *MIR34A regulates autophagy and apoptosis by targeting HMGB1 in the retinoblastoma cell*. *Autophagy*, 2014. **10**(3): p. 442-52.
124. Song, L., et al., *MicroRNA-34a Suppresses Autophagy in Alveolar Type II Epithelial Cells in Acute Lung Injury by Inhibiting FoxO3 Expression*. *Inflammation*, 2017. **40**(3): p. 927-936.
125. Lv, X., et al., *miR-34a-5p was involved in chronic intermittent hypoxia-induced autophagy of human coronary artery endothelial cells via Bcl-2/beclin 1 signal transduction pathway*. *J Cell Biochem*, 2019. **120**(11): p. 18871-18882.
126. Zhang, Y., et al., *MicroRNA-34c-5p provokes isoprenaline-induced cardiac hypertrophy by modulating autophagy via targeting ATG4B*. *Acta Pharm Sin B*, 2022. **12**(5): p. 2374-2390.
127. Kim, Y.S., et al., *Liver X Receptor Alpha Activation Inhibits Autophagy and Lipophagy in Hepatocytes by Dysregulating Autophagy-Related 4B Cysteine Peptidase and Rab-8B, Reducing Mitochondrial Fuel Oxidation*. *Hepatology*, 2021. **73**(4): p. 1307-1326.
128. Tai, Y., et al., *miR-34a-5p regulates PINK1-mediated mitophagy via multiple modes*. *Life Sci*, 2021. **276**: p. 119415.
129. Bouznad, N., et al., *miR-34a and IRE1A/XBP-1(S) Form a Double-Negative Feedback Loop to Regulate Hypoxia-Induced EMT, Metastasis, Chemo-Resistance and Autophagy*. *Cancers (Basel)*, 2023. **15**(4).
130. Myatt, S.S. and E.W. Lam, *The emerging roles of forkhead box (Fox) proteins in cancer*. *Nat Rev Cancer*, 2007. **7**(11): p. 847-59.
131. Khan, M.A., et al., *FOX M1: A small fox that makes more tracks for cancer progression and metastasis*. *Semin Cancer Biol*, 2023. **92**: p. 1-15.
132. Gentles, A.J., et al., *The prognostic landscape of genes and infiltrating immune cells across human cancers*. *Nat Med*, 2015. **21**(8): p. 938-945.
133. Weng, W., et al., *FOX M1 and FOX Q1 Are Promising Prognostic Biomarkers and Novel Targets of Tumor-Suppressive miR-342 in Human Colorectal Cancer*. *Clin Cancer Res*, 2016. **22**(19): p. 4947-4957.

134. Fischer, M., et al., *Coordinating gene expression during the cell cycle*. Trends Biochem Sci, 2022.
135. Engeland, K., *Cell cycle arrest through indirect transcriptional repression by p53: I have a DREAM*. Cell Death Differ, 2018. **25**(1): p. 114-132.
136. Hamurcu, Z., et al., *FOXM1 plays a role in autophagy by transcriptionally regulating Beclin-1 and LC3 genes in human triple-negative breast cancer cells*. J Mol Med (Berl), 2019. **97**(4): p. 491-508.
137. Lin, J.Z., et al., *FOXM1 contributes to docetaxel resistance in castration-resistant prostate cancer by inducing AMPK/mTOR-mediated autophagy*. Cancer Lett, 2020. **469**: p. 481-489.
138. Chen, X., et al., *The forkhead transcription factor FOXM1 controls cell cycle-dependent gene expression through an atypical chromatin binding mechanism*. Mol Cell Biol, 2013. **33**(2): p. 227-36.
139. Li, Y., et al., *Reciprocal Regulation Between Forkhead Box M1/NF- κ B and Methionine Adenosyltransferase 1A Drives Liver Cancer*. Hepatology, 2020. **72**(5): p. 1682-1700.
140. Hou, Y., et al., *The transcription factor Foxm1 is essential for the quiescence and maintenance of hematopoietic stem cells*. Nat Immunol, 2015. **16**(8): p. 810-8.
141. Xu, X., et al., *miR-34a induces cellular senescence via modulation of telomerase activity in human hepatocellular carcinoma by targeting FoxM1/c-Myc pathway*. Oncotarget, 2015. **6**(6): p. 3988-4004.
142. Bayraktar, R., et al., *Dual Suppressive Effect of miR-34a on the FOXM1/eEF2-Kinase Axis Regulates Triple-Negative Breast Cancer Growth and Invasion*. Clin Cancer Res, 2018. **24**(17): p. 4225-4241.
143. Barger, C.J., et al., *Genetic determinants of FOXM1 overexpression in epithelial ovarian cancer and functional contribution to cell cycle progression*. Oncotarget, 2015. **6**(29): p. 27613-27.
144. Ran, F.A., et al., *Genome engineering using the CRISPR-Cas9 system*. Nat Protoc, 2013. **8**(11): p. 2281-2308.
145. Kaller, M., U. Götz, and H. Hermeking, *Loss of p53-inducible long non-coding RNA LINC01021 increases chemosensitivity*. Oncotarget, 2017. **8**(61): p. 102783-102800.
146. Zheng, R., et al., *Cistrome Data Browser: expanded datasets and new tools for gene regulatory analysis*. Nucleic Acids Res, 2019. **47**(D1): p. D729-d735.
147. Siemens, H., et al., *Repression of c-Kit by p53 is mediated by miR-34 and is associated with reduced chemoresistance, migration and stemness*. Oncotarget, 2013. **4**(9): p. 1399-415.
148. Hamidi, H., J. Lilja, and J. Ivaska, *Using xCELLigence RTCA Instrument to Measure Cell Adhesion*. Bio Protoc, 2017. **7**(24).
149. Risso, D., et al., *Normalization of RNA-seq data using factor analysis of control genes or samples*. Nat Biotechnol, 2014. **32**(9): p. 896-902.
150. Love, M.I., W. Huber, and S. Anders, *Moderated estimation of fold change and dispersion for RNA-seq data with DESeq2*. Genome Biol, 2014. **15**(12): p. 550.
151. Rokavec, M., Z. Huang, and H. Hermeking, *Meta-analysis of miR-34 target mRNAs using an integrative online application*. Comput Struct Biotechnol J, 2023. **21**: p. 267-274.
152. Wu, T., et al., *clusterProfiler 4.0: A universal enrichment tool for interpreting omics data*. Innovation (Camb), 2021. **2**(3): p. 100141.
153. Bordi, M., et al., *A gene toolbox for monitoring autophagy transcription*. Cell Death Dis, 2021. **12**(11): p. 1044.
154. Liberzon, A., et al., *The Molecular Signatures Database (MSigDB) hallmark gene set collection*. Cell Syst, 2015. **1**(6): p. 417-425.
155. Hänzelmann, S., R. Castelo, and J. Guinney, *GSVA: gene set variation analysis for microarray and RNA-seq data*. BMC Bioinformatics, 2013. **14**: p. 7.

156. Chen, Y., A.T. Lun, and G.K. Smyth, *From reads to genes to pathways: differential expression analysis of RNA-Seq experiments using Rsubread and the edgeR quasi-likelihood pipeline*. *F1000Res*, 2016. **5**: p. 1438.
157. Grossman, R.L., et al., *Toward a Shared Vision for Cancer Genomic Data*. *N Engl J Med*, 2016. **375**(12): p. 1109-12.
158. Martinez-Romero, J., et al., *Survival marker genes of colorectal cancer derived from consistent transcriptomic profiling*. *BMC Genomics*, 2018. **19**(Suppl 8): p. 857.
159. Colaprico, A., et al., *TCGAbiolinks: an R/Bioconductor package for integrative analysis of TCGA data*. *Nucleic Acids Res*, 2016. **44**(8): p. e71.
160. Robinson, M.D., D.J. McCarthy, and G.K. Smyth, *edgeR: a Bioconductor package for differential expression analysis of digital gene expression data*. *Bioinformatics*, 2010. **26**(1): p. 139-40.
161. Robinson, M.D. and A. Oshlack, *A scaling normalization method for differential expression analysis of RNA-seq data*. *Genome Biol*, 2010. **11**(3): p. R25.
162. Carvalho, B.S. and R.A. Irizarry, *A framework for oligonucleotide microarray preprocessing*. *Bioinformatics*, 2010. **26**(19): p. 2363-7.
163. Stein, C.K., et al., *Removing batch effects from purified plasma cell gene expression microarrays with modified ComBat*. *BMC Bioinformatics*, 2015. **16**: p. 63.
164. Eide, P.W., et al., *CMScaller: an R package for consensus molecular subtyping of colorectal cancer pre-clinical models*. *Sci Rep*, 2017. **7**(1): p. 16618.
165. Hoshida, Y., *Nearest template prediction: a single-sample-based flexible class prediction with confidence assessment*. *PLoS One*, 2010. **5**(11): p. e15543.
166. Barretina, J., et al., *The Cancer Cell Line Encyclopedia enables predictive modelling of anticancer drug sensitivity*. *Nature*, 2012. **483**(7391): p. 603-7.
167. Iorio, F., et al., *A Landscape of Pharmacogenomic Interactions in Cancer*. *Cell*, 2016. **166**(3): p. 740-754.
168. Ianevski, A., A.K. Giri, and T. Aittokallio, *SynergyFinder 2.0: visual analytics of multi-drug combination synergies*. *Nucleic Acids Res*, 2020. **48**(W1): p. W488-w493.
169. Loewe, S., *The problem of synergism and antagonism of combined drugs*. *Arzneimittelforschung*, 1953. **3**(6): p. 285-90.
170. Vassilev, L.T., et al., *In vivo activation of the p53 pathway by small-molecule antagonists of MDM2*. *Science*, 2004. **303**(5659): p. 844-8.
171. Tazawa, H., et al., *Tumor-suppressive miR-34a induces senescence-like growth arrest through modulation of the E2F pathway in human colon cancer cells*. *Proc Natl Acad Sci U S A*, 2007. **104**(39): p. 15472-7.
172. Poillet-Perez, L., J.E. Sarry, and C. Joffre, *Autophagy is a major metabolic regulator involved in cancer therapy resistance*. *Cell Rep*, 2021. **36**(7): p. 109528.
173. Kaizuka, T., et al., *An Autophagic Flux Probe that Releases an Internal Control*. *Mol Cell*, 2016. **64**(4): p. 835-849.
174. Yoshii, S.R. and N. Mizushima, *Monitoring and Measuring Autophagy*. *Int J Mol Sci*, 2017. **18**(9).
175. Jain, A., et al., *p62/SQSTM1 is a target gene for transcription factor NRF2 and creates a positive feedback loop by inducing antioxidant response element-driven gene transcription*. *J Biol Chem*, 2010. **285**(29): p. 22576-91.
176. Bellezza, I., et al., *ROS-independent Nrf2 activation in prostate cancer*. *Oncotarget*, 2017. **8**(40): p. 67506-67518.
177. Liberzon, A., et al., *Molecular signatures database (MSigDB) 3.0*. *Bioinformatics*, 2011. **27**(12): p. 1739-40.

-
178. Cao, H.X., et al., *Circ_0009910 promotes imatinib resistance through ULK1-induced autophagy by sponging miR-34a-5p in chronic myeloid leukemia*. Life Sci, 2020. **243**: p. 117255.
 179. Pang, J., et al., *Activation of miR-34a impairs autophagic flux and promotes cochlear cell death via repressing ATG9A: implications for age-related hearing loss*. Cell Death Dis, 2017. **8**(10): p. e3079.
 180. Bartoszewska, S., et al., *miR-34c-5p modulates X-box-binding protein 1 (XBP1) expression during the adaptive phase of the unfolded protein response*. Faseb j, 2019. **33**(10): p. 11541-11554.
 181. Cheng, X., et al., *miR-34a inhibits progression of neuroblastoma by targeting autophagy-related gene 5*. Eur J Pharmacol, 2019. **850**: p. 53-63.
 182. Krammes, L., et al., *Induction of the Endoplasmic-Reticulum-Stress Response: MicroRNA-34a Targeting of the IRE1 α -Branch*. Cells, 2020. **9**(6).
 183. Bjørkøy, G., et al., *p62/SQSTM1 forms protein aggregates degraded by autophagy and has a protective effect on huntingtin-induced cell death*. J Cell Biol, 2005. **171**(4): p. 603-14.
 184. Laoukili, J., et al., *FoxM1 is required for execution of the mitotic programme and chromosome stability*. Nat Cell Biol, 2005. **7**(2): p. 126-36.
 185. *Comprehensive molecular characterization of human colon and rectal cancer*. Nature, 2012. **487**(7407): p. 330-7.
 186. Cano, A., et al., *The transcription factor snail controls epithelial-mesenchymal transitions by repressing E-cadherin expression*. Nat Cell Biol, 2000. **2**(2): p. 76-83.
 187. Battle, E., et al., *The transcription factor snail is a repressor of E-cadherin gene expression in epithelial tumour cells*. Nat Cell Biol, 2000. **2**(2): p. 84-9.
 188. Tan, T.Z., et al., *Epithelial-mesenchymal transition spectrum quantification and its efficacy in deciphering survival and drug responses of cancer patients*. EMBO Mol Med, 2014. **6**(10): p. 1279-93.
 189. Liao, H., et al., *Methylation-induced silencing of miR-34a enhances chemoresistance by directly upregulating ATG4B-induced autophagy through AMPK/mTOR pathway in prostate cancer*. Oncol Rep, 2016. **35**(1): p. 64-72.
 190. Jin, H.Y., et al., *Transfection of microRNA Mimics Should Be Used with Caution*. Front Genet, 2015. **6**: p. 340.
 191. Shibue, T. and R.A. Weinberg, *EMT, CSCs, and drug resistance: the mechanistic link and clinical implications*. Nat Rev Clin Oncol, 2017. **14**(10): p. 611-629.
 192. Tanida, I., et al., *Lysosomal turnover, but not a cellular level, of endogenous LC3 is a marker for autophagy*. Autophagy, 2005. **1**(2): p. 84-91.
 193. Zhang, X.J., et al., *Why should autophagic flux be assessed?* Acta Pharmacol Sin, 2013. **34**(5): p. 595-9.
 194. Ganley, I.G., et al., *Distinct autophagosomal-lysosomal fusion mechanism revealed by thapsigargin-induced autophagy arrest*. Mol Cell, 2011. **42**(6): p. 731-43.
 195. Bonetti, P., et al., *Dual role for miR-34a in the control of early progenitor proliferation and commitment in the mammary gland and in breast cancer*. Oncogene, 2019. **38**(3): p. 360-374.
 196. Ahn, Y.H., et al., *ZEB1 drives prometastatic actin cytoskeletal remodeling by downregulating miR-34a expression*. J Clin Invest, 2012. **122**(9): p. 3170-83.
 197. Isosaka, M., et al., *A Screen for Epigenetically Silenced microRNA Genes in Gastrointestinal Stromal Tumors*. PLoS One, 2015. **10**(7): p. e0133754.
 198. Mackiewicz, M., et al., *Identification of the receptor tyrosine kinase AXL in breast cancer as a target for the human miR-34a microRNA*. Breast Cancer Res Treat, 2011. **130**(2): p. 663-79.

199. Engkvist, M.E., et al., *Analysis of the miR-34 family functions in breast cancer reveals annotation error of miR-34b*. Sci Rep, 2017. **7**(1): p. 9655.
200. Bianchi, E., et al., *Role of miR-34a-5p in Hematopoietic Progenitor Cells Proliferation and Fate Decision: Novel Insights into the Pathogenesis of Primary Myelofibrosis*. Int J Mol Sci, 2017. **18**(1).
201. Navarro, F., et al., *miR-34a contributes to megakaryocytic differentiation of K562 cells independently of p53*. Blood, 2009. **114**(10): p. 2181-92.
202. Silber, J., et al., *miR-34a repression in proneural malignant gliomas upregulates expression of its target PDGFRA and promotes tumorigenesis*. PloS one, 2012. **7**(3): p. e33844-e33844.
203. Yang, J. and A.M. Davidoff, *Remarkable Synergy When Combining EZH2 Inhibitors with YM155 Is H3K27me3-Independent*. Cancers (Basel), 2022. **15**(1).
204. Wu, J., et al., *MicroRNA-34 Family Enhances Wound Inflammation by Targeting LGR4*. J Invest Dermatol, 2020. **140**(2): p. 465-476.e11.
205. Daige, C.L., et al., *Systemic delivery of a miR34a mimic as a potential therapeutic for liver cancer*. Mol Cancer Ther, 2014. **13**(10): p. 2352-60.
206. Mantione, K.J., et al., *Comparing bioinformatic gene expression profiling methods: microarray and RNA-Seq*. Med Sci Monit Basic Res, 2014. **20**: p. 138-42.
207. Kim, J., et al., *AMPK and mTOR regulate autophagy through direct phosphorylation of Ulk1*. Nat Cell Biol, 2011. **13**(2): p. 132-41.
208. De Tito, S., et al., *The Golgi as an Assembly Line to the Autophagosome*. Trends Biochem Sci, 2020. **45**(6): p. 484-496.
209. Chipuk, J.E., L. Bouchier-Hayes, and D.R. Green, *Mitochondrial outer membrane permeabilization during apoptosis: the innocent bystander scenario*. Cell Death Differ, 2006. **13**(8): p. 1396-402.
210. Ow, Y.P., et al., *Cytochrome c: functions beyond respiration*. Nat Rev Mol Cell Biol, 2008. **9**(7): p. 532-42.
211. Zauli, G., et al., *miR-34a induces the downregulation of both E2F1 and B-Myb oncogenes in leukemic cells*. Clin Cancer Res, 2011. **17**(9): p. 2712-24.
212. Sadasivam, S., S. Duan, and J.A. DeCaprio, *The MuvB complex sequentially recruits B-Myb and FoxM1 to promote mitotic gene expression*. Genes Dev, 2012. **26**(5): p. 474-89.
213. Li, D., et al., *The critical role of dysregulated FOXM1-PLAUR signaling in human colon cancer progression and metastasis*. Clin Cancer Res, 2013. **19**(1): p. 62-72.
214. Lamark, T., S. Svenning, and T. Johansen, *Regulation of selective autophagy: the p62/SQSTM1 paradigm*. Essays Biochem, 2017. **61**(6): p. 609-624.
215. Pohl, C. and I. Dikic, *Cellular quality control by the ubiquitin-proteasome system and autophagy*. Science, 2019. **366**(6467): p. 818-822.
216. Vomund, S., et al., *Nrf2, the Master Regulator of Anti-Oxidative Responses*. Int J Mol Sci, 2017. **18**(12).
217. Komatsu, M., et al., *The selective autophagy substrate p62 activates the stress responsive transcription factor Nrf2 through inactivation of Keap1*. Nat Cell Biol, 2010. **12**(3): p. 213-23.
218. Nguyen, T., P. Nioi, and C.B. Pickett, *The Nrf2-antioxidant response element signaling pathway and its activation by oxidative stress*. J Biol Chem, 2009. **284**(20): p. 13291-5.
219. Jaramillo, M.C. and D.D. Zhang, *The emerging role of the Nrf2-Keap1 signaling pathway in cancer*. Genes Dev, 2013. **27**(20): p. 2179-91.
220. Guardia, C.M., et al., *Structure of Human ATG9A, the Only Transmembrane Protein of the Core Autophagy Machinery*. Cell Rep, 2020. **31**(13): p. 107837.
221. Mari, M., et al., *An Atg9-containing compartment that functions in the early steps of autophagosome biogenesis*. J Cell Biol, 2010. **190**(6): p. 1005-22.

-
222. Yamamoto, H., et al., *Atg9 vesicles are an important membrane source during early steps of autophagosome formation*. J Cell Biol, 2012. **198**(2): p. 219-33.
 223. Suzuki, K., et al., *Fine mapping of autophagy-related proteins during autophagosome formation in Saccharomyces cerevisiae*. J Cell Sci, 2013. **126**(Pt 11): p. 2534-44.
 224. Kotani, T., et al., *The Atg2-Atg18 complex tethers pre-autophagosomal membranes to the endoplasmic reticulum for autophagosome formation*. Proc Natl Acad Sci U S A, 2018. **115**(41): p. 10363-10368.
 225. Osawa, T., et al., *Atg2 mediates direct lipid transfer between membranes for autophagosome formation*. Nat Struct Mol Biol, 2019. **26**(4): p. 281-288.
 226. Sawa-Makarska, J., et al., *Reconstitution of autophagosome nucleation defines Atg9 vesicles as seeds for membrane formation*. Science, 2020. **369**(6508).
 227. Maeda, S., et al., *Structure, lipid scrambling activity and role in autophagosome formation of ATG9A*. Nat Struct Mol Biol, 2020. **27**(12): p. 1194-1201.
 228. McIntosh, H.M., *Chloroquine or amodiaquine combined with sulfadoxine-pyrimethamine for treating uncomplicated malaria*. Cochrane Database Syst Rev, 2001(4): p. Cd000386.
 229. Cohen, H.G. and T.B. Reynolds, *Comparison of metronidazole and chloroquine for the treatment of amoebic liver abscess. A controlled trial*. Gastroenterology, 1975. **69**(1): p. 35-41.
 230. Dörner, T., *Therapy: Hydroxychloroquine in SLE: old drug, new perspectives*. Nat Rev Rheumatol, 2010. **6**(1): p. 10-1.
 231. Mauthe, M., et al., *Chloroquine inhibits autophagic flux by decreasing autophagosome-lysosome fusion*. Autophagy, 2018. **14**(8): p. 1435-1455.
 232. Ferreira, P.M.P., et al., *Chloroquine and hydroxychloroquine in antitumor therapies based on autophagy-related mechanisms*. Pharmacol Res, 2021. **168**: p. 105582.
 233. Kinsey, C.G., et al., *Protective autophagy elicited by RAF → MEK → ERK inhibition suggests a treatment strategy for RAS-driven cancers*. Nat Med, 2019. **25**(4): p. 620-627.
 234. Sasaki, K., et al., *Resistance of colon cancer to 5-fluorouracil may be overcome by combination with chloroquine, an in vivo study*. Anticancer Drugs, 2012. **23**(7): p. 675-82.
 235. Hashimoto, D., et al., *Autophagy is needed for the growth of pancreatic adenocarcinoma and has a cytoprotective effect against anticancer drugs*. Eur J Cancer, 2014. **50**(7): p. 1382-90.
 236. Hu, J., X. Hu, and T. Kan, *MiR-34c Participates in Diabetic Corneal Neuropathy Via Regulation of Autophagy*. Invest Ophthalmol Vis Sci, 2019. **60**(1): p. 16-25.

8. Appendix

Table S1. List of mRNAs to generate the K-means clustering heatmap.

Gene symbol	Cluster	MiR34_targets	DREAM_targets	E2F_targets
<i>PADI3</i>	1	No	No	No
<i>ID3</i>	1	No	No	No
<i>IFI6</i>	1	No	No	No
<i>PIFO</i>	1	No	No	No
<i>SH2D1B</i>	1	No	No	No
<i>DUSP10</i>	1	No	No	No
<i>LINC01814</i>	1	No	No	No
<i>ID2-AS1</i>	1	No	No	No
<i>LBH</i>	1	No	No	No
<i>AC019069.1</i>	1	No	No	No
<i>PROM2</i>	1	No	No	No
<i>FN1</i>	1	Predicted	No	No
<i>GRIP2</i>	1	No	No	No
<i>VILL</i>	1	No	No	No
<i>TMEM158</i>	1	No	No	No
<i>HYAL1</i>	1	No	No	No
<i>TNNC1</i>	1	No	No	No
<i>MITF</i>	1	No	No	No
<i>ZBED2</i>	1	No	No	No
<i>SPICE1</i>	1	No	No	No
<i>MUC13</i>	1	No	No	No
<i>RBP1</i>	1	No	No	No
<i>LIPH</i>	1	No	No	No
<i>WDR53</i>	1	No	No	No
<i>APBB2</i>	1	No	No	No
<i>DAPP1</i>	1	No	No	No
<i>LINC02273</i>	1	No	No	No
<i>GASK1B</i>	1	No	No	No
<i>CEP72</i>	1	No	Yes	No
<i>DOK3</i>	1	No	No	No
<i>JARID2</i>	1	No	No	No
<i>CLIC5</i>	1	No	No	No
<i>AL135905.2</i>	1	No	No	No
<i>RAET1E</i>	1	No	No	No
<i>SUGCT</i>	1	No	No	No
<i>ERV3-1</i>	1	No	No	No
<i>AC016831.6</i>	1	No	No	No
<i>MNX1</i>	1	No	No	No
<i>MYOM2</i>	1	No	No	No
<i>AC018398.1</i>	1	No	No	No
<i>BAALC-AS1</i>	1	No	No	No
<i>SYBU</i>	1	No	No	No
<i>MTBP</i>	1	No	Yes	No
<i>TBC1D31</i>	1	No	Yes	No
<i>AC016074.2</i>	1	No	No	No
<i>LRATD2</i>	1	No	No	No
<i>CASC8</i>	1	No	No	No
<i>ADGRB1</i>	1	No	No	No
<i>LY6K</i>	1	No	No	No
<i>MINCR</i>	1	No	No	No
<i>MROH6</i>	1	No	No	No

<i>WDR97</i>	1	No	No	No
<i>KIFC2</i>	1	No	No	No
<i>RECQL4</i>	1	No	Yes	No
<i>DMRT1</i>	1	No	No	No
<i>PSAT1</i>	1	No	No	No
<i>FGD3</i>	1	No	No	No
<i>LCN2</i>	1	No	No	No
<i>LINP1</i>	1	No	No	No
<i>HKDC1</i>	1	No	No	No
<i>PRXL2A</i>	1	No	No	No
<i>NEURL1</i>	1	No	No	No
<i>ACSL5</i>	1	No	No	No
<i>LMNTD2-AS1</i>	1	No	No	No
<i>DGAT2</i>	1	No	No	No
<i>TMPRSS4</i>	1	No	No	No
<i>NINJ2-AS1</i>	1	No	No	No
<i>VWF</i>	1	No	No	No
<i>C1R</i>	1	No	No	No
<i>GPRC5A</i>	1	No	No	No
<i>KRT80</i>	1	No	No	No
<i>HSD17B6</i>	1	No	No	No
<i>AC025419.1</i>	1	No	No	No
<i>CPM</i>	1	No	No	No
<i>OAS1</i>	1	No	No	No
<i>EPST11</i>	1	No	No	No
<i>AL606834.1</i>	1	No	No	No
<i>DGLUCY</i>	1	No	No	No
<i>IFI27</i>	1	No	No	No
<i>RASGRF1</i>	1	No	No	No
<i>ALPK3</i>	1	No	No	No
<i>NR2F2</i>	1	No	No	No
<i>HAS3</i>	1	No	No	No
<i>FOXL1</i>	1	No	No	No
<i>WNK4</i>	1	No	No	No
<i>EPN3</i>	1	No	No	No
<i>CACNA1G</i>	1	No	No	No
<i>MYO15B</i>	1	No	No	No
<i>UNC13D</i>	1	No	No	No
<i>SPHK1</i>	1	No	No	No
<i>RAB27B</i>	1	No	No	No
<i>HCN2</i>	1	No	No	No
<i>FUT3</i>	1	No	No	No
<i>ZNF567</i>	1	No	No	No
<i>CD33</i>	1	No	No	No
<i>ZNF350</i>	1	No	No	No
<i>ZNF525</i>	1	No	No	No
<i>ZNF530</i>	1	No	Yes	No
<i>AL035661.1</i>	1	No	No	No
<i>FER1L4</i>	1	No	No	No
<i>WFDC3</i>	1	No	No	No
<i>B3GALT5-AS1</i>	1	No	No	No
<i>SH3BP1</i>	1	No	No	No
<i>CSDC2</i>	1	No	No	No
<i>PRR34-AS1</i>	1	No	No	No
<i>KLF8</i>	1	No	No	No
<i>PWWP3B</i>	1	No	No	No
<i>FHL1</i>	1	Predicted	No	No
<i>HAUS7</i>	1	No	Yes	No

<i>AL691432.2</i>	2	No	No	No
<i>GABRD</i>	2	No	No	No
<i>AL139423.1</i>	2	No	No	No
<i>DRAXIN</i>	2	No	No	No
<i>OTUD3</i>	2	No	No	No
<i>HTR1D</i>	2	No	No	No
<i>E2F2</i>	2	No	Yes	No
<i>IL22RA1</i>	2	No	No	No
<i>IFNLR1</i>	2	No	No	No
<i>GRHL3</i>	2	No	No	No
<i>GPR3</i>	2	Predicted	No	No
<i>PTAFR</i>	2	No	No	No
<i>LAPTM5</i>	2	No	No	No
<i>GJB3</i>	2	No	No	No
<i>MFSD2A</i>	2	No	No	No
<i>ZNF684</i>	2	No	Yes	No
<i>RAD54L</i>	2	No	Yes	No
<i>JUN</i>	2	No	No	No
<i>STXBP3</i>	2	No	No	No
<i>WDR47</i>	2	No	No	No
<i>TENT5C</i>	2	No	No	No
<i>TMEM81</i>	2	No	No	No
<i>TMCC2</i>	2	No	No	No
<i>SLC41A1</i>	2	No	No	No
<i>YOD1</i>	2	No	No	No
<i>GRHL1</i>	2	Predicted	No	No
<i>RRM2</i>	2	Predicted	Yes	Yes
<i>SLC30A3</i>	2	Predicted	No	No
<i>CYP1B1</i>	2	No	No	No
<i>EMX1</i>	2	No	No	No
<i>SFXN5</i>	2	No	No	No
<i>BCL2L11</i>	2	No	No	No
<i>TFCP2L1</i>	2	Predicted	No	No
<i>DHRS9</i>	2	No	No	No
<i>C2orf88</i>	2	No	No	No
<i>NRP2</i>	2	No	No	No
<i>VIL1</i>	2	No	No	No
<i>TUBA4A</i>	2	No	No	No
<i>DOCK10</i>	2	No	No	No
<i>GBX2</i>	2	No	No	No
<i>ERFE</i>	2	No	No	No
<i>HES6</i>	2	No	No	No
<i>AC022007.1</i>	2	No	No	No
<i>EOMES</i>	2	No	No	No
<i>SNRK</i>	2	No	No	No
<i>UBA7</i>	2	No	No	No
<i>SEMA3F</i>	2	No	No	No
<i>SLC38A3</i>	2	No	No	No
<i>DUSP7</i>	2	Predicted	No	No
<i>KBTD8</i>	2	No	No	No
<i>CEP97</i>	2	No	Yes	No
<i>C3orf52</i>	2	No	No	No
<i>GCSAM</i>	2	No	No	No
<i>HEG1</i>	2	Predicted	No	No
<i>LAMP3</i>	2	No	No	No
<i>EPHB3</i>	2	No	No	No
<i>IL1RAP</i>	2	No	No	No
<i>N4BP2</i>	2	No	No	No

<i>NIPAL1</i>	2	No	No	No
<i>CNGA1</i>	2	No	No	No
<i>AREG</i>	2	Published	No	No
<i>LIN54</i>	2	No	Yes	No
<i>ABCG2</i>	2	No	No	No
<i>ZGRF1</i>	2	No	Yes	No
<i>CLGN</i>	2	No	No	No
<i>OTULINL</i>	2	No	No	No
<i>TNFAIP8</i>	2	No	No	No
<i>MARCHF3</i>	2	No	No	No
<i>SOWAHA</i>	2	No	No	No
<i>HBEGF</i>	2	No	No	No
<i>GPRIN1</i>	2	No	No	No
<i>MAK</i>	2	No	No	No
<i>SMIM13</i>	2	No	No	No
<i>CD83</i>	2	No	No	No
<i>TCF19</i>	2	No	Yes	Yes
<i>ATP6V1G2-DDX39B</i>	2	No	No	No
<i>C2</i>	2	No	No	No
<i>C4B</i>	2	No	No	No
<i>ETV7</i>	2	No	No	No
<i>MDF1</i>	2	No	No	No
<i>ULBP2</i>	2	Published	No	No
<i>SYNJ2</i>	2	Predicted	No	No
<i>AC007566.1</i>	2	No	No	No
<i>AC105052.2</i>	2	No	No	No
<i>STRIP2</i>	2	No	No	No
<i>KDM7A</i>	2	No	No	No
<i>EZH2</i>	2	No	Yes	Yes
<i>NKX3-1</i>	2	No	No	No
<i>TACC1</i>	2	No	No	No
<i>GINS4</i>	2	Predicted	Yes	Yes
<i>MYBL1</i>	2	No	Yes	No
<i>RDH10</i>	2	No	No	No
<i>PAG1</i>	2	No	No	No
<i>FSBP</i>	2	No	No	No
<i>SPAG1</i>	2	No	No	No
<i>MAFA</i>	2	No	No	No
<i>TONSL</i>	2	No	Yes	No
<i>CD274</i>	2	Published	No	No
<i>KIF24</i>	2	No	Yes	No
<i>SERPINH1P1</i>	2	No	No	No
<i>AL162231.2</i>	2	No	No	No
<i>GLIPR2</i>	2	No	No	No
<i>ANKRD20A1</i>	2	No	No	No
<i>CENPP</i>	2	No	Yes	No
<i>ZBTB34</i>	2	No	No	No
<i>HSPA14_1</i>	2	No	No	No
<i>CDK1</i>	2	No	Yes	Yes
<i>ARID5B</i>	2	No	No	No
<i>EGR2</i>	2	No	No	No
<i>UNC5B</i>	2	No	No	No
<i>PANK1</i>	2	No	No	No
<i>ENTPD1-AS1</i>	2	No	No	No
<i>SLF2</i>	2	No	Yes	No
<i>ELOVL3</i>	2	No	No	No
<i>PLEKHA1</i>	2	Predicted	No	No
<i>NKX1-2</i>	2	No	No	No

<i>ADAM12</i>	2	Published	No	No
<i>DPYSL4</i>	2	Predicted	No	No
<i>DUSP8</i>	2	No	No	No
<i>H19</i>	2	No	No	No
<i>RRM1</i>	2	No	Yes	No
<i>E2F8</i>	2	No	Yes	Yes
<i>CCDC34</i>	2	No	Yes	No
<i>PRRG4</i>	2	No	No	No
<i>TP53I11</i>	2	No	No	No
<i>CHRM4</i>	2	No	No	No
<i>CLP1</i>	2	No	No	No
<i>FAM111A</i>	2	No	Yes	No
<i>NXF1</i>	2	No	No	No
<i>FRMD8</i>	2	No	No	No
<i>OVOL1</i>	2	No	No	No
<i>P2RY2</i>	2	No	No	No
<i>AP002761.4</i>	2	No	No	No
<i>RELT</i>	2	No	No	No
<i>DDIAS</i>	2	No	Yes	No
<i>BIRC3</i>	2	No	No	No
<i>MPZL2</i>	2	No	No	No
<i>SCN3B</i>	2	Predicted	No	No
<i>CCDC15</i>	2	No	Yes	No
<i>DDX12P</i>	2	No	No	No
<i>AC092821.2</i>	2	No	No	No
<i>RAPGEF3</i>	2	No	No	No
<i>VDR</i>	2	No	No	No
<i>FMNL3</i>	2	Predicted	No	No
<i>PMEL</i>	2	No	No	No
<i>NEMP1</i>	2	No	Yes	No
<i>E2F7</i>	2	No	Yes	No
<i>TMTC3</i>	2	Predicted	No	No
<i>TMPO-AS1</i>	2	No	No	No
<i>OAS3</i>	2	No	No	No
<i>BICDL1</i>	2	No	No	No
<i>BCL7A</i>	2	No	No	No
<i>GJB2</i>	2	No	No	No
<i>LACC1</i>	2	No	No	No
<i>CDH24</i>	2	No	No	No
<i>BRMS1L</i>	2	No	No	Yes
<i>TRIM9</i>	2	No	No	No
<i>GPR137C</i>	2	No	Yes	No
<i>GCH1</i>	2	No	No	No
<i>PPM1A</i>	2	Predicted	No	No
<i>SIX1</i>	2	No	No	No
<i>ARG2</i>	2	Predicted	No	No
<i>STON2</i>	2	No	No	No
<i>CHRFAM7A</i>	2	No	No	No
<i>INAFM2</i>	2	No	No	No
<i>OIP5</i>	2	No	Yes	No
<i>ITPKA</i>	2	No	No	No
<i>CEP152</i>	2	No	Yes	No
<i>CA12</i>	2	No	No	No
<i>CORO2B</i>	2	Predicted	No	No
<i>THAP10</i>	2	No	No	No
<i>CEMIP</i>	2	No	No	No
<i>MEX3B</i>	2	No	No	No
<i>PKMYT1</i>	2	No	Yes	No

AC026401.3	2	No	No	No
CCP110	2	No	No	Yes
SBK1	2	No	No	No
NETO2	2	Predicted	No	No
RRAD	2	No	No	No
AC020763.4	2	No	No	No
MARVELD3	2	No	No	No
AC092718.8	2	No	No	No
FOXF1	2	No	No	No
DOC2B	2	No	No	No
TRPV3	2	No	No	No
SLC52A1	2	No	No	No
LINC00324	2	No	No	No
AC005747.1	2	No	No	No
SARM1	2	No	No	No
SLC46A1	2	No	No	No
TOP2A	2	No	Yes	Yes
TUBG1	2	No	Yes	Yes
HROB	2	No	Yes	No
SP6	2	No	No	No
NGFR	2	Predicted	No	No
COIL	2	No	No	No
SEPTIN4	2	No	No	No
RAD51C	2	No	Yes	Yes
C17orf80	2	No	No	No
CDR2L	2	No	No	No
FBF1	2	No	No	No
TEN1-CDK3	2	No	No	No
AC015802.6	2	No	No	No
METRNL	2	No	No	No
LPIN2	2	No	No	No
CEP76	2	No	No	No
AP005482.4	2	No	No	No
PMAIP1	2	No	Yes	No
RNF152	2	No	No	No
SERPINB8	2	No	No	No
PARD6G	2	No	No	No
DOT1L	2	No	No	No
TINCR	2	No	No	No
ANGPTL4	2	No	No	No
ZNF699	2	No	No	No
SPC24	2	Predicted	Yes	Yes
ZNF441	2	No	No	No
ZNF440	2	No	No	No
ZNF564	2	No	No	No
C19orf57	2	No	No	No
NOTCH3	2	Predicted	No	No
AC005336.1	2	No	No	No
CYP4F11	2	No	No	No
ANKLE1	2	Predicted	No	No
AC008397.2	2	No	No	No
ZNF101	2	No	No	No
ZNF506	2	No	No	No
CCNE1	2	Published	Yes	Yes
DPF1	2	No	No	No
SERTAD1	2	No	No	No
PLAUR	2	No	No	No
LYPD5	2	No	No	No

<i>RELB</i>	2	No	No	No
<i>LIG1</i>	2	No	No	Yes
<i>KCNA7</i>	2	No	No	No
<i>ZNF845</i>	2	No	No	No
<i>PCNA</i>	2	No	Yes	Yes
<i>MGME1</i>	2	No	No	No
<i>NANP</i>	2	No	No	No
<i>NOL4L</i>	2	No	No	No
<i>KCNB1</i>	2	No	No	No
<i>HELZ2</i>	2	No	No	No
<i>FP565260.3</i>	2	No	No	No
<i>BTG3</i>	2	No	No	No
<i>SYNJ1</i>	2	Predicted	No	No
<i>ICOSLG</i>	2	No	No	No
<i>PDXP</i>	2	No	No	No
<i>NCAPH2</i>	2	No	Yes	No
<i>GK</i>	2	No	No	No
<i>PIM2</i>	2	No	No	No
<i>RADX</i>	2	No	No	No
<i>LONRF3</i>	2	No	No	No
<i>ELF4</i>	2	No	No	No
<i>INTS6L</i>	2	No	No	No
<i>F8A3</i>	2	No	No	No
<i>RNF207</i>	3	No	No	No
<i>SPCS2P4</i>	3	No	No	No
<i>AZIN2</i>	3	No	No	No
<i>BMP8A</i>	3	No	No	No
<i>PPIEL</i>	3	No	No	No
<i>ABCA4</i>	3	No	No	No
<i>AC093157.1</i>	3	No	No	No
<i>PBXIP1</i>	3	No	No	No
<i>RIT1</i>	3	No	No	No
<i>TGFB2</i>	3	Predicted	No	No
<i>TRIM67</i>	3	No	No	No
<i>SLC35F3</i>	3	No	No	No
<i>FAM49A</i>	3	No	No	No
<i>DNAJC27-AS1</i>	3	No	No	No
<i>WBP1</i>	3	No	No	No
<i>LINC00342</i>	3	No	No	No
<i>LIMS2</i>	3	No	No	No
<i>COL4A3</i>	3	No	No	No
<i>DNER</i>	3	Predicted	No	No
<i>ARL4C</i>	3	No	No	No
<i>PLCD1</i>	3	No	No	No
<i>TCTA</i>	3	No	No	No
<i>DNAH12</i>	3	No	No	No
<i>TMEM45A</i>	3	No	No	No
<i>PLD1</i>	3	No	No	No
<i>NAALADL2</i>	3	No	No	No
<i>CXCL8</i>	3	No	No	No
<i>ARHGAP24</i>	3	No	No	No
<i>INPP4B</i>	3	No	No	No
<i>FSTL5</i>	3	No	No	No
<i>AC138866.2</i>	3	No	No	No
<i>AC010501.2</i>	3	No	No	No
<i>VCAN</i>	3	No	No	No
<i>EFNA5</i>	3	No	No	No
<i>EPB41L4A</i>	3	No	No	No

<i>SIL1</i>	3	No	No	No
<i>NRG2</i>	3	No	No	No
<i>PCDHGB7</i>	3	No	No	No
<i>STK32A</i>	3	No	No	No
<i>ADAM19</i>	3	Predicted	No	No
<i>DRD1</i>	3	No	No	No
<i>H3C6</i>	3	No	No	No
<i>AL645929.1</i>	3	No	No	No
<i>AL662795.2</i>	3	No	No	No
<i>PHF1</i>	3	No	No	No
<i>EFHC1</i>	3	No	Yes	No
<i>AL359715.1</i>	3	No	No	No
<i>TARID</i>	3	No	No	No
<i>TCF21</i>	3	No	No	No
<i>TMEM184A</i>	3	No	No	No
<i>AC007009.1</i>	3	No	No	No
<i>HDAC9</i>	3	No	No	No
<i>ITGB8</i>	3	No	No	No
<i>HECW1</i>	3	No	No	No
<i>STAG3L1</i>	3	No	No	No
<i>BHLHA15</i>	3	No	No	No
<i>FOXP2</i>	3	Published	No	No
<i>AASS</i>	3	No	No	No
<i>LINC01006</i>	3	No	No	No
<i>AC027117.1</i>	3	No	No	No
<i>DUSP4</i>	3	No	No	No
<i>AC090578.3</i>	3	No	No	No
<i>SNTB1</i>	3	No	No	No
<i>KCNQ3</i>	3	No	No	No
<i>GLIS3</i>	3	No	No	No
<i>FAM189A2</i>	3	No	No	No
<i>MAMDC2</i>	3	Predicted	No	No
<i>CEMIP2</i>	3	No	No	No
<i>TNFSF15</i>	3	No	No	No
<i>TLL11</i>	3	Predicted	No	No
<i>AL162586.1</i>	3	No	No	No
<i>AL157935.3</i>	3	No	No	No
<i>ST6GALNAC4</i>	3	No	No	No
<i>PIP5KL1</i>	3	No	No	No
<i>CERCAM</i>	3	No	No	No
<i>QRFP</i>	3	No	No	No
<i>STKLD1</i>	3	No	No	No
<i>SLC2A6</i>	3	No	No	No
<i>DBH-AS1</i>	3	No	No	No
<i>AJM1</i>	3	No	No	No
<i>CLIC3</i>	3	No	No	No
<i>PNPLA7</i>	3	No	No	No
<i>VIM</i>	3	No	No	No
<i>SGMS1-AS1</i>	3	No	No	No
<i>SPOCK2</i>	3	No	No	No
<i>ANKRD1</i>	3	No	No	No
<i>PAOX</i>	3	No	No	No
<i>SPON1</i>	3	No	No	No
<i>SERPING1</i>	3	No	No	No
<i>SLC3A2</i>	3	No	Yes	No
<i>ALDH3B1</i>	3	No	No	No
<i>AP001972.5</i>	3	No	No	No
<i>MMP13</i>	3	No	No	No

<i>PDE3A</i>	3	No	No	No
<i>SLCO1B3</i>	3	No	No	No
<i>CNTN1</i>	3	No	No	No
<i>GLT8D2</i>	3	No	No	No
<i>DCLK1</i>	3	No	No	No
<i>KCTD12</i>	3	No	No	No
<i>GAS6-AS1</i>	3	No	No	No
<i>AL138479.2</i>	3	No	No	No
<i>LTK</i>	3	No	No	No
<i>HOMER2</i>	3	No	No	No
<i>ADAMTS17</i>	3	No	No	No
<i>MSLN</i>	3	No	No	No
<i>ENO3</i>	3	No	No	No
<i>ZNF594</i>	3	No	No	No
<i>ARL4D</i>	3	No	No	No
<i>SPATA20</i>	3	No	No	No
<i>CUEDC1</i>	3	Predicted	No	No
<i>WIP1</i>	3	Predicted	No	No
<i>DTNA</i>	3	Predicted	No	No
<i>CCDC102B</i>	3	No	No	No
<i>CYB5A</i>	3	No	No	No
<i>AC004623.1</i>	3	No	No	No
<i>ANO8</i>	3	No	No	No
<i>ZNF91</i>	3	No	No	No
<i>ZNF30</i>	3	No	No	No
<i>THAP8</i>	3	No	No	No
<i>MIA</i>	3	No	No	No
<i>GFY</i>	3	No	No	No
<i>ZNF134</i>	3	No	No	No
<i>AC020915.3</i>	3	No	No	No
<i>L3MBTL1</i>	3	No	No	No
<i>LINC01271</i>	3	No	No	No
<i>FNDC11</i>	3	No	No	No
<i>AL121845.1</i>	3	No	No	No
<i>RUNX1</i>	3	No	Yes	No
<i>AP001066.1</i>	3	No	No	No
<i>SCARF2</i>	3	No	No	No
<i>CASTOR1</i>	3	No	No	No
<i>RNF215</i>	3	No	No	No
<i>C1QTNF6</i>	3	Predicted	No	No
<i>NHS</i>	3	No	No	No
<i>WAS</i>	3	No	No	No
<i>TSC22D3</i>	3	No	No	No
<i>ARHGEF6</i>	3	No	No	No
<i>L1CAM</i>	3	Published	No	No
<i>SCNN1D</i>	4	No	No	No
<i>MXRA8</i>	4	No	No	No
<i>HES2</i>	4	No	No	No
<i>TNFRSF9</i>	4	No	No	No
<i>KLHDC7A</i>	4	No	No	No
<i>HSPG2</i>	4	No	No	No
<i>NCMAP</i>	4	No	No	No
<i>SERINC2</i>	4	No	No	No
<i>TINAGL1</i>	4	No	No	No
<i>COL16A1</i>	4	No	No	No
<i>COL9A2</i>	4	No	No	No
<i>BTBD19</i>	4	No	No	No
<i>TSPAN1</i>	4	No	No	No

<i>ECHDC2</i>	4	No	No	No
<i>WDR78</i>	4	No	No	No
<i>SLC44A5</i>	4	No	No	No
<i>ST6GALNAC5</i>	4	No	No	No
<i>SLC44A3-AS1</i>	4	No	No	No
<i>INKA2-AS1</i>	4	No	No	No
<i>S100A10</i>	4	No	No	No
<i>HRNR</i>	4	No	No	No
<i>S100A2</i>	4	No	No	No
<i>LMNA</i>	4	Predicted	No	No
<i>AL590560.3</i>	4	No	No	No
<i>GPA33</i>	4	No	No	No
<i>PTPRVP</i>	4	No	No	No
<i>MFSD4A</i>	4	No	No	No
<i>C1orf116</i>	4	No	No	No
<i>LAMB3</i>	4	No	No	No
<i>PXDN</i>	4	No	No	No
<i>TP53I3</i>	4	No	No	No
<i>EFR3B</i>	4	No	No	No
<i>KIF3C</i>	4	Predicted	No	No
<i>UCN</i>	4	No	No	No
<i>XDH</i>	4	No	No	No
<i>CRIM1</i>	4	No	No	No
<i>TTC7A</i>	4	No	No	No
<i>DYSF</i>	4	No	No	No
<i>AC159540.2</i>	4	No	No	No
<i>AC092683.1</i>	4	No	No	No
<i>EDAR</i>	4	No	No	No
<i>MIR4435-2HG</i>	4	No	No	No
<i>GALNT5</i>	4	No	No	No
<i>AC009299.1</i>	4	No	No	No
<i>SCN2A</i>	4	No	No	No
<i>MAP2</i>	4	Predicted	No	No
<i>ABCA12</i>	4	No	No	No
<i>AC068946.1</i>	4	No	No	No
<i>GPR55</i>	4	No	No	No
<i>TMPPE</i>	4	No	No	No
<i>TRANK1</i>	4	No	No	No
<i>KIF9-AS1</i>	4	No	No	No
<i>LAMB2</i>	4	No	No	No
<i>AC104452.1</i>	4	No	No	No
<i>NICN1</i>	4	No	No	No
<i>DOCK3</i>	4	No	No	No
<i>NR112</i>	4	No	No	No
<i>CSTA</i>	4	No	No	No
<i>ALDH1L1</i>	4	No	No	No
<i>AMOTL2</i>	4	No	No	No
<i>IL20RB</i>	4	No	No	No
<i>LPP-AS2</i>	4	No	No	No
<i>MYL5</i>	4	No	No	No
<i>IDUA</i>	4	No	No	No
<i>CTBP1-DT</i>	4	No	No	No
<i>MXD4</i>	4	No	No	No
<i>HGFAC</i>	4	No	No	No
<i>DOK7</i>	4	No	No	No
<i>MSX1</i>	4	No	No	No
<i>SORCS2</i>	4	Predicted	No	No
<i>AC093827.4</i>	4	No	No	No

<i>SPRY1</i>	4	No	No	No
<i>TRIML2</i>	4	No	No	No
<i>ADAMTS16</i>	4	No	No	No
<i>DAB2</i>	4	No	No	No
<i>AC025171.2</i>	4	No	No	No
<i>PLK2</i>	4	No	No	No
<i>KRT8P33</i>	4	No	No	No
<i>AC011346.1</i>	4	No	No	No
<i>SH3TC2</i>	4	No	No	No
<i>GM2A</i>	4	No	No	No
<i>FAT2</i>	4	No	No	No
<i>CPLX2</i>	4	No	No	No
<i>MYLK4</i>	4	No	No	No
<i>C6orf52</i>	4	No	No	No
<i>EDN1</i>	4	No	No	No
<i>CDKN1A</i>	4	No	No	Yes
<i>MDGA1</i>	4	Predicted	No	No
<i>AL365205.1</i>	4	No	No	No
<i>PTCHD4</i>	4	No	No	No
<i>AL590428.1</i>	4	No	No	No
<i>COL12A1</i>	4	Predicted	No	No
<i>LAMA4</i>	4	No	No	No
<i>AL096711.2</i>	4	No	No	No
<i>SYNE1</i>	4	No	No	No
<i>AC073957.3</i>	4	No	No	No
<i>AP5Z1</i>	4	No	No	No
<i>RASA4CP</i>	4	No	No	No
<i>LINC02604</i>	4	No	No	No
<i>PMS2P3</i>	4	No	No	No
<i>SEMA3C</i>	4	No	No	No
<i>MYH16</i>	4	No	No	No
<i>SLC12A9</i>	4	No	No	No
<i>IFRD1</i>	4	No	Yes	No
<i>CICP14</i>	4	No	No	No
<i>CPA4</i>	4	No	No	No
<i>ATP6V0A4</i>	4	No	No	No
<i>TMEM139</i>	4	No	No	No
<i>SSPO</i>	4	No	No	No
<i>ATG9B</i>	4	No	No	No
<i>FGF17</i>	4	No	No	No
<i>CLU</i>	4	No	No	No
<i>LINC00589</i>	4	No	No	No
<i>AC131254.1</i>	4	No	No	No
<i>AC027702.2</i>	4	No	No	No
<i>DNAJC5B</i>	4	No	No	No
<i>AC132219.2</i>	4	No	No	No
<i>AF117829.1</i>	4	No	No	No
<i>AC087752.3</i>	4	No	No	No
<i>AC067930.5</i>	4	No	No	No
<i>TMEM249</i>	4	No	No	No
<i>ABCA1</i>	4	No	No	No
<i>AL138756.1</i>	4	No	No	No
<i>SUSD1</i>	4	No	No	No
<i>CEL</i>	4	No	No	No
<i>NALT1</i>	4	No	No	No
<i>CYSRT1</i>	4	No	No	No
<i>MIR1915HG</i>	4	No	No	No
<i>NRP1</i>	4	No	No	No

<i>HSD17B7P2</i>	4	No	No	No
<i>AL022344.1</i>	4	No	No	No
<i>ANXA8</i>	4	No	No	No
<i>AL591684.2</i>	4	No	No	No
<i>ZNF365</i>	4	No	No	No
<i>COL13A1</i>	4	No	No	No
<i>PPP3CB-AS1</i>	4	No	No	No
<i>C10orf55</i>	4	No	No	No
<i>KLLN</i>	4	No	No	No
<i>FGFBP3</i>	4	No	No	No
<i>MORN4</i>	4	Predicted	No	No
<i>LOXL4</i>	4	No	No	No
<i>PYROXD2</i>	4	No	No	No
<i>SEC31B</i>	4	No	No	No
<i>SFXN3</i>	4	No	No	No
<i>COL17A1</i>	4	No	No	No
<i>DMBT1</i>	4	No	No	No
<i>AL731571.1</i>	4	No	No	No
<i>CEND1</i>	4	No	No	No
<i>TRIM22</i>	4	No	No	No
<i>KIAA1549L</i>	4	No	No	No
<i>DAGLA</i>	4	No	No	No
<i>ROM1</i>	4	No	No	No
<i>LBHD1</i>	4	No	No	No
<i>CCDC88B</i>	4	No	No	No
<i>AP003068.2</i>	4	No	No	No
<i>CST6</i>	4	No	No	No
<i>USP35</i>	4	No	No	No
<i>UPK2</i>	4	No	No	No
<i>SNX19</i>	4	No	No	No
<i>LINC02827</i>	4	No	No	No
<i>LRMP</i>	4	No	No	No
<i>MUC19</i>	4	No	No	No
<i>GPD1</i>	4	No	No	No
<i>KRT7</i>	4	No	No	No
<i>KRT81</i>	4	No	No	No
<i>AC121757.2</i>	4	No	No	No
<i>IGFBP6</i>	4	No	No	No
<i>AC076968.2</i>	4	No	No	No
<i>TAFA2</i>	4	No	No	No
<i>MDM2</i>	4	No	No	No
<i>BTBD11</i>	4	Predicted	No	No
<i>SDSL</i>	4	No	No	No
<i>ABCB9</i>	4	No	No	No
<i>DNAH10</i>	4	No	No	No
<i>GAS6-DT</i>	4	No	No	No
<i>RTN1</i>	4	No	No	No
<i>TMEM229B</i>	4	No	No	No
<i>DPF3</i>	4	No	No	No
<i>AHNAK2</i>	4	Predicted	No	No
<i>CRIP1</i>	4	No	No	No
<i>HERC2P3</i>	4	No	No	No
<i>THBS1</i>	4	Predicted	No	No
<i>CCDC9B</i>	4	No	No	No
<i>CHAC1</i>	4	No	No	No
<i>AC087482.1</i>	4	No	No	No
<i>SEMA7A</i>	4	No	No	No
<i>ST20-AS1</i>	4	No	No	No

<i>ISG20</i>	4	No	No	No
<i>VPS33B-DT</i>	4	No	No	No
<i>MSLNL</i>	4	No	No	No
<i>EME2</i>	4	No	No	No
<i>PDPK2P</i>	4	No	No	No
<i>AC092117.1</i>	4	No	No	No
<i>PRSS30P</i>	4	No	No	No
<i>ABAT</i>	4	No	No	No
<i>NUPR1</i>	4	No	No	No
<i>AC026471.1</i>	4	No	No	No
<i>AC007906.2</i>	4	No	No	No
<i>KIFC3</i>	4	No	No	No
<i>NDRG4</i>	4	No	No	No
<i>FBXL8</i>	4	No	No	No
<i>HSF4</i>	4	No	No	No
<i>C17orf107</i>	4	No	No	No
<i>AC004771.4</i>	4	No	No	No
<i>ALOX12P2</i>	4	No	No	No
<i>TOM1L2</i>	4	Predicted	No	No
<i>SLC47A2</i>	4	No	No	No
<i>LGALS9B</i>	4	No	No	No
<i>AC022916.2</i>	4	No	No	No
<i>MMP28</i>	4	No	No	No
<i>TBC1D3L</i>	4	No	No	No
<i>KRT16</i>	4	No	No	No
<i>JUP</i>	4	No	No	No
<i>OSBPL7</i>	4	No	No	No
<i>LINC02086</i>	4	No	No	No
<i>TTL6</i>	4	No	No	No
<i>LRRC37A3</i>	4	No	No	No
<i>AC018665.1</i>	4	No	No	No
<i>TSPAN10</i>	4	No	No	No
<i>AC132938.6</i>	4	No	No	No
<i>AP000919.2</i>	4	No	No	No
<i>AC016588.2</i>	4	No	No	No
<i>GZMM</i>	4	No	No	No
<i>VMAC</i>	4	No	No	No
<i>CAPS</i>	4	No	No	No
<i>NWD1</i>	4	No	No	No
<i>IQCN</i>	4	No	No	No
<i>C19orf33</i>	4	No	No	No
<i>PRKCG</i>	4	No	No	No
<i>LENG8</i>	4	No	No	No
<i>BCL2L1</i>	4	No	No	No
<i>ABALON</i>	4	No	No	No
<i>MYL9</i>	4	Predicted	No	No
<i>NNAT</i>	4	No	No	No
<i>ARHGAP40</i>	4	No	No	No
<i>PABPC1L</i>	4	No	No	No
<i>TMEM189-UBE2V1</i>	4	No	No	No
<i>LIME1</i>	4	No	No	No
<i>SSR4P1</i>	4	No	No	No
<i>ZNF70</i>	4	No	No	No
<i>SUSD2</i>	4	No	No	No
<i>POM121L9P</i>	4	No	No	No
<i>TCN2</i>	4	No	No	No
<i>APOBEC3D</i>	4	No	No	No
<i>APOBEC3H</i>	4	No	No	No

<i>PDGFB</i>	4	No	No	No
<i>MIRLET7BHG</i>	4	No	No	No
<i>ADM2</i>	4	No	No	No
<i>ARSA</i>	4	No	No	No
<i>RPL23AP82</i>	4	No	No	No
<i>ASMTL-AS1</i>	4	No	No	No
<i>GRPR</i>	4	No	No	No
<i>AC078993.1</i>	4	No	No	No
<i>OPHN1</i>	4	No	No	No
<i>SRPX2</i>	4	No	No	No
<i>COL4A6</i>	4	No	No	No
<i>SMIM10L2A</i>	4	No	No	No
<i>PLXNB3</i>	4	No	No	No
<i>LINC01770</i>	5	No	No	No
<i>SMIM1</i>	5	No	No	No
<i>TNFRSF8</i>	5	No	No	No
<i>CCDC24</i>	5	No	No	No
<i>FPGT-TNNI3K</i>	5	No	No	No
<i>AC097059.1</i>	5	No	No	No
<i>VTCN1</i>	5	No	No	No
<i>PHGDH</i>	5	No	No	No
<i>LINC00623</i>	5	No	No	No
<i>LINC00869</i>	5	No	No	No
<i>SELL</i>	5	No	No	No
<i>CRYZL2P</i>	5	No	No	No
<i>ZNF648</i>	5	No	No	No
<i>HLX</i>	5	No	No	No
<i>ODC1-DT</i>	5	No	No	No
<i>ATP6V1C2</i>	5	No	No	No
<i>CCDC121</i>	5	No	No	No
<i>C2orf81</i>	5	No	No	No
<i>TMSB10</i>	5	No	No	No
<i>SH2D6</i>	5	No	No	No
<i>C2orf15</i>	5	No	No	No
<i>IL18R1</i>	5	No	No	No
<i>SULT1C2</i>	5	No	No	No
<i>ACOXL</i>	5	No	No	No
<i>MZT2A</i>	5	No	No	No
<i>GPR39</i>	5	No	No	No
<i>DPP4</i>	5	No	No	No
<i>TTC30A</i>	5	No	No	No
<i>ZNF385B</i>	5	No	No	No
<i>IKZF2</i>	5	No	No	No
<i>AC012512.1</i>	5	No	No	No
<i>AC077690.1</i>	5	No	No	No
<i>PRRT3-AS1</i>	5	No	No	No
<i>SLC6A20</i>	5	No	No	No
<i>C3orf18</i>	5	No	No	No
<i>ACOX2</i>	5	No	No	No
<i>AC093010.3</i>	5	No	No	No
<i>PLCH1</i>	5	No	No	No
<i>C4orf48</i>	5	No	No	No
<i>CC2D2A</i>	5	No	No	No
<i>FGFBP1</i>	5	No	No	No
<i>DANCR</i>	5	No	No	No
<i>EREG</i>	5	No	No	No
<i>CXXC4</i>	5	No	No	No
<i>SPEF2</i>	5	No	No	No

<i>AC008957.1</i>	5	No	No	No
<i>GPX8</i>	5	No	No	No
<i>MEF2C</i>	5	No	No	No
<i>KIAA0825</i>	5	No	No	No
<i>SPATA24</i>	5	No	No	No
<i>FABP6</i>	5	No	No	No
<i>RAB24</i>	5	No	No	No
<i>HULC</i>	5	No	No	No
<i>LST1</i>	5	No	No	No
<i>ARMC12</i>	5	No	No	No
<i>SUPT3H</i>	5	No	No	No
<i>EYS</i>	5	No	No	No
<i>CD24</i>	5	Published	No	No
<i>STX7</i>	5	No	No	No
<i>PACRG</i>	5	No	No	No
<i>RNASET2</i>	5	No	No	No
<i>ELFN1</i>	5	No	No	No
<i>ELFN1-AS1</i>	5	No	No	No
<i>BBS9</i>	5	No	No	No
<i>TRG-AS1</i>	5	No	No	No
<i>ASNS</i>	5	No	No	No
<i>LAMB1</i>	5	No	No	No
<i>LRRC61</i>	5	No	No	No
<i>AC022239.1</i>	5	No	No	No
<i>NCALD</i>	5	Predicted	No	No
<i>MAL2</i>	5	No	No	No
<i>CCN3</i>	5	No	No	No
<i>GSDMC</i>	5	No	No	No
<i>MAPK15</i>	5	No	No	No
<i>MFSD3</i>	5	No	No	No
<i>FRG1HP</i>	5	No	No	No
<i>TMC1</i>	5	No	No	No
<i>ANXA1</i>	5	No	No	No
<i>SUSD3</i>	5	No	No	No
<i>AL590705.1</i>	5	No	No	No
<i>KIF12</i>	5	No	No	No
<i>ECHDC3</i>	5	No	No	No
<i>FAM107B</i>	5	No	No	No
<i>ADAMTS14</i>	5	No	No	No
<i>SCD</i>	5	Predicted	No	No
<i>FANK1</i>	5	No	No	No
<i>LRRC27</i>	5	No	No	No
<i>AL451069.1</i>	5	No	No	No
<i>FUOM</i>	5	No	No	No
<i>RPL26P30</i>	5	No	No	No
<i>LINC02724</i>	5	No	No	No
<i>CDC42EP2</i>	5	No	No	No
<i>NEAT1</i>	5	No	No	No
<i>FOLR1</i>	5	No	No	No
<i>GSEC</i>	5	No	No	No
<i>GRIN2B</i>	5	No	No	No
<i>TSPAN8</i>	5	No	No	No
<i>AC090015.1</i>	5	No	No	No
<i>AC089983.1</i>	5	No	No	No
<i>TCP11L2</i>	5	No	No	No
<i>LINC00173</i>	5	No	No	No
<i>ADGRD1</i>	5	No	No	No
<i>AC126564.1</i>	5	No	No	No

<i>FLT3</i>	5	No	No	No
<i>GGACT</i>	5	No	No	No
<i>ITGBL1</i>	5	No	No	No
<i>LINC00460</i>	5	No	No	No
<i>CARMIL3</i>	5	No	No	No
<i>PCK2</i>	5	No	No	No
<i>AKAP6</i>	5	Predicted	No	No
<i>NKX2-8</i>	5	No	No	No
<i>AL365295.1</i>	5	No	No	No
<i>PAPLN</i>	5	Predicted	No	No
<i>PIF1</i>	5	No	Yes	No
<i>AP3B2</i>	5	No	No	No
<i>AC013489.1</i>	5	No	No	No
<i>NPW</i>	5	No	No	No
<i>HCFC1R1</i>	5	No	No	No
<i>MT1E</i>	5	No	No	No
<i>MT1F</i>	5	No	No	No
<i>TSNAXIP1</i>	5	No	No	No
<i>CTRL</i>	5	No	No	No
<i>SLC16A13</i>	5	No	No	No
<i>TMEM256</i>	5	No	No	No
<i>STX8</i>	5	No	No	No
<i>LYRM9</i>	5	No	No	No
<i>GHDC</i>	5	No	No	No
<i>CNTNAP1</i>	5	Predicted	No	No
<i>IFI35</i>	5	Predicted	No	No
<i>RND2</i>	5	No	No	No
<i>CCDC103</i>	5	No	No	No
<i>HEXIM2</i>	5	No	No	No
<i>HOXB8</i>	5	Predicted	No	No
<i>LIMD2</i>	5	Published	No	No
<i>BAIAP2-DT</i>	5	No	No	No
<i>AC027601.1</i>	5	No	No	No
<i>OXL1</i>	5	No	No	No
<i>MRO</i>	5	No	No	No
<i>CCDC68</i>	5	No	No	No
<i>PCSK4</i>	5	No	No	No
<i>TJP3</i>	5	No	No	No
<i>BST2</i>	5	No	No	No
<i>MAP4K1</i>	5	No	No	No
<i>PPM1N</i>	5	No	No	No
<i>SULT2B1</i>	5	No	No	No
<i>FCGRT</i>	5	No	No	No
<i>CPT1C</i>	5	No	No	No
<i>TMEM74B</i>	5	No	No	No
<i>FRG1BP</i>	5	No	No	No
<i>HNF4A</i>	5	Published	No	No
<i>PLTP</i>	5	No	No	No
<i>AL133335.2</i>	5	No	No	No
<i>HMGB1P1</i>	5	No	No	No
<i>PPP1R3D</i>	5	No	No	No
<i>RPS21</i>	5	No	No	No
<i>LINC01694</i>	5	No	No	No
<i>GAL3ST1</i>	5	No	No	No
<i>ATF4</i>	5	No	Yes	No
<i>ASB9</i>	5	No	No	No
<i>AC112493.1</i>	5	No	No	No
<i>MAOB</i>	5	No	No	No

<i>RRAGB</i>	5	No	No	No
<i>TCEAL4</i>	5	No	No	No
<i>DUSP9</i>	5	No	No	No
<i>TP73</i>	6	Predicted	No	No
<i>LINC01355</i>	6	No	No	No
<i>AUNIP</i>	6	No	Yes	No
<i>CEP85</i>	6	No	Yes	No
<i>RPA2</i>	6	No	Yes	Yes
<i>IQCC</i>	6	No	No	No
<i>ZBTB8B</i>	6	No	No	No
<i>CLSPN</i>	6	No	Yes	No
<i>BMP8B</i>	6	No	No	No
<i>NASP</i>	6	No	Yes	Yes
<i>STIL</i>	6	No	Yes	No
<i>CDKN2C</i>	6	No	Yes	Yes
<i>ORC1</i>	6	No	Yes	No
<i>USP1</i>	6	No	Yes	Yes
<i>ALG6</i>	6	No	No	No
<i>ITGB3BP</i>	6	No	Yes	No
<i>CDC7</i>	6	No	Yes	No
<i>DIPK1A</i>	6	No	No	No
<i>TLCD4</i>	6	No	No	No
<i>SASS6</i>	6	No	Yes	No
<i>RBM15</i>	6	No	No	No
<i>DCLRE1B</i>	6	No	Yes	Yes
<i>H2BC19P</i>	6	No	No	No
<i>C1orf61</i>	6	No	No	No
<i>C1orf112</i>	6	No	Yes	No
<i>CENPL</i>	6	Predicted	Yes	No
<i>KIF14</i>	6	No	Yes	No
<i>UBE2T</i>	6	No	Yes	Yes
<i>ELK4</i>	6	No	No	No
<i>DYRK3</i>	6	No	No	No
<i>INTS7</i>	6	No	Yes	No
<i>DTL</i>	6	No	Yes	No
<i>LIN9</i>	6	Predicted	Yes	No
<i>CCSAP</i>	6	No	Yes	No
<i>EXO1</i>	6	No	Yes	No
<i>KLF11</i>	6	No	No	No
<i>GEN1</i>	6	No	Yes	No
<i>CENPO</i>	6	No	Yes	No
<i>GPATCH11</i>	6	No	Yes	No
<i>PRKD3</i>	6	No	No	No
<i>MSH2</i>	6	No	Yes	Yes
<i>MSH6</i>	6	No	Yes	No
<i>CHAC2</i>	6	No	No	No
<i>AC010733.2</i>	6	No	No	No
<i>PELI1</i>	6	No	No	No
<i>GMCL1</i>	6	No	No	No
<i>ALMS1-IT1</i>	6	No	No	No
<i>NCAPH</i>	6	Predicted	Yes	No
<i>ZC3H6</i>	6	Predicted	No	No
<i>TTL</i>	6	No	No	No
<i>CKAP2L</i>	6	No	Yes	No
<i>LRP1B</i>	6	No	No	No
<i>KLHL23</i>	6	Predicted	Yes	No
<i>HAT1</i>	6	No	Yes	No
<i>CDCA7</i>	6	No	Yes	No

<i>NAB1</i>	6	No	No	No
<i>STK17B</i>	6	No	Yes	No
<i>TMEM237</i>	6	No	No	No
<i>BARD1</i>	6	No	Yes	Yes
<i>USP37</i>	6	No	Yes	No
<i>NHEJ1</i>	6	No	No	No
<i>HJURP</i>	6	No	Yes	No
<i>PASK</i>	6	No	Yes	No
<i>SETMAR</i>	6	No	No	No
<i>RAD18</i>	6	No	Yes	No
<i>SGO1</i>	6	No	Yes	No
<i>ZNF620</i>	6	No	No	No
<i>ABHD5</i>	6	No	No	No
<i>KIF15</i>	6	No	Yes	No
<i>CDC25A</i>	6	Published	Yes	Yes
<i>ATRIP</i>	6	No	No	No
<i>PFKFB4</i>	6	No	No	No
<i>TRAIP</i>	6	No	Yes	No
<i>IL17RB</i>	6	No	No	No
<i>KCTD6</i>	6	No	No	No
<i>NFKBIZ</i>	6	No	No	No
<i>LRRRC58</i>	6	No	No	No
<i>POLQ</i>	6	No	Yes	No
<i>OSBPL11</i>	6	No	No	No
<i>MCM2</i>	6	Predicted	Yes	Yes
<i>GATA2</i>	6	Published	No	No
<i>TOPBP1</i>	6	No	Yes	No
<i>DIPK2A</i>	6	No	No	No
<i>ARHGEF26</i>	6	No	No	No
<i>SMC4</i>	6	No	Yes	Yes
<i>B3GNT5</i>	6	No	No	No
<i>RFC4</i>	6	No	Yes	No
<i>RNF168</i>	6	No	No	No
<i>FBXO45</i>	6	No	No	No
<i>ANKRD18DP</i>	6	No	No	No
<i>SLBP</i>	6	No	Yes	Yes
<i>NSD2</i>	6	No	Yes	No
<i>HAUS3</i>	6	No	Yes	No
<i>NCAPG</i>	6	No	Yes	No
<i>RFC1</i>	6	No	Yes	Yes
<i>CEP135</i>	6	No	Yes	No
<i>DCK</i>	6	No	Yes	Yes
<i>PAQR3</i>	6	Predicted	No	No
<i>HADH</i>	6	No	Yes	No
<i>FAM241A</i>	6	No	No	No
<i>TIFA</i>	6	No	No	No
<i>CCNA2</i>	6	Predicted	Yes	No
<i>PLK4</i>	6	No	Yes	Yes
<i>MND1</i>	6	No	Yes	No
<i>C4orf46</i>	6	No	Yes	No
<i>FNIP2</i>	6	No	No	No
<i>NEIL3</i>	6	Predicted	Yes	No
<i>ING2</i>	6	No	No	No
<i>CASP3</i>	6	No	No	No
<i>CENPU</i>	6	No	Yes	No
<i>PDLIM3</i>	6	No	No	No
<i>OTULIN</i>	6	No	No	No
<i>RAD1</i>	6	No	Yes	Yes

<i>NUP155</i>	6	No	Yes	No
<i>C5orf34</i>	6	No	Yes	No
<i>HCN1</i>	6	No	No	No
<i>DEPDC1B</i>	6	No	Yes	No
<i>CENPH</i>	6	No	Yes	No
<i>ARRDC3</i>	6	No	Yes	No
<i>SLF1</i>	6	No	Yes	No
<i>TRIM36</i>	6	No	No	No
<i>KIF20A</i>	6	Predicted	Yes	No
<i>CDC25C</i>	6	No	Yes	No
<i>EGR1</i>	6	No	No	No
<i>SPRY4</i>	6	No	No	No
<i>N4BP3</i>	6	No	No	No
<i>SNRNP48</i>	6	No	No	No
<i>DEK</i>	6	No	Yes	Yes
<i>GMNN</i>	6	Predicted	Yes	No
<i>ZNF165</i>	6	No	No	No
<i>PGBD1</i>	6	No	No	No
<i>HSPA1B</i>	6	No	No	No
<i>KIFC1</i>	6	No	Yes	No
<i>FKBP5</i>	6	Predicted	Yes	No
<i>BRPF3</i>	6	Predicted	No	No
<i>CENPQ</i>	6	No	Yes	No
<i>MCM3</i>	6	Predicted	Yes	Yes
<i>RAB23</i>	6	No	No	No
<i>CASP8AP2</i>	6	No	Yes	No
<i>MMS22L</i>	6	No	Yes	Yes
<i>MYB</i>	6	Published	No	No
<i>HECA</i>	6	No	No	No
<i>EPM2A</i>	6	No	No	No
<i>FBXO5</i>	6	No	Yes	No
<i>ZNRF2</i>	6	No	No	No
<i>LINC00997</i>	6	No	No	No
<i>ANLN</i>	6	No	Yes	No
<i>FIGNL1</i>	6	No	Yes	No
<i>ZNF273</i>	6	No	Yes	No
<i>ZNF92</i>	6	No	Yes	No
<i>RFC2</i>	6	No	Yes	Yes
<i>DBF4</i>	6	No	Yes	No
<i>MCM7</i>	6	No	Yes	Yes
<i>TMEM209</i>	6	No	Yes	No
<i>XRCC2</i>	6	No	Yes	No
<i>NCAPG2</i>	6	No	Yes	No
<i>AGPAT5</i>	6	No	Yes	No
<i>LONRF1</i>	6	No	No	No
<i>EGR3</i>	6	No	No	No
<i>CDCA2</i>	6	No	Yes	No
<i>ESCO2</i>	6	No	Yes	No
<i>PBK</i>	6	No	Yes	No
<i>MCM4</i>	6	No	Yes	Yes
<i>JPH1</i>	6	No	No	No
<i>IMPA1</i>	6	No	No	No
<i>SNX16</i>	6	No	No	No
<i>GEM</i>	6	No	No	No
<i>RAD54B</i>	6	No	Yes	No
<i>CCNE2</i>	6	Published	No	No
<i>DSCC1</i>	6	No	Yes	Yes
<i>AC021945.1</i>	6	No	No	No

ATAD2	6	No	Yes	Yes
HAUS6	6	No	Yes	No
MYORG	6	No	No	No
MELK	6	No	Yes	Yes
AL513165.2	6	No	No	No
BX664727.3	6	No	No	No
CEP78	6	No	Yes	No
RMI1	6	No	Yes	No
ZNF367	6	No	Yes	No
SMC2	6	No	Yes	No
TMEM38B	6	No	No	No
PTPN3	6	No	No	No
ZNF483	6	No	No	No
KIAA1958	6	No	No	No
ZFP37	6	No	No	No
MIR600HG	6	No	No	No
LHX2	6	Predicted	No	No
NUP188	6	No	No	No
TUBB4B	6	No	No	No
NRARP	6	No	No	No
PRKCQ	6	Predicted	No	No
MCM10	6	No	Yes	No
HSPA14_2	6	No	No	No
SUV39H2	6	No	Yes	No
MASTL	6	No	Yes	No
ZWINT	6	No	Yes	No
TFAM	6	No	No	No
DNA2	6	No	Yes	No
DNAJC9	6	No	Yes	No
KIF20B	6	No	Yes	No
KIF11	6	No	Yes	No
HHEX	6	No	No	No
PLCE1	6	No	No	No
HELLS	6	Predicted	Yes	Yes
ARHGAP19	6	No	Yes	No
CHUK	6	No	No	No
PCGF6	6	No	No	No
TAF5	6	Predicted	Yes	No
ITPRIP	6	No	No	No
SMC3	6	No	Yes	Yes
ZDHHC6	6	No	No	No
ZRANB1	6	No	No	No
MKI67	6	No	Yes	Yes
WEE1	6	No	Yes	Yes
NUP160	6	No	Yes	No
SLC43A3	6	No	No	No
FAM111B	6	No	Yes	No
FEN1	6	No	Yes	No
INCENP	6	Predicted	Yes	No
CDCA5	6	No	Yes	No
POLA2	6	No	Yes	Yes
AP000944.5	6	No	No	No
TIGD3	6	No	No	No
PGM2L1	6	No	No	No
POLD3	6	No	Yes	Yes
EMSY	6	No	No	No
EED	6	No	No	Yes
SLC36A4	6	No	No	No

<i>SMCO4</i>	6	No	No	No
<i>CEP295</i>	6	No	Yes	No
<i>NPAT</i>	6	No	Yes	No
<i>CHEK1</i>	6	No	Yes	Yes
<i>PRDM10</i>	6	No	No	No
<i>CCDC77</i>	6	No	Yes	No
<i>FOXM1</i>	6	Published	Yes	No
<i>RAD51AP1</i>	6	No	Yes	Yes
<i>GPR19</i>	6	Predicted	Yes	No
<i>TMEM106C</i>	6	No	No	No
<i>SENP1</i>	6	Predicted	Yes	No
<i>RHEBL1</i>	6	No	No	No
<i>RACGAP1</i>	6	No	Yes	Yes
<i>ESPL1</i>	6	No	Yes	Yes
<i>CDK2</i>	6	No	Yes	No
<i>TIMELESS</i>	6	Predicted	Yes	Yes
<i>PRIM1</i>	6	No	Yes	No
<i>ATP23</i>	6	No	Yes	No
<i>YEATS4</i>	6	No	Yes	No
<i>TBC1D15</i>	6	No	No	No
<i>CSRP2</i>	6	No	No	No
<i>TMPO</i>	6	No	Yes	Yes
<i>UHRF1BP1L</i>	6	No	No	No
<i>UNG</i>	6	No	Yes	Yes
<i>FAM222A</i>	6	No	No	No
<i>RFC5</i>	6	No	Yes	No
<i>KNTC1</i>	6	No	Yes	No
<i>MPHOSPH9</i>	6	No	Yes	No
<i>AC073857.1</i>	6	No	No	No
<i>BRI3BP</i>	6	No	No	No
<i>POLE</i>	6	No	Yes	Yes
<i>SKA3</i>	6	No	Yes	No
<i>CENPJ</i>	6	No	Yes	No
<i>NUP58</i>	6	No	Yes	No
<i>B3GLCT</i>	6	No	No	No
<i>BRCA2</i>	6	No	Yes	Yes
<i>RFC3</i>	6	No	Yes	Yes
<i>DGKH</i>	6	No	No	No
<i>CKAP2</i>	6	No	Yes	No
<i>FBXL3</i>	6	No	No	No
<i>CLYBL</i>	6	No	No	No
<i>TEX30</i>	6	No	Yes	No
<i>ING1</i>	6	No	Yes	No
<i>TUBGCP3</i>	6	Predicted	No	No
<i>CHAMP1</i>	6	No	No	No
<i>PARP2</i>	6	No	Yes	No
<i>LINC00641</i>	6	No	No	No
<i>AL132780.1</i>	6	No	No	No
<i>BAZ1A</i>	6	No	No	No
<i>FANCM</i>	6	No	Yes	No
<i>LRR1</i>	6	No	Yes	No
<i>POLE2</i>	6	No	Yes	No
<i>TXNDC16</i>	6	No	No	No
<i>WDHD1</i>	6	No	Yes	No
<i>HSPA2</i>	6	No	No	No
<i>LIN52</i>	6	No	Yes	No
<i>ACYP1</i>	6	No	No	No
<i>FOS</i>	6	No	No	No

<i>GON7</i>	6	No	No	No
<i>UBR7</i>	6	No	Yes	Yes
<i>XRCC3</i>	6	No	Yes	No
<i>CDCA4</i>	6	No	Yes	No
<i>TUBGCP5</i>	6	No	No	No
<i>BUB1B</i>	6	No	Yes	Yes
<i>KNL1</i>	6	No	Yes	No
<i>RAD51</i>	6	Published	Yes	No
<i>NUSAP1</i>	6	Predicted	Yes	No
<i>HAUS2</i>	6	No	Yes	No
<i>TUBGCP4</i>	6	No	No	No
<i>WDR76</i>	6	Predicted	Yes	No
<i>CTDSPL2</i>	6	No	Yes	No
<i>PCLAF</i>	6	No	Yes	No
<i>PARP16</i>	6	No	No	No
<i>CALML4</i>	6	No	No	No
<i>KIF23</i>	6	No	Yes	No
<i>LRRC49</i>	6	No	No	No
<i>CHRNA5</i>	6	No	No	No
<i>FANCI</i>	6	Predicted	Yes	No
<i>TICRR</i>	6	No	Yes	No
<i>BLM</i>	6	No	Yes	No
<i>PRC1</i>	6	No	Yes	No
<i>AC068831.8</i>	6	No	No	No
<i>CCNF</i>	6	Predicted	Yes	No
<i>EMP2</i>	6	Predicted	No	No
<i>REXO5</i>	6	No	No	No
<i>ZKSCAN2-DT</i>	6	No	No	No
<i>SHCBP1</i>	6	Predicted	Yes	No
<i>ORC6</i>	6	No	Yes	Yes
<i>GINS3</i>	6	Predicted	Yes	Yes
<i>RFWD3</i>	6	No	Yes	No
<i>ZFP1</i>	6	No	No	No
<i>TMEM170A</i>	6	No	No	No
<i>CENPN</i>	6	No	Yes	No
<i>AC092718.4</i>	6	No	No	No
<i>GAN</i>	6	No	No	No
<i>GINS2</i>	6	No	Yes	No
<i>CDT1</i>	6	No	Yes	No
<i>FANCA</i>	6	Predicted	Yes	No
<i>RFLNB</i>	6	No	No	No
<i>SMYD4</i>	6	No	No	No
<i>HASPIN</i>	6	No	Yes	No
<i>USP6</i>	6	No	No	No
<i>MIS12</i>	6	No	Yes	No
<i>WRAP53</i>	6	No	Yes	No
<i>TOP3A</i>	6	No	Yes	No
<i>SPAG5</i>	6	No	Yes	Yes
<i>ATAD5</i>	6	No	Yes	No
<i>SUZ12</i>	6	No	Yes	No
<i>RHBDL3</i>	6	No	No	No
<i>CDK5R1</i>	6	No	No	No
<i>MYO19</i>	6	Predicted	Yes	No
<i>PPP1R1B</i>	6	No	No	No
<i>CDC6</i>	6	No	Yes	No
<i>PSMC3IP</i>	6	No	Yes	Yes
<i>BRCA1</i>	6	No	Yes	Yes
<i>KIF18B</i>	6	No	Yes	Yes

<i>EME1</i>	6	Predicted	Yes	No
<i>TUBD1</i>	6	No	Yes	No
<i>BRIP1</i>	6	No	Yes	No
<i>TCAM1P</i>	6	No	No	No
<i>GNA13</i>	6	No	No	No
<i>SLC25A19</i>	6	No	Yes	No
<i>CBX2</i>	6	No	No	No
<i>YES1</i>	6	No	No	No
<i>METTL4</i>	6	No	Yes	No
<i>NDC80</i>	6	No	Yes	No
<i>RBBP8</i>	6	No	No	No
<i>SKA1</i>	6	Predicted	Yes	No
<i>C18orf54</i>	6	Predicted	Yes	No
<i>ONECUT2</i>	6	No	No	No
<i>BCL2</i>	6	Published	No	No
<i>EFNA2</i>	6	No	No	No
<i>ZNF555</i>	6	No	No	No
<i>CHAF1A</i>	6	No	Yes	No
<i>UHRF1</i>	6	Predicted	Yes	No
<i>ZNF266</i>	6	No	No	No
<i>ZNF562</i>	6	No	No	No
<i>DNMT1</i>	6	No	Yes	Yes
<i>KANK2</i>	6	Predicted	No	No
<i>ZNF887P</i>	6	No	No	No
<i>ZNF823</i>	6	No	No	No
<i>ZNF700</i>	6	No	No	No
<i>ZNF136</i>	6	No	No	No
<i>ZNF44</i>	6	No	No	No
<i>ZNF799</i>	6	No	No	No
<i>ZNF443</i>	6	No	No	No
<i>RNASEH2A</i>	6	No	Yes	Yes
<i>IL27RA</i>	6	No	No	No
<i>SAMD1</i>	6	No	No	No
<i>ASF1B</i>	6	No	Yes	Yes
<i>HAUS8</i>	6	No	Yes	No
<i>UNC13A</i>	6	No	No	No
<i>UBA2</i>	6	No	No	No
<i>WDR62</i>	6	No	Yes	No
<i>ZNF45</i>	6	No	Yes	No
<i>ZNF230</i>	6	No	No	No
<i>AC021092.2</i>	6	No	No	No
<i>RNF24</i>	6	No	No	No
<i>MCM8</i>	6	No	Yes	No
<i>GINS1</i>	6	Predicted	Yes	Yes
<i>AL035071.1</i>	6	No	No	No
<i>E2F1</i>	6	Published	Yes	No
<i>DSN1</i>	6	Predicted	Yes	No
<i>RBL1</i>	6	No	Yes	No
<i>MYBL2</i>	6	Published	Yes	Yes
<i>CSE1L</i>	6	No	Yes	Yes
<i>SNAI1</i>	6	Published	No	No
<i>CABLES2</i>	6	No	No	No
<i>AL121832.3</i>	6	No	No	No
<i>SIK1B</i>	6	No	No	No
<i>CU638689.4</i>	6	No	No	No
<i>AP000295.1</i>	6	No	No	No
<i>DONSON</i>	6	No	No	Yes
<i>CHAF1B</i>	6	No	No	No

ZBTB21	6	No	No	No
PKNOX1	6	Predicted	Yes	No
CDC45	6	No	Yes	No
CHEK2	6	No	Yes	Yes
CCDC117	6	No	No	No
YWHAH	6	No	No	No
CENPM	6	No	Yes	Yes
RIBC2	6	No	No	No
GTSE1	6	Predicted	Yes	No
FANCB	6	No	Yes	No
PIGA	6	No	Yes	No
SCML1	6	No	No	No
SCML2	6	Predicted	No	No
KLHL15	6	No	No	No
SUV39H1	6	No	Yes	Yes
SMC1A	6	No	Yes	Yes
SPIN4	6	No	No	No
ERCC6L	6	No	Yes	No
TAF9B	6	No	No	No
GABRQ	6	No	No	No
AL590822.3	7	No	No	No
EPHA10	7	No	No	No
FGGY	7	No	No	No
PDE4B	7	Predicted	No	No
ST6GALNAC3	7	No	No	No
SAMD13	7	No	No	No
AP4B1-AS1	7	No	No	No
S100A5	7	No	No	No
DPM3	7	No	No	No
AL590560.2	7	No	No	No
PBX1	7	No	No	No
HMCN1	7	No	No	No
AC108488.2	7	No	No	No
EIF3FP3	7	No	No	No
PAIP2B	7	No	No	No
KCNIP3	7	No	No	No
LONRF2	7	No	No	No
NR4A2	7	Published	No	No
PDE11A_1	7	No	No	No
KLF7	7	Predicted	No	No
IL17RD	7	No	No	No
MAG11	7	No	No	No
AC046134.2	7	No	No	No
SLC9A9	7	No	No	No
TLR6	7	No	No	No
FRAS1	7	No	No	No
GPRIN3	7	No	No	No
CCSER1	7	No	No	No
PDE5A	7	No	No	No
SLC7A11	7	No	No	No
NR3C2	7	No	No	No
TRIM2	7	No	No	No
CTSO	7	No	No	No
PDGFC	7	No	No	No
GUSBP1	7	No	No	No
SELENOP	7	No	No	No
ADAMTS6	7	No	No	No
IQGAP2	7	No	No	No

ZBED3-AS1	7	No	No	No
ATP6AP1L	7	No	No	No
GLRX	7	No	No	No
STARD4-AS1	7	No	No	No
NREP	7	No	No	No
ZNF608	7	No	No	No
SYNPO	7	Predicted	No	No
ADAMTS2	7	No	No	No
GMDS-DT	7	No	No	No
SAPCD1	7	No	No	No
HLA-DMB	7	No	No	No
RCAN2	7	No	No	No
AL080250.1	7	No	No	No
RPS6KA2	7	No	No	No
PRKAR1B	7	No	No	No
GPER1	7	No	No	No
HOXA4	7	Predicted	No	No
SEMA3A	7	No	No	No
SEMA3D	7	No	No	No
PPP1R9A	7	No	No	No
TECPR1	7	No	No	No
UFSP1	7	No	No	No
WNT16	7	No	No	No
FAM180A	7	No	No	No
ZNF467	7	No	No	No
NUDT18	7	No	No	No
HAS2	7	No	No	No
AL354707.1	7	No	No	No
FAM201A	7	No	No	No
FRG1JP	7	No	No	No
AL161457.2	7	No	No	No
SHC3	7	No	No	No
SARDH	7	No	No	No
LCN12	7	No	No	No
AL136982.1	7	No	No	No
KAZALD1	7	No	No	No
SLC22A18	7	No	No	No
OR51B4	7	No	No	No
CAVIN3	7	No	No	No
ACCS	7	No	No	No
SLC43A1	7	No	No	No
ARHGAP42	7	No	No	No
KBTD3	7	No	No	No
SPSB2	7	No	No	No
BHLHE41	7	No	No	No
FAR2	7	No	No	No
AC008014.1	7	No	No	No
METTL7A	7	No	No	No
TNS2	7	No	No	No
METTL7B	7	No	No	No
TMEM198B	7	No	No	No
CAPS2	7	No	No	No
RPS2P5	7	No	No	No
AC004812.2	7	No	No	No
LINC01089	7	No	No	No
AC084018.2	7	No	No	No
STARD13	7	No	No	No
LINC02331	7	No	No	No

<i>BMP4</i>	7	No	No	No
<i>SERPINA5</i>	7	No	No	No
<i>DICER1-AS1</i>	7	No	No	No
<i>PLCB2</i>	7	No	No	No
<i>AC090517.4</i>	7	No	No	No
<i>AC009065.3</i>	7	No	No	No
<i>LDHD</i>	7	No	No	No
<i>CDH15</i>	7	No	No	No
<i>VPS9D1</i>	7	No	No	No
<i>TLCD2</i>	7	No	No	No
<i>SERPINF2</i>	7	No	No	No
<i>SREBF1</i>	7	No	No	No
<i>AC073508.2</i>	7	No	No	No
<i>NAGLU</i>	7	No	No	No
<i>FZD2</i>	7	No	No	No
<i>ACE</i>	7	No	No	No
<i>MILR1</i>	7	No	No	No
<i>CEP112</i>	7	No	No	No
<i>ARSG</i>	7	No	No	No
<i>SLC16A6</i>	7	No	No	No
<i>LINC00482</i>	7	No	No	No
<i>FGF22</i>	7	No	No	No
<i>TLE6</i>	7	No	No	No
<i>NDUFB7</i>	7	No	No	No
<i>KCNN1</i>	7	No	No	No
<i>AC020910.6</i>	7	No	No	No
<i>ETV2</i>	7	No	No	No
<i>RABAC1</i>	7	No	No	No
<i>LRRC4B</i>	7	No	No	No
<i>SPACA6</i>	7	No	No	No
<i>NDUFV2P1</i>	7	No	No	No
<i>BFSP1</i>	7	No	No	No
<i>CYP24A1</i>	7	No	No	No
<i>LSS</i>	7	Predicted	No	No
<i>LINC00896</i>	7	No	No	No
<i>SCUBE1</i>	7	No	No	No
<i>ODF3B</i>	7	No	No	No
<i>CA5B</i>	7	No	No	No
<i>FAAH2</i>	7	No	No	No
<i>AMOT</i>	7	No	No	No
<i>MBNL3</i>	7	No	No	No
<i>DNASE1L1</i>	7	No	No	No
<i>CDA</i>	8	Predicted	No	No
<i>EXTL1</i>	8	No	No	No
<i>SPOCD1</i>	8	No	No	No
<i>TMEM234</i>	8	No	No	No
<i>TMEM125</i>	8	No	No	No
<i>SLC6A9</i>	8	Predicted	No	No
<i>BEST4</i>	8	No	No	No
<i>AL604028.1</i>	8	No	No	No
<i>TMEM61</i>	8	No	No	No
<i>GSTM2</i>	8	No	No	No
<i>BCL2L15</i>	8	No	No	No
<i>PEX11B</i>	8	No	No	No
<i>PDIA3P1</i>	8	No	No	No
<i>MINDY1</i>	8	No	No	No
<i>TRIM46</i>	8	No	No	No
<i>THBS3</i>	8	No	No	No

<i>AL592435.1</i>	8	No	No	No
<i>AL645568.1</i>	8	No	No	No
<i>CAPN8</i>	8	No	No	No
<i>ZNF670-ZNF695</i>	8	No	No	No
<i>INO80B</i>	8	No	No	No
<i>AC022210.2</i>	8	No	No	No
<i>CYTOR</i>	8	No	No	No
<i>LINC01123</i>	8	No	No	No
<i>ZBTB45P2</i>	8	No	No	No
<i>AC105402.3</i>	8	No	No	No
<i>AC012443.2</i>	8	No	No	No
<i>TTC30B</i>	8	No	No	No
<i>ALPP</i>	8	No	No	No
<i>EFHD1</i>	8	No	No	No
<i>LMCD1-AS1</i>	8	No	No	No
<i>PRRT3</i>	8	No	No	No
<i>CMTM7</i>	8	No	No	No
<i>FBXL2</i>	8	No	No	No
<i>TTC21A</i>	8	No	No	No
<i>PRKAR2A-AS1</i>	8	No	No	No
<i>HEMK1</i>	8	No	No	No
<i>AC097358.2</i>	8	No	No	No
<i>TMCC1-AS1</i>	8	No	No	No
<i>NUDT16P1</i>	8	No	No	No
<i>NME9</i>	8	No	No	No
<i>ERICH6-AS1</i>	8	No	No	No
<i>VEPH1</i>	8	No	No	No
<i>TMEM44-AS1</i>	8	No	No	No
<i>CFAP99</i>	8	No	No	No
<i>FGFBP2</i>	8	No	No	No
<i>UBA6-AS1</i>	8	No	No	No
<i>ANK2</i>	8	No	No	No
<i>LINC02236</i>	8	No	No	No
<i>AC008957.3</i>	8	No	No	No
<i>LINC02065</i>	8	No	No	No
<i>AC022107.1</i>	8	No	No	No
<i>LINC02163</i>	8	No	No	No
<i>MIR3936HG</i>	8	No	No	No
<i>ATOX1</i>	8	No	No	No
<i>STC2</i>	8	No	No	No
<i>RGS14</i>	8	No	No	No
<i>DDAH2</i>	8	No	No	No
<i>PRRT1</i>	8	No	No	No
<i>AL451165.2</i>	8	No	No	No
<i>PLA2G7</i>	8	No	No	No
<i>GSTA2</i>	8	No	No	No
<i>CITED2</i>	8	Predicted	No	No
<i>UTRN</i>	8	No	No	No
<i>C6orf99</i>	8	No	No	No
<i>AGPAT4</i>	8	No	No	No
<i>AL596442.3</i>	8	No	No	No
<i>AC004982.2</i>	8	No	No	No
<i>HOXA1</i>	8	No	No	No
<i>NPC1L1</i>	8	No	No	No
<i>PSPH</i>	8	No	No	No
<i>ZNF117</i>	8	No	No	No
<i>SAMD9</i>	8	No	No	No
<i>AC254629.1</i>	8	No	No	No

<i>CDHR3</i>	8	No	No	No
<i>AC002066.1</i>	8	No	No	No
<i>LINC00513</i>	8	No	No	No
<i>FMC1</i>	8	No	No	No
<i>WEE2-AS1</i>	8	No	No	No
<i>CLCN1</i>	8	No	No	No
<i>NOS3</i>	8	Predicted	No	No
<i>CDK5</i>	8	No	No	No
<i>AC021218.1</i>	8	No	No	No
<i>AC022784.1</i>	8	No	No	No
<i>PIWIL2</i>	8	No	No	No
<i>SCARA5</i>	8	No	No	No
<i>SLC20A2</i>	8	No	No	No
<i>AP002851.1</i>	8	No	No	No
<i>SAMD12</i>	8	No	No	No
<i>ERICD</i>	8	No	No	No
<i>AC067930.8</i>	8	No	No	No
<i>AC109322.1</i>	8	No	No	No
<i>AC233992.2</i>	8	No	No	No
<i>LRRC24</i>	8	No	No	No
<i>SPATA6L</i>	8	No	No	No
<i>LURAP1L</i>	8	No	No	No
<i>TLE1</i>	8	No	No	No
<i>PTCH1</i>	8	Predicted	No	No
<i>OLFML2A</i>	8	No	No	No
<i>PLPP7</i>	8	No	No	No
<i>SKIDA1</i>	8	No	No	No
<i>ITGB1-DT</i>	8	No	No	No
<i>RASSF4</i>	8	No	No	No
<i>AL356056.2</i>	8	No	No	No
<i>BEND3P1</i>	8	No	No	No
<i>ZNF503-AS1</i>	8	No	No	No
<i>IFIT1</i>	8	No	No	No
<i>PDZD7</i>	8	No	No	No
<i>AFAP1L2</i>	8	No	No	No
<i>LRRC56</i>	8	No	No	No
<i>LMNTD2</i>	8	No	No	No
<i>GATD1</i>	8	No	No	No
<i>CARS1</i>	8	No	No	No
<i>OR51B3P</i>	8	No	No	No
<i>AP001453.4</i>	8	No	No	No
<i>ZNHIT2</i>	8	No	No	No
<i>POLD4</i>	8	No	No	No
<i>LINC02701</i>	8	No	No	No
<i>LINC02700</i>	8	No	No	No
<i>LINC02732</i>	8	No	No	No
<i>TMEM25</i>	8	Predicted	No	No
<i>C11orf45</i>	8	No	No	No
<i>CACNA2D4</i>	8	No	No	No
<i>SCNN1A</i>	8	No	No	No
<i>ING4</i>	8	No	No	No
<i>FAM90A1</i>	8	No	No	No
<i>ARHGDIIB</i>	8	Published	No	No
<i>PLEKHA8P1</i>	8	No	No	No
<i>AC021066.1</i>	8	No	No	No
<i>KRT83</i>	8	No	No	No
<i>ITGA7</i>	8	No	No	No
<i>AC009779.3</i>	8	No	No	No

<i>NDUFA4L2</i>	8	No	No	No
<i>SLC26A10</i>	8	No	No	No
<i>PTPRR</i>	8	No	No	No
<i>AC078923.1</i>	8	No	No	No
<i>AC078820.3</i>	8	No	No	No
<i>NAV3</i>	8	Predicted	No	No
<i>TRPV4</i>	8	No	No	No
<i>HRK</i>	8	No	No	No
<i>AC131009.3</i>	8	No	No	No
<i>AC148477.3</i>	8	No	No	No
<i>AC148477.2</i>	8	No	No	No
<i>TPTE2P1</i>	8	No	No	No
<i>UBAC2-AS1</i>	8	No	No	No
<i>LINC00346</i>	8	No	No	No
<i>NFATC4</i>	8	Published	No	No
<i>ATL1</i>	8	No	No	No
<i>JDP2</i>	8	No	No	No
<i>FOXN3-AS1</i>	8	No	No	No
<i>RPS3AP6</i>	8	No	No	No
<i>ANXA2</i>	8	No	No	No
<i>SMAD6</i>	8	No	No	No
<i>NOX5</i>	8	No	No	No
<i>GDPGP1</i>	8	No	No	No
<i>RPL3L</i>	8	No	No	No
<i>ELOB</i>	8	No	No	No
<i>AC108134.1</i>	8	No	No	No
<i>AC126755.7</i>	8	No	No	No
<i>AC008915.3</i>	8	No	No	No
<i>AC106782.1</i>	8	No	No	No
<i>CES3</i>	8	No	No	No
<i>AC027682.6</i>	8	No	No	No
<i>PKD1L2</i>	8	No	No	No
<i>MLYCD</i>	8	No	No	No
<i>SLC7A5</i>	8	No	No	No
<i>TNFSF12</i>	8	No	No	No
<i>TRIM16</i>	8	No	No	No
<i>AC104024.4</i>	8	No	No	No
<i>MYO15A</i>	8	No	No	No
<i>AC004477.1</i>	8	No	No	No
<i>TOB1-AS1</i>	8	No	No	No
<i>AC007114.1</i>	8	No	No	No
<i>SOX9-AS1</i>	8	No	No	No
<i>TTYH2</i>	8	No	No	No
<i>MGAT5B</i>	8	No	No	No
<i>TNRC6C-AS1</i>	8	No	No	No
<i>TMC8</i>	8	No	No	No
<i>C1QTNF1</i>	8	No	No	No
<i>PCYT2</i>	8	No	No	No
<i>AC132872.5</i>	8	No	No	No
<i>LINC01910</i>	8	No	No	No
<i>ZNF516</i>	8	No	No	No
<i>AC018413.1</i>	8	No	No	No
<i>AC005775.1</i>	8	No	No	No
<i>AC005256.1</i>	8	No	No	No
<i>IZUMO4</i>	8	No	No	No
<i>FXD1</i>	8	No	No	No
<i>AC002398.1</i>	8	No	No	No
<i>LINC01534</i>	8	No	No	No

<i>SNHG11</i>	8	No	No	No
<i>PTK6</i>	8	No	No	No
<i>B3GALT5</i>	8	No	No	No
<i>TMEM191B</i>	8	No	No	No
<i>AIFM3</i>	8	No	No	No
<i>SLC2A11</i>	8	No	No	No
<i>RHBDD3</i>	8	No	No	No
<i>LINC01521</i>	8	No	No	No
<i>TMPRSS6</i>	8	No	No	No
<i>EFCAB6</i>	8	No	No	No
<i>AC207130.1</i>	8	No	No	No
<i>CSF2RA</i>	8	No	No	No
<i>CLCN4</i>	8	No	No	No
<i>SH3KBP1</i>	8	No	No	No
<i>YY2</i>	8	No	No	No
<i>SLC35A2</i>	8	No	No	No

Acknowledgements

First, I would like to thank my supervisor Prof. Dr. Heiko Hermeking for offering me the opportunity to work in such a great laboratory and his continuous support, scientific input as well as his help during my doctoral study. His visionary advice and scientific insight helped me a lot with my PhD project. Therefore, I could not have undertaken this journey without his invaluable patience and support. I have learned much from him about how to become a qualified scientist. He is not only an excellent supervisor, a talented scientist, but also a great friend.

In addition, I am grateful to Dr. Markus Kaller for his supervision and kind help in bioinformatics analysis of this project. He also assisted me a lot to solve experimental and scientific problems during my study.

I would like to express my gratitude to all members of the group for their help and valuable scientific support. In particular, I would like to thank Ursula Götz, our technician, for her full technical support in the lab. Also, I would like to thank Esra Cetin for the generation of *miR-34a*-gRNA-plasmids and Raffaele Conca (Dr. von Haunersches Children's Hospital, Munich) for FACS sorting. I had the pleasure of working with my colleagues Dr. Matjaz Rokavec, Dr. Xiaolong Shi, Chunfeng Liu, Jinjiang Chou, Fangteng Liu, Dr. Nassim Bouznad, Janine König, Dr. Markus Winter, Xiaoyan Chen, Yuyun Du and AG Peter Jung.

Furthermore, I would like to thank my parents for their support and encouragement. And I thank my girlfriend, Chenyue Dai, for her support. Last but not least, I would like to thank China Scholarship Council (CSC) for supporting me for 4 years to achieve my doctor degree.

Affidavit



LUDWIG-
MAXIMILIANS-
UNIVERSITÄT
MÜNCHEN

Promotionsbüro
Medizinische Fakultät



Affidavit

Huang, Zekai

Surname, first name

Street

Zip code, town, country

I hereby declare, that the submitted thesis entitled:

Characterization of miR-34 effectors in colorectal cancer

.....

is my own work. I have only used the sources indicated and have not made unauthorised use of services of a third party. Where the work of others has been quoted or reproduced, the source is always given.

I further declare that the dissertation presented here has not been submitted in the same or similar form to any other institution for the purpose of obtaining an academic degree.

Munich, 13.03.2024

place, date

Zekai Huang

Signature doctoral candidate

Confirmation of congruency



LUDWIG-
MAXIMILIANS-
UNIVERSITÄT
MÜNCHEN

Promotionsbüro
Medizinische Fakultät



**Confirmation of congruency between printed and electronic version of
the doctoral thesis**

Huang, Zekai

Surname, first name

Street

Zip code, town, country

I hereby declare, that the submitted thesis entitled:

Characterization of miR-34 effectors in colorectal cancer

.....

is congruent with the printed version both in content and format.

Munich, 13.03.2024

place, date

Zekai Huang

Signature doctoral candidate

Curriculum vitae

Zekai Huang

Education:

- 2011-2016 Southern Medical University, Guangzhou, China
Major subject: Clinical Medicine
- 06.2016 Bachelor Degree of Medicine
- 2016-2019 Peking University, Beijing, China
Major subject: Oncology
- 06.2019 Master Degree of Medicine

Research experience:

- Since 10.2019 PhD student,
Supervisor: Prof. Dr. rer. nat. Heiko Hermeking
(Head of Experimental and Molecular Pathology,
Institute of Pathology, LMU, Munich, Germany)

List of publications

1. **Huang, Z.**, Kaller, M. & Hermeking, H. CRISPR/Cas9-mediated inactivation of *miR-34a* and *miR-34b/c* in HCT116 colorectal cancer cells: comprehensive characterization after exposure to 5-FU reveals EMT and autophagy as key processes regulated by miR-34. *Cell Death Differ* 30, 2017–2034 (2023). <https://doi.org/10.1038/s41418-023-01193-2>
2. Rokavec, M., **Huang, Z.**, Hermeking, H. Meta-analysis of miR-34 target mRNAs using an integrative online application. *Comput Struct Biotechnol J*, 2023. 21: p. 267-274. <https://doi.org/10.1016/j.csbj.2022.12.003>
3. Liu, C., Rokavec, M., **Huang, Z.** & Hermeking, H. Curcumin activates a ROS/KEAP1/NRF2/*miR-34a/b/c* cascade to suppress colorectal cancer metastasis. *Cell Death Differ* 30, 1771–1785 (2023). <https://doi.org/10.1038/s41418-023-01178-1>
4. **Huang Z.**, Ma Y, Zhang P, Si J, Xiong Y, Yang Y, Long non-coding RNA H19 confers resistance to gefitinib via miR-148b-3p/DDAH1 axis in lung adenocarcinoma. *Anticancer Drugs*, 2020. 31(1): p. 44-54. <https://doi.org/10.1097/CAD.0000000000000831>
5. **Huang Z.**, Li S, Yang X, Lu F, Huang M, Zhang S, et al. Long-term survival of patients with locally advanced esophageal squamous cell carcinoma receiving esophagectomy following neoadjuvant chemotherapy: a cohort study. *Cancer Manag Res*. 2019. 11:1299-1308. <https://doi.org/10.2147/CMAR.S195355>